



HAL
open science

Random and Out-of-Equilibrium Potts models

Christophe Chatelain

► **To cite this version:**

Christophe Chatelain. Random and Out-of-Equilibrium Potts models. Statistical Mechanics [cond-mat.stat-mech]. Université de Lorraine, 2012. tel-00959733

HAL Id: tel-00959733

<https://theses.hal.science/tel-00959733>

Submitted on 15 Mar 2014

HAL is a multi-disciplinary open access archive for the deposit and dissemination of scientific research documents, whether they are published or not. The documents may come from teaching and research institutions in France or abroad, or from public or private research centers.

L'archive ouverte pluridisciplinaire **HAL**, est destinée au dépôt et à la diffusion de documents scientifiques de niveau recherche, publiés ou non, émanant des établissements d'enseignement et de recherche français ou étrangers, des laboratoires publics ou privés.

Habilitation à Diriger des Recherches

**Modèles de Potts
désordonnés et hors de l'équilibre**

Christophe Chatelain

Soutenance publique prévue le 17 décembre 2012

Membres du jury :

Rapporteurs :	Werner Krauth	École Normale Supérieure, Paris
	Marco Picco	Université Pierre et Marie Curie, Paris 6
	Heiko Rieger	Université de Saarbrücken, Allemagne
Examineurs :	Dominique Mouhanna	Université Pierre et Marie Curie, Paris 6
	Wolfhard Janke	Université de Leipzig, Allemagne
	Bertrand Berche	Université de Lorraine

TABLE OF CONTENTS

1. Random and Out-of-Equilibrium Potts models	4
1.1. Introduction	4
1.2. Random Potts models	6
1.2.1. The pure Potts model	6
1.2.1.1. Fortuin-Kasteleyn representation	7
1.2.1.2. From loop and vertex models to the Coulomb gas	9
1.2.1.3. Coulomb gas and minimal models	12
1.2.2. Smoothing of first-order transitions by inhomogeneous perturbations	14
1.2.2.1. Heuristic arguments and correspondence with the RFIM	14
1.2.2.2. Effect of disorder on two-dimensional Potts models	19
1.2.2.3. Three-dimensional random Potts models	24
1.2.2.4. Two-dimensional Potts models on irregular graphs	28
1.2.2.5. Anisotropic perturbations of the two-dimensional Potts model	29
1.2.3. The random Potts fixed point	37
1.2.3.1. The Harris criterion	37
1.2.3.2. Critical behaviour at the two-dimensional random fixed point	39
1.2.3.3. Three-dimensional random fixed point	44
1.2.3.4. Aperiodic and irregular graphs in the second-order regime	46
1.2.3.5. Multifractality at the random fixed-point	49
1.2.3.6. Replica-symmetry breaking	56
1.2.4. Conformal invariance of two-dimensional random systems	57
1.2.4.1. Conformal covariance of correlation functions	58
1.2.4.2. Conformal covariance of profile	61
1.2.4.3. Stochastic Schramm-Loewner Evolution	63
1.2.5. Conclusions	72
1.3. Out-of-equilibrium processes	73
1.3.1. Phenomenology and scaling theory of aging ferromagnets	75
1.3.1.1. Lifschitz-Cahn-Allen growth law	75
1.3.1.2. Initial-slip and autocorrelation exponents	78
1.3.1.3. Scaling theory of aging two-point functions	79
1.3.1.4. Response functions and violation of the FDT	81
1.3.1.5. Local Scale Invariance	84

1.3.2. Out-of-equilibrium dynamics of the Potts model	85
1.3.2.1. Aging in one-dimensional spin models	86
1.3.2.2. Aging in two-dimensional models in the Potts universality class . . .	89
1.3.2.3. Potts models with an irreversible dynamics	94
1.3.3. Aging in fully-frustrated models	100
1.3.3.1. Fully-Frustrated Ising Model	100
1.3.3.2. Fully-Frustrated XY Model	104
1.3.4. Jarzynski relation	109
1.3.5. Conclusions	114
1.4. Simulations of experimental systems	116
1.4.1. Magnetic systems	116
1.4.2. Electronic systems	117

1. RANDOM AND OUT-OF-EQUILIBRIUM POTTS MODELS

1.1. Introduction

This dissertation is an attempt to give a coherent presentation of my research activities during the last fifteen years. I would not have imagined spending such a long time on the Potts model when I started my Ph.D. thesis under the supervision of Bertrand Berche. Neither would I have foretold the recent theoretical developments involving this very simple model. At that time, the critical behaviour of the two-dimensional model was conjectured to be known exactly, thanks to Conformal Theory and a sequence of mappings on different cluster, loop, and vertex representations leading finally to a correspondence with a Coulomb gas. The introduction of cluster algorithms and multicanonical sampling techniques, combined with an exponential increase of computer power, had opened the way to accurate and large-scale Monte Carlo simulations. In the second half of the 1990's decade, the question regarding the critical behaviour of the two-dimensional random Potts model was more or less believed to be settled. Only mere refinements were expected. The idea that the Ising universality class could encompass many, if not all, random systems was attractive, probably too attractive to avoid the fate of being swept completely. Only a few months after I started to run my first Monte Carlo simulations of the random Potts model, Jacobsen and Cardy published on the `arXiv` a ground-breaking preprint showing that the critical behaviour of the q -state random Potts model depends on the number of states q . This paper determined the subject of my Ph.D. thesis and an important part of my activities of these last fifteen years.

In parallel, I was more and more interested in out-of-equilibrium processes, more specifically aging. The latter had been extensively studied in the context of glasses before it was realised that ferromagnets could also undergo a simpler form of aging. In the last two decades, new ideas have regularly emerged. The specific role of domain walls was identified and the particular scaling behaviour of autocorrelation functions was associated to the existence of a growing length scale. The violation of the Fluctuation-Dissipation Theorem attracted a lot of attention, especially because it was believed to offer a possible definition of an out-of-equilibrium temperature. I studied the aging properties of several models, more or less related to the Potts model, quenched at the critical temperature or below.

This dissertation is organised as follows. The first chapter starts with a short presentation of the known critical properties of the pure Potts model, mainly in two dimensions. The influence of disorder coupled to the energy density is then discussed in the general context of temperature-driven phase transitions. A physical explanation for the smoothing of the transition, due to Imry and Wortis, is presented and then applied to explain the phase diagram of the homogeneous random two and three-dimensional Potts

models. It is then extended to the Potts model on irregular graphs and with layered randomness. In the third section, the critical properties at the random fixed point are examined in the light of the series expansion obtained by Renormalisation Group. The multifractal spectrum of scaling dimensions is discussed in the two-dimensional case and a new symmetry is proposed. The predictions of conformal invariance for profiles and correlation functions are compared with numerical data for the two-dimensional random Potts model in strip or square geometries. Finally, the geometrical properties of interfaces induced by symmetry-breaking boundary conditions are analysed in the context of the recent Stochastic Schramm-Loewner Evolution theory.

The second chapter is devoted to the aging properties of homogeneous or frustrated Potts models submitted to a quench below or at their critical temperature. The scaling theory of two-time functions, as well as the more recent Local Scale Invariance theory, are presented in the first section. The violation of the Fluctuation-Dissipation theorem is described and the interpretation of the so-called Fluctuation-Dissipation Ratio as an out-of-equilibrium effective temperature is discussed. These ideas are applied to different spin models. First, one-dimensional systems with the Ising symmetry are considered. The equivalence of the KDH model with a gas of immobile particles subjected to pair-annihilation is exploited to obtain new analytical results. The question of the universality of dynamical exponents and ratios is then addressed in the two-dimensional case. Several lattices and several models in different universality classes are compared. A new model with the same symmetry as the three-state Potts model but with an irreversible dynamics is introduced. Its phase diagram in the steady state is determined and its aging properties on the critical line are studied. Finally, the aging of the Fully-Frustrated Ising and XY models are examined. Emphasis is put on the presence of logarithmic corrections due to the existence of topological defects. Two applications of the Jarzynski relation to the Potts model are presented at the end of the chapter.

A short third chapter introduces the numerical simulations employed to analyse different set of experimental data. Monte Carlo simulations were used to reproduced some magnetic phase transitions in layered nanostructures. Spectroscopic data of surface reconstructions were compared to the electronic band structure obtained by computing the first eigenvectors of the Bloch-Schrödinger equation with a projective technique combined with a multiscale approach.

In the four chapter, I performed the difficult exercise to draw the future orientations of my research activity.

The fifth chapter presents a shorter version of my research activities in french, followed by a curriculum vitæ and a list of publications.

1.2. Random Potts models

1.2.1. The pure Potts model

The Potts model is a particularly rich and thus interesting toy model in statistical mechanics. It was introduced as a simple generalisation of the Ising model [265]. While spins are allowed to take only two possible values in the Ising model, the degrees of freedom of the q -state Potts model are chosen to be the variables

$$\sigma_i \in \{0; 1; \dots; q - 1\}.$$

The Hamiltonian of the Potts model ⁽¹⁾ is written as [32, 494, 495]

$$H = -J \sum_{(i,j)} \delta_{\sigma_i, \sigma_j} - h \sum_i \delta_{\sigma_i, 0}. \quad (1)$$

The first term is a generalisation of the spin-spin exchange interaction to q -state spins. In this thesis, we will consider only interactions between nearest neighbours on the lattice. The second term is the Zeeman interaction with a magnetic field h . It breaks the \mathbb{Z}_q symmetry, i.e. the invariance under the cyclic permutation $\sigma_i \rightarrow (\sigma_i + 1) \bmod q$, by favouring the state $\sigma = 0$. At zero magnetic field, this symmetry is spontaneously broken at low temperatures and the system is in a ferromagnetic phase characterised by a non-vanishing order parameter

$$\rho = \frac{q \max_{\sigma=0 \dots q-1} \rho(\sigma) - 1}{q - 1},$$

where

$$\rho(\sigma) = \frac{1}{N} \sum_i \delta_{\sigma_i, \sigma}$$

is the density of spins in the state σ . Depending on the number of states q , the pure Potts model undergoes a second-order ($q \leq q_c$) or a first-order ($q > q_c$) temperature-driven phase transition. In two dimensions, the continuous regime was proved to extend up to $q_c = 4$ [43] (see figure 1). In dimension $d = 3$, Monte Carlo simulations showed that the Ising model ($q = 2$) undergoes a continuous phase transition whereas it is weakly first-order for the 3-state Potts model.

The first-order phase transition of the Potts model is of mean-field type which means that it occurs above the upper critical dimension d_c . From the above discussion, it follows that d_c depends on the number of states q . For the four-state Potts model for instance, the upper-critical dimension is $d_c = 2$. Some exact results are known at the transition temperature: energy density [46], magnetisation [45] and correlation length [83]. At surfaces, the transition is continuous for any value of q . In the second-order regime, i.e. when $d \leq d_c(q)$, the critical behaviour is known exactly only in the case of the $q = 2$ Ising model [403]. Exact values of the bulk and surface critical exponents

⁽¹⁾ The model suggested by C. Domb to his Ph.D. student R.B. Potts is actually not this one but the so-called clock model. The Potts model appears only in a small note at the end of the paper 32.

were conjectured for the two-dimensional Potts model. The assumptions behind this conjecture are presented in the following.

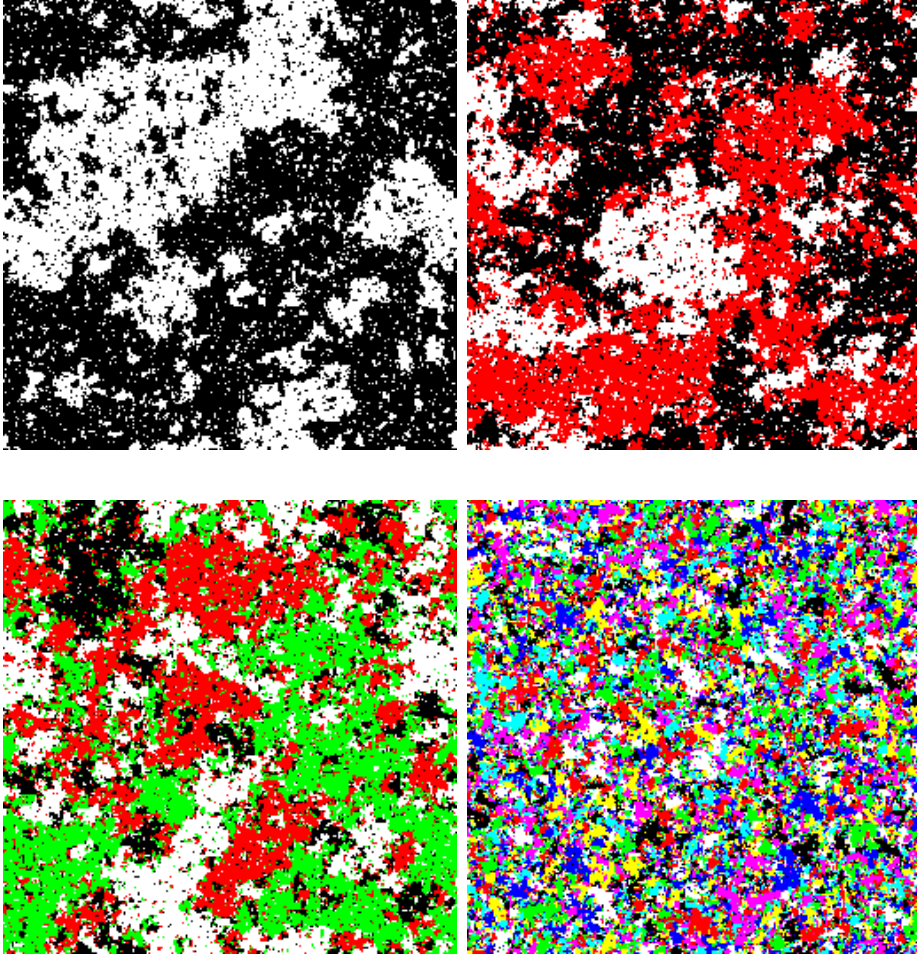


Figure 1 : Typical spin configurations of the q -state Potts models for $q = 2, 3, 4$ and 8 at their respective transition temperatures.

1.2.1.1. Fortuin-Kasteleyn representation

The Potts model can be mapped onto a random cluster model ^[185] that allowed for many analytical as well as numerical developments. For each link joining the neighbouring sites i and j , introduce a variable $b_{ij} \in \{0; 1\}$. The partition function of the q -state Potts model without magnetic field can be written

$$\begin{aligned} \mathcal{Z} &= \sum_{\{\sigma\}} \prod_{(i,j)} [(e^K - 1) \delta_{\sigma_i, \sigma_j} + 1] \\ &= \sum_{\{\sigma\}} \prod_{(i,j)} \left[\sum_{b_{ij}=0}^1 (e^K - 1) \delta_{\sigma_i, \sigma_j} \delta_{b_{ij}, 1} + \delta_{b_{ij}, 0} \right], \end{aligned}$$

where $K = \beta J$. A link in the state $b_{ij} = 1$ is said to be active or frozen. It indicates that the two spins at its edges are in the same state, i.e. $\sigma_i = \sigma_j$. In contradistinction, the

state $b_{ij} = 0$ does not provide any information on the relative state of these two spins. The spin degrees of freedom can be integrated out and the partition function reads

$$\begin{aligned} \mathcal{Z} &= \sum_{\{b_{ij}\}} (e^K - 1)^{\sum_{ij} b_{ij}} \sum_{\{\sigma_i\}} \prod_{(i,j)} \delta_{\sigma_i, \sigma_j} \delta_{b_{ij}, 1} \\ &= \sum_{G=\{b_{ij}\}} (e^K - 1)^{b(G)} q^{C(G)}, \end{aligned} \quad (2)$$

where $G = \{b_{ij}\}$ is the graph formed by the frozen links. $b(G) = \sum_{ij} b_{ij}$ is the total number of frozen links in the graph G and $C(G)$ the number of connected clusters. This model can also be seen as a generalisation of percolation. Setting $p = 1 - e^{-K}$, the partition function becomes

$$\mathcal{Z} = (1 - p)^{-N} \sum_G p^{b(G)} (1 - p)^{N - b(G)} q^{C(G)}, \quad (3)$$

where N is the total number of links, frozen or not, of the lattice. When $q = 1$, the partition function of the percolation problem is recovered. In the two-dimensional case, the phase transition of the Potts model occurs at the same temperature as the percolation transition of the Fortuin-Kasteleyn clusters. The number of states q enters into the partition function as a simple parameter and nothing constrains it to take integer values only. The Fortuin-Kasteleyn random cluster model can thus be extended to real values of q . A transfer matrix can be constructed in this representation [69]. It has been widely used to study the random-bond Potts model and will be mentioned at multiple occasions in this chapter.

The duality transformation was introduced by Kramers and Wannier for the two-dimensional Ising model [306] and later generalised to the Potts model by Potts himself [423]. Under the assumption of self-duality of the partition function at the critical point, the critical coupling K_c can be determined exactly ⁽²⁾ :

$$K_c = \ln(1 + \sqrt{q}). \quad (4)$$

The duality transformation can also be defined in the Fortuin-Kasteleyn representation. Each link of the lattice is associated to a link of the dual lattice, geometrically constructed as the link joining the centres of the two plaquettes (dual sites) at both sides of the original link. The states b_{ij}^* of these dual links are

$$b_{ij}^* = 1 - b_{ij},$$

i.e. a frozen link in a graph G is inactive in the dual graph G^* . The number of frozen dual links is thus $b(G^*) = N - b(G)$. Moreover each cluster of a graph G is surrounded by a loop of frozen dual links, i.e. $l(G^*) = C(G)$. Using these two equalities together with the Euler relation

$$C(G) = V - b(G) + l(G) - 1,$$

⁽²⁾ A rigorous proof that does not rely on the self-duality assumption was given only recently [51].

where V is the number of vertices, the partition function can be written as ^[213]

$$\begin{aligned}\mathcal{Z}^* &= \sum_{G^*} (u^*)^{b(G^*)} q^{C(G^*)} \\ &= \sum_G (u^*)^{N-b(G)} q^{C(G)+V-N+b(G)-1} \\ &= q^{V-1} \left(\frac{u^*}{q}\right)^N \sum_G \left(\frac{q}{u^*}\right)^{b(G)} q^{C(G)},\end{aligned}$$

where $u^* = e^{K^*} - 1$. The partition function (2) is recovered (up to a multiplicative constant) if

$$u u^* = q \Leftrightarrow (e^K - 1)(e^{K^*} - 1) = q. \quad (5)$$

The duality transformation maps the ferromagnetic phase onto the paramagnetic one, and vice versa. The critical temperature is thus given by the self-duality condition (4).

1.2.1.2. From loop and vertex models to the Coulomb gas

The Fortuin-Kasteleyn representation (2) of the q -state Potts model can be mapped onto a loop model on the so-called medial lattice whose sites are at the centres of the links of the original lattice. For a square lattice, the medial lattice is also a square lattice but rotated by an angle of 45° and shrunk by a factor $\sqrt{2}$. At each site of the medial lattice, four links meet. To construct the loop model, these links should be first grouped into pairs. For a given Fortuin-Kasteleyn graph, the two links of the medial lattice belonging to such a pair should be on the same side of a link of the original lattice if it is frozen in the FK graph, while it should be on different sides if the bond is inactive (figure 2). As a consequence, the links of the medial lattice form loops that do not cross any frozen Fortuin-Kasteleyn bond. Each cluster of a FK graph is then enclosed by a loop. More details of this construction can be found in references 47 and 46. Using the Euler relation, the partition function can be expressed as a sum over loop configurations:

$$\mathcal{Z} = q^{N/2} \sum_{\{\text{loops}\}} v^n \sqrt{q}^\ell,$$

where ℓ denotes the number of loops, n the total number of FK bonds (or equivalently of sites of the medial lattice) that are enclosed by loops and $v = u/\sqrt{q}$.

This loop model can then be mapped onto a 6-vertex model (or ice model) ^[46, 2, 47, 46]. An orientation is assigned to each loop in such a way that at each site of the medial lattice there are exactly two incoming bonds and two outgoing. There are six such configurations. Let the bonds that form loops meet again at the sites of the medial lattice. During the last step, these four bonds were given a direction. The medial lattice has then to be divided into plaquettes, each one containing a single site of the medial lattice at its centre. The six possible configurations of the plaquettes are represented on figure 3. One can show that the statistical weight of a Fortuin-Kasteleyn graph can be decomposed as a product over the plaquettes. Each one of them contains a single bond of the original lattice and the information about its state b_{ij} is recovered from

the orientations of the arrows of the plaquette. Consider figure 3 again. If the plaquette is centred on a horizontal bond then only the first, second and fifth configurations can correspond to a frozen bond. These configurations should be given a weight u . Since horizontal and vertical bonds should be treated differently, one obtains a staggered six-vertex model. The number of Fortuin-Kasteleyn clusters, or equivalently the number of loops is a non-local information. To distribute the information among the plaquettes, a weight $z^{\alpha_i/2\pi}$ where $\sqrt{q} = 2 \cosh z$ is assigned to each plaquette where a loop undergoes a rotation by an angle α_i . Collecting all the terms coming from a loop, the weight $z^{\sum_i \alpha_i/2\pi}$ gives either z or z^{-1} upon its orientation and leads to the appropriate factor \sqrt{q} in the partition function after performing the sum over all vertex configurations and therefore over the two orientations of the loop.

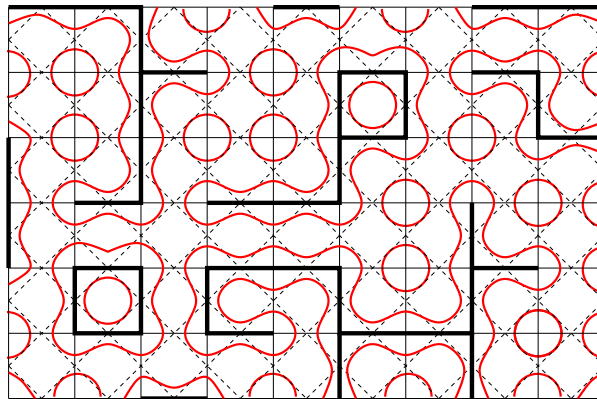


Figure 2 : Construction of a loop configuration on the medial lattice from a Fortuin-Kasteleyn graph. The original square lattice is represented as thin continuous lines and the corresponding medial lattice as the dashed lines. The frozen links of the Fortuin-Kasteleyn graph are the bold segments and the associated loop configuration is drawn in red.

To be exhaustive, one should mention that this six-vertex model can be mapped onto a Solid-On-Solid model (SOS). Each site of the dual lattice is assigned an integer height or a multiple of a minimal height. When going from one point to one of its neighbours, an oriented bond of the six-vertex model is crossed. Depending on the orientation of this bond, the height decreases or increases.



Figure 3 : The six possible configurations of a plaquette around a site of the medial lattice. The loops are represented as dashed curves. They are deformed to meet at the centres of the plaquette and the orientation of the loops are affected to the four branches.

The six-vertex model displays a line of fixed points on which it is exactly solvable and which is given in the Potts language by the self-duality condition (4). Such a critical line is also encountered in several other models, for instance, the Ashkin-Teller model, the $O(n)$ model or the Solid-On-Solid model. In the late 1970s, it was suspected that

all these models could be mapped onto a Coulomb gas model where a line of fixed point is also observed. Some models, like the $O(2)$ model, usually known as the XY model, and the Solid-On-Solid model, can be mapped exactly onto a Coulomb gas. After integrating out the spin-wave degrees of freedom of the XY model, the partition function reduces to that of magnetic charges, topologically associated to vortices of the XY model and interacting through a logarithmic Coulombian potential. For non-quadratic Hamiltonians, such a mapping cannot be obtained exactly. However, using Renormalisation Group arguments, it can be argued that the six-vertex model is related to a more general Coulomb gas of electric and magnetic charges [389, 390]:

$$\begin{aligned}
H = & \frac{1}{2g} \sum_{i,j \neq i} e_i G(\vec{r}_i - \vec{r}_j) e_j + \frac{g}{2} \sum_{i,j \neq i} m_i G(\vec{r}_i - \vec{r}_j) m_j \\
& + i \sum_{i,j} e_i \Phi(\vec{r}_i - \vec{r}_j) m_j + \sum_i \ln X^e(\vec{r}_i) + \sum_i \ln Y^m(\vec{r}_i),
\end{aligned} \tag{6}$$

where $e_i \in \mathbb{Z}$ is the electric charge at lattice site i , $m_i \in \mathbb{Z}$ the magnetic charge. $G(\vec{r}) \sim \ln r$ is the Coulombian interaction between electric charges and between magnetic charges. Φ is also a Coulombian potential describing the fact that when an electric charge moves around a magnetic charge, and therefore moves in a magnetic field, it gains a phase factor. X^e and Y^m play the role of fugacities associated to electric and magnetic charges on a given site of the lattice. At high temperatures, the charges are free while they are bounded at low temperatures. Under real-space renormalisation, the fugacities X^e and Y^m acquire contributions from the Coulombian potential at small distances. For different values of e (resp. m), the fugacities X^e (resp. Y^m) form a set of independent scaling operators. Two infinite sets of correlation functions can therefore be defined:

$$\begin{aligned}
C^e(\vec{r}_i - \vec{r}_j) = \langle e_i e_j \rangle &= \frac{\partial^2 \ln \mathcal{Z}}{\partial X^e(\vec{r}_i) \partial X^e(\vec{r}_j)}, \\
C^m(\vec{r}_i - \vec{r}_j) = \langle m_i m_j \rangle &= \frac{\partial^2 \ln \mathcal{Z}}{\partial Y^m(\vec{r}_i) \partial Y^m(\vec{r}_j)}
\end{aligned}$$

that decay algebraically on the critical line as

$$C^e(r) \sim r^{-e^2/g}, \quad C^m(r) \sim r^{-m^2g}.$$

As a consequence, the scaling dimensions of the operators X^e and Y^m are respectively $2 - e^2/2g$ and $2 - gm^2/2$.

On the basis of already known estimations of the thermal exponent y_t of the q -state Potts model, a simple relation was conjectured between y_t and the thermal exponent y_t^{8v} of the exactly-solved eight-vertex model [146]:

$$(y_t^{8v} - 2)(y_t - 3) = 3. \tag{7}$$

Plugging the exact value of y_t^{8v} gives ⁽³⁾

$$y_t = 3 \frac{y - 1}{y - 2}, \quad q = 4 \cos^2 \frac{\pi y}{2}. \tag{8}$$

(3) This parameter y can be introduced already in the loop model equivalent to the Fortuin-Kasteleyn representation of the Potts model. Extending statistical weight to complex values, a weight $[e^{i\pi y/2}]^{i\alpha/2}$ is assigned to each plaquette where the loops performs an angle α . Taking into account the two possible orientations of the loop, its weight in the partition function is $2 \cos \pi y/2$. To recover the expected factor \sqrt{q} , the relation (8) between q and y has to be imposed.

The Ising model corresponds to $y = 1/2$ and the four-state Potts model to $y = 0$. Shortly after, the thermal exponent y_t was calculated exactly using the transfer matrix formalism introduced by Temperley and Lieb and the den Nijs conjecture (7) was confirmed [64]. Using Renormalisation Group, such a relation was then identified between the magnetic exponent y_h of the Potts model and $y_t^{8\nu}$ [393, 409]:

$$y_h = d - x_\sigma, \quad x_\sigma = \frac{1 - y^2}{4(2 - y)}. \quad (9)$$

Since a mapping between the eight-vertex model and the Coulomb gas was known [290, 147], a relation could be established between the Potts model and the Coulomb gas.

1.2.1.3. Coulomb gas and minimal models

The Coulomb gas Hamiltonian (6) can be conveniently replaced by the Gaussian action

$$S = \frac{g}{4\pi} \int (\nabla\varphi)^2 d^2x$$

that can also be seen as the continuum limit of the XY model. The scaling dimension of the scalar field φ vanishes in dimension $d = 2$. Other observables should thus be considered, as for example $O_e(\vec{r}) = e^{ie\varphi(\vec{r})}$. It can be shown that the correlation function $\langle O_e(\vec{r})O_{-e}(\vec{r}') \rangle$ decays algebraically with the same exponent as the electric density correlation $C^e(|\vec{r} - \vec{r}'|)$ of the Coulomb gas. The correlations of the dual field O_m of O_e can be shown to behave as the correlation C^m between magnetic charges. In the complex plane, the Gaussian action reads

$$S = \frac{g}{4\pi} \int \partial_z\varphi\partial_{\bar{z}}\varphi d^2z.$$

Consider the vertex operators

$$V_\alpha(z, \bar{z}) = e^{i\alpha\varphi(z, \bar{z})}.$$

Their correlation functions decay as

$$\langle V_\alpha(z_1, \bar{z}_1)V_{-\alpha}(z_2, \bar{z}_2) \rangle = \frac{1}{|z_{12}|^{4\alpha^2}}$$

which means in the language of conformal field theory (CFT) that the conformal weight of V_α is $\Delta_\alpha = \alpha^2$. Since the model is nothing but a Gaussian action for a scalar field, the central charge is expected to be $c = 1$. Dotsenko and Fateev introduced a modification of this CFT resulting into a central charge that can be freely tuned by changing the value of an external parameter [163]. They introduced a charge $-2\alpha_0$ at infinity and calculated the new central charge

$$c = 1 - 24\alpha_0^2$$

from the correlations of the energy-momentum tensor, and the conformal weights of the operators V_α

$$\Delta_\alpha = \alpha^2 - 2\alpha\alpha_0$$

from the correlations $\langle V_\alpha V_{-\alpha} \rangle$. They also computed the four-point correlation functions and showed that this model provides a representation of minimal models [190].

The four-point correlations had already been calculated for the q -state Potts model. By identifying them with the same quantities for the deformed Coulomb gas, the Potts model with $q \leq 4$ can be put into correspondence with the minimal models. In the latter, the central charge is quantised by the constraint of unitarity (or reflexion positivity) and can be parametrised by an integer m as

$$c = 1 - \frac{6}{m(m+1)}. \quad (10)$$

The Ising model ($c = 1/2$), the 3 and 4-state Potts models ($c = 4/5$, and $c = 1$) correspond to $m = 3$, $m = 5$ and $m \rightarrow +\infty$, respectively. More generally, any integer $m \geq 2$ corresponds to a Potts model with a (non-integer) number of states

$$q = 4 \cos^2 \left(\frac{\pi}{m+1} \right). \quad (11)$$

In terms of the parameter y used in the loop model and the six-vertex model, this relation reads

$$y = \frac{2}{m+1}.$$

Thermal and magnetic exponents then follow from (8) and (9):

$$\nu = \frac{2m}{3(m-1)}, \quad \eta = \frac{(m+3)(m-1)}{4m(m+1)}.$$

The scaling dimensions of the bulk and surface scaling fields are finally

$$x_\varepsilon = \frac{m+3}{m}, \quad x_\sigma = \frac{(m+3)(m-1)}{8m(m+1)}, \quad x_\sigma^1 = \frac{m-1}{m+1}.$$

The values of these exponents are given in Table 1 for integer numbers of states q .

	$q = 2$	3	4	$q > 4$
ν	1	5/6	2/3	1 st order
$x_\varepsilon = \frac{1-\alpha}{\nu}$	1	4/5	1/2	-
$x_\sigma = \beta/\nu$	1/8	2/15	1/8	-
$x_\sigma^1 = \beta_1/\nu$	1/2	2/3	1	3

Tableau 1 : Bulk and surface scaling dimensions of the two-dimensional pure q -state Potts model.

Being at the frontier between the second-order and first-order regimes, the four-state Potts model corresponds to a tricritical point. In the late 1970s, real-space Renormalisation Group analysis showed that the existence of such a point is due to a scaling field associated to the fugacity of vacancies that becomes marginal at $q = 4$ [391]. It induces logarithmic corrections that were later determined by assuming appropriate renormalisation flow equations involving the fugacity of vacancies [387, 99].

1.2.2. Smoothing of first-order transitions by inhomogeneous perturbations

Disorder may produce important changes to a phase transition. All people living in northern countries have already observed the shift of melting temperature of ice when salt is thrown onto the roads in winter. Besides the transition temperature, the order of the phase transition may also change. The smoothing of first-order phase transitions has been observed in a large number of physical systems. In some cases, the diminution of the latent heat is replaced by a complete disappearance. The transition is then continuous. Such a drastic change of the order of the phase transition was observed, for example in the 4' - n - octyl - 4 - cyanobiphenyl (8CB) liquid crystal [497]. The pure system undergoes a weak nematic-isotropic first-order phase transition with a correlation length $\xi \simeq 200 \text{ \AA}$. When this fluid was introduced into the pores of a silica aerogel, the diffusion of polarised light revealed that the transition had become continuous. The same effect was observed in the temperature-driven first-order order-disorder phase transition of the interstitial alloy V_2H [470]. X-ray diffraction showed a continuous phase transition due to defects when a thin layer was deposited. The mechanism governing this change of the order of the phase transition was identified as due to disorder fluctuations that destabilise the low-temperature phase. A detailed presentation of this mechanism will be given in the first section of this chapter. The specific case of the Potts model will then be considered. Different kinds of disorder, homogeneous or correlated, will be presented for this model and discussed in the light of their corresponding fluctuations.

1.2.2.1. Heuristic arguments and correspondence with the RFIM

Consider a system that undergoes a temperature-driven first-order phase transition, as for example the q -state Potts model with $q > 4$. At a temperature close, but below the transition temperature T_t , the system essentially consists of clusters in different ordered phases. The characteristic length ℓ of these clusters is of the same order of magnitude as the correlation length ξ ⁽⁴⁾ so the correlations between degrees of freedom in different clusters can be neglected. If the surface tension $\sigma_{o,o}$ between different ordered phases is large, then thermal fluctuations, i.e. subdomains in other phases, will only appear inside a cluster with a very small probability. Therefore, they can be safely neglected and the clusters can be considered as homogeneous. The free energy of the system is the sum of the bulk free energy $f_o(T) \ell^d$ of each cluster, where $f_o(T)$ is the free energy of the infinite homogeneous ordered phase, and of the surface free energy $\sigma_{o,o} \ell^{d-1}$ ⁽⁵⁾. When the temperature is increased, the clusters are expected to undergo a transition to the disordered phase. At thermodynamic equilibrium, the system chooses the phase with the lowest free energy so the transition temperature T_t is determined by the equality

$$f_o(T_t)\ell^d + \sigma_{o,o}\ell^{d-1} = f_d(T_t)\ell^d.$$

The surface tension $\sigma_{o,d}$ between the ordered and disordered phases is not involved in the definition of the equilibrium state because all clusters will switch to the disordered phase at the same temperature. In a real experiment, this is no longer the case since the transformations are never perfectly quasi-static, and thus some of the clusters may

⁽⁴⁾ It was shown for the q -state Potts model that the radii ℓ of the correlated clusters are distributed according to the law $\wp(\ell) = \mathcal{A} e^{-\ell/\xi}$ so that the average radius is $\langle \ell \rangle = \xi$ [74].

⁽⁵⁾ It can be shown that the exponent is $d-2$ when the Hamiltonian is invariant under a continuous symmetry [263].

be trapped in one of the metastable ordered phases at the expense of an interface free energy $\sigma_{o,d}\ell^{d-1}$.

Now imagine that impurities are randomly introduced in the system with a given concentration p . They are supposed to be frozen and thus shall not be considered as additional degrees of freedom of the system. By altering the local interactions, these impurities will shift the temperature $T_t(p)$ at which the free energies of the ordered and disordered phases are equal. The number of impurities in a cluster is $p\ell^d$ on average but it fluctuates from a cluster to the other with an amplitude $\Delta p\ell^d \sim \ell^{d/2}$ according to the central limit theorem. A local transition temperature $T_t(p + \Delta p)$ may thus be defined for each cluster depending on the local concentration $p + \Delta p$ of impurities. However, as emphasised by Imry and Wortis ^[263], the clusters are interacting and cannot freely jump from one phase to the other. If the neighbouring clusters stay unchanged, the transition will also create an interface between disordered and ordered phases. A transition to a disordered phase will only occur if

$$\ell^d f_d(T, p + \Delta p) + \sigma_{o,d}\ell^{d-1} < \ell^d f_o(T, p + \Delta p) + \sigma_{o,o}\ell^{d-1}. \quad (12)$$

For a temperature $T = T_t(p) - \Delta T$ close but below the average transition temperature $T_t(p)$, the difference between the two free energies reads

$$\begin{aligned} f_d(T_t - \Delta T, p + \Delta p) - f_o(T_t - \Delta T, p + \Delta p) \\ \simeq -\Delta T \frac{\partial}{\partial T} [f_d(T, p) - f_o(T, p)]_{T_t} + \Delta p \frac{\partial}{\partial p} [f_d(T_t, p) - f_o(T_t, p)] \\ = -LT_t(p)\Delta T + \Delta p \frac{\partial}{\partial T_t} [f_d(T_t, p) - f_o(T_t, p)] \frac{dT_t}{dp} \\ = -LT_t(p)\Delta T + T_t(p)L \frac{dT_t}{dp} \Delta p, \end{aligned}$$

where $L = E_o - E_d$ is the latent heat. The condition (12) may be written as

$$\frac{dT_t}{dp} \Delta p < \Delta T + \frac{\sigma_{o,o} - \sigma_{o,d}}{LT_t(p)} \ell^{-1},$$

where the left-hand side of the inequality corresponds to the shift of the transition temperature of an infinite homogeneous phase under a shift Δp of the concentration of impurities. Since $\Delta p \sim \ell^{-d/2}$, the cluster will undergo a transition at the temperature

$$T_t(p) - \Delta T = T_t - \frac{dT_t}{dp} \ell^{-d/2} + \frac{\sigma_{o,o} - \sigma_{o,d}}{LT_t(p)} \ell^{-1}.$$

In dimensions $d > 2$, the fluctuations are larger than the interface free energy for sufficiently small clusters. On the other hand, in dimensions $d < 2$, the largest clusters are the more sensible to fluctuations. The two-dimensional case appears as a marginal situation. If the considerations presented above explain the rounding of a first-order transition in presence of impurities, it does not predict under which conditions the discontinuity of the energy will be completely eliminated.

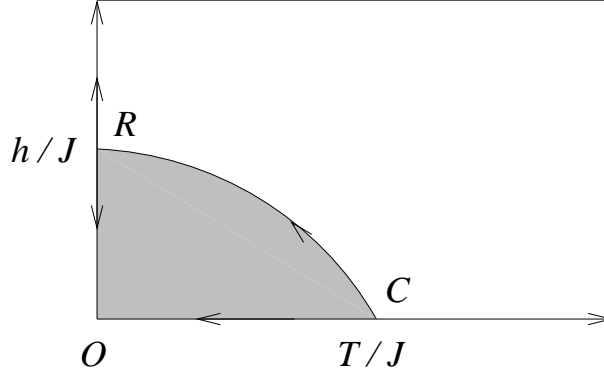


Figure 4 : Phase diagram of the Random-Field Ising Model in the (h, T) plane where h is the amplitude of the random-field and T is the temperature.

The picture presented above is similar to the one that was employed a few years before by Imry and Ma to study the stability of the ferromagnetic phase of the Ising model in presence of a random magnetic field [262]. The essential difference is that in this case the first-order transition is driven by the magnetic field and not by the temperature. Below the critical temperature, a change of the sign of the magnetic field is followed by a transition from one ferromagnetic phase to the opposite one. Suppose that the system is initially in the ferromagnetic phase of positive magnetisation, i.e. $\sigma_i = +1$ for all sites i at sufficiently low temperature. Consider a sub-domain of characteristic size ℓ . A random magnetic field $h_i = \pm h$ is applied. The energy of the infinite ferromagnetic phase is unchanged because the average field vanishes, $\bar{h} = 0$, but, within a small cluster the fluctuations of the number of positive and negative fields may induce a significant energy change:

$$\Delta E = - \sum_i h_i \sigma_i = - \sum_i h_i \simeq \pm \Delta h \ell^{d/2}, \quad (13)$$

where $\Delta h = \sqrt{\overline{h_i^2}}$. If $\sum_i h_i > 0$, the cluster is tempted to undergo a transition to the opposite ferromagnetic phase since the free energies of the two ferromagnetic phases now differ by $2 \sum_i h_i \sim 2 \Delta h \ell^{d/2}$. Like in the case of the temperature-driven first-order phase transition, this is not a sufficient condition for the cluster to undergo the transition. One has to take into account the free energy $\sigma \ell^{d-1}$ of the interface that is created between the cluster and the rest of the system. The transition of the cluster to the opposite ferromagnetic phase is thus energetically favourable if

$$\sigma \ell^{d-1} < \Delta h \ell^{d/2}. \quad (14)$$

For large clusters, it is clear that the ferromagnetic phase is unstable for $d < 2$ and will break into small clusters whose state depends on the local fluctuations of the random magnetic field. Thus $d_c = 2$ is again the lower critical dimension. Renormalisation group studies in dimensions $d = 2 + \epsilon$ allowed to go beyond these heuristic arguments [80]. The phase diagram of the RFIM is schematically presented on figure 4. The pure Ising model fixed point is located at $h = 0$ and $T = T_c$. At zero magnetic field, temperature is a relevant scaling field that brings the system to the stable $T = 0$ and $h = 0$ ferromagnetic fixed point denoted O on the figure. The shaded region corresponds to the basin of

attraction of this fixed point. In this region, the ferromagnetic phase is stable and the system undergoes a first-order phase transition when the sign of the magnetic field is changed. Outside the shaded region, the ferromagnetic phase is unstable. At the critical point C of the pure Ising model, the random magnetic field is a relevant scaling field. The RG flow brings the system to a new $T = 0$ and $h = h_R$ fixed point, the Random-Field fixed point, denoted R on the figure. Above this line, the system is in the paramagnetic phase. The Random-Field fixed-point is thus a tricritical point. In dimension $d = 2$, RG calculations show that this fixed point goes down to $h_R = 0$, confirming the Imry-Ma prediction of the instability of the ferromagnetic phase.

From the Imry-Ma criterion (14), an analogy can be drawn between the Random-Field Ising Model (RFIM) and temperature-driven first-order transitions in presence of impurities. In both cases, the fluctuations Δh of the random magnetic field or Δp of the concentration of impurities induce a shift of the temperature at which the stability of the phases gets interchanged. The two quantities Δp (or more precisely the fluctuations of the energy density) and Δh thus play the same role and can be put into correspondence. The surface tension σ counterbalances this effect and prevents a cluster from undergoing a transition to the other phase at this temperature. This analogy, put forward by Hui and Berker, was tested on the random Blume-Emery-Griffiths model [248, 249 177]. The pure model is defined by the Hamiltonian

$$-\beta H = J \sum_{(i,j)} \sigma_i \sigma_j + K \sum_{(i,j)} \sigma_i^2 \sigma_j^2 - \Delta \sum_i \sigma_i^2, \quad \sigma_i \in \{-1; 0; +1\}.$$

At low temperatures, a non-magnetic phase ($\sigma_i = 0$) is favoured if $\Delta > 0$. When the sign of Δ is changed, the system undergoes a first-order transition into a magnetic phase ($\sigma_i = +1$ or -1). The non-magnetic phase is destroyed by thermal fluctuations before the magnetic phase because the latter is stabilised by the exchange interactions. The line of first-order phase transition ends at a tricritical point. At high temperatures, the system behaves as the Ising model and thus undergoes a second-order ferromagnetic-paramagnetic phase transition. Like in the RBPM, disorder is introduced into the system by replacing the exchange coupling J by quenched random variables. Under renormalisation, the three couplings J , K and Δ become random variables. Because of the local fluctuations of Δ , the magnetic and non-magnetic phases may be locally destabilised in the very same way as the ferromagnetic phases are destabilised by a random magnetic field. The first-order transition is smoothed and the tricritical point moves towards lower temperatures. Interestingly, the real-space RG calculations show the total elimination of the first-order transition line at $d = 2$. This result was rigorously proved in the case of the q -state Potts model in the next article of the same journal by Aizenman, and Wehr [11, 12]! In two-dimensional systems, an infinitesimal amount of disorder is sufficient to smooth completely a first-order phase transition. This statement was recently extended to quantum systems [211].

In the case of the Random-Bond Potts Model (RBPM), the correspondence with the RFIM is more than a simple analogy. An exact mapping onto the RFIM can be constructed in the Fortuin-Kasteleyn representation (3) in the limit $q \rightarrow +\infty$ [98, 268, 96, 294]. The RBPM is defined from the Hamiltonian (1) of the pure Potts model by replacing the exchange couplings by frozen random variables, i.e.

$$-\beta H = \sum_{(i,j)} K_{ij} \delta_{\sigma_i, \sigma_j}, \quad (15)$$

where K_{ij} is distributed according to the law $\wp(K_{ij})$. In the following, the disorder is assumed to be homogeneous in the sense that the probability distribution $\wp(K_{ij})$ is the same for all bonds of the lattice. Since the RBPM with a given disorder realisation $\{K_{ij}\}$ is mapped under the duality transformation onto a RBPM with the disorder realisation $\{K_{ij}^*\}$, self-duality is ensured on average if ^[286]

$$\wp(K) = \wp(K^*), \quad \forall K.$$

A popular choice is the binary distribution

$$\wp(K_{ij}) = \frac{1}{2}\delta(K_{ij} - K_1) + \frac{1}{2}\delta(K_{ij} - K_2) \quad (16)$$

with the relation

$$K_1 = K_2^* \Leftrightarrow (e^{K_1} - 1)(e^{K_2} - 1) = q, \quad (17)$$

where the expression (5) of K^* was used. The amplitude of disorder is usually measured as $r = K_2/K_1$. To reveal the correspondence with the RFIM, write this relation as

$$(e^{K_1} - 1) = \sqrt{q} e^h, \quad (e^{K_2} - 1) = \sqrt{q} e^{-h}.$$

In the Fortuin-Kasteleyn representation of the RBPM, a weight

$$u_{ij} = (e^{K_{ij}} - 1) = \sqrt{q} e^{h_{ij}},$$

with $h_{ij} = \pm h$, is assigned to a frozen bond $b_{ij} = 1$. The partition function then becomes

$$\mathcal{Z}_{K_{ij}} = \sum_G \prod_{(i,j)} [\sqrt{q} e^{h_{ij}}]^{b_{ij}} q^{C(G)} = \sum_G \sqrt{q}^{b(G)} q^{C(G)} e^{\sum_{(i,j)} h_{ij} b_{ij}}.$$

In the limit $q \rightarrow +\infty$, the partition function of the 2D pure Potts model is dominated by two terms: the empty graph $G = \emptyset$ ($b(G) = 0$ and $C(G) = N$) and the full graph ($b(G) = 2N$ and $C(G) = 1$) corresponding to the paramagnetic phase and the q ferromagnetic phases. For weak disorder, the partition function of the 2D RBPM is expected to be

$$\mathcal{Z}_{K_{ij}} \simeq q^N \left(1 + q e^{\sum_{(i,j)} h_{ij}} \right)$$

The free energy of the paramagnetic phase is

$$e^{-\beta F_d} = q^N \Leftrightarrow f_d = -k_B T \ln q$$

while the free energy of the ferromagnetic phase is

$$e^{-\beta F_o} = q^{N+1} e^{\sum_{(i,j)} h_{ij}} \Leftrightarrow f_o \simeq -k_B T \ln q - \frac{k_B T}{N} \sum_{(i,j)} h_{ij}.$$

The last term is analogous to the Zeeman energy (13) associated to a random magnetic field h_{ij} acting on a ferromagnetic phase. One may thus analyse the stability of the

ordered phase using the Imry-Ma argument. The first sub-dominant terms of the large- q expansion of \mathcal{Z} are the graphs with a line of inactive bonds spanning the lattice and separating two subgraphs either empty or full. These graphs correspond to different phases separated by an interface. The number of bonds that are removed by forming this interface is proportional to its length ℓ . The weight of such a graph is thus of order $q^{N-\ell}$. The free energy of the interface, i.e. per unit of length the surface tension, is therefore

$$e^{-\sigma\ell} \sim q^{-\ell} \Leftrightarrow \sigma \sim \ln q.$$

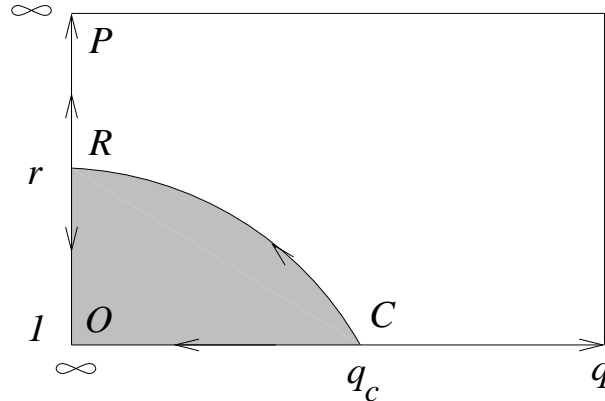


Figure 5 : Phase diagram of the self-dual Random-Bond Potts model in the (r, q) plane where r is the amplitude of the disorder and q the number of states of the Potts model. The x -axis corresponds to the pure Potts model. The large- q limit is on the y -axis.

This completes the correspondence with the Imry-Ma description of the RFIM which is expected to hold for a sufficiently large number of states q . The phase diagram of the RBPM is thus similar to that of the RFIM (figure 4). As shown in figure 5, the temperature-driven first-order phase transition of the q -state Potts model is preserved for sufficiently small fluctuations of the randomness $r < r^*(q)$ and large number of states q (shaded region on the figure). Outside this region, the phase transition is continuous, at least as long as the strongest exchange couplings form a percolating cluster. At the tricritical point q_c of the pure model, the RG flow brings the system to the RFIM fixed point at $q \rightarrow +\infty$. Along this line, the critical exponents of the RBPM are expected to be the same as the RFIM. This prediction has been checked numerically.

1.2.2.2. Effect of disorder on two-dimensional Potts models

1.2.2.2.1. The random-bond Potts model

The two-dimensional random-bond Potts model has been extensively studied. In the first-order regime of the pure model, the case $q = 8$ was often considered in numerical studies because the transition is sufficiently strong to be observed with a reasonable lattice size. The correlation length is indeed $\xi \simeq 24$ at the transition temperature [83]. The complete smoothing of the first-order transition was first reported by Chen *et al.* [123, 124]. The typical spin configurations sampled by Monte Carlo simulation clearly show percolating clusters, as expected for a second-order phase transition (see figure 6).

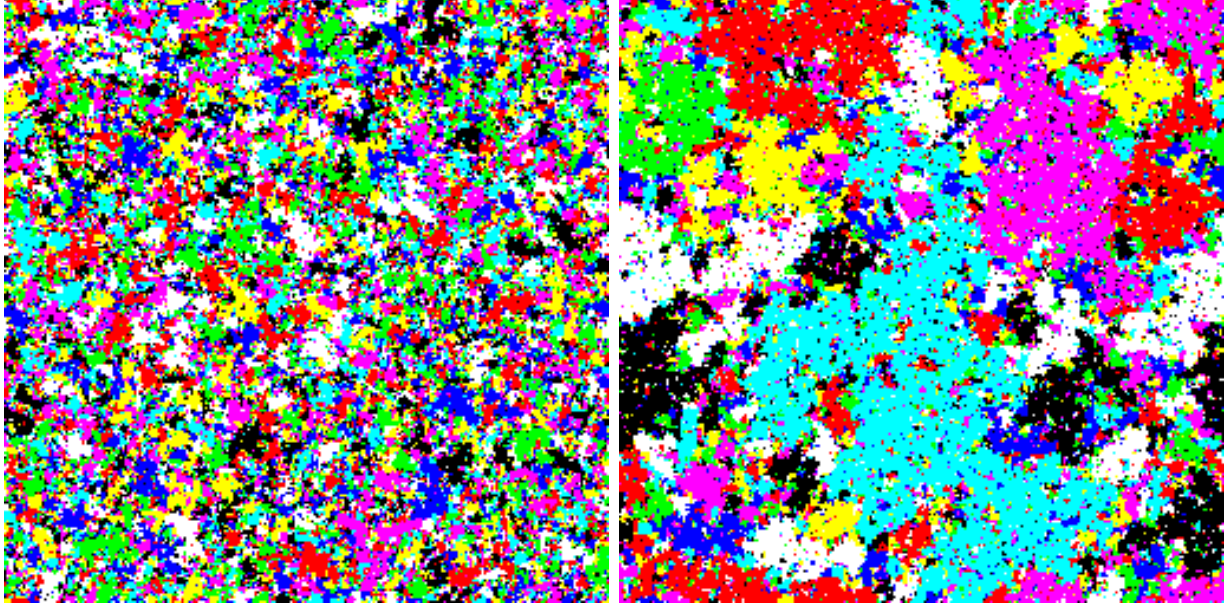


Figure 6 : Typical spin configurations produced by Monte Carlo simulations for the pure eight-state Potts model (on the left) and the random-bond model (on the right).

More quantitatively, Chen *et al.* studied the behaviour of the average probability distribution of the energy $\wp_L(E)$ with the lattice size L . At the transition temperature, this distribution has two peaks, corresponding to the system being either in a paramagnetic or a ferromagnetic phase. In between, the mixed states have a lower probability of order $e^{-\beta\Delta F}$ where the free-energy barrier $\Delta F \sim 2\sigma_{o,d}\ell^{d-1}$ is due to the interfaces between the coexisting ordered and disordered phases. In the case of a first-order phase transition, ΔF is expected to grow with the lattice size L . In contrast, the surface tension $\sigma_{o,d}$ vanishes at the critical point of a second-order phase transition. Therefore, the free-energy barrier for a finite system shrinks as the lattice size increases. As suggested, by Lee and Kosterlitz, these two very different behaviours can be exploited to distinguish a first-order from a continuous transition with Monte Carlo simulations^[315]. The free-energy barrier ΔF can be estimated as

$$\Delta F = -k_B T \ln \frac{\wp_L(E_{\text{mixed}})}{\wp_L(E_o)}, \quad (18)$$

where E_o is the energy of one of the homogeneous phases, i.e. the location of one of the peaks and E_{mixed} is the energy of smallest probability in the mixed state. In practise, the method of histogram reweighting is usually employed to find the precise temperature at which the two peaks have equal weights^[180]. An example of such an analysis of the free-energy barrier is given on figure 9 in the case of the three-dimensional four-state Potts model to be discussed later. The data presented by Chen *et al.*, and later by Yaşar *et al.*^[501], for the two-dimensional eight-state Potts model unambiguously show a vanishing of the free-energy barrier and thus prove that randomness induces a second-order phase transition. The case $q = 5$, for which the pure model undergoes a weak first-order phase transition, was also studied by Monte Carlo simulations^[408]. The magnetic susceptibility and specific heat were shown to diverge, respectively, as $L^{\gamma/\nu}$

and $L^{\alpha/\nu}$ with $\gamma/\nu \simeq 1.72(1)$ and $\alpha \simeq 0$, and not as L^d as expected for a first-order phase transition. The transition is thus continuous.

The transition being continuous, the question of its universality class naturally arises. Chen *et al.* estimated the critical exponents by Finite-Size Scaling of various observables (magnetisation, susceptibility, specific heat, derivatives with respect to β of the logarithm of various moments of the magnetisation, shift of the critical temperature). For two different strengths of disorder, $r = K_1/K_2 = 2$ and $r = 10$, the estimations are in agreement with the exact values of the pure Ising model. Earlier Monte Carlo studies of the site-diluted Baxter-Wu model [395], of the Baxter model [354], and of the random Ashkin-Teller at the four-state-Potts point [490] had already provided evidences of a random fixed point belonging to the Ising universality class. Renormalisation Group calculations for the Baxter model [159, 160, 158], and the Ashkin-Teller model [288] supported the idea of super-universality for two-dimensional random models. These results are however surprising because they contradict RG calculations of the random Potts model in the $q \leq 4$ regime that predict a new universality class for all Potts models [336]. The latter was confirmed by a transfer matrix calculation of the central charge c in both regimes $q \leq 4$ and $q > 4$ [414]. The numerical estimates of c are generally not multiples of $1/2$, the value of the central charge of the pure Ising model. Therefore, the random fixed point of the Potts model cannot correspond to an integer number of decoupled Ising models. However, in the special case $q = 8$ studied by Chen *et al.*, the estimate of the central charge is compatible with the value $3/2$ and therefore allows for an Ising universality class. A more systematic study was accomplished by Cardy and Jacobsen [98, 268]. By means of transfer matrix calculations, the magnetic scaling dimension was estimated to be $x_\sigma = 0.1415(36)$ in the case $q = 8$. This excludes completely the possibility of an Ising universality class (for which $x_\sigma = 0.125$). The correlation length critical exponent $\nu = 1.01(2)$ is however still compatible with the one of the Ising model. In 1997, we have studied the critical behaviour of the random eight-state Potts model by Monte Carlo simulations [110]. Using Finite-Size Scaling of various observables (figure 7), we estimated the critical exponents:

$$\frac{\beta}{\nu} = 0.153(3), \quad \frac{\gamma}{\nu} = 1.701(8), \quad \nu = 1.023(20).$$

These values corroborate the incompatibility with the pure Ising model universality class ($\beta/\nu = 0.125$, $\gamma/\nu = 1.75$, and $\nu = 1$). They are still up-to-date and were not contradicted by further numerical estimations (see table 2). It is now well established that the magnetic scaling dimension $x_\sigma = \beta/\nu$ grows continuously with the number of states q and reaches the asymptotic value $(3 - \sqrt{5})/4$ in the limit $q \rightarrow +\infty$. The thermal exponent ν of the correlation length displays a much slower evolution with the number of states and remains very close to the value $\nu = 1$ of the pure Ising model.

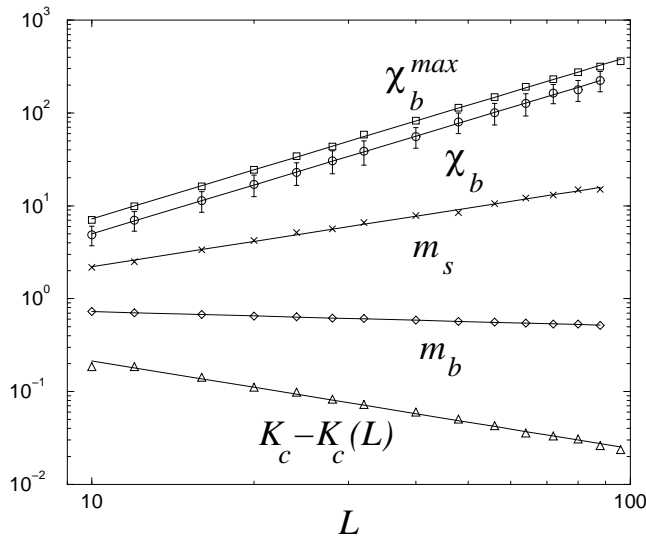


Figure 7 : Finite-Size Scaling of the maximum of the bulk susceptibility χ_b^{\max} , susceptibility χ_b at T_c , excess magnetisation m_s at the surface, bulk magnetisation m_b and shift of critical coupling $|K - K_c|$ for the eight-state Random-Bond Potts model.

The limit $q \rightarrow +\infty$ is particularly interesting because it can be studied directly using combinatorial techniques. The self-duality condition (17) imposes the scaling $K_{ij} \sim \ln q$ of the exchange coupling. To get rid of these logarithmically diverging terms, define $K_{ij} = \tilde{K}_{ij} \ln q$. The partition function in the Fortuin-Kasteleyn representation (3) then reads

$$\mathcal{Z} = \sum_G \prod_{(i,j)} (q^{\tilde{K}_{ij}} - 1)^{b_{ij}} q^{C(G)} \underset{q \rightarrow +\infty}{\sim} \sum_G q^{\sum_{(i,j)} b_{ij} \tilde{K}_{ij} + C(G)}.$$

In the limit $q \rightarrow +\infty$, only those graphs that maximise the function $\phi(G) = \sum_{(i,j)} b_{ij} \tilde{K}_{ij} + C(G)$ will contribute to the sum. While in the pure case the sum is dominated by only two graphs (the full and the empty graphs), an infinite number of graphs have a non-vanishing contribution in the limit $q \rightarrow +\infty$. The calculation of the partition function has thus been reduced to an optimisation problem with a cost function $\phi(G)$. The determination of the set of graphs G^* such that $\phi(G^*) = \max \phi(G)$, or at least of a finite subset of them, was done using the simulated annealing technique and an optimisation algorithm [289]. The scaling dimension $x_\sigma = \frac{\beta}{\nu} \simeq 0.18(2)$ was found to be compatible with the extrapolated value 0.192(2) obtained with the transfer matrix technique [270]. A more elaborated combinatorial optimisation algorithm, the optimal cooperation algorithm, was later developed [23]. It allowed for much more accurate estimates of the critical exponents [22, 365]. The latter were shown to be compatible with the exact values $\beta = (3 - \sqrt{5})/4$ and $\nu = 1$ of the infinite-randomness fixed point of the random transverse-field Ising spin chain. This point will be further discussed in § 1.2.2.5.1..

Authors	Year	Numerical technique	β/ν
Chen, Ferrenberg, and Landau ^[123]	1992	Monte Carlo	0.118(8)
Cardy, and Jacobsen ^[98, 268]	1997	Transfer matrix	0.142(1)
Chatelain, and Berche ^[110]	1998	Monte Carlo	0.153(3)
Picco ^[415]	1998	Monte Carlo	0.153(1)
Chatelain, and Berche ^[109, 56]	1998	Monte Carlo	0.1499(1)
		Transfer matrix	0.1496(9)
Olson, and Young ^[397]	1999	Monte Carlo	0.159(3)
Chatelain, and Berche ^[111]	1999	Transfer matrix	0.1505(31)
		Monte Carlo	0.152(3)
		Monte Carlo	0.1487(32)
Jacobsen, and Picco ^[270]	2000	Transfer matrix	0.1535(10)
Ying, and Harada ^[507]	2000	Short-Time Dyn.	0.151(3)
Chatelain, Berche, and Shchur ^[115]	2001	Transfer matrix	0.1514(2)
Yin, Zheng, and Trimper ^[505]	2004	Short Time Dyn.	0.157(2)
Fan, and Zhong ^[179]	2009	Dynamical MCRG	0.167(14)

Tableau 2 : Estimates of the critical exponent β/ν of the random eight-state Potts model.

We have also studied the surface critical behaviour of the finite RBPM. The (ordinary) surface transition is already continuous in the absence of disorder with a magnetic critical exponent $\beta_1/\nu = 3$. From Finite-Size Scaling of the surface magnetisation m_1 , the magnetic susceptibility χ_{11} associated to a surface field and the excess magnetisation $\sum_i(m_i - m_b)$, we extracted the following surface critical exponents:

$$\frac{\beta_1}{\nu} = 0.467(6), \quad \frac{\gamma_{11}}{\nu} = 0.099(9), \quad \frac{\beta_s}{\nu} = -0.852(4). \quad (19)$$

These values are remarkably different from those of the pure model and, surprisingly much closer to the surface exponents of the pure Ising model ($\beta_1/\nu = 1/2$, $\gamma_{11}/\nu = 0$ and $\beta_s/\nu = \beta/\nu - 1 = -0.875$), albeit error bars exclude the Ising values. We also performed an analysis of the scaling behaviour away from the critical point. The scaling behaviour with the reduced critical temperature allowed us to estimate these surface exponents independently and not as a ratio with ν ^[406]. Unfortunately, unlike the bulk quantities, the surface behaviour is strongly influenced by scaling corrections. The comparison of the magnetisation profile with conformal predictions, to be presented in chapter § 1.2.4., confirmed the presence of these corrections and the values (19). The cases $q = 3, 4$ and 6 were also considered. Interestingly, the magnetic surface exponent β_1/ν was shown to increase with the number of states in a very similar way as the bulk magnetic exponent (with roughly the relation $\beta_1 \simeq 4\beta$). In the limit $q \rightarrow +\infty$, the magnetic surface exponent was conjectured to be $\beta_1/\nu = 1/2$ ^[22]. This is a further

evidence that there is not a single random fixed point in the Ising universality class but a line of fixed points.

1.2.2.3. Three-dimensional random Potts models

The three-dimensional random Potts model is expected to display a richer phase diagram than the two-dimensional one. As predicted by Hui and Berker, a first-order phase transition line should survive at weak disorder and eventually terminate at a tricritical point. The transition is then continuous as long as the strongest bonds form a percolating cluster. The study of the three-dimensional random Potts model is however more difficult because the most successful techniques in two-dimensions are not available anymore in three dimensions: RG group calculations based on deformed Coulomb-gas representations of the conformal minimal models are limited to two dimensions and transfer matrices would demand a huge amount of memory. Monte Carlo simulations are essentially the only technique to study the three-dimensional Potts model.

Motivated by experiments on the liquid crystal 8CB in an aeorgel, the three-state and four-state Potts models were studied numerically on three-dimensional graphs obtained by diffusion-limited cluster-cluster aggregation [476, 475]. A change of the order of the transition, from first-order to second-order, was observed under an increase of the disorder strength. The determination of the critical exponents along the continuous transition line was possible only with large-scale Monte Carlo simulations. This was achieved in the case of the site-diluted three-state Potts model by Ballesteros *et al.* [36]. The pure system undergoes a very weak first-order phase transition with a small latent heat $\Delta e \simeq 0.1614(3)$ per site and a surface tension $2\sigma_{o,d} \simeq 0.00163(3)$ [278]. A second-order phase transition is clearly observed in the random case. In this regime, critical exponents were measured using the so-called quotient method. The scaling behaviour of any observable O being $O(L, |T - T_c|) \sim L^{-x_O} \mathcal{O}(L/\xi)$, the critical exponent x_O can be estimated from the comparison of O at two different lattice sizes L and L' as

$$x_O \simeq - \frac{\ln O(L', |T' - T_c|) - \ln O(L, |T - T_c|)}{\ln L' - \ln L}. \quad (20)$$

The usual Finite-Size Scaling technique consists in choosing the temperatures T and T' as the critical temperature T_c of the infinite system and in assuming that the scaling corrections can be neglected. In the quotient method, the simulations are performed away from the critical point at two different temperatures T and T' such that

$$\frac{L}{\xi(T)} = \frac{L'}{\xi(T')}.$$

Since the scaling function depends only on L/ξ , its value is identical for the two simulations. Therefore, the scaling corrections cancel exactly in the expression (20) of the critical exponent. Using this technique, the critical exponents of the site-diluted three-state Potts model were shown to be independent of the disorder strength for several points on the transition line:

$$\eta = 0.078(4), \quad \nu = 0.690(5). \quad (21)$$

Again, this means that the critical behaviour is governed by a single random fixed point. Moreover, the numerical estimates (21) are incompatible with those of the Ising

model. Scaling corrections were shown to be strong with an exponent $\omega \simeq 0.4$ for the first subdominant correction. For weak disorder, Ballesteros *et al.* suspected the presence of a first-order phase transition. The location of the tricritical point was later estimated using Short Time Dynamics simulations in the case of the random-bond three-state Potts model [506]. For the binary distribution of exchange couplings (16) that was considered, the tricritical point was observed at $r = K_1/K_2 \simeq 2.3$. At strong disorder $r = 10$, the magnetic critical exponent was estimated to be $0.548(13)$, in agreement with Ballesteros' value ($\beta/\nu \simeq 0.539(2)$). More recently, the site-diluted three-state Potts model has been studied in a series of papers by Murtazaev *et al.* [379, 385, 380, 381, 382, 378]. The order of the phase transition was confirmed by the study of the Binder cumulant. The critical exponents were estimated by Finite-Size Scaling at several points on the transition line ($p = 0.95$ to 0.65). Even though a small evolution with the impurity concentration is observed, the critical exponents are nevertheless in good agreement: ν goes from $0.671(5)$ to $0.688(9)$, $\alpha \simeq -0.001(12)$ to $-0.0027(14)$, $\beta \simeq 0.364(6)$ to $0.376(6)$ (which leads to $\beta/\nu \simeq 0.544$). Extremely surprisingly, a recent study based on an original time-dependent Monte Carlo Renormalisation Group technique [204] led to critical exponents at strong disorder $\nu \simeq 0.568(2)$, $\beta \simeq 0.32(4)$, and $\alpha \simeq 0.29(6)$ in contradiction with all previous simulations [498]. This disagreement has not been explained yet. Additional simulations are needed using more standard Monte Carlo simulations to confirm or infirm this large positive value of the specific heat exponent.

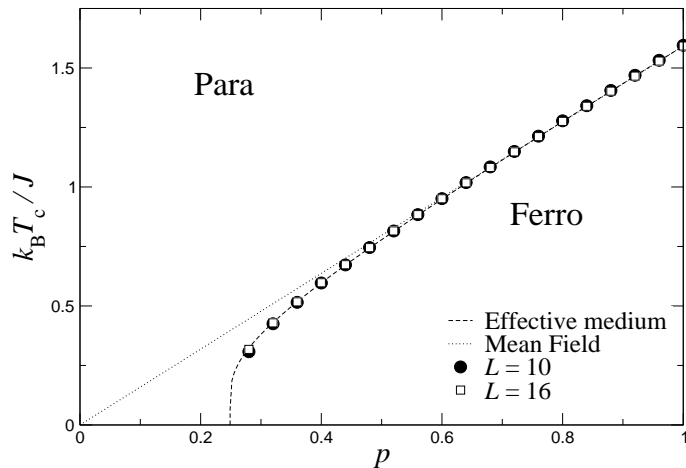


Figure 8 : Transition temperature of the bond-diluted three-dimensional four-state Potts model as a function of the bond concentration p . The dashed line is an estimation based on an effective-medium approximation. Its intersection with the x -axis corresponds to bond percolation.

After Ballesteros *et al.*'s work, we considered the bond-diluted four-state Potts model [113, 118, 114]. This choice was motivated by the fact that the pure four-state Potts model undergoes a much stronger first-order phase transition than the three-state one. We therefore hoped that a first-order regime would be easier to observe. In the second-order regime, the system was studied using the Swendsen-Wang algorithm [459]. In the first-order regime, this cluster algorithm is not able to force the system to tunnel through the free energy barrier and explore both the low and high-temperature phases. In that situation, we used a multi-canonical Monte Carlo algorithm based on the Fortuin-Kasteleyn formulation of the Potts model, the multi-bondic algorithm [273]. We

determined the transition temperature as the location of the maximum of the magnetic susceptibility (figure 8). The data are nicely reproduced by a simple effective-medium approximation [472, 471]. The order of the phase transition was then determined by the Finite-Size Scaling of the free-energy barrier using the Lee and Kosterlitz method (18). At weak disorder, a first-order regime persists up to a tricritical point occurring at the concentration $p_{TC} \simeq 0.76(8)$. At smaller bond concentration, the transition is continuous as shown by the vanishing of the surface tension in the thermodynamic limit (figure 9). The phase diagram was later confirmed by series expansions of the magnetic susceptibility up to the 18th-order [233, 234]. Using Finite-Size Scaling, we estimated the critical exponents at different concentrations. The different values of $1/\nu$ are compatible within error bars, as expected for a single random fixed point. Unfortunately, this is not the case for γ/ν . We studied in details the scaling corrections but were not able, using non-linear interpolation of the Monte Carlo data, to estimate the exponent ω of the first sub-dominant correction. At the concentration $p = 0.56$, where the scaling corrections appeared to be the weaker, we obtained the values:

$$\frac{\beta}{\nu} \simeq 0.732(24), \quad \frac{\gamma}{\nu} \simeq 1.535(30), \quad \nu \simeq 0.7468(14),$$

that we expect to be the closest to the critical exponents at the random fixed point. Like in Ballesteros *et al.* work, a precise localisation of the tricritical point, and therefore an estimation of the critical exponents at that point, was out of reach. The bond-diluted four-state Potts model was later studied using Short-Time Dynamics [504]. The tricritical point was found at a concentration $p_{TC} \simeq 0.74(2)$, compatible with our estimate (0.76(8)). The critical exponents were determined at three different concentrations in the continuous regime. Again, only the estimates of the exponent ν appear to be disorder-independent. At the concentration $p = 0.56$, the values

$$\frac{\beta}{\nu} \simeq 0.653(14), \quad \nu \simeq 0.702(25)$$

were measured. The site-diluted four-state Potts model was considered by Murtzahev *et al.* [383, 378]. From the behaviour of the Binder cumulant, they showed the existence of the continuous transition at the site concentration $p = 0.65$ and estimated the critical exponents at this point using Finite-Size Scaling:

$$\beta \simeq 0.514(24), \quad \gamma \simeq 1.133(30), \quad \nu \simeq 0.745(13)$$

or, for comparison, $\beta/\nu \simeq 0.69(4)$ and $\gamma/\nu \simeq 1.52(7)$, compatible both with our estimates and Yin *et al.*'s one for β/ν .

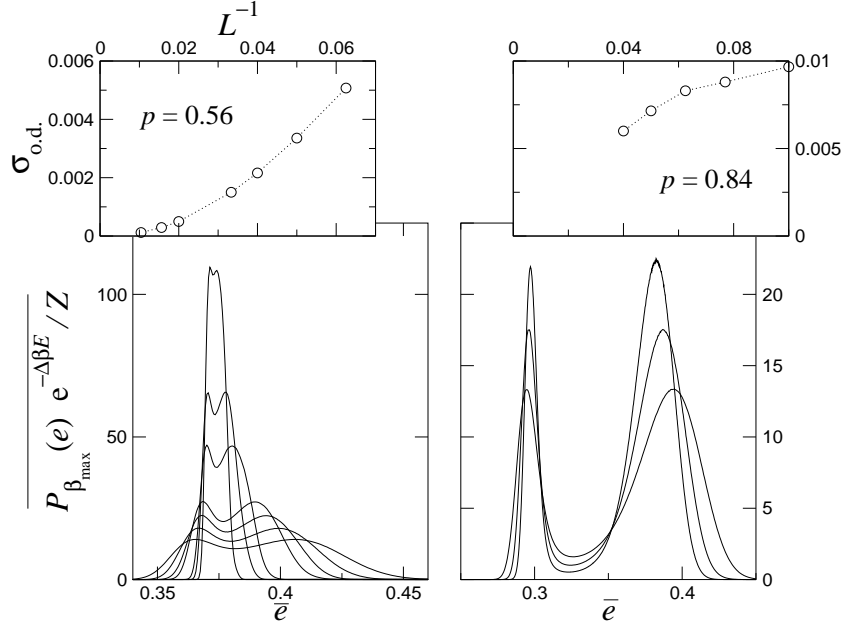


Figure 9 : Probability distribution of the energy of the tree-dimensional bond-diluted four-state Potts model at two concentrations ($p = 0.56$ on the left and $p = 0.84$ on the right). The surface tension $\sigma_{o,d}$ is extracted from the barrier between the two peaks corresponding respectively to the ordered and disordered phases.

The limit $q \rightarrow +\infty$ of the random-bond Potts model was studied using combinatorial techniques for the bimodal distribution $K_1 = K_c(1 + \delta)$ and $K_2 = K_c(1 - \delta)$ [366, 367]. In the second-order regime, the critical exponents were estimated to be

$$\frac{\beta}{\nu} = 0.60(2), \quad \nu = 0.73(1),$$

independently of the value of δ . The tricritical point was found at $\delta_{PT} \simeq 0.658(1)$. In contradistinction to Monte Carlo simulations for finite numbers of states q , the accuracy on the location of this point was sufficient to measure the critical exponents:

$$\frac{\beta}{\nu} = 0.10(2), \quad \nu = 0.67(4).$$

Using the mapping of the RBPM onto the RFIM, these exponents are expected to be related to those of the RFIM by [98, 268]

$$\nu_{\text{Tri.}} = \frac{\nu_{\text{RFIM}}}{\beta_{\text{RFIM}} + \gamma_{\text{RFIM}}}.$$

Monte Carlo estimates of the critical exponents of the RFIM [370] ($\nu_{\text{RFIM}} \simeq 1.37(9)$, $\beta_{\text{RFIM}} \simeq 0.017(5)$, $\gamma_{\text{RFIM}} \simeq 2.04(14)$) lead to $\nu_{\text{Tri.}} \simeq 0.66(9)$.

1.2.2.4. Two-dimensional Potts models on irregular graphs

Randomness coupled to the energy density may be introduced in different ways in the Potts model. Besides the case of random exchange couplings that we have discussed above, one may also consider quenched non-regular lattices. The exchange coupling is assumed to be identical for all bonds but coordination numbers, i.e. the number of bonds attached to a given site, can now fluctuate from site to site. Two classes of irregular graphs have been considered in the literature: quasi-periodic tilings and random graphs. Even though we did not contribute to these works, a presentation of these results is useful to understand the general picture of randomness-induced continuous transitions.

Following the discovery of quasi-crystals, many lattice models have been studied on quasi-periodic structures [436]. Surprisingly, simulations of the q -state Potts model in the first-order regime reported a softening of the transition but no complete elimination of the latent heat, in apparent contradiction with the Aizenman-Wehr theorem. The $q = 5$ -Potts model was studied on the Penrose quasi-periodic tiling using an original multicanonical algorithm [487, 489]. The eight-state Potts model was later considered on an octagonal quasi-periodic tiling. The analysis of the free energy barrier (18) showed an incomplete smoothing of the first-order transition [314]. The introduction of two different couplings J and $10J$ on some definite links of the quasi-periodic lattice was shown not to be sufficient to change the order of the transition [312]. A continuous phase transition, separated from the first-order line by a tricritical point, was finally observed in the five-state Potts model but only after random removal of a fraction of the seven nearest neighbours of the Penrose lattice [488].

Planar random graphs are easily obtained using the Voronoi-Delaunay algorithm: choose randomly N points inside a square and then construct the segments joining these points. Consider only those segments forming triangles such that their circumcircles do not contain any other random points. This construction is called the Delaunay triangulation. Construct now the bisector of these segments. They should meet at the centres of the circumcircles of the Delaunay triangles and form a lattice known as Voronoi diagram. At each site of this diagram, a q -state Potts spin σ_i is placed. The Hamiltonian (1) of the pure Potts model is unchanged, except that the interaction involves now pairs of nearest neighbours spins on the Voronoi diagram. This model was studied by means of Monte Carlo simulations in the case $q = 10$ which corresponds to a very strong first-order phase transition on regular lattices [276, 277]. The inverse transition temperature was estimated to be $\beta_t \simeq 0.83362(13)$, a value close to that of the triangular lattice. Indeed, it can be shown that each site of a planar Voronoi diagram has on average six neighbours, i.e. the same number as a triangular lattice. Like on quasi-periodic lattices, the transition was shown to remain of first-order. Both the susceptibility and the specific heat scale as N , the number of lattice points, while the Binder cumulant vanishes as $1/N$. The contradiction with the Aizenman-Wehr theorem was explained by the fact that the fluctuations of the coordination number scale as $L^{(d-1)/2}$ and not as $L^{d/2}$ [96, 281]. Since the free energy of an interface behaves as L^{d-1} , it is always dominant for large clusters and there is no lower critical dimension d_c . The transition remains of first-order at weak disorder and might become continuous at strong disorder. The Potts model on Voronoi-Delaunay graphs was later considered with an exchange coupling depending on the distance between the two sites: $J_{ij} = J_0 e^{-a\|\vec{r}_i - \vec{r}_j\|}$ [324]. The additional parameter a controls the strength of the disorder. For large values of a , a continuous transition is observed in the cases $q = 6$ and $q = 8$.

The 10-state Potts model was later studied on planar Φ^3 gravity graphs [33, 271, 272]. In the context of 2D quantum gravity, space-time interacts with matter so its geometry is annealed and not quenched. Here, we are discussing the case of quenched gravity graphs. In contradistinction to Voronoi diagrams, these gravity graphs are fractal. As a consequence, their intrinsic Hausdorff dimension d_f takes non-trivial values different from 2 and the characteristic length scale of these planar lattices is not \sqrt{N} , where N is the number of points, but N^{1/d_f} . The 10-state Potts model on these graphs was studied by Monte Carlo simulations. A continuous phase transition is clearly observed, at least for the number of points considered. As expected, the critical inverse temperature $\beta_c \simeq 2.244(1)$ is close to the one of the triangular lattice. The Finite-Size Scaling of various observables, among which the specific heat ($C \sim N^{\alpha/\nu d_f}$) and the susceptibility ($\chi \sim N^{\gamma/\nu d_f}$), was studied. The critical exponents were estimated to be

$$\frac{1}{\nu d_f} \simeq 0.58(1), \quad \frac{\alpha}{\nu d_f} \simeq 0.21(1), \quad \frac{\gamma}{\nu d_f} \simeq 0.71(1), \quad \frac{\beta}{\nu d_f} \simeq 0.12(1).$$

These values are incompatible with the critical exponents of the 2D pure Ising model. Again, to understand why in this case the first-order was completely smoothed, one has to study the fluctuations of the coordination number z . In a cluster of size ℓ , they are expected to grow algebraically as $\langle z^2 \rangle - \langle z \rangle^2 \sim \ell^{d_f \omega} \sim N^\omega$. The wandering exponent was estimated numerically to be $\omega \simeq 0.751(9)$ [281]. As a consequence, the fluctuations of the coordination number grow faster than the interface free energy $\sigma \ell^{d-1} \sim N^{(d-1)/d_f}$ for any dimension d such as $d-1 < \omega d_f$. Since $1 \leq d_f \leq 2$ and $\omega \simeq 3/2$, one can predict that disorder fluctuations will completely smooth the first-order transition.

1.2.2.5. Anisotropic perturbations of the two-dimensional Potts model

In the previous sections, disorder was assumed to be homogeneous, i.e. the probability distribution of the exchange couplings was site-independent. We now consider an anisotropic perturbation of the exchange couplings of the two-dimensional Potts models. Using the lattice coordinates (x, y) instead of the site label i , the Potts Hamiltonian (15) reads

$$-\beta H = \sum_{x,y} [K_{x,y}^1 \delta_{\sigma_{x,y}, \sigma_{x+1,y}} + K_{x,y}^2 \delta_{\sigma_{x,y}, \sigma_{x,y+1}}].$$

The exchange couplings are chosen to be constant in one direction, i.e. $K_{x,y}^i = K(x)$, and randomly distributed or deterministically defined in the other direction:

$$-\beta H = \sum_{x,y} K_x [\delta_{\sigma_{x,y}, \sigma_{x+1,y}} + \delta_{\sigma_{x,y}, \sigma_{x,y+1}}]. \quad (22)$$

The reason for such an apparently unphysical choice is that many analytical calculations can be performed in the case of the Ising model. Applying the technique of transfer matrices, McCoy and Wu determined the expression of the free-energy in the random case [361]. They showed that the transition is of infinite order and consequently that the specific heat displays an essential singularity [361, 360]. The spin-spin correlation functions both in the bulk and at the surface of a finite system were then considered [362, 359]. From the latter, the critical exponent $\beta_1 = 1/2$ was extracted. The bulk critical exponents

$$\beta = \frac{3 - \sqrt{5}}{2}, \quad \nu = 2$$

were later obtained by Fisher by applying the Dasgupta-Ma Renormalisation Group technique [137] to the spin-1/2 quantum chain in a transverse magnetic field obtained from the transfer matrix in the extreme anisotropic limit. The layered structure of the model leads to an infinite anisotropy exponent z . The calculation of the surface magnetisation was shown to be equivalent to the problem of the survival probability of a walker in the neighbourhood of an absorbing surface [260].

Following the discovery of quasi-crystals [436], one-dimensional aperiodic perturbations of the Ising model were studied using the same techniques. The relevance of these perturbations was shown to depend on the scaling of the fluctuations of the exchange couplings [335, 259, 334]. Different examples of relevant, marginal and irrelevant aperiodic sequences were systematically studied [474, 473, 293].

1.2.2.5.1. McCoy-Wu perturbation of the Potts model

In the extreme anisotropic limit, the transfer matrix of the random Potts model (22) is mapped onto an evolution operator for a random quantum Potts chain. The latter has been studied using Dasgupta-Ma Renormalisation Group [443]. The universality class was shown to be same as the Ising chain in a random transverse field independently of the number of states q . This result is especially interesting because the random fixed point of this anisotropic model was numerically shown to also control the isotropic random-bond Potts model in the limit $q \rightarrow +\infty$.

The regime $q > 4$, where the pure Potts model undergoes a first-order transition, has been much less explored. We studied the $q = 6$ case by means of Density Matrix Renormalisation Group (DMRG) [100]. As expected, randomness induces a continuous transition. Our estimate of the magnetic critical exponent, $\beta/\nu \simeq 0.190(2)$, is compatible with the value $\frac{3-\sqrt{5}}{4}$, which is exact in the case $q = 2, 3$ and 4. The situation is therefore remarkably different from the one of the homogeneous random-bond Potts model. In the latter, the critical behaviour is governed by a line of fixed points depending on the number of states q . As will be discussed in § 1.2.3.2., the disorder strength r^* at these fixed points increases as $\ln q$. In the present situation, the fixed point corresponds to an infinite disorder for all values of the number of states q . There is a single fixed point and thus a single set of critical exponents. Note that the line of fixed points of the random-bond Potts model terminates at such an infinite-randomness fixed point in the limit $q \rightarrow +\infty$. [22, 365].

1.2.2.5.2. Aperiodic perturbations of the Potts model

We have studied by means of Monte Carlo simulations the phase transition of the eight-state Potts model with different aperiodic sequences of the exchange couplings [57, 117, 116].

$$K_x^1 = K_x^2 = K_0 \delta_{n(x),0} + K_1 \delta_{n(x),1},$$

where the sequence $n(x) \in \{0; 1\}$ is constructed recursively using substitution rules. In the simple example of the so-called Thue-Morse sequence, these rules are

$$0 \longrightarrow S(0) = 01, \quad 1 \longrightarrow S(1) = 10.$$

When they are iterated, the following sequences are successively generated:

0,
01,
0110,
01101001,
0110100110010110,
...

In the case of the Thue-Morse aperiodic sequence, the length is doubled at each iteration. Other aperiodic sequences with longer substitution rules may display a faster increase of their length. The geometrical properties of the sequence are derived from the so-called substitution matrix whose elements M_{ij} correspond to the number of figures $i \in \{0; 1\}$ in the substitution pattern $S(j)$. For the Thue-Morse sequence, $M_{ij} = 1$ for all i, j . At the N -th iteration, the number n_i^N of figures i in the full sequence is linearly related to the numbers n_i^{N-1} at the previous one:

$$n_i^N = M_{ij} n_j^{N-1}.$$

Given an initial distribution n_i^0 , the number of couplings reads after N iterations

$$|n^N\rangle = M^N |n^0\rangle = \sum_i \lambda_i^N \langle \phi_i | n^0 \rangle | \phi_i \rangle \underset{N \rightarrow +\infty}{\sim} \lambda_0^N | \phi_0 \rangle \langle \phi_0 | n^0 \rangle, \quad (23)$$

where $|\phi_i\rangle$ are the right eigenvectors of the substitution matrix for the eigenvalues λ_i and $\langle \phi_i|$ are their duals defined by $\langle \phi_i | \phi_j \rangle = \delta_{i,j}$. The largest eigenvalue is denoted λ_0 . The length $L_N = \sum_{i=0}^1 n_i$ of the sequence is obtained by a projection on the dual vector $\langle \mathbf{1} | = (1 \ 1 \ \dots)$:

$$L_N \underset{N \rightarrow +\infty}{\sim} \lambda_0^N \langle \mathbf{1} | \phi_0 \rangle \langle \phi_0 | n^0 \rangle.$$

In a similar way, a projection on $\langle 0 | = (1 \ 0 \ \dots)$ gives the number of couplings K_0 in the sequence after N iterations

$$n^N(K_0) = \sum_i \lambda_i^N \langle 0 | \phi_i \rangle \langle \phi_i | n^0 \rangle \underset{N \rightarrow +\infty}{\sim} \lambda_0^N \langle 0 | \phi_0 \rangle \langle \phi_0 | n^0 \rangle.$$

The average density of couplings K_0 is therefore

$$\rho^N(K_0) = \frac{n^N(K_0)}{L_N} = \frac{1}{L_N} \sum_i \lambda_i^N \langle 0 | \phi_i \rangle \langle \phi_i | n^0 \rangle \underset{N \rightarrow +\infty}{\sim} \frac{\langle 0 | \phi_0 \rangle}{\langle \mathbf{1} | \phi_0 \rangle}.$$

The fluctuations of the finite-size density around its asymptotic value are calculated from (23):

$$\begin{aligned} \Delta \rho_N(K_0) &= \rho_N(K_0) - \rho_{+\infty}(K_0) \\ &= \frac{\sum_i \lambda_i^N \langle 0 | \phi_i \rangle \langle \phi_i | n(0) \rangle - \lambda_0^N \langle 0 | \phi_0 \rangle \langle \phi_0 | n(0) \rangle}{\lambda_0^N \langle \mathbf{1} | \phi_0 \rangle \langle \phi_0 | n(0) \rangle} \\ &\underset{N \rightarrow +\infty}{\sim} \left(\frac{\lambda_1}{\lambda_0} \right)^N \frac{\langle 0 | \phi_1 \rangle \langle \phi_1 | n(0) \rangle}{\langle \mathbf{1} | \phi_0 \rangle \langle \phi_0 | n(0) \rangle}. \end{aligned}$$

Introducing the length L_n of the sequence, these fluctuations scale as

$$\Delta\rho_N(K_0) \underset{N \rightarrow +\infty}{\sim} L_n^{\omega-1}, \quad (24)$$

where the wandering exponent is defined as

$$\omega = \frac{\ln |\lambda_1|}{\ln \lambda_0}.$$

The Luck criterion (38) states that an aperiodic sequence is a relevant perturbation at the critical point of a second-order phase transition if $\omega > 1 - 1/\nu$ [335, 259, 334]. For the moment, we are only interested in the first-order regime of the $q > 4$ pure Potts model. The Luck criterion is often invoked, with a correlation length exponent ν replaced by $1/d$, to decide whether the order of the transition will be changed or not. This quick and dirty generalisation is not justified, apart from the agreement with some still rare *a-posteriori* Monte Carlo simulations. According to the Imry-Wortis criterion, the lower critical dimension at which the low-temperature phase is stable may be obtained from the comparison between the fluctuations of the density of couplings K_0 and the surface free-energy. Consider a cluster of size ℓ . According to (24), the fluctuations of the total number of couplings K_0 scale as $\ell^{\omega-1} \times \ell^d = \ell^{1+\omega}$. The surface free energy behaves as $\sigma\ell$. Therefore, the marginal situation described by Imry and Wortis in the case of homogeneous disorder corresponds to $\omega = 0$ in the case of aperiodic sequences. One may thus conjecture a complete smoothing of the first-order phase transition by the aperiodic sequence if the wandering exponent is positive or zero, $\omega \geq 0$.

We have studied several aperiodic sequences. The Thue-Morse one has already been presented above. Its wandering exponent is $\omega = -\infty$. As a check, we considered the periodic sequence

0101010101010...

that can be obtained with the substitution rules

$$0 \longrightarrow S(0) = 01, \quad 1 \longrightarrow S(1) = 01.$$

The substitution matrix is the same as for the Thue-Morse sequence and thus $\omega = -\infty$. At a large scale, we expect the periodic sequence to be equivalent to an homogeneous system with an average exchange coupling $(K_0 + K_1)/2$. The transition of the eight-state Potts model should therefore remain of first-order. The Paper-Folding sequence is defined by the more complex substitution rules

$$\begin{aligned} 00 &\longrightarrow S(00) = 1000, & 01 &\longrightarrow S(01) = 1001, \\ 10 &\longrightarrow S(10) = 1100, & 11 &\longrightarrow S(11) = 1101, \end{aligned}$$

and the Three-folding sequence by

$$0 \longrightarrow S(0) = 010, \quad 1 \longrightarrow S(1) = 011.$$

Both sequences possess a vanishing wandering exponent.

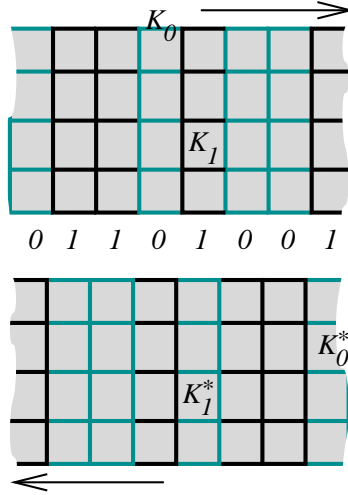


Figure 10 : Duality transformation applied to an aperiodic system.

The two couplings were chosen dual of each other, i.e. $K_0 = K_1^*$. The duality transformation maps the aperiodic system onto a new one which is oriented in the other direction (see figure 10). A rotation by 180° is therefore needed to bring the dual system into the same orientation of the couplings as the original lattice. Because of this rotation and of the condition $K_0 = K_1^*$, the resulting aperiodic sequence is $n^*(x) = 1 - n(L - x)$. For this reason, the system is self-dual only if the sequence is anti-symmetric under a reflexion, i.e. $1 - n(L - x) = n(x)$. This is the case for the periodic sequence, Thue-Morse after an even number of iterations, and Paper-Folding and Three-Folding sequences when the last figure $n(L)$ is omitted, which should result only in a surface effect. It is of course not a general property of aperiodic sequences. The so-called Rudin-Shapiro sequence is not anti-symmetric.

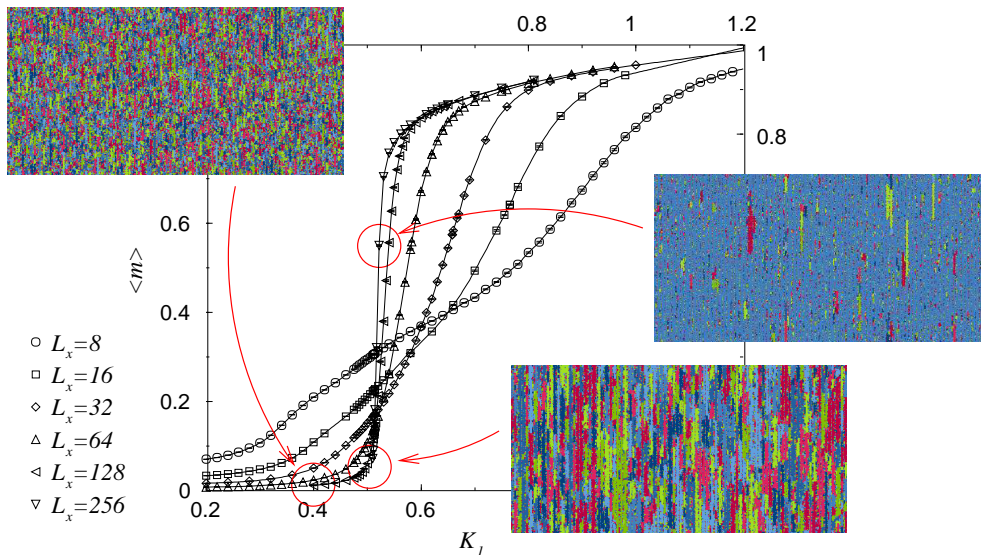


Figure 11 : Magnetisation versus the exchange coupling K_1 for the aperiodic sequence Thue-Morse. The different curves correspond to different lattice sizes. The insets show typical spin configurations for the couplings $K_1 = 0.4, 0.5$ and 0.52 .

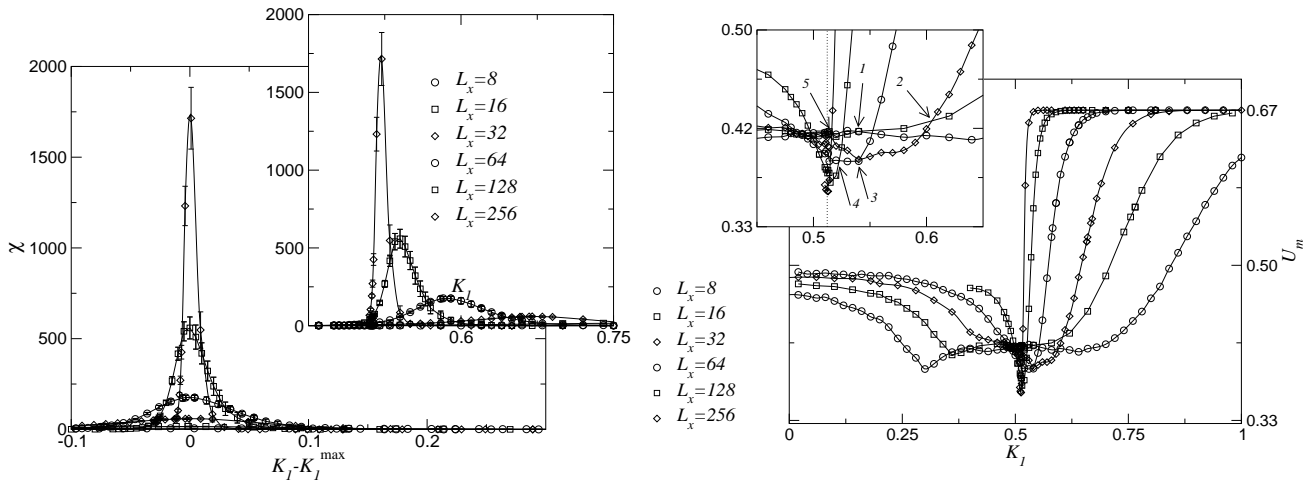


Figure 12 : On the left, magnetic susceptibility versus the exchange coupling K_1 for the aperiodic sequence Thue-Morse. The different curves correspond to different lattice sizes. On the right, Binder cumulant of the magnetisation versus K_1 .

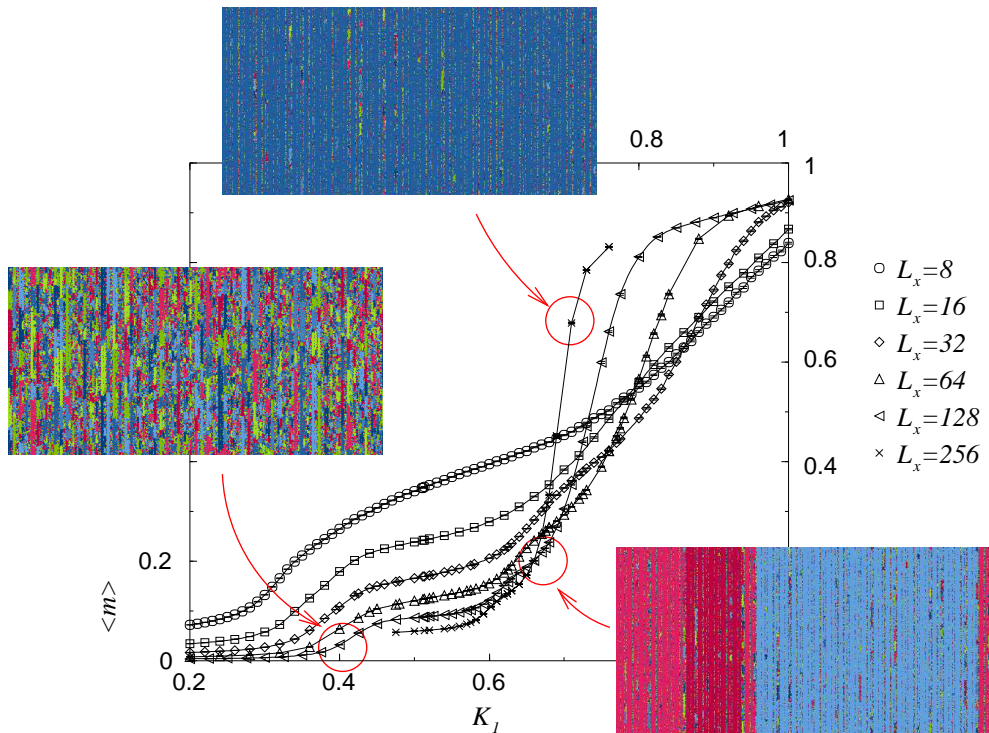


Figure 13 : Magnetisation versus the exchange coupling K_1 for the aperiodic sequence Paper-Folding. The different curves correspond to different lattice sizes. The insets show typical spin configurations for the couplings $K_1 = 0.4, 0.67$ and 0.7 .

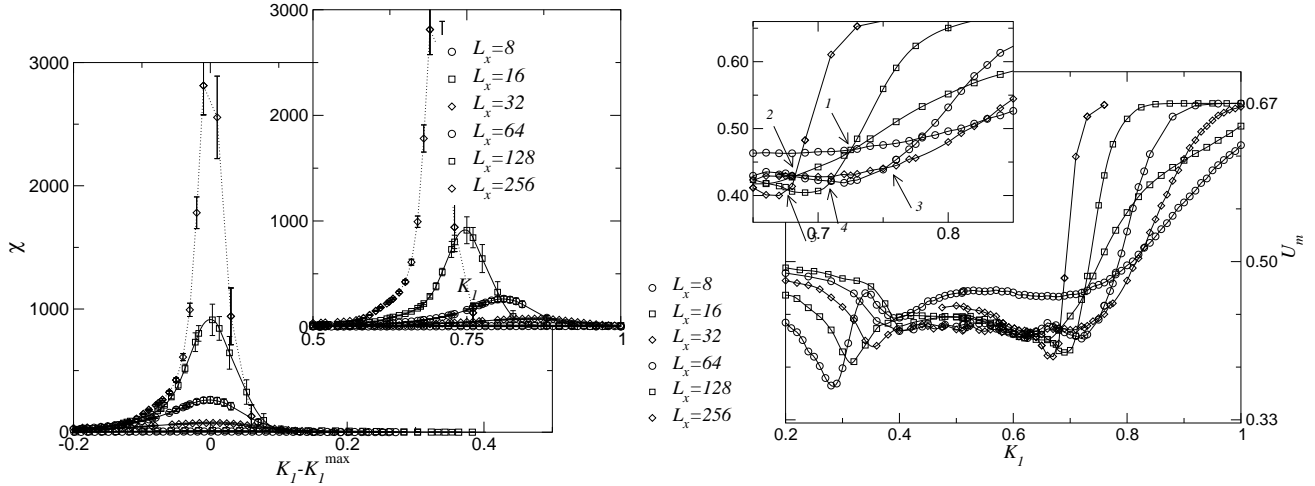


Figure 14 : On the left, magnetic susceptibility versus the exchange coupling K_1 for the aperiodic sequence Paper-Folding. The different curves correspond to different lattice sizes. On the right, Binder cumulant of the magnetisation versus K_1 .

We first studied the average magnetisation, the magnetic susceptibility and the Binder cumulant away from the transition temperature. The numerical data are presented for the Thue-Morse and Paper-Folding sequences on figures 11, 12, 13, and 14. Unfortunately, the lattice sizes are still too small to draw any definitive conclusion on the order of the phase transition from the shape of the Binder cumulant. We estimated temperature-dependent effective critical exponents by combining data at two different lattice sizes L and L' :

$$\left(\frac{\beta}{\nu}\right)_{\text{eff.}} = -\frac{\ln m(T, L') - \ln m(T, L)}{\ln L' - \ln L}$$

for example in the case of magnetisation. If the system undergoes a second-order phase transition, the magnetisation is expected to behave as $m(T, L) = L^{-\beta/\nu} \mathcal{M}(L|T - T_c|^\nu)$. In the vicinity of the transition temperature T_c , the effective exponent should approach the true critical exponent β/ν . For a first-order phase transition, magnetisation is discontinuous and therefore the effective exponent should vanish in the thermodynamic limit. Similarly, the effective exponent calculated from the susceptibility should tend to the value $d = 2$. These tendencies are clearly observed for the aperiodic eight-state Potts model: the periodic and True-Morse sequences exhibit a first-order behaviour while Paper-Folding and Three-Folding lead to a critical behaviour with exponents $\gamma/\nu \simeq 1$ and $\beta/\nu \simeq 1/2$. More accurate estimates of these exponents were then obtained using Finite-Size Scaling at the transition temperature. The magnetic susceptibility is shown on figure 15. Effective critical exponents γ/ν were calculated by power law interpolation. The sequences Paper-Folding and Three-Folding show a nice power-law behaviour with an exponent $\gamma/\nu \simeq 1$. In contradistinction, the magnetic susceptibility displays strong cross-over effects for the periodic and Thue-Morse sequences. The first regime corresponds to a lattice size smaller than the correlation length. Percolating clusters can still appear, in a way that is similar to a system undergoing a second-order phase transition. The second regime $L > \xi$ is characteristic of a first-order phase transition with an effective exponent approaching $d = 2$. Our estimates of the critical

exponents show a small dependence on the ratio K_0/K_1 . However, a tendency toward a single value is observed as the lattice size is increased. No tricritical point was observed at large values of this ratio for the periodic and Thue-Morse sequences or at small values for Paper-Folding and Three-Folding.

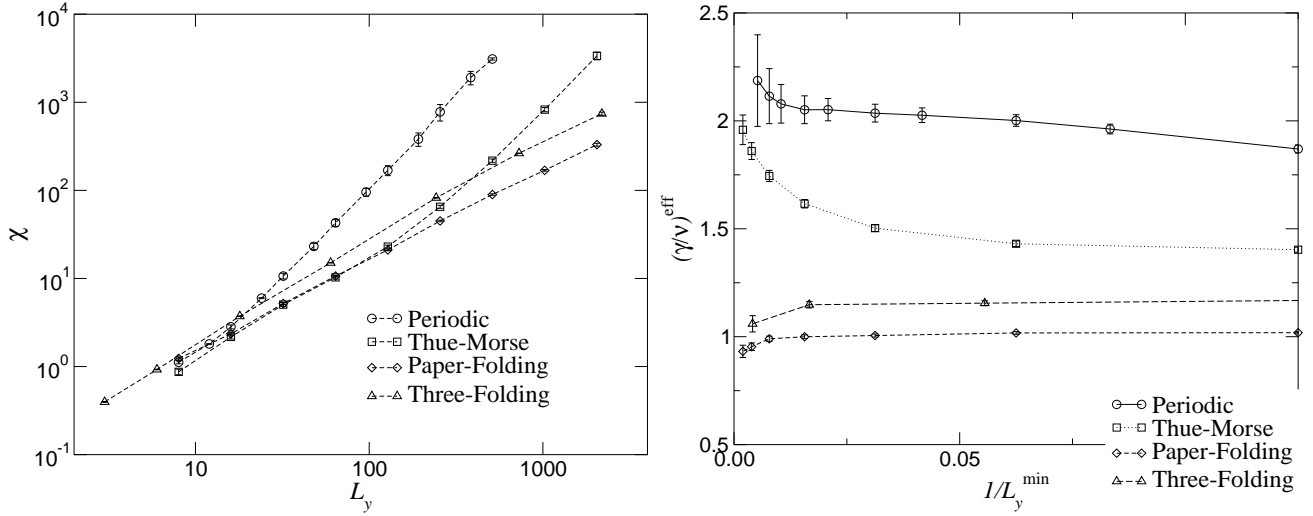


Figure 15 : On the left, magnetic susceptibility at the transition temperature versus the lattice size L_y for different aperiodic sequences. On the right, effective critical exponent γ/ν versus the inverse of the smallest lattice size L_y^{\min} . that was taken into account in the power-law interpolation of the susceptibility.

The $q = 6$ and $q = 15$ Potts models perturbed by the Thue-Morse, Paper-Folding and Three-Folding aperiodic sequences were recently studied by Monte Carlo simulations [198]. The order of the phase transition was determined from the behaviour of the free energy barrier (18) as the lattice size is increased. As expected, this barrier vanishes at large lattice sizes for the Paper-Folding and Three-Folding sequences while it grows quickly for the Thue-Morse one. The critical exponents were estimated using Finite-Size Scaling. Interestingly, together with our results for $q = 8$, the exponent β/ν displays a slow growth with the number of states (table 3). The situation is very similar to the case of homogeneous disorder.

	$q = 6$	$q = 8$	$q = 15$
Paper-Folding	0.469(5)	0.49(1)	0.509(16)
Three-Folding	0.433(4)	0.44(2)	0.47(2)

Tableau 3 : Estimation of the critical exponents β/ν for the q -state Potts model perturbed by Paper-Folding and Three-Folding aperiodic sequences.

The results presented above are consistent with the Imry-Wortis criterion. For the periodic and Thue-Morse sequences ($\omega = -\infty$), the fluctuations of the exchange couplings remain finite and cannot compensate the effect of the surface tension. The low-temperature phase is stable and the transition remains first-order. For the Paper-Folding and Three-Folding sequences ($\omega = 0$), the fluctuations scale with the cluster size in the same way as the interface free energy. Like in the case of homogeneous disorder, $d = 2$ is

the lower critical dimension when $\omega = 0$. A continuous phase transition is observed for all ratios K_0/K_1 . It would be interesting to study other aperiodic sequences, especially with a negative but finite wandering exponent. One would expect in this case a richer phase diagram with a tricritical point separating a first-order line at small ratios K_0/K_1 from an inhomogeneity-induced continuous transition at large ratios.

1.2.3. The random Potts fixed point

So far we have discussed the random Potts model only in the regime where the pure model undergoes a first-order phase transition. Numerical calculations allowed for the estimation of the critical exponents in the cases where a second-order phase transition is induced by the introduction of disorder. But no analytical calculation was possible in this regime, essentially because a critical point cannot be reached perturbatively from a first-order transition. In contradistinction, many analytical developments could be achieved in the regime where the pure model undergoes a second-order phase transition. Relevance criterions predict whether disorder will be a relevant perturbation or not, i.e. whether the critical behaviour of the pure system will be altered or not. Series expansions of the critical exponents were obtained using Renormalisation Group techniques, combined with conformal invariance results in the two-dimensional case. After two decades of efforts, a very good agreement between numerical and RG calculations has been reached. The critical behaviour is governed by a line of fixed points depending on the number of states q , that starts at a tricritical point in dimensions $d > 2$, and ends at an infinite-randomness fixed point. The magnetic critical exponent shows a monotonous increase with no special behaviour at $q = 4$, where the order of the phase transition of the pure model changes. Remarkably, in the case of the layered random Potts model, there is a single infinite-randomness fixed point independently of the number of states.

1.2.3.1. The Harris criterion

Consider a model whose degrees of freedom are spins σ_i located on the nodes of a lattice. They interact through the Hamiltonian

$$-\beta H_0(\sigma) = K \sum_{(i,j)} \varepsilon_{ij}(\sigma),$$

where σ denotes the set of spins $\{\sigma_i\}_i$ and ε_{ij} is the local energy on the bond (i, j) . In the case of the q -state Potts model, $\sigma_i \in \{0; \dots; q-1\}$ and $\varepsilon_{ij} = \delta_{\sigma_i, \sigma_j}$. Randomness is introduced in the system as site-dependent couplings:

$$-\beta H(\sigma) = \sum_{(i,j)} (\bar{K} + \delta K_{ij}) \varepsilon_{ij}(\sigma) = -\beta H_0 - \beta W. \quad (25)$$

The couplings are random variables distributed according to a probability law $\wp(K_{ij})$. Consider a given realisation $\{K_{ij}\}$ of exchange couplings. The free energy reads

$$F = -k_B T \ln \mathcal{Z} = -k_B T \ln \left[\sum_{\sigma} e^{\sum_{(i,j)} (K + \delta K_{ij}) \varepsilon_{ij}(\sigma)} \right].$$

In the limit of weak disorder, i.e. $\delta K_{ij} \ll \bar{K}$, it can be expanded as

$$\begin{aligned}
F &\simeq -k_B T \ln \left[\sum_{\sigma} e^{-\beta H_0(\sigma)} \left(1 + \sum_{(i,j)} \delta K_{ij} \varepsilon_{ij} + \frac{1}{2} \left[\sum_{(i,j)} \delta K_{ij} \varepsilon_{ij} \right]^2 + \dots \right) \right] \\
&= -k_B T \ln \left[\mathcal{Z}_0 \left(1 + \sum_{(i,j)} \delta K_{ij} \langle \varepsilon_{ij} \rangle_0 + \frac{1}{2} \sum_{\substack{(i,j) \\ (k,l)}} \delta K_{ij} \delta K_{kl} \langle \varepsilon_{ij} \varepsilon_{kl} \rangle_0 + \dots \right) \right] \quad (26) \\
&\simeq F_0 - k_B T \sum_{(i,j)} \delta K_{ij} \langle \varepsilon_{ij} \rangle_0 - \frac{k_B T}{2} \sum_{\substack{(i,j) \\ (k,l)}} \delta K_{ij} \delta K_{kl} \left[\langle \varepsilon_{ij} \varepsilon_{kl} \rangle_0 - \langle \varepsilon_{ij} \rangle_0 \langle \varepsilon_{kl} \rangle_0 \right] + \dots
\end{aligned}$$

where \mathcal{Z}_0 is the partition function of the pure system and $\langle \dots \rangle_0 = \frac{1}{\mathcal{Z}_0} \sum \dots e^{-\beta H_0}$ the unperturbed thermodynamic averages. The average free energy reads

$$\bar{F} \simeq F_0 - k_B T \sum_{(i,j)} \overline{\delta K_{ij}} \langle \varepsilon_{ij} \rangle_0 - \frac{k_B T}{2} \sum_{\substack{(i,j) \\ (k,l)}} \overline{\delta K_{ij} \delta K_{kl}} \left[\langle \varepsilon_{ij} \varepsilon_{kl} \rangle_0 - \langle \varepsilon_{ij} \rangle_0 \langle \varepsilon_{kl} \rangle_0 \right] + \dots \quad (27)$$

Since \bar{K} was defined as the average coupling, it implies that $\overline{\delta K_{ij}} = 0$. Therefore the first-order term of the expansion vanishes and the free energy difference between random and pure systems is proportional to the variance of disorder $\sigma^2 = \overline{\delta K_{ij} \delta K_{kl}}$ and to the unperturbed energy-energy connected correlation. In the continuum limit, the free energy difference (26) becomes

$$\Delta F \simeq -\frac{k_B T V}{2} \int_V \sigma^2(\vec{r}) \left[\langle \varepsilon(0) \varepsilon(\vec{r}) \rangle_0 - \langle \varepsilon \rangle_0^2 \right] d^d \vec{r}.$$

Away from the critical point, the unperturbed energy-energy correlation function decays exponentially as $e^{-r/\xi}$. Therefore, the integration domain is essentially restricted to the correlation volume ξ^d instead of the volume V of the system. Inside this volume, the system develops critical correlation functions:

$$\langle \varepsilon(0) \varepsilon(\vec{r}) \rangle_0 - \langle \varepsilon \rangle_0^2 \underset{r \gg 1}{\sim} r^{-2x_\varepsilon}, \quad (28)$$

where x_ε is the scaling dimension of the energy density. In the case of uncorrelated disorder, i.e. when $\sigma^2(\vec{r}) = \sigma^2 \delta(\vec{r})$, the fluctuations scale as $\sigma^2(\vec{r}) = b^{-d} \sigma^2(\vec{r}/b)$. As a consequence, the difference of free energy density Δf reads

$$\Delta f \simeq b^{-2x_\varepsilon} \int_{(\xi/b)^d} \sigma^2(\vec{u}) \left[\langle \varepsilon(0) \varepsilon(\vec{u}) \rangle_0 - \langle \varepsilon \rangle_0^2 \right] d^d \vec{u}.$$

The dependence of the integral on the correlation length is removed by setting $b = \xi$. In the neighbourhood of the critical point, the difference of free energy density behaves as

$$\Delta f \sim \xi^{-2x_\varepsilon} \underset{T \rightarrow T_c}{\sim} |T - T_c|^{2(d\nu-1)},$$

where the relations $\xi \sim |T - T_c|^{-\nu}$ and $x_\varepsilon = d - 1/\nu$ have been used. On the other hand, the unperturbed free energy density is singular:

$$f_0 \sim \xi^{-d} \underset{T \rightarrow T_c}{\sim} |T - T_c|^{\nu d}.$$

The dominant scaling behaviour of the random free energy is dictated by disorder if

$$2x_\varepsilon < d \Leftrightarrow \alpha > 0$$

when the hyperscaling relation $\alpha = 2 - \nu d$ holds. Since the free energy is the generating function of all thermodynamic quantities, the critical exponents will be changed if $\alpha > 0$. In the opposite case, i.e. $\alpha \leq 0$, the expansion (26) has to be extended to highest orders. This result, known as Harris criterion, also constrains the specific-heat exponent at the random fixed point. Strengthening the disorder by a small amount is equivalent to adding a weak perturbation $\sum_{(i,j)} \delta K_{ij} \varepsilon_{i,j}$ to the random fixed point. According to the Harris criterion, the latter is expected to be unstable if the specific heat exponent of the random system is positive. The stability of the random fixed point requires ^[122]

$$\alpha \leq 0 \Leftrightarrow \nu \geq 2/d.$$

The particular distribution of random exchange couplings or impurities, either fixed number or fixed average, was shown to be irrelevant ^[9].

1.2.3.2. Critical behaviour at the two-dimensional random fixed point

According to the Harris criterion, the universality class of the two-dimensional q -state Potts model in the second-order regime $q < 4$ is expected to be affected by the introduction of disorder in the cases $q = 3$ and $q = 4$, or more generally for $2 < q \leq 4$ in the Fortuin-Kasteleyn representation. The case of the Ising model, which corresponds to a marginal situation $\alpha = 0$, was widely debated in the literature. It is now established that the disorder is marginally irrelevant and manifests itself only by logarithmic corrections and a double logarithmic behaviour of the specific heat ^[444, 445, 337, 446]:

$$\chi \sim t^{-7/4} (\ln |t|)^{7/8}, \quad C \sim \frac{1}{g_0} \ln \left[1 + \frac{4g_0}{\pi} \ln \frac{1}{|t|} \right],$$

where g_0 depends on the strength of disorder and t denotes the reduced temperature $T - T_c$. These theoretical predictions were extensively tested by numerical simulations ^[143, 2, 3, 358] and high-temperature series expansions ^[429]. In the cases $2 < q \leq 4$, the first analytical studies, based on the Migdal-Kadanoff real-space Renormalisation Group procedure ^[302, 17] or the renormalisation on hierarchical lattices ^[150] confirmed the prediction of the Harris criterion and suggested an evolution of the critical exponents with the number of states q .

The full calculation of these critical exponents by Renormalisation Group techniques was pioneered by Ludwig ^[336]. Several difficulties had to be overcome to reach this result. First, the calculation of the average of the free energy is more complicated in the case of random system because the expression of F involves the logarithm of the partition function. Equation (26) gives an example of such a calculation up to second order. A much more convenient approach is to make use of the identity ^[175]

$$\bar{F} = -k_B T \overline{\ln \mathcal{Z}} = \lim_{n \rightarrow 0} \frac{\overline{\mathcal{Z}^n} - 1}{n} \quad (29)$$

known as replica trick. Forgetting for a moment that n is not an integer, \mathcal{Z}^n can be interpreted as the partition function of n uncoupled replicas of the system with the

same perturbed couplings K_{ij} . The average over randomness will couple these replicas. Consider again the Hamiltonian (25). The average partition function of n replicas is in the limit of weak disorder:

$$\begin{aligned} \overline{\mathcal{Z}^n} &= \sum_{\sigma^{(1)}, \dots, \sigma^{(n)}} \overline{e^{\sum_{\alpha=1}^n [H_0(\sigma^{(\alpha)}) + \sum_{(i,j)} \delta K_{ij} \varepsilon_{ij}(\sigma^{(\alpha)})]}} \\ &\simeq \mathcal{Z}_0^n \left[1 + \sum_{\alpha=1}^n \sum_{(i,j)} \overline{\delta K_{ij}} \langle \varepsilon_{ij}(\sigma^{(\alpha)}) \rangle_0 \right. \\ &\quad \left. + \frac{1}{2} \sum_{\alpha, \beta=1}^n \sum_{\substack{(i,j), \\ (k,l)}} \overline{\delta K_{ij} \delta K_{kl}} (\langle \varepsilon_{ij}(\sigma^{(\alpha)}) \varepsilon_{kl}(\sigma^{(\beta)}) \rangle_0 - \langle \varepsilon_{ij}(\sigma^{(\alpha)}) \rangle_0 \langle \varepsilon_{kl}(\sigma^{(\beta)}) \rangle_0) + \dots \right]. \end{aligned} \quad (30)$$

If $\overline{\delta K_{ij}} = 0$, the coupling between replicas is proportional to the variance of disorder. Since the replicas were uncorrelated in the pure model, the unperturbed connected correlation $\langle \varepsilon_{ij}(\sigma^{(\alpha)}) \varepsilon_{kl}(\sigma^{(\beta)}) \rangle_0 - \langle \varepsilon_{ij}(\sigma^{(\alpha)}) \rangle_0 \langle \varepsilon_{kl}(\sigma^{(\beta)}) \rangle_0$ vanishes unless $\alpha = \beta$. The pure Hamiltonian being the same for all replicas ⁽⁶⁾, the partition function is

$$\overline{\mathcal{Z}^n} \simeq \mathcal{Z}_0^n \left[1 + \frac{n}{2} \sum_{\substack{(i,j), \\ (k,l)}} \overline{\delta K_{ij} \delta K_{kl}} (\langle \varepsilon_{ij}(\sigma) \varepsilon_{kl}(\sigma) \rangle_0 - \langle \varepsilon_{ij}(\sigma) \rangle_0 \langle \varepsilon_{kl}(\sigma) \rangle_0) + \dots \right]$$

The last step is to assume that this expansion, obtained with an integer number of replicas, is also true for real values of n in order to be allowed to use the replica trick (29). As expected, the expansion (27) is recovered:

$$\begin{aligned} \lim_{n \rightarrow 0} \frac{\overline{\mathcal{Z}^n} - 1}{n} &\simeq \lim_{n \rightarrow 0} \left[\frac{\overline{\mathcal{Z}_0^n} - 1}{n} + \frac{\mathcal{Z}_0^n}{2} \sum_{\substack{(i,j), \\ (k,l)}} \overline{\delta K_{ij} \delta K_{kl}} (\langle \varepsilon_{ij} \varepsilon_{kl} \rangle_0 - \langle \varepsilon_{ij} \rangle_0 \langle \varepsilon_{kl} \rangle_0) \right] \\ &= \overline{\ln \mathcal{Z}_0} + \frac{1}{2} \sum_{\substack{(i,j), \\ (k,l)}} \overline{\delta K_{ij} \delta K_{kl}} (\langle \varepsilon_{ij} \varepsilon_{kl} \rangle_0 - \langle \varepsilon_{ij} \rangle_0 \langle \varepsilon_{kl} \rangle_0). \end{aligned}$$

The second difficulty in the analytical study of the random Potts model is that, in contradistinction to the $O(n)$ model [225], there is no Ginzburg-Landau action for the pure Potts model with $q > 2$. However, conformal invariance constrains the various correlation functions $\langle \varepsilon_{ij}(\sigma^{(\alpha)}) \varepsilon_{kl}(\sigma^{(\beta)}) \dots \rangle_0$ that may appear in the expansion of the partition function $\overline{\mathcal{Z}^n}$. At the operator level, these constraints take the form of the Operator Product Expansion (OPE)

$$\phi_i(\vec{r}) \phi_j(\vec{r}') \xrightarrow{\vec{r}' \rightarrow \vec{r}} \sum_k \frac{c_{ijk}}{r^{x_i + x_j - x_k}} \phi_k(\vec{r}),$$

where x_i is the scaling dimension of ϕ_i . The coefficients c_{ijk} are universal quantities whose values are known for the minimal models and thus for the Potts model with $q \leq 4$.

⁽⁶⁾ This calculation is meant as a basic example. As will be discussed later (§ 1.2.3.6) the symmetry between replicas may be broken during the Renormalisation Group process.

Using these techniques together with a real-space Renormalisation Group approach, Ludwig computed the scaling behaviour of the specific heat of the random-bond Potts model [336]. The expansion parameter is $1 - x_\varepsilon$, where x_ε is the scaling dimension of the energy density in the pure system. As a consequence, the calculation holds in the neighbourhood of the Ising model for which $x_\varepsilon = 1$. The thermal exponent was calculated to two-loop order:

$$y_t = 1 - \frac{1}{2}(1 - x_\varepsilon)^2 + O((1 - x_\varepsilon)^3).$$

The expansion can be recast as a series in powers of the small parameter ⁽⁷⁾ $y = 2(1 - x_\varepsilon) = 2(y_t - 1) = \frac{\alpha}{\nu}$

$$y_t = 1 + \frac{1}{8}y^2 + O(y^3). \quad (32)$$

Finally the expression of the thermal exponents as a function of $q - 2$ may be obtained using the known expression (8) for y_t . In a similar way, the central charge was later computed to three-loop order [339]:

$$c(q) = \frac{1}{2} \left(1 + \frac{7}{4}y - \frac{9}{16}y^2 - \frac{5}{64}y^3 \right) + O(y^4). \quad (33)$$

The calculation of the magnetic scaling dimension was more involved because the first non-vanishing correction appears only at third order [165, 166, 164]:

$$x_\sigma = x_\sigma^{\text{Pure}} + \frac{\Gamma^2(-\frac{2}{3})\Gamma^2(\frac{1}{6})}{32\Gamma^2(-\frac{1}{3})\Gamma^2(-\frac{1}{6})}y^3 + O(y^4), \quad (34)$$

where x_σ^{Pure} is the magnetic scaling dimension of the pure Potts model.

A very good agreement has been achieved between the series expansions (33) and (34) and the numerical estimates of the central charge and of the magnetic scaling dimension. This was made possible by a detailed analysis of the strength of disorder r^* that minimises the scaling corrections due to the pure and percolation fixed points. r^* is expected to reflect the location of the random fixed point. It is efficiently determined by the study of the effective central charge $c(r)$. The latter can be computed by transfer matrices using the Finite-Size Scaling [67]

$$\bar{f}(L) = \bar{f}(\infty) - \frac{\pi c}{6L^2} + O\left(\frac{1}{L^4}\right) \quad (35)$$

of the free energy density on a strip of width L . In practice, the next-order term A/L^4 has to be taken into account in the interpolation. As observed by Jacobsen and

⁽⁷⁾ This parameter y is not the same as the one introduced in equation (8). The latter, that will be denoted y' here, is related to y by

$$\frac{y}{2} = \frac{2y' - 1}{y' - 2} \Leftrightarrow y' = 2\frac{1 - y}{4 - y} = \frac{2}{\pi} \arccos \frac{\sqrt{q}}{2}. \quad (31)$$

Cardy [98, 268], the effective central charge c measured in this way depends on the strength of disorder r and displays a maximum at a finite value of r which is interpreted as r^* . The apparent contradiction with Zamolodchikov's theorem, that states that the effective central charge should decay along the renormalisation flow, is due to the fact that this theorem holds only for unitary conformal theories. As shown on figure 16, the optimal disorder strength r^* depends on the number of states q as $r^* \sim \ln q$. The value $c(r^*)$ of the central charge at this maximum is in excellent agreement with the series expansion (33) (figure 17). The data for a number of states $q > 4$, unreachable by RG calculations, seem to fall nicely on the same smooth curve as the values in the regime $q \leq 4$ (figure 17). Based on data for large numbers of states, a simple law $c(q) = \frac{1}{2} \ln_2 q$, was conjectured [270]. The comparison with the data is presented on figure 17.

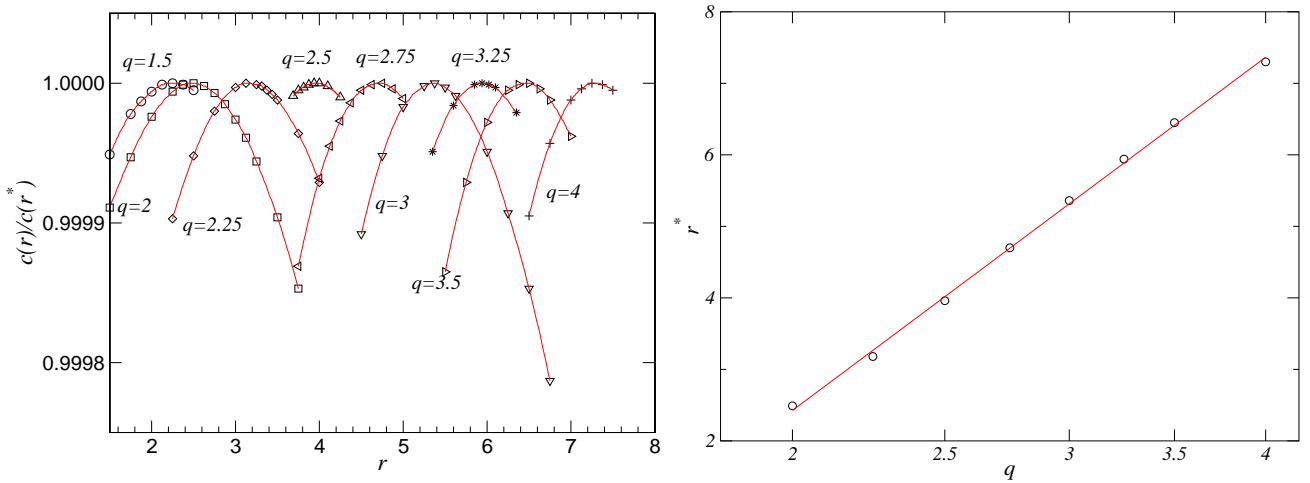


Figure 16 : Effective central charge $c(r)$ of the random Potts model as a function of the strength of disorder r for several numbers of states q . To make comparison easier, the data were normalised by dividing them by their value at the maximum r^* . On the right, the location r^* of the maximum is plotted versus q in a logarithmic scale.

The more accurate estimates of the magnetic scaling dimension x_σ were obtained from the exponential decay of the spin-spin correlation functions on the strip, accessible by transfer matrices [98, 268, 111, 112, 270], and by interpolating the magnetisation profile in a square calculated by Monte Carlo simulations with the conformal prediction [111]. As can be seen on figure 18, a good agreement is achieved with the series expansion (34) (see also table 4). The same result was obtained for bond-diluted Potts models [115] and for different distributions of exchange couplings in the random-bond case [397, 112]. As for the central charge, the estimates of the magnetic scaling dimension that were obtained in the regime $q > 4$ and discussed in § 1.2.2.2. seem to fall on the same curve as the data for $q \leq 4$ (figure 18). The surface magnetic exponent was shown to follow the same trend [406], going from $\beta_1 = 0.542(10)$ for $q = 3$ to $0.597(23)$ for $q = 8$. We may thus conclude that the (yet unknown) effective theory describing the random Potts model depends on the number of states q in a way that is not related to the order of the phase transition in the pure model.

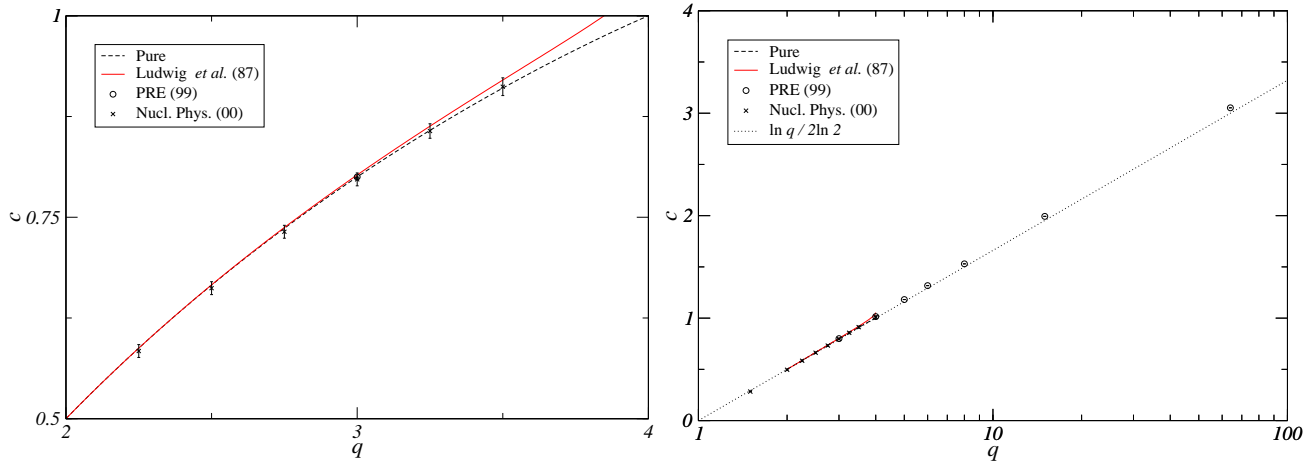


Figure 17 : Central charge c of the random Potts model. The dashed curve corresponds to the pure model. The red curve is the series expansion (33). The symbols correspond to numerical estimates as published in 111 (PRE 99) and 112 (Nucl. Phys. 00).

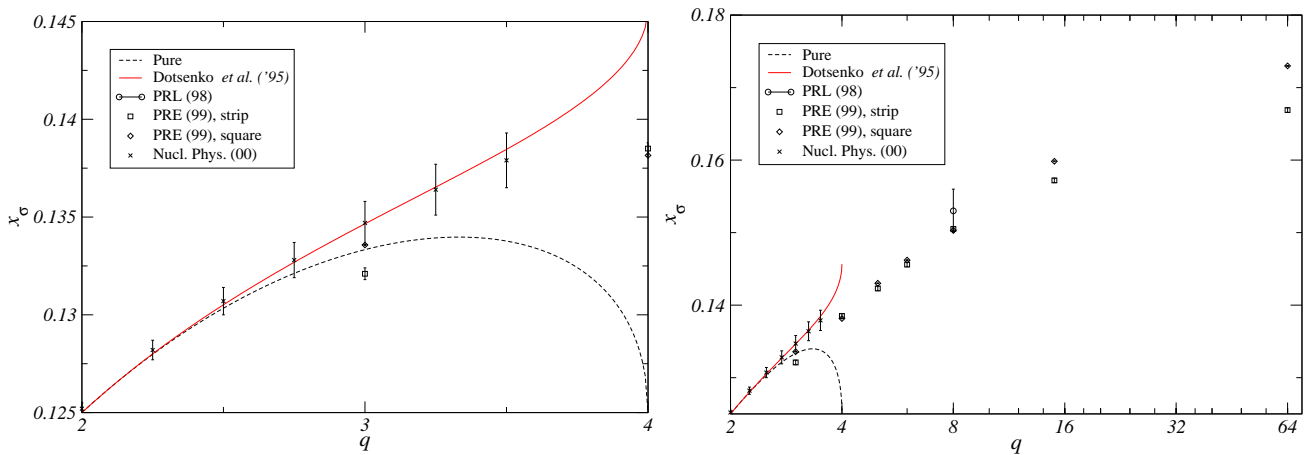


Figure 18 : Magnetic scaling dimension x_σ of the random Potts model in the regime where the pure system undergoes a continuous transition. The dashed curve corresponds to the pure model. The red curve is the series expansion (34). The symbols correspond to numerical estimates as published in 110 (PRL 98), 111 (PRE 99) and 112 (Nucl. Phys. 00).

The thermal scaling dimension y_t is more difficult to estimate numerically [268, 397, 406]. Moreover, a comparison with the series expansion (32) requires a high accuracy because y_t remains very close to the value $y_t = 1$ of the Ising model.

Authors	Year	Numerical technique	$q = 3$	$q = 4$
Wiseman and Domany [490]	1995	Monte Carlo		0.125(2)
Kim [300]	1996	Monte Carlo	0.133(6)	
Picco [413]	1996	Monte Carlo	0.1337(7)	
Cardy and Jacobsen [98,268]	1997-98	Transfer matrix	0.13467(13)	0.1396(5)
Olson and Young [397]	1999	Monte Carlo	0.1345(20)	0.1435(35)
Chatelain and Berche [111]	1999	Transfer matrix	0.1321(3)	0.1385(3)
		Monte Carlo	0.13357(3)	0.13815(4)
Chatelain and Berche [112]	2000	Transfer matrix	0.1347(11)	
Chatelain, Berche, Shchur [115]	2001	Transfer matrix	0.13495(6)	0.1419(1)

Tableau 4 : Magnetic critical exponents β/ν obtained by numerical simulations for the $q = 3$ and $q = 4$ two-dimensional random Potts models.

1.2.3.3. Three-dimensional random fixed point

Because the specific heat exponent α of the three-dimensional Ising model is positive ($\alpha \simeq 0.1103(1)$), the Harris criterion predicts a change of universality class upon the introduction of disorder. The first Renormalisation Group studies of the $O(n)$ model in dimension $d = 4 - \varepsilon$ predicted a new fixed point for $1 < n \leq 4 - 4\varepsilon$ but were inconclusive in the case $n = 1$ corresponding to the Ising model [225, 333]. Shortly after, it was understood that the random fixed point was reachable with a series expansion in powers of $\sqrt{\varepsilon}$, and not of ε , when $n = 1$ [215]. The critical exponents were estimated to be $\eta \simeq -0.0094$ and $\nu \simeq 0.6277$ for the three-dimensional diluted Ising model. The calculation was extended up to six-loop order [410]. As in the two-dimensional case, an agreement between analytical predictions and numerical estimations was not reached before the second half of the 1990s. No change of universality class could be observed in the first Monte Carlo simulations [308]. The magnetic critical exponent β was later shown to be larger ($\beta \simeq 0.39(3)$) than in the pure model ($\beta \simeq 0.304(3)$) [75]. Because of strong scaling corrections, the effective critical exponents that were obtained numerically showed a dependence on the strength of disorder [244]. Accurate measurements were achieved in the case of the site-diluted Ising model by Ballesteros *et al.* [35]. By a careful analysis of the data, the following values were obtained:

$$\frac{\beta}{\nu} \simeq 0.519(3), \quad \frac{\gamma}{\nu} \simeq 1.963(5), \quad \nu \simeq 0.6839(53) \quad (36)$$

in excellent agreement with RG calculations at six-loop order [410]. Strong scaling corrections were observed and the exponent of the sub-dominant one was estimated to be $\omega \simeq 0.37(6)$. Compatible values were reported at the concentration $p = 0.8$ [91]. The site-diluted Ising model was later studied by Murtazaev *et al.* [384, 377] and Prudnikov *et al.* [425]. We studied the bond-diluted Ising model [58, 59, 54]. The critical line, joining the pure fixed point for $p = 1$ to the percolation fixed point $p_c \simeq 0.2488$, was estimated

from the location of the maximum of the magnetic susceptibility (figure 19). The strong cross-overs with the pure and percolation fixed points, make extremely difficult the estimation of the critical exponents by the Finite-Size Scaling technique. We had resort to an analysis of the temperature behaviour in the neighbourhood of the critical line and estimated the critical exponents:

$$\frac{\beta}{\nu} \simeq 0.515(5), \quad \frac{\gamma}{\nu} \simeq 1.97(2), \quad \nu \simeq 0.68(2).$$

Even though less precise, these values are compatible with (36). A larger-scale Monte Carlo simulation allowed for the determination of the exponents by Finite-Size scaling [229]:

$$\frac{\beta}{\nu} \simeq 0.518(3), \quad \nu \simeq 0.683(2).$$

The exponent $\gamma \simeq 1.305(5)$ was obtained by series expansion. Recent Monte Carlo estimations of the critical exponents for the random-bond three-dimensional Ising model showed a good agreement with the results previously obtained for the site-diluted and bond-diluted model [193, 463, 499].

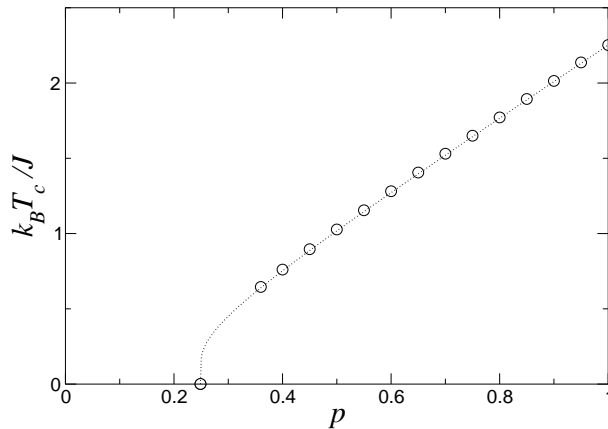


Figure 19 : Critical line of the bond-diluted three-dimensional Ising model as a function of the concentration p of bonds. The dashed curve is the result of an effective-medium approximation [472, 471]. Its intersection with the x -axis corresponds to bond-percolation.

For a number of states $q > 2$, the pure three-dimensional Potts model undergoes a first-order phase transition. As previously discussed, a second-order regime is induced at large disorder (§ 1.2.2.3.). In the very same way as the two-dimensional random Potts model, the critical exponent β/ν in the second-order regime displays a smooth increase with the number of states q , regardless of the order of the transition of the pure model.

1.2.3.4. Aperiodic and irregular graphs in the second-order regime

1.2.3.4.1. Potts models on irregular graphs

In the spirit of the Harris and Luck criterions, a relevance criterion was established for random graphs [281]. We give here another derivation, much closer to the presentation of the Harris criterion given above. For a given graph, the Potts Hamiltonian is written as

$$-\beta H = \sum_{i,j} A_{ij} \varepsilon_{ij},$$

where A is the so-called connectivity matrix whose elements A_{ij} are equal to one if the sites i and j are nearest neighbours on the graph and zero otherwise. Introduce the connectivity matrix $A^{(0)}$ of the closest regular lattice and denote $\delta A_{ij} = A_{ij} - A_{ij}^{(0)} \in \{-1; 0; 1\}$. In the limit of small differences, the average free energy can be expanded in a way similar to (26)

$$\begin{aligned} \bar{F} &\simeq -k_B T \ln \left[\sum_{\sigma} e^{\sum_{i,j} A^{(0)} \varepsilon_{ij}} \left(1 + \sum_{i,j} \delta A_{ij} \varepsilon_{ij} + \frac{1}{2} \left[\sum_{i,j} \delta A_{ij} \varepsilon_{ij} \right]^2 + \dots \right) \right] \\ &\simeq F_0 - k_B T \sum_{i,j} \overline{\delta A_{ij}} \langle \varepsilon_{ij} \rangle_0 - \frac{k_B T}{2} \sum_{\substack{i,j \\ k,l}} \overline{\delta A_{ij} \delta A_{kl}} \left[\langle \varepsilon_{ij} \varepsilon_{kl} \rangle_0 - \langle \varepsilon_{ij} \rangle_0 \langle \varepsilon_{kl} \rangle_0 \right] + \dots \end{aligned}$$

With an appropriate choice of $A^{(0)}$, the average difference $\overline{\delta A_{ij}}$ vanishes on average. To evaluate the second-order term, the approximation

$$\sum_{i,j} \delta A_{ij} \varepsilon_{ij} \simeq \sum_i \left[\sum_j \delta A_{ij} \right] \left[\sum_j \varepsilon_{ij} \right] = \sum_i \delta A_i \varepsilon_i$$

is used. The sum $\sum_j \varepsilon_{ij}$ is the total energy on site i . Since $\sum_j A_{ij}$ is the number of neighbours of site i , $\sum_j \delta A_{ij} = \delta A_i$ is the variation of this number with respect to the regular lattice. As a consequence, the second-order term of the expansion of the free energy involves the product of the fluctuations of the number of neighbours with the energy-energy correlation function:

$$\bar{F} \simeq F_0 - \frac{k_B T}{2} \sum_{i,k} \overline{\delta A_i \delta A_k} \left[\langle \varepsilon_i \varepsilon_k \rangle_0 - \langle \varepsilon_i \rangle_0 \langle \varepsilon_k \rangle_0 \right].$$

The latter behaves in the neighbourhood of the critical point as (28). The former is assumed to decay algebraically as

$$\overline{\delta A_i \delta A_k} \underset{\|\vec{r}_i - \vec{r}_k\| \gg 1}{\sim} \|\vec{r}_i - \vec{r}_k\|^{-a/d_h}.$$

i.e. the random graph corresponds to a wandering exponent $\omega = 1 - a/2d_h$ where d_h is its Hausdorff dimension. In the continuum limit, sums are replaced by integrals but since $\sum_i 1 = N = L^{d_h}$ and not L^d , the integrals should be corrected by a power $L^{d_h/d}$. Under rescaling, the free energy behaves therefore in the continuum limit as

$$\bar{f} = f_0 - \frac{k_B T}{2} \left[b^{-a/d_h - 2x_\varepsilon + d} \int_{(\xi/b)^d} \overline{\delta A(0) \delta A(\vec{r})} r^{-2x_\varepsilon} d^d \vec{r} \right]^{d_h/d}.$$

The choice $b = \xi$ suppresses the dependence on ξ of the integral and leads to $\bar{f} \sim \xi^{(-a-2x_\varepsilon+d)d_h/d}$. Comparing to the behaviour $f_0 \sim \xi^{-d_h}$ of the unperturbed free energy, it can be concluded that the perturbation is relevant if

$$-a/d_h - 2x_\varepsilon + d > -d \Leftrightarrow \frac{a}{d_h} < \frac{2}{\nu}.$$

As discussed in § 1.2.2.4., the fluctuations of the coordination number scale as $L^{(d-1)/2}$ on a Voronoi-Delaunay random graph [96, 281]. In the notations used above, this corresponds to $a/d_h = (d-1)$. As a consequence, the perturbation is expected to be relevant if $\nu < 2/(d-1)$. In the two-dimensional case, this inequality is satisfied by Potts models with $q = 2, 3$ and 4 states (see table 1). The three-state Potts model was studied by Lima [324]. Interestingly, in the three-dimensional case, the Ising model, which is the only Potts model that undergoes a continuous transition, seems to fall in the same universality class as the random-bond Ising model [279, 280].

In the case of Φ^3 gravity graphs, the wandering exponent was estimated numerically to be $\omega \simeq 0.751(9)$ [281]. As a consequence, the perturbation is relevant if $\nu < 4$ which is realised by all Potts models with $q = 2, 3$ and 4 states. The cases $q = 2$ and $q = 4$ were studied numerically [271]. As expected, the critical exponents are different from the pure models: $\beta/\nu d_h \simeq 0.10(1)$ and $\alpha/\nu d_h \simeq -0.32(1)$ for $q = 2$ and $\beta/\nu d_h \simeq 0.11(1)$ and $\alpha/\nu d_h \simeq -0.16(1)$ for $q = 4$.

On the octagonal quasi-periodic tiling, Monte Carlo simulations showed that the universality class of the Ising model is not affected whereas the three-state Potts model displays new critical exponents: $\nu \simeq 0.85(2)$ and $\gamma \simeq 1.40(5)$ [313].

1.2.3.4.2. Aperiodic perturbation of the Potts model

Consider now the case of inhomogeneous but deterministic couplings K_{ij} . The main difference is that no average over randomness needs to be taken. An average coupling may still be defined as the average over the lattice: $\bar{K} = \frac{1}{2N} \sum_{(i,j)} K_{ij}$. In the limit of small variations $\delta K_{ij} = K_{ij} - \bar{K}$ of the exchange couplings, the expansion (26) of the free energy holds. Since the unperturbed average energy is uniform, i.e. $\langle \varepsilon_{ij} \rangle_0 = \langle \varepsilon \rangle_0$, the first-order term of the expansion vanishes

$$\sum_{(i,j)} \delta K_{ij} \langle \varepsilon_{ij} \rangle_0 = \sum_{(i,j)} \delta K_{ij} \langle \varepsilon \rangle_0 = 0.$$

In the continuum limit, the free energy becomes

$$F \simeq F_0 - \frac{k_B T}{2} \int_V \delta K(\vec{r}) \delta K(\vec{r}') [\langle \varepsilon(\vec{r}) \varepsilon(\vec{r}') \rangle_0 - \langle \varepsilon \rangle_0^2] d^d \vec{r} d^d \vec{r}' + \dots \quad (37)$$

Restrict now the discussion to the aperiodic sequences introduced in section § 1.2.2.5.2.. The local fluctuations of the exchange couplings are quite complicated. Assume that they can be replaced by spatially averaged quantities:

$$\delta K(0) \delta K(L) \simeq \left[\frac{1}{L} \sum_x \delta K(x) \right]^2 \simeq (\rho - \rho_\infty)^2 \sim L^{2(\omega-1)},$$

where the definition (24) of the wandering exponent ω was used. The integration domain of (37) is restricted to the correlation volume ξ^d by the exponential decay of the energy-energy correlation function. Inside this volume, the correlation decays algebraically as

(28) so the difference of free energy density Δf between the perturbed and pure models can be written as

$$\Delta f \sim b^{2(\omega-1)-2x_\varepsilon+2} \int_{(\xi/b)^d} \delta K(x) \delta K(x') r^{-2x_\varepsilon} dx dy.$$

The dependence of the integral on the correlation length is removed by the choice $b = \xi$ so

$$\Delta f \sim \xi^{2+2(\omega-1)-2x_\varepsilon} \underset{T \rightarrow T_c}{\sim} |T - T_c|^{-\nu(\omega+2+2/\nu)},$$

where the relations $\xi \sim |T - T_c|^{-\nu}$ and $x_\varepsilon = d - 1/\nu$ were used. Comparing with the singular behaviour $f_0 \sim \xi^{-2} \underset{T \rightarrow T_c}{\sim} |T - T_c|^{2\nu}$ of the unperturbed free energy, the dominant scaling behaviour will be affected by the aperiodic perturbation if [335, 259, 334]

$$1 - \omega < 2 - x_\varepsilon = 1/\nu \Leftrightarrow \omega > 1 - 1/\nu. \quad (38)$$

In the case of the Ising model, for which $\nu = 1$, the aperiodic sequence is relevant if $\omega > 0$. For the q -state Potts model, the perturbation is relevant when $\omega > \omega_c$ with $\omega_c = -1/5$ for $q = 3$ and $\omega_c = -1/2$ for $q = 4$.

As discussed in § 1.2.2.5., the critical exponents of the McCoy-Wu model, i.e. the layered random-bond Ising model, are known exactly. The calculations have been made possible by the equivalence in the extreme anisotropic limit of the transfer matrix with the evolution operator of a quantum Ising chain in a transverse field. The latter can then be studied by the Ma-Dasgupta real-space Renormalisation Group. The critical exponents differ from the pure Ising model ($\nu = 1$) as predicted by the Luck criterion with a wandering exponent $\omega = 1/2$. The same method was applied to the generalisation of the McCoy-Wu model to three and four-state Potts models by Senthil and Majumdar [443]. The Luck criterion predicts a new universality class in both cases. Senthil *et al.* showed that the critical exponents are the same as in the original McCoy-Wu model. In contradistinction to the homogeneous random Potts model, the critical exponents do not depend on the number of states q . We confirmed this result by means of Density Matrix Renormalisation Group (DMRG) [100]. The surface exponents β_1 were shown to be equal to $\beta_1 = 1/2$ for all values of q .

The influence of aperiodic sequences was studied only in the case of the Ising model and not for $q = 3$ or 4 states.

1.2.3.5. Multifractality at the random fixed-point

1.2.3.5.1. Non self-averaging thermodynamic quantities

In random systems, thermodynamic quantities are the result of two different averages: first an average over thermal fluctuations, denoted $\langle \dots \rangle$ in this thesis and second an average over disorder realisations $\overline{\dots}$. In the case of the random-bond Potts model, the average spin-spin correlation function reads for example

$$\overline{C(\vec{r})} = \overline{\langle \sigma(0)\sigma(\vec{r}) \rangle} = \int \langle \sigma(0)\sigma(\vec{r}) \rangle_{K_{ij}} \prod_{(i,j)} \wp(K_{ij}) dK_{ij},$$

where $\wp(K_{ij})$ is the probability distribution of the random bonds. The correlation $C(\vec{r})$ may decay very differently in two independent disorder realisations. Indeed, for some of them, a higher density of strong couplings might be found in some regions of the lattice, and, as a result, spins will be much strongly correlated. These rare events can even dominate the average over randomness and dictate the behaviour of the average decay of the correlation function. A simple example is provided by the random Ising chain [152]. The spin-spin correlation function decays as

$$\overline{C(r)} = \overline{\left[\prod_{i=1}^r \tanh K_i \right]} = \left[\overline{\tanh K} \right]^r$$

if the couplings are independent random variables. The average spin-spin correlation function therefore decays as $e^{-r/\xi_{av}}$ with an average correlation length $\xi_{av} = -\left[\overline{\ln \tanh K} \right]^{-1}$. Consider now the quantity

$$\overline{\ln C(r)} = \overline{\left[\sum_{i=1}^r \ln \tanh K_i \right]} = r \overline{\ln \tanh K}.$$

The function $e^{\overline{\ln C(r)}}$, obviously identical to the average correlation function in the absence of disorder, decays exponentially but with a different correlation length $\xi_{typ} = -\left[\overline{\ln \tanh K} \right]^{-1}$. In contradistinction to $C(r)$, the probability distribution $\wp_r(\ln C)$ of $\ln C(r)$ is predicted to be Gaussian by the Central Limit Theorem in the thermodynamic limit. Since the maximum of a Gaussian is equal to its average, $\overline{\ln C}$ is the most probable value. For a single disorder realisation, the typical correlation is therefore $e^{\overline{\ln C(r)}}$ and not $\overline{C(r)}$. Unlike $\wp_r(\ln C)$, the probability distribution $\wp_r(C)$ of the correlation displays a long tail:

$$\wp_r(C) = \wp_r(\ln C) \left| \frac{d \ln C}{dC} \right| = \frac{1}{\sqrt{2\pi\sigma_{\ln C}^2}} e^{-\frac{(\ln C - \overline{\ln C})^2}{2\sigma_{\ln C}^2}}.$$

This distribution is plotted in the case of the two-dimensional random-bond Potts model on figure 20. The long tail corresponds to rare events where the connected correlation decays faster because of a larger number of strong couplings. As a consequence of the asymmetry of the probability distribution, the typical correlation, i.e. the most probable value, may be different from the average one. A thermodynamic quantity is said to be self-averaging if its typical and average values are identical.

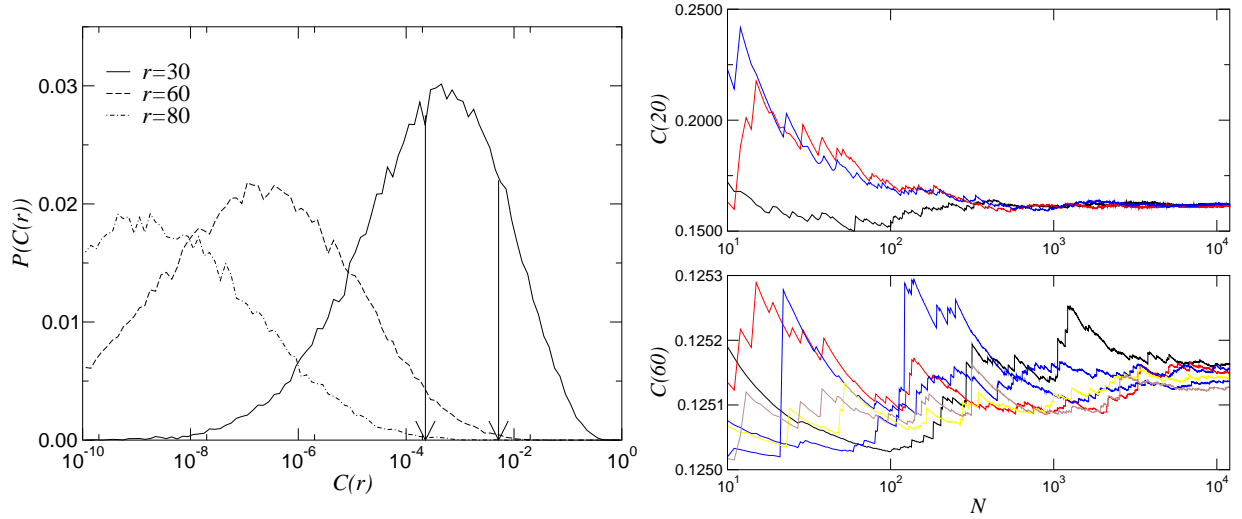


Figure 20 : On the left, probability distribution $\wp_r(C)$ of the spin-spin correlation function in the random-bond Potts model for three different distances $r = 30, 60$ and 80 . Note that the scale is logarithmic on the x -axis. On the right, evolution of the average spin-spin correlation function versus the number of disorder realisations used to perform the average. Above, the graph corresponds to a distance $r = 20$ and below, to $r = 60$.

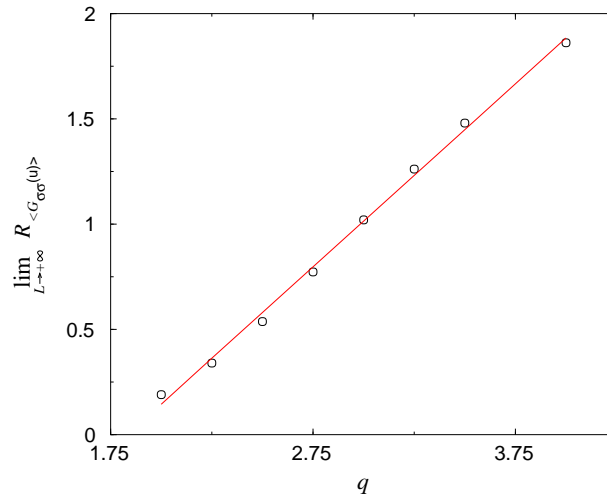


Figure 21 : Square width R_C of the average spin-spin correlation function of the random Potts model versus the number of states q .

To be more quantitative, one may consider the square width of the probability distribution of any quantity X

$$R_X = \frac{\overline{\langle X \rangle^2} - \overline{\langle X \rangle}^2}{\overline{\langle X \rangle}^2}$$

which is expected to vanish in the thermodynamic limit for a self-averaging quantity. A non-zero ratio indicates that the observable $\langle X \rangle$ fluctuates from sample-to-sample even

in the thermodynamic limit. In random ferromagnets, non vanishing ratios were first reported in the case of the random Ashkin-Teller model by Wiseman and Domany [49¹] and then extensively studied by Aharony and Harris [8]. As expected when disorder is irrelevant, the observables of the two-dimensional random Ising model were shown to be self-averaging, even at the critical point [46⁵]. In contradistinction, disorder is relevant for the $q > 2$ -state Potts model and, as can be seen on figure 21, spin-spin correlation functions for example are non self-averaging.

As emphasised by Derrida and Hilhorst, this may have dramatic consequences on numerical simulations [15²]. Indeed, during any numerical simulation, the average over disorder is usually approximated by a sum over a few thousands of disorder realisations only. If this number is too small, the numerical estimate of a non self-averaging quantity may be closer to the typical value than the average one, causing a systematic deviation. The problem is usually believed to be circumvented by considering a cumulant expansion. In the case of the correlation function $C(r)$, the latter reads

$$\overline{C} = e^{\overline{\ln C}} = \sum_{p=0}^{+\infty} \frac{1}{p!} \overline{[\ln C]^p} = e^{\overline{\ln C} + \frac{1}{2} [\overline{(\ln C)^2} - \overline{\ln C}^2] + \dots}.$$

Since the probability distribution of $\ln C$ is Gaussian in the one-dimensional case and not far from such a distribution in higher dimensions, the cumulants $\overline{[\ln C - \overline{\ln C}]^p}$ are small for $p > 2$ and thus the expansion is expected to converge rapidly. The flaw in this reasoning is to consider that the observable $\ln C$ is sampled by the simulation with a Gaussian distribution. The independent random variables of the system are the exchange couplings K_{ij} . To each disorder realisation $\{K_{ij}\}$ is associated a correlation function $C_{\{K_{ij}\}}(r)$. The problem is now that rare disorder realisations may induce weak correlation functions with a dominant contribution. These rare events may be undersampled by the numerical simulation. If this is the case, the transformed random variables $\ln C_{\{K_{ij}\}}$ will not be distributed according to a Gaussian law but to an asymmetric deformed one with too low probabilities in the region corresponding to these rare events. There is no way to circumvent undersampling by a simple transformation of variables.

1.2.3.5.2. Multifractal spectrum of random Potts models

As a consequence of the absence of self-averaging, the different moments $\overline{\langle X \rangle^n}^{1/n}$ of a quantity X take different values depending on the order n . In the example of the random Ising chain, the moments of the spin-spin correlation function reads

$$\overline{[C(r)]^n}^{1/n} = \overline{\tanh^n K}^{r/n}.$$

An infinite set of correlation lengths $\xi_n = -n / \overline{\ln \tanh^n K}$ can thus be defined. The average one corresponds to $n = 1$ while the typical one is recovered in the limit $n \rightarrow 0$. In the case of the two-dimensional random Potts model, Ludwig showed that these correlation lengths diverge as the critical temperature is approached, with the same exponent ν (at two-loop order). However, the algebraic decay of the different moments of the spin-spin correlation functions involve independent scaling dimensions $2x_\sigma(n)$:

$$\overline{\langle \sigma(0)\sigma(\vec{r}) \rangle^n}^{1/n} \underset{T=T_c, r \gg 1}{\sim} r^{-2x_\sigma(n)}.$$

In contradistinction to the fixed point of a pure ferromagnet which is usually characterised by two scaling dimensions y_t and y_h , the random fixed point possesses an infinite set of independent scaling dimensions $x_\sigma(n)$, called multifractal exponents. In the neighbourhood of the $q = 2$ Ising model, a series expansion of these exponents was computed, first to one-loop order [338] and then to two-loop [321,322]:

$$x_\sigma(n) = x_\sigma^{\text{Pur}} - \frac{n-1}{16} \left\{ y + \left[\frac{11}{12} - 4 \ln 2 + \frac{n-2}{24} \left(33 - \frac{29\pi}{\sqrt{3}} \right) \right] \frac{y^2}{2} \right\} + \mathcal{O}(y^3), \quad (39)$$

where $y = \alpha/\nu$. In the case of the Ising model, i.e. $q = 2$ and $y = 0$, the scaling dimensions $x_\sigma(n)$ are independent of the order n of the moment, as expected since disorder is marginally irrelevant at the pure fixed point. However, the logarithmic corrections still depend on n [337]:

$$\overline{\langle \sigma(0)\sigma(r) \rangle^n}^{1/n} \sim r^{-1/4} (\ln r)^{(n-1)/8}.$$

Numerical calculations using transfer matrices confirmed that behaviour [320].

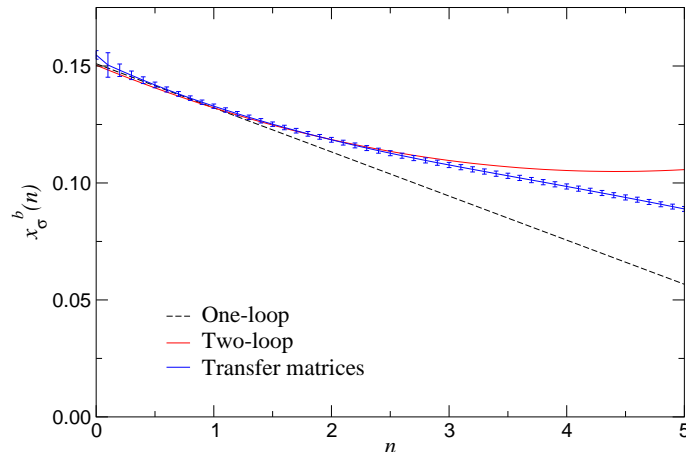


Figure 22 : Multifractal exponents of the moments of the spin-spin correlation functions of the $q = 2.75$ -state Potts model. The continuous curves are the series expansion.

In the case of the two-dimensional random Potts model, the numerical calculations confirmed that the multifractal exponents $x_\sigma(n)$ decay more rapidly with n for larger values of the number of states q [397, 406, 112, 115]. The use of transfer matrices in the Fortuin-Kasteleyn representation, instead of Monte Carlo simulations, allowed for much more accurate estimates of the spin-spin correlations. On figure 22, the scaling dimensions $x_\sigma(n)$ of the n -th moment for $q = 2.75$ are compared to the series expansions. As the average exponent $x_\sigma = x_\sigma(1)$, the multifractal exponents evolve smoothly with the number of states q and do not allow to distinguish between the regime of second-order regime ($q > 4$) induced by disorder and the regime $q \leq 4$ (see figure 23). Moreover, it was shown numerically that these multifractal exponents are the same for several

distributions of exchange couplings, including a continuous one, and for random-bond or site-diluted Potts models. The multifractal exponents $x_\sigma^1(n)$ associated to the boundary spin-spin correlation functions follow the same trend [406].

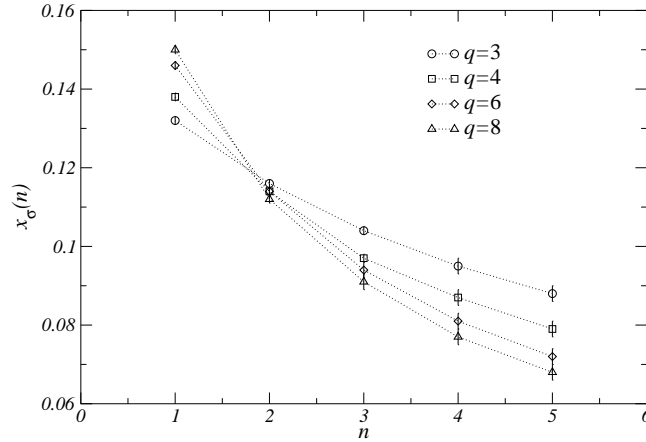


Figure 23 : Magnetic scaling dimensions of the first five moments of the spin-spin correlation function of various random Potts models.

The multifractal exponents have not been determined yet for the three-dimensional Potts model. The only known result concerns the lack of self-averaging at the critical point of the three-dimensional site-diluted Ising model [493, 492]. In the case of the Potts model on random gravity graphs, the multifractal exponents were computed exactly by Cardy [95]. This prediction has not been confronted to numerical simulations yet.

1.2.3.5.3. Legendre transform of the multifractal exponents

The multifractal exponents $x_\sigma(n)$ are fully determined by the probability distribution $\wp_r(C)$ of the spin-spin correlation function. Its n -th moment is indeed given by

$$\overline{\langle C(r) \rangle^n} = \int_0^1 \wp_r(C) C^n dC \sim \mathcal{A}_n r^{-2X(n)}, \quad (40)$$

where $X(n) = nx_\sigma(n)$. Under the change of variable $y = -\ln C$, the probability distribution $\tilde{\wp}_r(y)$ satisfies the equation $\tilde{\wp}_r(y) dy = \wp_r(C) dC$ and therefore the n -th moment can be written as

$$\int_0^{+\infty} dy e^{-ny} \tilde{\wp}_r(y) \sim \mathcal{A}_n r^{-2X(n)}.$$

The Laplace transform can be inverted via a Mellin-Fourier transform :

$$\tilde{\wp}_r(y) \sim \frac{1}{2i\pi} \int_{\delta-i\infty}^{\delta+i\infty} dn e^{ny-2X(n) \ln r + \ln \mathcal{A}_n}.$$

Let $\alpha = y/2 \ln r$ and then use the saddle-point approximation of the integrand to get

$$\tilde{\wp}_r(y) \sim \frac{1}{2i\pi} \int_{\delta-i\infty}^{\delta+i\infty} dn e^{-2 \ln r [X(n) - n\alpha]} \sim e^{-2 \ln r H(\alpha)},$$

where the multifractal spectrum $H(\alpha)$ is the Legendre transform of $X(n)$:

$$H(\alpha) = X(n^*) - \alpha n^*, \quad \alpha = \left(\frac{\partial X(n)}{\partial n} \right)_{n^*}. \quad (41)$$

In the case of the two-dimensional random Potts model, a series expansion in powers of $y = \alpha/\nu$ of this Legendre transform was calculated to one-loop order [338] and then to two-loop [321,322]. The multifractal spectrum $H(\alpha)$ was numerically reconstructed for the random eight-state Potts model from the scaling dimensions $x_\sigma(n)$ with $n = 0, 1, 2, 3,$ and 4 , estimated by means of Monte Carlo simulations [397]. A better accuracy was achieved using transfer matrices [112]. Since the spin-spin correlation functions decay exponentially along the strip, and not algebraically, the equation (40) had to be adapted. As shown on figure 24, the numerical data are in good agreement with series expansions.

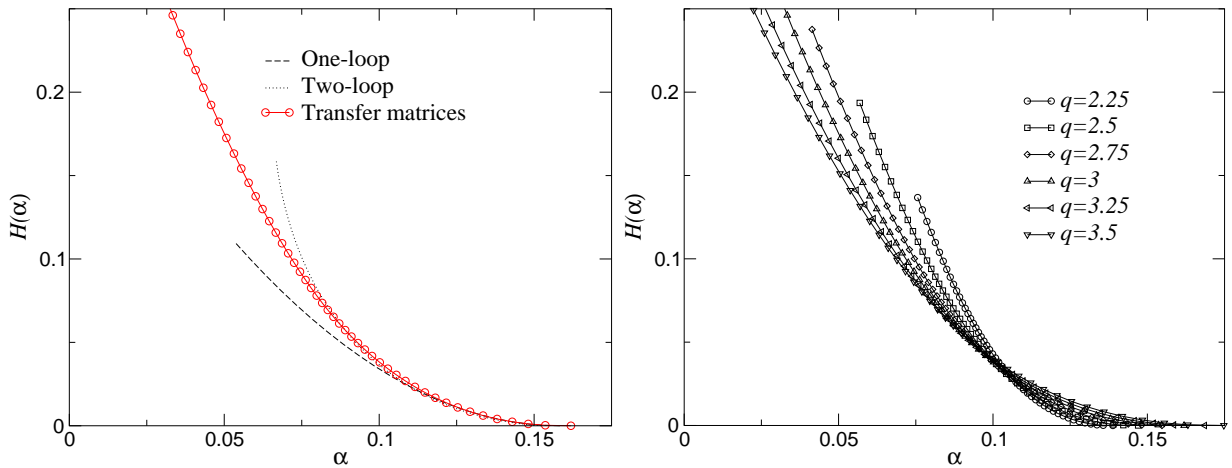


Figure 24 : On the left, multifractal spectrum $H(\alpha)$, i.e. Legendre transform of the exponents $X(n) = nx_\sigma(n)$ of the random $q = 3$ -state Potts model, versus α . The dashed curves correspond to the series expansions. On the right, the multifractal spectrum is represented for different numbers of states q .

Lack of self-averaging and multifractality are general features of random systems. They were observed for example in random resistors networks [138], diffusion-limited aggregation [224] and Anderson localisation [18, 283]. In the latter, electrons are coupled to a random potential $V(\vec{r})$. For strong enough disorder, the electronic wavefunction undergoes a transition from a delocalised state over the system to a localised state in regions of smaller potential. At the macroscopic level, the system becomes insulator. A simple model of electrons hopping over a one-dimensional sequence of random potential steps can be solved with a transfer matrix formalism that displays many similarities with the random Ising chain. In particular, the quantum transmission amplitude behaves as the spin-spin correlation and the probability distribution of conductivity is log-normal. A multifractal behaviour is displayed by the wavefunction at the critical point. As the system-size L is increased, the electronic probability density $|\psi(\vec{r})|^2$ does not scale as L^{-d} but with an exponent which is position-dependent. On a lattice, the number of points where the density scales as $|\psi(\vec{r})|^2 \sim L^{-\alpha}$ is $N(\alpha) \sim L^{f(\alpha)}$. Consequently, the

order parameters of the transition, the so-called inverse participation ratios, behave as

$$Y_q(L) = \int |\psi(\vec{r})|^{2q} d^d \vec{r} \sim \int L^{-q\alpha} L^{f(\alpha)} d\alpha. \quad (42)$$

In the insulating phase $f(\alpha) = q\alpha$ while in the metallic state, $f(\alpha) - q\alpha = -d(q-1)$. At the critical point, $f(\alpha) - q\alpha$ takes non-trivial values. In the thermodynamic limit $L \rightarrow +\infty$, the integral (42) can be estimated via a saddle-point approximation:

$$Y_q(L) \sim L^{-\tau(q)}, \quad \tau(q) = \max_{\alpha} [f(\alpha) - q\alpha] \quad (43)$$

i.e. $\tau(q)$ is the Legendre transform of $f(\alpha)$. The normalisation of the wavefunction implies that $\tau(1) = 0$. The equation (43) is mathematically equivalent to the inverse Legendre transform of (41) for the random Potts model if the two variables α are put into correspondence. Therefore, the analogy between the Anderson localisation and the random Potts model relies on

$$\begin{aligned} f(\alpha) &\longleftrightarrow H(\alpha), \\ q &\longleftrightarrow n, \\ \tau(q) &\longleftrightarrow X(n). \end{aligned} \quad (44)$$

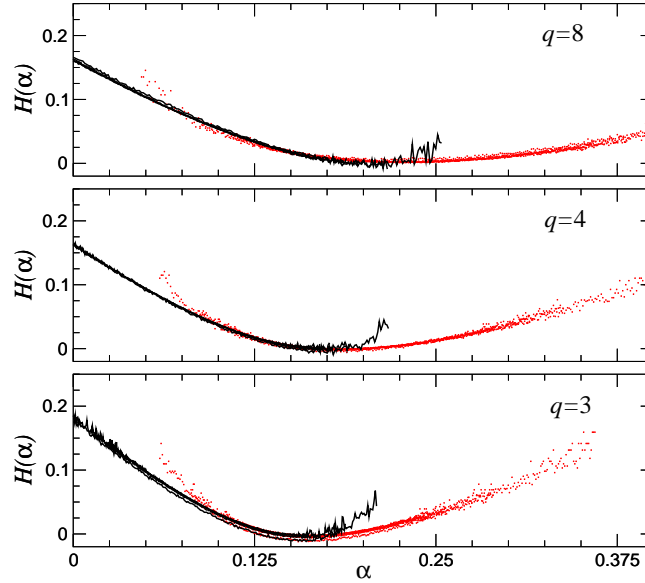


Figure 25 : Multifractal spectrum $H(\alpha)$ versus α for three random q -state Potts models. The black dots correspond to the numerical data while the red ones were obtained by applying the transformation $H(2X(1) - \alpha) - \alpha + X(1)$. The symmetry (45) holds if the two curves fall on top of each other.

Recently, the symmetry relation

$$f(2d - \alpha) = f(\alpha) + d - \alpha$$

was conjectured for Anderson transitions in the conventional symmetry class [372] and checked numerically for different systems. Using (43), the symmetry of $f(\alpha)$ around $\alpha = d$ becomes a symmetry of $\tau(q)$ around $q = 1/2$:

$$\tau(q) - \tau(1 - q) = d(2q - 1).$$

We conjectured that these symmetries can be extended to the random Potts model using the correspondence (44) [375]:

$$\begin{aligned} H(2X(1) - \alpha) &= H(\alpha) + \alpha - X(1), \\ X(n) - X(1 - n) &= X(1)(2n - 1). \end{aligned} \tag{45}$$

Our numerical data for $X(n)$ and $H(\alpha)$ are in good agreement with these relations (see figure 25). However, we should mention that the symmetries (45) are not satisfied by the series expansion (39). They are therefore probably not exact but only approximate.

1.2.3.6. Replica-symmetry breaking

Analytically, the critical behaviour of random systems is usually studied via perturbative Renormalisation Group. Short-distance fluctuations around the ground state are integrated out to define an effective Hamiltonian from which renormalised couplings will be extracted. In the case of a pure ferromagnet, this ground state is unique and easily determined. This is generally not the case for a random system. For each disorder realisation, the energy landscape may display a large number of local minima. Spin glasses and Random-Field models are the more studied examples [369, 508]. In the case of random ferromagnets at the critical point, some regions may be in a ferromagnetic phase because of a higher density of strong bonds. Because there are several ferromagnetic phases, each such region introduces a degeneracy of the ground state [157]. The integration of short-distance fluctuations has to be done for each minima. Applying now the replica trick (29) to cope with the average over disorder, the last term of (30) can now couple the energy densities of two replicas in the neighbourhood of two different minima. As a result, the symmetry between replicas may be spontaneously broken and the Renormalisation Group techniques have to be applied to an effective potential

$$\frac{1}{2} \int \sum_{\alpha, \beta=1}^n g_{\alpha\beta} \varepsilon^{(\alpha)}(\vec{r}) \varepsilon^{(\beta)}(\vec{r})(\sigma) d^d \vec{r}.$$

The random fixed point obtained with a symmetric coupling between replicas becomes unstable. In the case of the two-dimensional random Potts model, the question of a possible spontaneously-broken replica-symmetry was raised by Dotensko *et al.* [162, 161]. They calculated in particular the magnetic scaling dimension $x_\sigma(2)$ of the second moment of the spin-spin correlation function. With broken replica-symmetry, this exponent is

$$x_\sigma(2) = x_\sigma^{b, \text{Pure}} - \frac{1}{16}y + \frac{1}{32} \left(4 \ln 2 - \frac{5}{12} \right) y^2 + \mathcal{O}(y^3),$$

while in the symmetric case, it reads

$$x_\sigma(2) = x_\sigma^{\text{Pure}} - \frac{1}{16}y + \frac{1}{32} \left(4 \ln 2 - \frac{11}{12} \right) y^2 + \mathcal{O}(y^3).$$

We estimated this exponent by means of transfer matrices. As seen on figure 26, a good agreement is observed with the scenario involving no breaking of the replica symmetry.

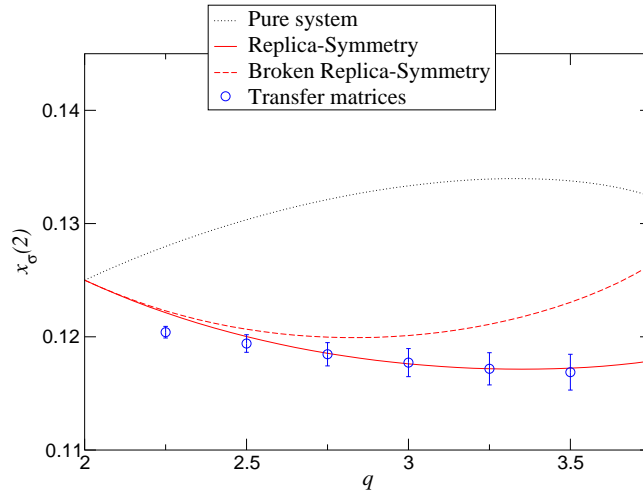


Figure 26 : Scaling dimension $x_\sigma(2)$ of the second moment of the spin-spin correlation function computed numerically versus the number of states q . The black dashed curve corresponds to the pure system and the red curves to series expansions when assuming replica-symmetry (continuous curve) or spontaneously-broken replica-symmetry (dashed curve).

1.2.4. Conformal invariance of two-dimensional random systems

Conformal Field Theory finds its root in high energy physics, more precisely in the so-called dual-resonance models which stands for the first string theory introduced to describe scattering caused by the strong interaction. During its time evolution, the string sweeps a two-dimensional sub-manifold $X^\mu(\sigma, \tau)$ of the four-dimensional Minkowski space-time [512, 363, 210]. In the case of a closed string, this world sheet looks like a tube. Both the Nambu-Goto and the Polyakov actions are invariant under reparametrisation of this surface. To reveal the conformal invariance of the theory, a complex parameter $z = \tau + i\sigma$ is formed from the space and time parameters σ and τ . The world sheet swept by the string is mapped onto the complex plane by the transformation $z \rightarrow z' = e^z$. The plane-wave decomposition of X^μ takes the form of a Laurent series in the complex plane. Since the time direction of the world sheet is mapped onto the radial direction of the complex plane, the Hamiltonian, i.e. the infinitesimal generator of time translations on the world sheet, is replaced by the generator $L_0 + \bar{L}_0$ of dilatations in the complex plane. The set of transformations leaving the action unchanged are the conformal transformations $z \rightarrow f(z)$ where f is an holomorphic function. While for classical fields the infinitesimal generators L_n and \bar{L}_n of these transformations satisfy a Virasoro algebra, in the case of quantum fields this algebra involves a central extension term.

Remarkably, this theory has become later one of the most important in the study of two-dimensional critical phenomena [235, 92, 65, 154, 208]. In statistical physics, the divergence of the correlation length induces a self-similarity of thermal fluctuations under scale transformations. This symmetry is exploited by the Renormalisation Group. When translation and rotation also leave the Hamiltonian invariant, one may assume

that this symmetry can be extended to conformal transformations. In dimensions $d > 2$, the conformal group comprehends translations, rotations, dilatation and the special conformal transformations that correspond to an inversion followed by a translation and a second inversion. Conformal invariance determines completely two and three-point correlation functions. In dimension $d = 2$, the conformal group is isomorphic to the set of holomorphic functions and therefore is infinite. Consequently, the requirement of conformal invariance imposes an infinite number of constraints on the theory. An infinite family of unitary representations of the Virasoro algebra with central extension was constructed. Among these so-called minimal models, because they owe no other symmetry than conformal invariance, one can identify the Ising model and the three and four-state Potts models. The scaling dimensions of the latter are given by some conformal weights.

Ironically, the cylindrical geometry resulting from the conformal transformation $z \rightarrow \ln z$ and which corresponds to the world sheet of the string plays also an important role in Statistical Physics. The iteration of a transfer matrix indeed generates such a cylindrical system. As discussed in the case of string theory, the Hamiltonian is the dilatation infinitesimal generator $L_0 + \bar{L}_0$ of the original complex plane. The Virasoro algebra leads to the already-mentioned finite-size expansion (35) of the free energy density where the central charge appears in the second-order term.

During the last decade, a bridge has been established between Stochastic Loewner Evolution (SLE) and Conformal Field Theory. The former offers a description of a certain family of stochastic fractal and non-intersecting curves of the complex half-plane. Some properties of these curves, as their Hausdorff dimensions or the probability for them to pass on the left of a given point, were exactly derived. Interfaces in Conformal Field Theories are good candidates for a description by SLE.

In the following, the extension of these ideas to random systems is discussed. There is no theoretical reason for conformal invariance to hold at the random fixed point. In the regime $2 < q \leq 4$, one may nevertheless note that the critical behaviour of the pure q -state Potts model is described by a Conformal Field Theory. For a given disorder realisation, translation, rotation, dilatation, and conformal invariances are broken. However, after an average over disorder, the homogeneity of the system is expected to be restored, implying translation and rotation invariance of the effective theory. When the transition is of second-order, the existence of a diverging correlation length proves the restoration of dilatation invariance. It is therefore tempting to assume that conformal invariance is also restored after the average over disorder. However, a famous counterexample is provided by randomly branched polymers for which conformal invariance is violated even though they display an isotropic critical behaviour with a correlation length that diverges as $\xi \sim L$ [371]. In the case of the random Potts model, we have already discussed the agreement of the central charge, estimated numerically by means of transfer matrix, with the series expansion in the regime $q \leq 4$. In the following, we present further numerical evidences in favour of the restoration of conformal invariance. We then discuss numerical tests of SLE predictions for the random Potts model.

1.2.4.1. Conformal covariance of correlation functions

Under a conformal transformation $z \rightarrow f(z)$, correlation functions of primary fields

are assumed to transform as

$$\begin{aligned} \langle \phi_1(z_1, \bar{z}_1) \phi_2(z_2, \bar{z}_2) \dots \rangle &= \left[\prod_i |f'(z_i)|^{\Delta_i} |\bar{f}'(\bar{z}_i)|^{\bar{\Delta}_i} \right] \\ &\times \langle \phi_1(f(z_1), \bar{f}(\bar{z}_1)) \phi_2(f(z_2), \bar{f}(\bar{z}_2)) \dots \rangle \end{aligned} \quad (46)$$

where the conformal weights Δ_i , and $\bar{\Delta}_i$ of the field ϕ_i are related to its scaling dimension and its spin. $|f'(z)|$ being the scale factor of the transformation at the point z , equation (46) should be understood as a generalisation of the scaling behaviour of correlation functions under a dilatation. In the following, we present some numerical tests of this equation in the case of the two-dimensional random Potts model.

We mentioned several times in the previous section the use of transfer matrices to compute spin-spin correlation functions. This technique implies to consider the Potts model on infinite strips or cylinders. Because of the finite-size in one of the two directions, the correlation functions do not decay algebraically at the critical point but exponentially. In the case of the cylinder, i.e. with periodic boundary conditions in the transverse direction, this behaviour is understood by considering the conformal transformation

$$f(z) = \frac{L}{2\pi} \ln z = u + iv$$

which maps the radial direction of the complex plane onto the longitudinal direction of the cylinder. Assuming now an algebraic decay of the two-point correlation function in the complex plane, i.e.

$$\langle \phi(z_1) \phi(z_2) \rangle \sim \frac{1}{|z_1 - z_2|^{2x_\phi}},$$

as imposed by conformal invariance, and applying equation (46), correlations on the cylinder are predicted to be [93]:

$$\langle \phi(u_1, v_1) \phi(u_2, v_2) \rangle = \frac{(2\pi/L)^{2x_\phi}}{\left[2 \cosh\left(\frac{2\pi}{L}(u_1 - u_2)\right) - 2 \cos\left(\frac{2\pi}{L}(v_1 - v_2)\right) \right]^{x_\phi}}.$$

In the longitudinal direction of the cylinder, an exponential decay is recovered at large distances:

$$\langle \phi(u_1, v_1) \phi(u_2, v_2 = v_1) \rangle \underset{|u_1 - u_2| \gg L}{\sim} \left(\frac{2\pi}{L}\right)^{2x_\phi} e^{-\frac{2\pi x_\phi}{L}(u_1 - u_2)}.$$

This equation was extensively used to analyse transfer matrix data and provided the more accurate estimates of the scaling dimension x_σ of the random Potts model. The good agreement of the latter with the series expansions gives additional strength to the assumption of restoration of conformal invariance by average over disorder.

We also studied the decay of spin-spin correlation functions in a square with free boundary conditions. The conformal mapping of the half-plane onto the square is performed by the Schwartz-Christoffel transformation

$$z' = f(z) = u + iv = \frac{N}{2K(k)} F(z, k), \quad (47)$$

where $(u, v) \in [-N/2; N/2] \times [0; N]$, $K(k)$ is the complete elliptic integral of the first kind, $F(z, k)$ the incomplete elliptic integral of the first kind and k satisfies the relation [4]

$$k = 4 \left[\frac{\sum_{p=0}^{+\infty} e^{-2\pi(p+1/2)^2}}{1 + 2 \sum_{p=1}^{+\infty} e^{-2\pi p^2}} \right]^2.$$

The vertices of the square are the points $z = -1/k, -1, 1/k,$ and 1 of the half-plane. Because of the presence of the free surface, the spin-spin correlation functions in the half-plane are not known exactly. In the upper half-plane $y > 0$, conformal invariance imposes the expression [94]

$$C(z_1, z_2) = \langle \phi(z_1) \phi(z_2) \rangle = |z_1 - z_2|^{-2x_\sigma} \psi \left(\frac{y_1 y_2}{|z_1 - z_2|^2} \right) \quad (48)$$

where $z_1 = x_1 + iy_1$ and $z_2 = x_2 + iy_2$ and ψ is an unknown scaling function that behaves asymptotically as $\psi(\omega) \sim \omega^{x_\sigma^1 - x_\sigma}$ when $\omega \rightarrow 0$ and goes to a constant limit when $\omega \rightarrow +\infty$. To get rid of this scaling function, we will restrict the study of the correlation functions to curves $\omega = \frac{y_1 y_2}{|z_1 - z_2|^2} = \text{Cst}$ of the half-plane. Consequently, a pure algebraic decay is expected:

$$C(z_1, z_2) \sim |z_1 - z_2|^{-2x_\sigma} = \left(\frac{y_1 y_2}{\omega} \right)^{-x_\sigma}.$$

According to (46), the average spin-spin correlation function of the random Potts model in the square will be

$$\overline{\langle C(z'_1, z'_2) \rangle} \sim \left[|f'(z_1)| |f'(z_2)| \Im(f^{-1}(z'_1)) \Im(f^{-1}(z'_2)) \right]^{-x_\sigma} \psi(\omega(f^{-1}(z'_1), f^{-1}(z'_2))).$$

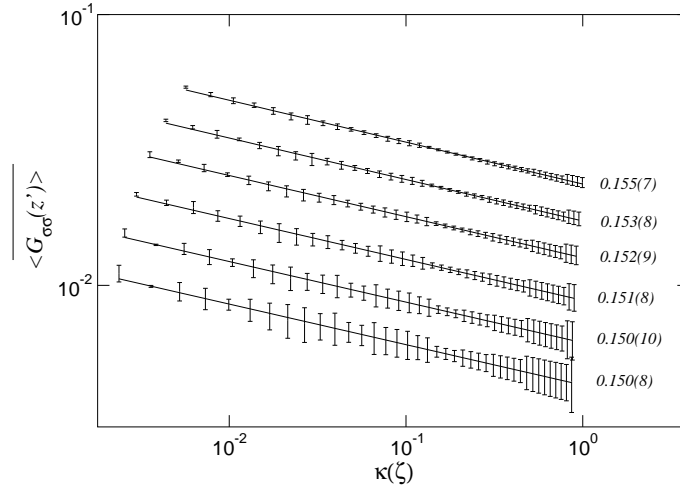


Figure 27 : Spin-spin correlation functions of the eight-state Potts model in a square measured along a curve $\omega = \text{Cst}$. On the right are displayed the scaling dimensions estimated by a power-law interpolation of the data.

We measured these spin-spin correlation functions for the eight-state random-bond Potts model by means of Monte Carlo simulations [109, 56, 111]. One of the point was

chosen close to the surface, i.e. $|z_1| \rightarrow 0$, while the second swept all lattice sites in the bulk of the square. The correlation was interpolated along the curves

$$\omega(f^{-1}(z'_1), f^{-1}(z'_2)) = \kappa(z'_1, z'_2) = \text{Cst.}$$

As seen on figure 27, the expected algebraic decay is indeed observed for different values of ω and the scaling dimensions are in very good agreement with the ones obtained by other methods.

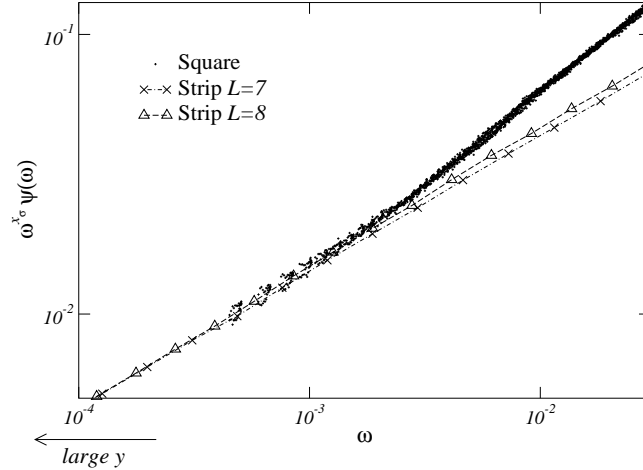


Figure 28 : Scaling function $\omega^{x_\sigma} \psi(\omega)$ versus ω for the eight-state random Potts model. The dots correspond to data obtained from the spin-spin correlation functions on the square with free boundary conditions. The symbols come from the analysis of the magnetisation profile on strips of length L .

According to equation (48), the scaling function $\psi(\omega)$ can be extracted from the spin-spin correlation function once the bulk scaling dimension x_σ is known:

$$\psi(\omega) = C(z_1, z_2) \left(\frac{y_1 y_2}{\omega} \right)^{x_\sigma} \underset{\omega \rightarrow 0}{\sim} \omega^{x_\sigma^1 - x_\sigma}.$$

On figure 28, the product $\omega^{x_\sigma} \psi(\omega)$ which is expected to scale as $\omega^{x_\sigma^1}$ is plotted versus ω . A power-law behaviour is observed for very small values of ω and the surface scaling dimension was estimated to be $x_\sigma^1 \simeq 0.47(3)$ in agreement with previous estimates.

1.2.4.2. Conformal covariance of profile

Besides spin-spin correlation functions, magnetisation profiles, i.e. one-point functions, were considered in both infinite strip and square geometries. On the strip, we studied systems with asymmetric boundary conditions: spins were fixed in the state $\sigma = 0$ on the left boundary and left free on the right one [406]. The system can be equivalently described as coupled to an infinite surface magnetic field on one of its boundaries. The half-plane is mapped onto such an infinite strip by the conformal transformation

$$f(z) = u + iv = \frac{L}{\pi} \ln z. \quad (49)$$

To obtain the correct boundary conditions on the strip, spins have to be fixed on the negative part of the real axis, i.e. $z \in \mathbb{R}^-$ and left free on the other one (\mathbb{R}^+). The

critical magnetisation profile is not known exactly in such a case but scaling arguments lead to the assumption

$$\langle \phi(x, y) \rangle \sim y^{-x_\phi} \mathcal{G}\left(\frac{x}{r}\right),$$

where the unknown scaling function \mathcal{G} is expected to decay algebraically with the surface exponent x_ϕ^1 . Applying the conformal transformation (49), one obtains on the strip [86]

$$\begin{aligned} \langle \phi(u, v) \rangle &\sim \left[\frac{L}{\pi} \sin\left(\frac{\pi v}{L}\right) \right]^{-x_\sigma} \mathcal{G}\left[\cos\left(\frac{\pi v}{L}\right)\right] \\ &\underset{L \rightarrow +\infty}{\sim} \left[\frac{L}{\pi} \sin\left(\frac{\pi v}{L}\right) \right]^{-x_\sigma} \left[\cos\left(\frac{\pi v}{2L}\right) \right]^{x_\sigma^1}. \end{aligned} \quad (50)$$

The magnetisation profile was computed numerically by transfer matrices for small widths L and by Monte Carlo simulations for larger ones, up to $L = 40$. In the second case, the length of the system in the longitudinal direction has to be finite. Several lengths were considered up to 500. However, as can be seen on figure 29, the lattice sizes are still too small and a systematic deviation from the predicted profile (50) is observed. We therefore interpolated the data and then extrapolated the resulting profiles to an infinite width. This extrapolation is plotted as black circles on figure 29. The agreement with the conformal prediction (50) is now much better and the surface scaling dimension x_σ^1 can be extracted numerically. The conformal prediction (50) for the magnetisation profile was assumed to hold also for the moments

$$\overline{\langle m(u) \rangle^n}^{1/n} = A \left[\frac{L}{\pi} \sin(\pi u/L) \right]^{-x_\sigma(n)} \left[\cos(\pi u/2L) \right]^{x_\sigma^1(n)}. \quad (51)$$

By the same technique as for the profile, a multifractal exponents $x_\sigma^1(n)$ can be estimated by the interpolation of the average moments with (51).

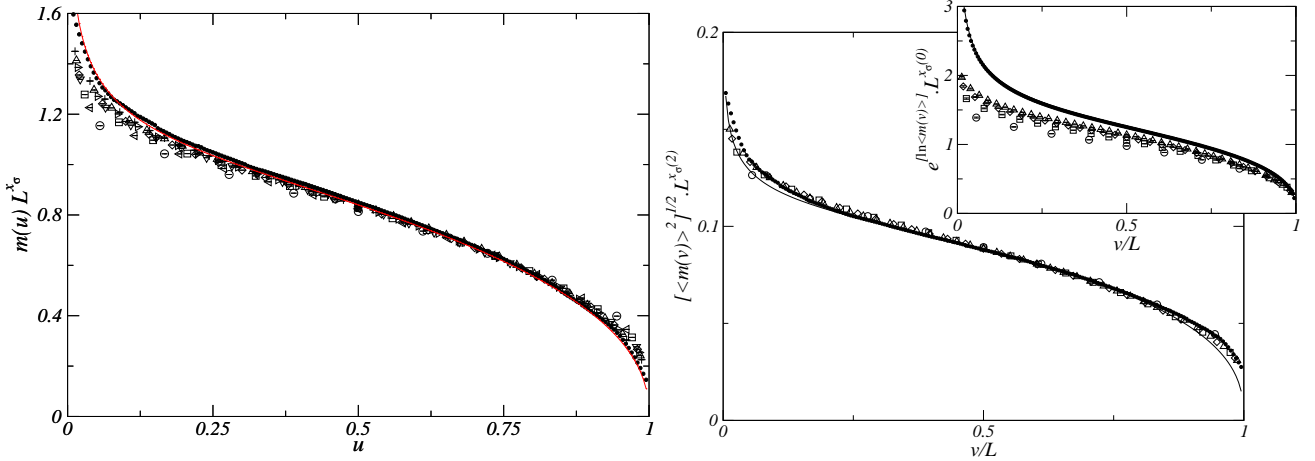


Figure 29 : On the left, rescaled magnetisation profile for the random eight-state Potts model. The symbols correspond to different strip widths. The small black circles were obtained by an extrapolation to infinite size. The red curve is the interpolation of these data with the conformal prediction (50). On the right, rescaled moment of order two (zero in the insert) of the magnetisation profile.

Lastly, the magnetisation profile was considered in a square with fixed boundary conditions. In the half-plane, the magnetisation is expected to decay algebraically, i.e. $\langle \phi(x, y) \rangle \sim y^{-x_\sigma}$. Using the Schwartz-Christoffel transformation (47) to map the half-plane onto the square, the transformation law (46) leads to [85, 84]

$$\overline{\langle m(z') \rangle} \sim |f'(z)|^{-x_\sigma} [\Im(f^{-1}(z'))]^{-x_\sigma} = \left[\frac{\Im(f^{-1}(z'))}{\sqrt{(1 - [f^{-1}(z')]^2)(1 - k^2[f^{-1}(z')]^2)}} \right]^{-x_\sigma}.$$

The logarithm of this expression depends linearly on the logarithm of the reduced variable

$$\kappa(z') = \frac{\Im(z(f^{-1}(z')))}{\sqrt{(1 - [f^{-1}(z')]^2)(1 - k^2[f^{-1}(z')]^2)}} \quad (52)$$

with a slope equal to the magnetic scaling dimension x_σ . We computed such magnetisation profile of the random Potts model by Monte Carlo simulations [109, 56, 111]. As seen on figure 30, the expected behaviour is indeed observed. The relative dispersion of the data is compensated by the number of points, equal to the number of sites in the square, which finally leads to an accurate estimate of the scaling dimension. The same procedure was applied to the energy profile, despite a faster decay and a larger dispersion of the data.

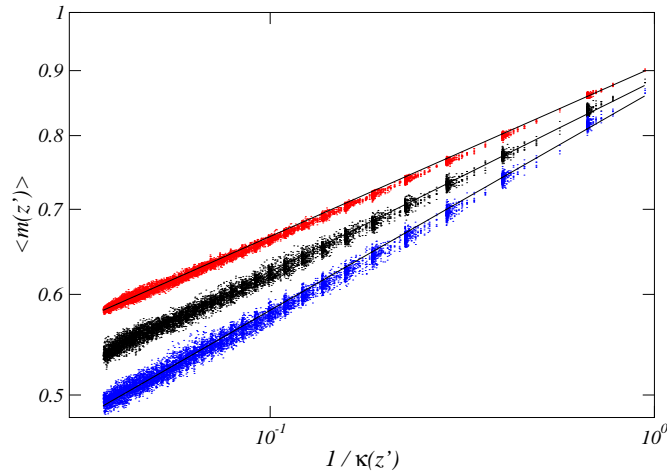


Figure 30 : Magnetisation profile of the random q -state Potts model in a square with fixed boundary conditions versus the inverse of the scaled variable (52). The dots correspond to the Monte Carlo data and the straight lines are the linear interpolation from which the scaling dimension x_σ was extracted. The different set of data are associated to different numbers of states $q = 3, 8,$ and 64 (from top to bottom).

1.2.4.3. Stochastic Schramm-Loewner Evolution

1.2.4.3.1. Random fractal curves in percolation and spin models

We briefly mentioned in the first chapter the fact that percolation corresponds to the limit $q \rightarrow 1$ of the Potts model. The phase transition between the percolating and non-percolating phases is purely geometrical. At a critical concentration p_c of sites, or bonds, randomly distributed on the lattice, one of the clusters expands up to the lattice boundaries (see figure 31). The fractal geometry of the clusters in the continuum limit was recognised by Stanley and Mandelbrot [453, 349]. The number of sites belonging to the percolating cluster diverges anomalously as L^{d_f} with a fractal dimension $d_f = 91/48$ in dimension $d = 2$. The perimeter of the hull of this cluster, i.e. the envelope obtained by removing all vacant sites not connected to infinity by a continuous path, scales as L^{d_h} with an exponent that was estimated numerically to be $d_h \simeq 1.74(2)$, i.e. a value compatible with the simple fraction $7/4$ [481, 511]. This perimeter has to be measured by sliding a rigid stick of length equal to the lattice size along the path joining the occupied sites at the frontier of the hull. On the square lattice, the stick is placed on the bonds between nearest neighbouring sites. Interestingly, a different result is obtained with the following procedure: a ball of radius equal to the lattice size rolls on the cluster and the length is computed as the number of turns that were made. Because the ball will roll over small cavities in the frontier, a shorter length is obtained. The latter is called the external perimeter of the cluster and scales as L^{d_e} with a new exponent $d_e \simeq 1.37(3)$ compatible with the fraction $4/3$ [217, 216]. These two fractal dimensions were later shown to be exactly equal to $d_h = 7/4$ and $d_e = 4/3$ by using the equivalence of the percolation problem with the Potts model in the limit $q \rightarrow 1$ and the mapping of the latter onto a Coulomb gas [434, 10].

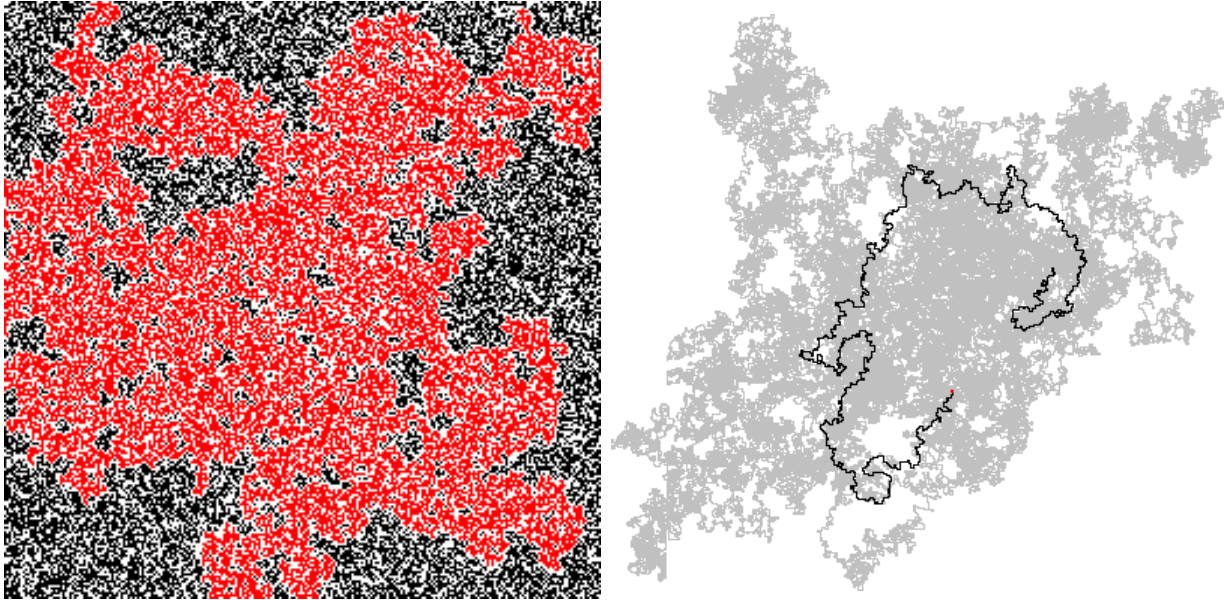


Figure 31 : On the left, typical configuration of site percolation at the concentration threshold p_c . The incipient cluster is coloured in red. On the right, example of loop-erased random walk. The loops that were erased are drawn in grey.

Similar quantities were defined for other models. Since the frontier of the hull does not have any intersection, one may study in the same way random curves with the

same property. The hull of a planar random walk forms at its frontier a self-avoiding walk whose fractal dimension was conjectured to be $d_h = 4/3$ [349]. This value was later shown to be exact using a quantum gravity formalism [171]. Self-intersections of the planar random walk can also be “manually” removed by erasing the loops (see figure 31). The length of the resulting loop-erased random walk was shown to scale with a fractal dimension $d_h = 5/4$ [346].

The same approach may be applied to the description of the geometrical properties of the frontiers between clusters in lattice spin models. In the case of the Ising model at the critical point, the clusters constructed from nearest-neighbouring spins in the same state, were indeed shown to be fractal [455]. However, because two spins can be in the same state even though they are not correlated, the Fortuin-Kasteleyn representation of the Potts model was believed to be better suited to a geometrical description. Moreover, the critical behaviour of the Potts model is encoded in the geometrical properties of the Fortuin-Kasteleyn clusters. From the scaling of the total number of sites in the percolating Fortuin-Kasteleyn cluster, the length of its hull and its external perimeter, fractal dimensions d_f , d_h and d_e were defined [126, 478, 731]. Their values are reported in table 5. The reader may check that the following relation between the fractal dimensions of the hull and the external perimeter holds:

$$(d_e - 1)(d_h - 1) = \frac{1}{4}. \quad (53)$$

It was much later proved by Duplantier in the more general context of SLE [172]. For the geometrical spin clusters, the fractal dimensions d_f , d_h and d_e take different values. The fact that the geometrical properties of Fortuin-Kasteleyn and spin clusters are different can be understood by considering the annealed site-diluted Potts model. This model has two non-trivial RG fixed points in the universality classes of the pure Potts model and of the tricritical Potts model, respectively [148]. Both fixed points have a representation in terms of a Coulomb gas with two couplings, $g = \frac{4}{\pi} \text{Arccos}(-\sqrt{q}/2)$ and g' respectively, related by $gg' = 16$. It is well known that the critical behaviour of the pure Potts model is encoded in the geometrical properties of the Fortuin-Kasteleyn clusters. It was shown that the tricritical Potts behaviour was related to the properties of the spin clusters of the original Potts model [274, 275]. Interestingly, the fractal dimensions d_h and d'_h of the critical and tricritical Potts model are related by $(d_h - 1)(d'_h - 1) = 1/4$. It means, according to (53), that the fractal dimension of the external perimeter of Fortuin-Kasteleyn clusters is equal to that of the hull of spin clusters.

	$q = 1$ (Perco.)	$q = 2$ (Ising)	$q = 3$	$q = 4$
d_f	91/48	15/8	28/15	15/8
d_h	7/4	5/3	8/5	3/2
d_e	4/3	11/8	17/12	3/2

Tableau 5 : Fractal dimensions of the Fortuin-Kasteleyn clusters of the q -state Potts model.

1.2.4.3.2. SLE and connection with minimal models

The so-called Stochastic Schramm-Loewner Evolution denotes a Markovian process that generates a one-parameter infinite family of fractal random planar curves without branching nor intersection [291, 97, 218, 40, 183]. It was constructed by Schramm [438] on the basis of a work performed by Loewner three quarters of century before [344]. Loewner's original idea was to describe conformally invariant non-intersecting and non-branching curves $\gamma(t)$ of the upper-half complex plane \mathbb{H} by their uniformising map $g_t(z)$. The latter is defined as the conformal transformation $g_t : \mathbb{H} \setminus \mathbb{K} \rightarrow \mathbb{H}$ that maps the hull \mathbb{K} of the curve, i.e. the curve itself and the domains that are enclosed by the curve, onto the real axis. The tip of the curve is sent to the origin O . Upon an infinitesimal variation of the parameter t , the new curve differs from $\gamma(t)$ by the addition at its tip of an infinitesimal segment γ_{dt} . Under the action of the uniformising map $g_t(z)$, the curve $\gamma(t)$ is mapped onto the real axis while the image of γ_{dt} is another infinitesimal segment $g_t(\gamma_{dt})$ which is attached by one end to the origin. Assuming that the curve $\gamma(t)$ is generated in such a way that γ_{dt} depends only on the location of the tip and not on the whole curve (Markovian assumption), the new uniformising map g_{t+dt} is the composition

$$g_{t+dt}(z) = g_{dt}(z) \circ g_t(z),$$

where $g_{dt}(z)$ maps the image of the infinitesimal segment γ_{dt} under $g_t(z)$ onto the real axis. Loewner showed that, together with the hydrodynamic normalisation condition $g_t(z) \underset{z \rightarrow +\infty}{\sim} z$, the uniformising map satisfies the differential equation

$$\frac{dg_t}{dt} = \frac{2}{g(t) - \xi_t}, \quad g_0(z) = z. \quad (54)$$

which is equivalent to say that the infinitesimal segment $g_t(\gamma_{dt})$ joins the origin and a point $\xi_t + 2i\sqrt{dt}$.

Schramm considered the family of random curves $\gamma : [0; \infty) \rightarrow \mathbb{H}$ of the upper-half plane generated by a Loewner chain when the driving function ξ_t is chosen to be the random Brownian motion $\sqrt{\kappa}B_t$ characterised by

$$\langle \xi_t \rangle = 0, \quad \langle \xi_t^2 \rangle = \kappa t. \quad (55)$$

This one-parameter family of random curves, called chordal SLE and denoted SLE_κ , possesses two important properties: conformal invariance and Markovian property. Consider a curve $\gamma(t)$ with $t \in [0; 1]$ joining the two points $\gamma(0) = a$ and $\gamma(1) = b$ in a domain \mathbb{D} . Under a conformal transformation $f(z)$, its image is a curve $f \circ \gamma(t)$ of the domain $f(\mathbb{D})$ that joins the points $f(a)$ and $f(b)$. The conformal invariance property is the equality of the probabilities of the curve and its image:

$$\wp_{f(\mathbb{D})}(f \circ \gamma) = \wp_{\mathbb{D}}(\gamma). \quad (56)$$

Consider now a point c on the same curve $\gamma(t)$, i.e. $c = \gamma(t_c)$ where $t_c \in]0; 1[$, and cut the curve into two pieces. The initial segment $\gamma_{<}(t) = \gamma(t/t_c)$ is a curve joining a and c while the final segment $\gamma_{>}(t) = \gamma((t - t_c)/(1 - t_c))$ joins c and b . The Markovian property holds if the conditional probability $\wp_{\mathbb{D}}(\gamma_{>}|\gamma_{<})$, i.e. the probability of the final

segment $\gamma_>$ knowing the initial one $\gamma_<$, is equal to the probability of the final segment $\gamma_>$ in a domain $\mathbb{D} \setminus \gamma_<$ where a cut has been performed along the initial segment $\gamma_<$:

$$\wp_{\mathbb{D}}(\gamma_>|\gamma_<) = \wp_{D \setminus \gamma_<}(\gamma_>). \quad (57)$$

Schramm showed that if conformal invariance and Markovian property both hold then the driving function ξ_t has to be a Brownian motion.

The curves, also called traces, of SLE_κ are simple curves when $\kappa < 4$. They present double points when $4 < \kappa \leq 8$ and fill densely their envelope when $\kappa > 8$. Their fractal dimension was shown to be [50]

$$d_h = 1 + \frac{\kappa}{8} \quad (58)$$

if $\kappa < 8$ and $d_h = 2$ above. From Duplantier's relation (53), the external perimeter of a SLE_κ trace has a fractal dimension

$$d_e = 1 + \frac{2}{\kappa}, \quad (\kappa \geq 4)$$

which is equivalent to say that the external perimeter of a SLE_κ trace is another trace $\text{SLE}_{\kappa'}$ with a diffusion constant $\kappa' = 16/\kappa$. Schramm showed that the probability that the SLE trace passes at the left of a given point $z = x + iy$ of the upper-half plane is [439]

$$\wp(z) = \frac{1}{2} + \frac{\Gamma(4/\kappa)}{\sqrt{\pi}\Gamma((8-\kappa)/2\kappa)} \frac{x}{y} {}_2F_1\left(\frac{1}{2}, \frac{4}{\kappa}, \frac{3}{2}, -\frac{x^2}{y^2}\right). \quad (59)$$

Note the dependence on $x/y = \cotan \theta$, where θ is the polar angle, in agreement with the assumption of invariance under dilatation.

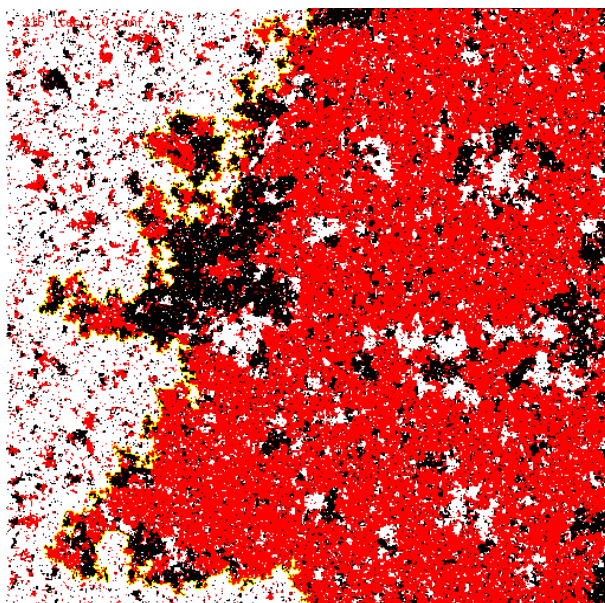


Figure 32 : Typical spin configuration of the three-state Potts model at the critical point. Spins are fixed to the state $\sigma = 0$ on the left part of the boundary

while they are free to take the values $\sigma = 1$ or 2 on the right. An interface is generated, depicted in yellow on the figure.

The continuum limit of the loop-erased random walk was shown to be SLE_2 [438, 311]. The percolation problem was conjectured to be SLE_6 by Schramm. A proof on the triangular lattice was given by Smirnov [449]. Since percolation corresponds to the limit $q \rightarrow 1$ of the Potts model, one may hope that the geometrical interfaces in the Potts models be SLE_κ traces in the continuum limit. As already discussed above, the frontiers of the spin and Fortuin-Kasteleyn clusters of the Potts model at the critical point are fractal curves too. By imposing boundary conditions that break the symmetry of the Hamiltonian, more convenient fractal interfaces can be generated. An example of such boundary conditions is presented on figure 32. The conformal property (56) of the distribution probability of the curves is expected to be inherited from the conformal invariance of the model. Markovian property (57) is also expected to hold in the case of short-range interactions. Indeed, when a cut is performed along a path $\gamma_<$ of the dual lattice, the weights of all the bonds perpendicular to that path have to be removed from the Boltzmann weight of the spin configuration. The result is identical to the Boltzmann weight that is obtained when an interface is present along this path, i.e. when the spin are in different states on both sides and therefore when the bonds are forced to be in an inactive state.

The connection between the Potts model and SLE was provided by the Coulomb gas and minimal models. From the study of the interfaces of the $O(n)$ model, the diffusion constant κ was inferred to be proportional to the inverse of the Coulomb gas coupling g [172]. The mapping of the Coulomb gas representation of the Potts model onto that of the tricritical Potts model is translated into the duality relation $\kappa\kappa' = 16$. Bauer and Bernard constructed an abstract SLE_κ process in the Virasoro Lie group and coupled it to Boundary Conformal Field Theory [38 39]. The central charge c of the CFT and the diffusion constant κ of SLE turned out to be constrained by the relation

$$c = \frac{(3\kappa - 8)(6 - \kappa)}{2\kappa}.$$

Interestingly, the duality transformation $\kappa \rightarrow 16/\kappa$, exchanging hull and external perimeters, does not change the central charge. The two fixed points of the annealed site-diluted Potts model have indeed the same central charge. Using relations (10) and (11), the diffusion constant of the SLE_κ associated to spin and Fortuin-Kasteleyn clusters are obtained:

$$\kappa_1 = \frac{4}{1 - \frac{1}{\pi} \text{Arccos}(\sqrt{q}/2)}, \quad \kappa_2 = 16/\kappa_1.$$

These predictions have found a mathematically rigorous confirmation in the case of the Ising model ($q = 2$). The frontier of the hull of Fortuin-Kasteleyn clusters was shown to have a well-defined continuum limit corresponding to SLE_3 [170]. The q -state Potts models with $q > 2$ were studied numerically (see figure 33). In the case $q = 3$, the fractal dimensions of the hull perimeter of the spin and Fortuin-Kasteleyn clusters were computed by Finite-Size scaling [195]. The estimates were shown to be compatible with the SLE predictions for the expected diffusion constants $\kappa = 10/3$ and $\kappa = 48/10$. The left-passage probability was compared with Schramm formula (59). Fractal dimensions

of the hull and external perimeters of the Fortuin-Kasteleyn clusters were estimated in the case $q = 1, 2, 3$ and 4 [6], for $q = (\sqrt{5} + 3)/2$ [200], and for half-integer values of q [509]. Finally, we note that the definition of the hull of spin clusters is not completely free of ambiguity. Apart from interfaces obtained from appropriate symmetry-breaking boundary conditions [195], domain walls between spin clusters usually intersect and branch. It was shown that in this case a continuous spectrum of fractal dimensions can be defined [168, 169]. Other models attracted a special attention, as the Ashkin-Teller whose underlying Conformal Field Theory is not minimal [416, 419, 417, 418, 101, 261].

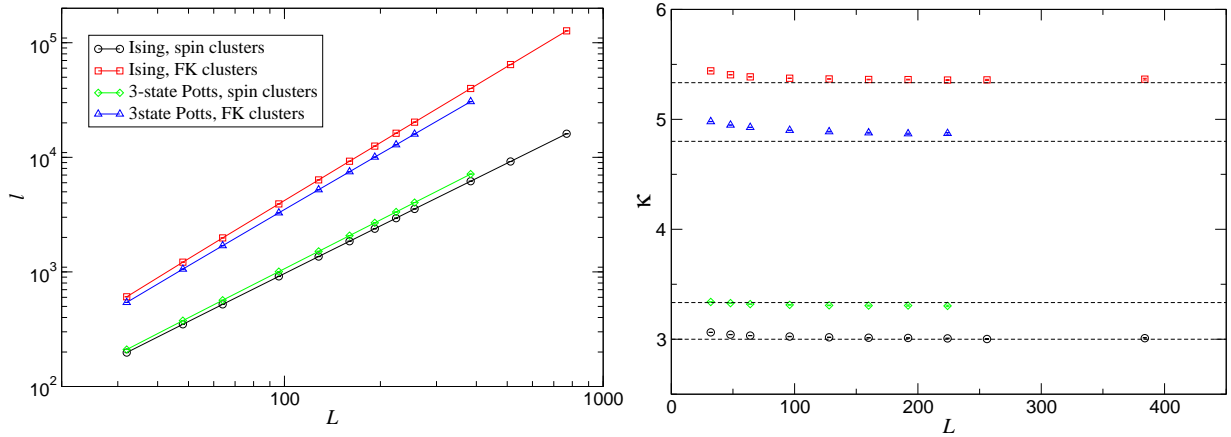


Figure 33 : On the left, length of the hull of the Fortuin-Kasteleyn and spin clusters of the Ising and three-state Potts models versus the lattice-size. On the right, effective diffusion constant κ obtained by power-law interpolation with respect to the largest lattice size used in the fit.

Few studies addressed the challenging case of random systems (see 108 for a review). For the random Potts model, numerical evidences of a restoration of conformal invariance after disorder average have been presented in the previous section. However, the simple argument in favour of Markovian property for pure systems with short-range interactions cannot be extended easily to the effective Boltzmann weight of a random system.

The first numerical evidences of the validity of SLE in a random system were obtained in the case of the Edwards-Anderson spin glass model

$$H = \sum_{(i,j)} J_{ij} \sigma_i \sigma_j,$$

where J_{ij} are quenched random couplings with a symmetric probability distribution $\varphi(J) = \varphi(-J)$. When reversing the sign of the exchange couplings J_{ij} along one row of the lattice, spins are usually flipped over a large region. An interface is therefore induced in the ground state between the region where the state of the spins did not change and the one where they flipped. Conformal property of the probability distribution of the interface was shown to hold with different configurations of cuts made in the lattice [16]. The driving function ξ_t was iteratively reconstructed from the interface $\gamma(t)$ using a lattice version of (54). The variance $\langle \xi_t^2 \rangle$ was shown to display the expected behaviour (55) of a Brownian motion and the estimate of the diffusion constant κ

is compatible with previous values of the fractal dimension d_h (58). Shortly after, further numerical compatibility tests with SLE were applied [61]. Among them, the left-passage probability was interpolated with Schramm formula (59). The diffusion constant obtained in this way was compatible with other independent estimates. Surprisingly, contradictory results were obtained with different coupling distributions $\wp(J)$ [428]. With a Gaussian distribution, instead of a bimodal one, incompatible values of the diffusion constant were estimated from the fractal dimension of the interface and the left-passage probability. This issue has remained unexplained.

SLE was also tested for the two-dimensional Random-Field Ising model [457, 458]. Even though the system does not undergo any phase transition, the size of the spin clusters diverges at zero temperature for a critical magnetic field h_c . The interfaces were believed to have the same geometrical properties as percolation and therefore correspond to SLE_6 traces in the continuum limit. The Markovian property was shown to hold. Left-passage probability, fractal dimension of the interface, variance of the reconstructed driving function and crossing probabilities of percolating clusters confirmed the SLE prediction $\kappa = 6$.

The two-dimensional Solid-On-Solid model on a random substrate was also considered [440]. However, even though the Schramm formula (59) was apparently well reproduced by the numerical left-passage probability, the resulting estimate $\kappa \simeq 4.00(1)$ of the diffusion constant was remarkably different from the one ($\kappa \simeq 2.00(8)$) obtained from the fractal dimension. This incompatibility has found no explanation.

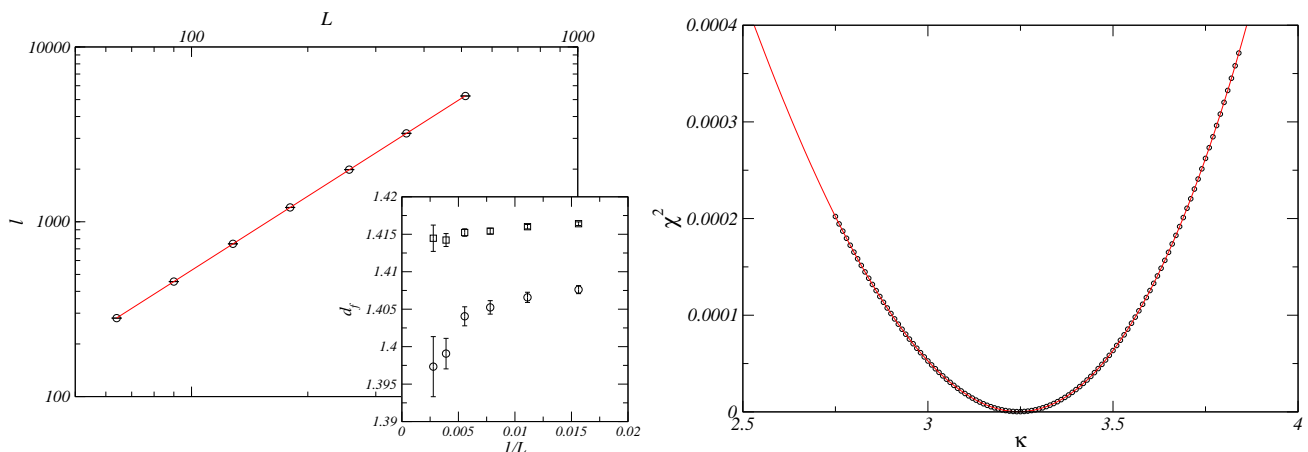


Figure 34 : On the left, scaling of the length of the interface between spin clusters in the random three-state Potts model with the lattice size. In the inset, the effective fractal dimension d_h of the pure (square) and random (circles) models are plotted with respect to the inverse of the smallest lattice size used in the interpolation. On the right, square deviation between the numerical left-passage probability and the Schramm formula as a function of κ .

Finally, the three-state (ferromagnetic) random-bond Potts model was studied both numerically and by Renormalisation Group techniques [269]. The latter predicted the fractal dimension of the Fortuin-Kasteleyn clusters to be $d_h \simeq 1.61433$. This value was confirmed by transfer matrices calculations ($d_h \simeq 1.615(2)$) and Monte Carlo simulations ($d_h \simeq 1.614(3)$). The fractal dimension of the hull of spin clusters ($d_h \simeq 1.401(3)$) was also estimated and the two diffusion constants κ (Fortuin-Kasteleyn) and

κ' (spin) were shown to satisfy the duality relation $\kappa' = 16/\kappa$. In this context, we studied the left-passage probability of the interface between spin clusters ^[107]. Despite a small systematic deviation in the region where the probability is large, a good agreement is obtained with the Schramm formula and the diffusion constant was estimated to be $\kappa = 3.245(10)$, in agreement with the value (3.208(24)) obtained from the fractal dimension (figure 34).

1.2.5. Conclusions

In this first chapter, the influence of inhomogeneous perturbations coupled to the energy density of the q -state Potts model was discussed. These perturbations can be either random or deterministic and correspond to a local modification of the exchange coupling or of the coordination number. When the pure system undergoes a first-order phase transition, i.e. when $q > 4$ in two dimensions or $q > 2$ in three dimensions, the Imry-Wortis criterion provides a heuristic explanation of the smoothing of the transition. The latter is caused by an interface free energy which is too small to prevent the ferromagnetic low-temperature phases to be destabilised by the local fluctuations of the perturbation. This criterion was discussed for homogeneous disorder, random graphs, layered randomness and aperiodic sequences. In the case of two-dimensional random bonds, the Aizenmann-Wehr theorem states that an infinitesimal amount of disorder is sufficient to smooth completely the discontinuous phase transition. The example of the eight-state Potts model was discussed. In higher dimensions, a tricritical point may separate a line of first-order transition at weak disorder from a regime of continuous transition. This scenario was encountered in particular in three-dimensional random Potts models.

When the pure Potts model undergoes a second-order phase transition, the critical behaviour may fall into a new universality class. The perturbation is relevant when its fluctuations dominate over the energy-energy correlation function at large-distances. We tried to give a coherent presentation of the different versions of this criterion for random bonds, aperiodic perturbations and random graphs. In the case of homogeneous disorder, the two-dimensional random fixed point has been widely studied both numerically and analytically. A very good agreement between the two approaches has been achieved for several distributions of random couplings and for site or bond dilution. The phase diagram involves a line of fixed points when the number of states q is increased, that is characterised by a monotonously increasing magnetic scaling dimension, and terminates at an infinite-randomness fixed point in the limit $q \rightarrow +\infty$. Interestingly, this fixed point governs also the critical behaviour of layered random (“McCoy-Wu”) Potts models for any number of states $q \geq 2$. In the three-dimensional case, the universality class at the tricritical point could not be determined by Monte Carlo simulations. It would be interesting to check the conjecture relating this fixed-point to the Random-Field Ising Model. The multifractal properties of the random fixed point were considered only in the two-dimensional case.

Finally, we presented numerical evidences of a restoration of conformal invariance of magnetisation profiles and two-point correlation functions at the two-dimensional random fixed point after averaging over disorder. This symmetry also seems to exist in the case where the pure system undergoes a first-order phase transition. More recently, the interest was focused on Stochastic Loewner Evolution. Interfaces are induced in spin systems by imposing symmetry-breaking boundary conditions. In the case of the random Potts model, the first calculations performed these last tree years show a compatibility of the geometrical properties of the interfaces between Fortuin-Kasteleyn and spin clusters with the predictions of SLE. Certainly more work needs to be done to achieve a better understanding of the connection between random systems and SLE.

1.3. Out-of-equilibrium processes

In the first chapter, only the static properties of the pure and random Potts models have been discussed. No dynamics was specified. In contradistinction to Hamiltonian dynamics, the Potts Hamiltonian (1) cannot be the infinitesimal generator of time translations because it does not involve any momentum conjugate to the spin variables σ_i . It has to be understood as an effective Hamiltonian resulting from the integration of the Boltzmann weight over momenta. Moreover, we are not interested in the dynamics of an isolated system but of a system in interaction with a thermal bath. Many different dynamics are therefore possible and have been studied in the literature. A classification was introduced by Hohenberg and Halperin [245]. In the following, we will focus mainly on the so-called model A where the dynamics does not conserve any global observable or momentum of the system.

Two routes have been explored. The first one consists in assuming that the dynamics of the system is stochastic because of the interaction with a thermal bath. A master equation is therefore postulated and the stationary distribution is imposed to be the Boltzmann weight. Glauber applied this procedure to the one-dimensional Ising model and calculated exactly time-dependent one-time and two-time averages [199]. These results will be discussed in more details later. This route is also naturally followed by Monte Carlo simulations. The Metropolis algorithm generates a Monte Carlo dynamics essentially equivalent to Glauber's one in the case of the one-dimensional Ising model [368]. Unfortunately, few analytical results can be obtained in this way. Like in the static case, continuous fields are more easily handled by analytical calculations and allow for sophisticated techniques as the Renormalisation Group. A more appropriate dynamics in this case is the Langevin equation [309]:

$$\partial_t \phi(\vec{r}, t) = -\Lambda \frac{\delta H[\phi]}{\delta \phi(\vec{r}, t)} + \eta(\vec{r}, t), \quad (60)$$

where $\phi(\vec{r}, t)$ is obtained from the local order-parameter after coarse-graining. $H[\phi]$ is a Ginzburg-Landau functional whose minimum defines the equilibrium state. η is a Gaussian noise describing in an effective way the effect of thermal fluctuations around the equilibrium state. Its variance $\langle \eta(t)\eta(s) \rangle = \sigma^2 \delta(t-s)$ is adjusted in such a way that the expected equilibrium fluctuations of ϕ are recovered. It is therefore a function of temperature.

Both the dynamical equations and the initial conditions should be specified to fully pose the problem. When the system is initially prepared at equilibrium, global observables are expected to be conserved. In the large-time limit, the two-time autocorrelation functions $\langle \phi(t)\phi(s) \rangle$ decay exponentially with a characteristic time τ corresponding to the relaxation time of the slowest mode of the system. As approaching the critical point, this relaxation time diverges as

$$\tau \sim \xi^{z_c} \sim |T - T_c|^{-\nu z_c}, \quad (61)$$

where z_c is the so-called dynamical exponent. In a finite system, the divergence is smoothed and the relaxation time scales as L^z at the critical temperature of the infinite system. The linear response to an external perturbation, for example a magnetic field, is related to autocorrelation functions by the Fluctuation-Dissipation Theorem (FDT):

$$R(t, s) = \lim_{h \rightarrow 0} \frac{\delta \langle \phi(t) \rangle}{\delta h(s)} = \beta \partial_s \langle \phi(t)\phi(s) \rangle, \quad (t > s).$$

The situation becomes more complicated when the system is initially prepared away from equilibrium. One can for example thermalise the system at a given temperature T_i and then suddenly quench it at a different temperature T . In the simplest cases, the system will relax to the new equilibrium state and, at large times, an exponential decay of the global observables will be observed:

$$\langle \phi(t) \rangle = \langle \phi \rangle_T + \mathcal{A}e^{-t/\tau}, \quad (62)$$

where $\langle \phi \rangle_T$ is the equilibrium average at temperature T and τ the relaxation time of the slowest mode. In some situations, this new equilibrium state cannot be reached. The paradigmatic example is provided by glass-forming liquids [21]. When the latter are cooled sufficiently fast, the crystallisation does not take place and the liquid enters into a super-cooled phase where it is trapped in an amorphous state. The viscosity η increases extremely rapidly as the temperature is decreased. The experimental data are well reproduced by the empirical Vogel-Fulcher law

$$\eta(t) = \eta_0 e^{A/(T-T_0)}$$

in the case of the so-called fragile liquids. Below the glass temperature $T_g > T_0$, the system appears completely frozen, at least at accessible time-scales. Time-translation invariance of the two-time functions is broken, i.e. $C(t, s) \neq C(t - s)$. Instead, the density-density autocorrelation functions display two distinct regimes. In the second one, which is also the slowest, the relaxation is often approximated by a Kohrausch stretched exponential [412]

$$\phi(t) \sim e^{-(t/\tau)^\beta}, \quad (63)$$

where the exponent β is smaller than one. A similar situation is encountered in spin-glasses where magnetic moments interact via exchange couplings with random signs. The latter are experimentally obtained by diluting magnetic ions into an insulator. The sign of the exchange couplings between them depends in a complicated way on the overlap of their wavefunctions. The same result is obtained with magnetic ions randomly distributed into a conductor. In this case, the interaction is mediated by the conduction electrons with an intensity that oscillates with the distance. The random sign of the couplings causes magnetic frustration, which is an essential ingredient of the glass transition. The static properties were captured by Parisi's solution of the mean-field Sherrington-Kirkpatrick model [369, 508]. In the p -spin model, autocorrelation functions were shown to display the same two-plateau behaviour as structural glasses [133]. The violation of the FDT was observed experimentally [256], numerically [129] and analytically for the p -spin model [134, 135, 136]. The following relation was conjectured to hold

$$R(t, s) = \beta X(t, s) \frac{\partial C(t, s)}{\partial s}, \quad (64)$$

where the Fluctuation-Dissipation Ratio (FDR) $X(t, s)$ is a function of the autocorrelation functions, i.e. $X(t, s) = X[C(t, s)]$, in the case of the p -spin model. $\beta X(t, s)$ has been interpreted as an effective inverse temperature [132].

1.3.1. Phenomenology and scaling theory of aging ferromagnets

The slow dynamics of glasses is usually referred to as aging. A decade ago, it was realised that homogeneous ferromagnets also undergo such a behaviour. Interestingly, unlike in glasses, aging in ferromagnets can be explained in a very simple manner.

1.3.1.1. Lifschitz-Cahn-Allen growth law

Consider a ferromagnet, for example the Ising model, initially prepared in the high-temperature phase. Suppose that the system is quenched at time $t = 0$ at a temperature T below its critical temperature T_c . The new equilibrium state consists of the two ferromagnetic phases. In contradistinction to the high-temperature phase, the typical spin configurations are not similar under the reversal of all spins, i.e. $\sigma_i \rightarrow -\sigma_i$. The transformation maps one ferromagnetic phase onto the other. During its time evolution, the system will therefore be forced to break the symmetry of its initial state. Since the dynamics is local, the choice can only be made locally. Different ferromagnetic domains will grow in different regions of the system, and enter into competition to impose the global state of the system. An example of typical spin configurations at different times is presented on figure 35. In a finite system, one domain will eventually win over all others. In the thermodynamic limit, the time needed to eliminate all domain walls diverge. Therefore, the system never reaches the equilibrium state.

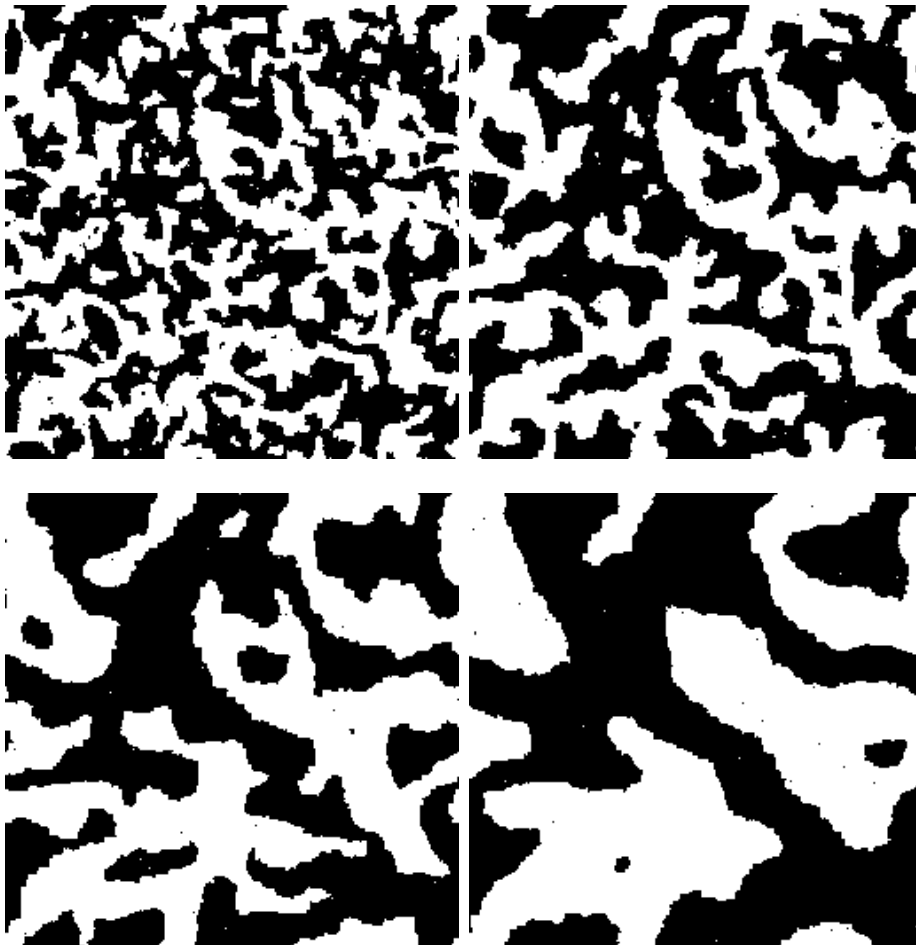


Figure 35 : Spin configurations of the Ising model during a quench in the low-temperature phase. The different snapshots correspond to times $t = 10, 30, 100,$ and 300 (from left to right and top to bottom).

Because of the surface tension between the ferromagnetic phases, the domain walls carry a non-vanishing free energy per unit of length. The dynamics being local, a domain wall will try to minimise this surface free energy by reducing its mean curvature κ . Using a simple phenomenological dynamical equation of the interface, it can be shown that the velocity of the wall should be $v = -(d-1)\kappa$ [14, 77]. For a domain whose characteristic size is L , the velocity behaves as $v \sim \frac{dL}{dt}$ while the curvature is $\kappa \sim 1/L$. The size of a domain is therefore expected to grow as

$$L(t) \sim t^{1/z}, \quad (65)$$

where the non-critical dynamical exponent z takes the value $z = 2$. Remarkably, this exponent does not depend on temperature. RG studies indeed suggest that the coarsening dynamics in the low-temperature phase is controlled by a $T = 0$ fixed point. The precise value $z = 2$ is imposed by the Langevin equation (60). For a dynamics conserving for example the global magnetisation (model B), the dynamical exponent is $z = 3$. More generally, a modified Cahn-Hilliard equation with $\Gamma \sim |k|^\mu$ as $k \rightarrow 0$, leads to $z = 1 + \mu$ [76]. In some models, the domain growth may be slowed down because the walls are pinned by topological defects, like in the XY model [1], or by impurities in random systems [253]. In these two cases, logarithmic corrections appear in the growth law:

$$L(t) \sim \left(\frac{t}{\ln t} \right)^{1/2}. \quad (66)$$

The typical domain size $L(t)$ appears in the scaling behaviour of equal-time correlation functions

$$C(\vec{r}, t) = \langle \phi(0, t) \phi(\vec{r}, t) \rangle = f(r/L(t)) \quad (67)$$

or equivalently, in the behaviour of the structure factor

$$S(\vec{k}, t) = \int C(\vec{r}, t) e^{i\vec{k} \cdot \vec{r}} d^d \vec{r} = [L(t)]^d \hat{f}(kL(t)). \quad (68)$$

These relations hold for the spherical model and the Ising-Glauber chain. They were also extensively tested for the Ising and Potts models by means of Monte Carlo simulations in the 1980s. Combined with the growth law (65), they were used to estimate the dynamical exponent z . While the earliest numerical calculations showed a dependence of the dynamical exponent on either the number of states of the Potts model or the temperature [432, 296], a perfect agreement with (65), (67) and (68) started emerging by the end of the decade [307, 310, 430, 250]. More recently, it was also shown that the distribution $n(A, t)$ of hull-enclosed areas can be obtained from the growth law (65). For a spherical domain of radius $L(t)$, the area A varies as

$$\frac{dA}{dt} = 2\pi L \frac{dL}{dt} \simeq 2\pi L v \simeq -2\pi(d-1)L\kappa \sim -2\pi(d-1).$$

This simple argument shows that all domain areas shrink at the same rate. The distribution $n(A, t)$ therefore can be easily obtained from the initial one. A good

agreement was achieved with numerical simulations in the case of the Ising model. The pure and random Potts models were also studied numerically [29, 332, 331].

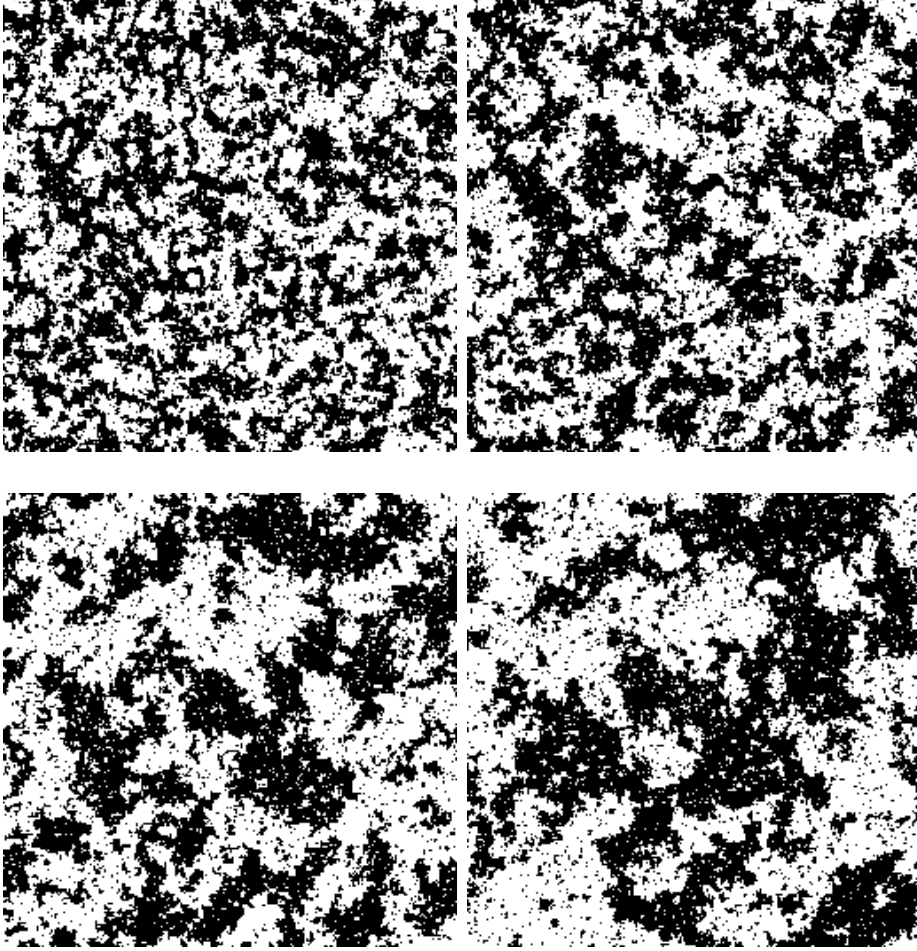


Figure 36 : Spin configurations of the Ising model during a quench at the critical temperature. The different snapshots correspond to times $t = 10, 30, 100,$ and 300 (from left to right and top to bottom).

When the system is quenched at the critical point, domains are observed at all length scales. Their interfaces develop a fractal structure because of the absence of surface tension. The characteristic length of the system is now the correlation length which grows as

$$\xi(t) \sim t^{1/z_c}, \quad (69)$$

where z_c is a non-trivial critical dynamical exponent. The equal-time correlation function is expected to decay as

$$C(r, t) = \langle \phi(0, t) \phi(\vec{r}, t) \rangle \sim r^{-(d-2+\eta)} f(r/\xi(t)), \quad (70)$$

and consequently the structure factor is

$$S(\vec{k}, t) = \int C(\vec{r}, t) e^{i\vec{k} \cdot \vec{r}} d^d \vec{r} = k^{-2+\eta} \hat{f}(k\xi(t)). \quad (71)$$

In this context, Renormalisation-Group techniques for the ϕ^4 model with a Langevin dynamics were introduced by Halperin *et al.* [221, 222] and further developed by Bausch *et al.* [42]. Soon after, series expansion of the critical dynamical exponent in dimension $d = 4 - \epsilon$ was obtained to order $\mathcal{O}(\epsilon^3)$ and shown to depend only on the static exponent η : $z_c \simeq 2 + [6 \ln \frac{4}{3} - 1]\eta$ [139]. In the case of the two-dimensional Ising model, the prediction is $z_c \simeq 2.1815$. A calculation was later performed in dimension $d = 1 + \epsilon$ and the results were combined with those at $d = 4 - \epsilon$ to provide a better accuracy at intermediate dimensions [41]. Monte Carlo simulations confirmed these values both for the two-dimensional Ising model [250, 267] and the three-dimensional one [485, 266]. The expressions (70) and (71) are well reproduced by the numerical data.

1.3.1.2. Initial-slip and autocorrelation exponents

At the end of the 1980's decade, the study of out-of-equilibrium dynamics was extended to other protocols. One of the most famous example was damage-spreading [454, 243]. The system is prepared at equilibrium. At time $t = 0$, a copy of the spin configuration is made. In one of the two replicas, one spin is flipped, thus creating a defect with respect to the other spin configuration. The two systems are evolved using the same sequence of random numbers. By monitoring the correlation between the two systems, the spreading of the defect can be traced. The growth of the defect is expected to follow the Lifschitz-Cahn-Allen law (65). Using this technique, more and more accurate estimates of the critical dynamical exponent z_c of the Ising model were obtained [251, 345, 356, 374, 209].

An interesting extension of damage spreading can be considered: at time $t = 0$, not only a spin is flipped but the temperature of one replica is also changed. If the system is initially prepared in the paramagnetic phase and quenched at the critical temperature, an initial spin-flip breaks the symmetry so that the spreading of the defect is actually given by the magnetisation. In this case, there is no need for a replica of the system anymore. The evolution of the magnetisation of the ϕ^4 field theory, when a small initial magnetisation is imposed, was studied by Renormalisation Group by Janssen *et al.* [282]. At large times t , magnetisation decays algebraically as $M(t) \sim t^{-\beta/\nu z}$. This behaviour can be obtained from simple scaling arguments by combining the growth law (69) and the relation $M \sim \xi^{\beta/\nu}$ between the equilibrium magnetisation and the correlation length. However, at short times t , the magnetisation was shown to first increase with time as $M(t) \sim t^\theta$. The so-called initial-slip exponent θ is a new critical dynamical exponent, independent of the static exponents. The counterintuitive behaviour of magnetisation at small times was exploited in the so-called Short-Time Dynamics Monte Carlo simulations [13]. The exponent θ was estimated to be equal to 0.191(3) for the two-dimensional Ising model, and 0.104(3) in the three-dimensional case [209].

When a small magnetisation is imposed in the initial state, the magnetisation $M(t)$ at time t can be shown to be equal to the magnetisation-magnetisation autocorrelation function $\langle M(0)M(t) \rangle$ [467]. Independently, autocorrelation functions $C(t, s)$ had already been studied in spin glasses and pure Ising models submitted to a quench and a new exponent λ had been introduced as [182, 252]

$$C(t, s) = \langle \sigma_i(t)\sigma_i(s) \rangle \underset{t \gg s}{\sim} t^{-\lambda/z}. \quad (72)$$

Monte Carlo simulations showed that the so-called autocorrelation exponent λ takes different values depending on whether the quench is performed at the critical temperature

or below. To distinguish between the two cases, the exponent is usually denoted λ_c at T_c and λ below. The autocorrelation exponent λ_c is related to the initial-slip exponent θ by

$$\lambda_c = d - z_c \theta, \quad (73)$$

where the appearance of the dimension d is due to the fact that equation (72) involves local spin-spin autocorrelation functions, while the initial-slip exponent is related to autocorrelations of the total magnetisation. Note that a surface autocorrelation exponent can be defined by considering the autocorrelation functions of a spin at the boundary of the system [348].

Below the critical temperature, the autocorrelation exponent λ was conjectured to be bounded by $d/2 \leq \lambda \leq d$ [182]. The lower bound was later shown rigorously by Yeung *et al.* [502]. The proof relies on the Cauchy-Schwartz inequality $C(r, t; 0, s) = \langle \sigma(r, t) \sigma(0, s) \rangle \leq \int \sqrt{S(k, t) S(k, s)} d^d k$. The integral is dominated by the small wavevectors, i.e. the large distances. Since the structure factor $S(k, s)$ is expected to be equal to the magnetisation M for small wavevectors k , the correlation is bounded as follows

$$C(r, t; 0, s) \sim [L(t)]^{-\lambda} \leq [L(t)]^{d/2} \sqrt{M} \int_0^{1/L(t)} \sqrt{f(kL(t))} d^d k \sim [L(t)]^{-d/2}$$

thus completing the proof. The numerical value of the autocorrelation exponents were estimated by means of Monte Carlo simulations [252, 329, 250]. For the two-dimensional Ising model, these estimates are $\lambda \simeq 1.24$, $\lambda_c/z_c \simeq 0.74(1)$ and therefore $\lambda_c \simeq 1.59(2)$. The autocorrelation exponent was shown to be affected by the presence of long-range correlations in the initial state [79]. If these correlations decay as $C(r, 0) \sim r^{-(d-\sigma)}$ then $\lambda = (d - \sigma)/4$ if $\sigma > d - 2\lambda$. The exponent is unchanged when $\sigma \leq d - 2\lambda$. Such a modification was also observed in the case of the spherical model [420].

It should be mentioned that the autocorrelation exponent, or equivalently the initial-slip exponent, is not the only exponent characterising the aging regime. The probability that a spin does not flip for a time t was shown to decay algebraically as $t^{-\theta'}$ in the one-dimensional Ising and Potts models [78, 149, 151]. In the same spirit, one may consider the probability that the sign of the total magnetisation does not change during a time t after a quench at the critical temperature [347]. If the dynamics of the global magnetisation is Markovian, which is usually not the case, then the persistence exponent is given by

$$z_c \theta' = \lambda_c - d + 1 - \eta/2.$$

1.3.1.3. Scaling theory of aging two-point functions

As discussed above, the recognition of the important role of autocorrelation functions in describing aging processes is a major achievement of the 1990's decade. A further step was made by Furukawa who first noticed that the scaling behaviour of autocorrelation functions

$$C(\vec{r}, t, s) = \langle \phi(\vec{r}, t) \phi(\vec{0}, s) \rangle \sim [L(t)]^{-\lambda} \mathcal{F}_C \left(\frac{r}{L(t)}, \frac{r}{L(s)} \right)$$

could equivalently be written as [192, 191]

$$C(\vec{r}, t, s) \sim [L(t)]^{-\lambda} \tilde{\mathcal{F}}_C \left(\frac{r}{L(t)}, \frac{L(t)}{L(s)} \right). \quad (74)$$

At the critical point, autocorrelation functions are expected to scale in a similar way:

$$C(\vec{r}, t, s) \sim [\xi(t)]^{-\lambda_c} \mathcal{F}_C \left(\frac{r}{\xi(t)}, \frac{\xi(t)}{\xi(s)} \right). \quad (75)$$

The dependence on the ratio $L(t)/L(s)$, or $\xi(t)/\xi(s)$ at the critical temperature, is a consequence of the self-similarity of domain walls. By looking at figures 35 and 36, the reader may convince herself that the system at time t' is similar to the one at time $t < t'$ when the lengths are appropriately rescaled. The state of the domains remains frozen if a dilatation with scale factor $1/L(t)$ is performed at each time t . It therefore seems more natural to assume that the “distance” between two domain configurations at times t and s is measured by the scale factor $L(t)/L(s)$ ($\xi(t)/\xi(s)$ at the critical temperature) that brings them to the same length scale. Note that the above discussion holds only if all length scales grow as (65). This is the case for domain walls but obviously not for thermal fluctuations whose characteristic length is the equilibrium correlation length. The full autocorrelation function can be decomposed into two independent contributions

$$C(t, s) = C_{\text{Therm.}}(t - s) + C_{\text{Ag.}}(t/s) \underset{\substack{t, s \gg \tau, \\ t - s \sim s}}{\sim} C_{\text{Ag.}}(t/s),$$

one corresponding to thermal fluctuations, and the other to domain walls. The scaling hypothesis presented above is therefore expected to hold only at time scales larger than the relaxation time τ of thermal fluctuations.

Below the critical temperature, spin-spin autocorrelation functions are expected to decay exponentially with the distance r . One may therefore assume that the scaling function (74) is of the form

$$C(\vec{r}, t, s) \sim [L(t)]^{-\lambda} \mathcal{F}_C \left(\frac{L(t)}{L(s)} \right) e^{-\frac{r}{L(t)}}.$$

The r -independent term is the one-site autocorrelation $C(0, t, s) = C(t, s)$. In the aging regime $t - s \sim s$, the scaling function $\mathcal{F}_C(L(t)/L(s))$ is approximated by $\mathcal{F}_C(1)$ that can be obtained from

$$C(s, s) \sim [L(s)]^{-\lambda} \mathcal{F}_C(1).$$

Spin-spin autocorrelation function scale finally in this regime as [203, 240]

$$C(t, s) \sim C(s, s) \left(\frac{L(t)}{L(s)} \right)^{-\lambda} \sim M_{\text{eq}}^2(s) \left(\frac{t}{s} \right)^{-\lambda/z}, \quad (76)$$

where $C(s, s) \sim M_{\text{eq}}^2(s)$ is the equilibrium magnetisation in a finite domain of size $L(s)$. At the critical temperature, spin-spin autocorrelation functions (75) are expected to decay algebraically with the distance r . One may assume

$$C(\vec{r}, t, s) \sim [\xi(t)]^{-\lambda_c} \mathcal{F}_C \left(\frac{\xi(t)}{\xi(s)} \right) \left(\frac{\xi(t)}{r} \right)^{d-2+\eta}.$$

In the aging regime $t - s \sim s$, the scaling function $\mathcal{F}_C(\xi(t)/\xi(s))$ is approximated by $\mathcal{F}_C(1)$ that can be obtained from

$$C(s, s) \sim [\xi(s)]^{-\lambda_c + d - 2 + \eta} \mathcal{F}_C(1).$$

Spin-spin autocorrelation functions are therefore expected to scale as

$$C(t, s) \sim C(s, s) [\xi(s)]^{-(d-2+\eta)} \left(\frac{\xi(t)}{\xi(s)} \right)^{-\lambda_c} \sim s^{-a_c} \left(\frac{t}{s} \right)^{-\lambda_c/z_c}, \quad (77)$$

where we have defined

$$a_c = (d - 2 + \eta)/z_c.$$

The autocorrelation function predicted by Renormalisation Group studies

$$C(\vec{r}, t; 0, s) = r^{-(d-2+\eta)} \left(\frac{t}{s} \right)^{1+(d-2+\eta-\lambda_c)/z_c} \tilde{\mathcal{F}}_C \left(\frac{r}{(t-s)^{1/z_c}}, \frac{t}{s} \right)$$

is consistent with this scaling behaviour [42, 282].

1.3.1.4. Response functions and violation of the FDT

The same scaling assumptions can be made for the response function too, leading below the critical temperature T_c to [203]

$$k_B T R(t, s) \underset{t, s \gg 1}{\sim} s^{-1-a} \left(\frac{t}{s} \right)^{-\lambda/z}. \quad (78)$$

The exponent appearing in the quasi-equilibrium prefactor is believed to be $a = 1/z$ when the correlation length is finite [238]. The dependence of the response on $L(t)/L(s)$ was confirmed by numerical simulations [62]. When combining (76) and (78), the FDR (64) reads

$$X(t, s) = k_B T R(t, s) [\partial_s C(t, s)]^{-1} \underset{t, s \gg 1}{\sim} s^{-a}.$$

The FDR vanishes in the limit $s \rightarrow +\infty$. As expected, the Fluctuation-Dissipation Theorem (64) is violated because the slow growth and coalescence of domain walls are irreversible processes. However, as shown by example by Monte Carlo simulations [37], the integrated response function displays a second regime at small times where the FDT holds. Reversible processes indeed take place at time scales smaller than the characteristic time of domain coarsening. When the size $L(t)$ of a domain becomes larger than the equilibrium correlation length ξ , the degrees of freedom inside the domain behave as in an homogeneous ferromagnetic phase. Reversible thermal fluctuations of energy $\Delta E \sim \sigma \ell^{d-1}$ occur during a time of order $e^{-\beta \Delta E}$.

At the critical temperature, the response function is assumed to scale as

$$k_B T_c R(t, s) \underset{t, s \gg 1}{\sim} (t-s)^{-1-a_c} \left(\frac{t}{s} \right)^{-\lambda_c/z_c}. \quad (79)$$

The autocorrelation exponent λ_c usually takes the same value for the autocorrelation and response functions. However, some counterexamples exist, like the XY model with an initially ordered state ^[63] or the spherical model with a correlated initial state ^[421]. Combining (77) and (79) leads to the FDR (64)

$$X(t, s) = k_B T R(t, s) [\partial_s C(t, s)]^{-1} \underset{t, s \gg 1}{\sim} \frac{A_R}{A_C} \left(\frac{\lambda_c}{z_c} - a_c \right)^{-1}.$$

The asymptotic value of the FDR

$$X_\infty = \lim_{s \rightarrow +\infty} \lim_{t \rightarrow +\infty} X(t, s)$$

depends only on critical exponents and on the ratio of amplitudes, and hence is believed to be universal ^[203]. In the simple cases of the random walk, the Gaussian model or the two-dimensional XY model in the spin-wave approximation, the autocorrelation and response functions are known exactly. In all these cases, the FDR takes the asymptotic value $X_\infty = 1/2$. Remarkably, the same value was obtained for the Ising-Glauber chain ^[201, 328] and for the spherical model in dimension $d > 4$ ^[202]. In lower dimension, the asymptotic FDR of the latter is different: $X_\infty = 1 - 2/d$. The field theory associated to the Langevin equation was extended by the introduction of a new field $\tilde{\phi}$ allowing for the calculation of the response as a correlation function $\langle \phi \tilde{\phi} \rangle$ ^[352]. RG estimations of the response of the ϕ^4 model in dimension $d = 4 - \epsilon$ calculated within this framework led to a FDR ^[88, 90, 194]

$$X_\infty(q = 0) = \frac{1}{2} \left[1 - \frac{\epsilon n + 2}{4 n + 8} \right] + \mathcal{O}(\epsilon^2).$$

The FDR was shown to be sensitive to correlated initial conditions. In the case of the Ising-Glauber chain, X_∞ takes two different values depending on whether the initial state has finitely many domain walls or not ^[242]. The same sensitivity to the initial correlations was observed in the spherical model ^[420]. A non-vanishing initial magnetisation m_0 also seems to be a relevant perturbation, thus inducing new exponents and ratios. In the long-range Ising model, the FDR was shown to be $X_\infty = 1/2$ if $m_0 = 0$ and $4/5$ for $m_0 > 0$ ^[197]. RG calculations for the ϕ^4 model in dimensions $d = 4 - \epsilon$ showed the same tendency, with a FDR

$$X_\infty = \frac{4}{5} \left[1 - \left(\frac{73}{480} - \frac{\pi^2}{80} \right) \epsilon \right] + \mathcal{O}(\epsilon^2)$$

in presence of non-vanishing initial magnetisation. The same observation was made for the spherical model in dimension $d > 4$ ^[24, 26]. Below $d = 4$, X_∞ depends on both the initial magnetisation and the dimension. While approaching $d = 2$, the FDR develops a singular behaviour.

As the experimental measure, the numerical calculation of the linear response is in principle impossible directly because it involves the estimation of the variation of magnetisation caused by the application of an extremely small magnetic field during a time extremely short. In a Monte Carlo simulation, a sufficiently strong magnetic field has to be applied to measure a response larger than the statistical noise due to the finite

number of histories. Therefore, a non-linear response is measured. Experimentally and numerically, it is easier to measure an integrated response, for example

$$\chi_{\text{TRM}}(t, s) = \int_0^s R(t, u) du$$

corresponding to the magnetisation at time t when a magnetic field $h = 1$ is applied between the times 0 and s . Under the assumption $X(t, s) = X(C)$, the FDR may be estimated as the slope of a plot of $R(t, s)$ versus $C(t, s)$ [37, 203]. The value $X_\infty \simeq 0.34$ was estimated in this way for the two-dimensional Ising model [357].

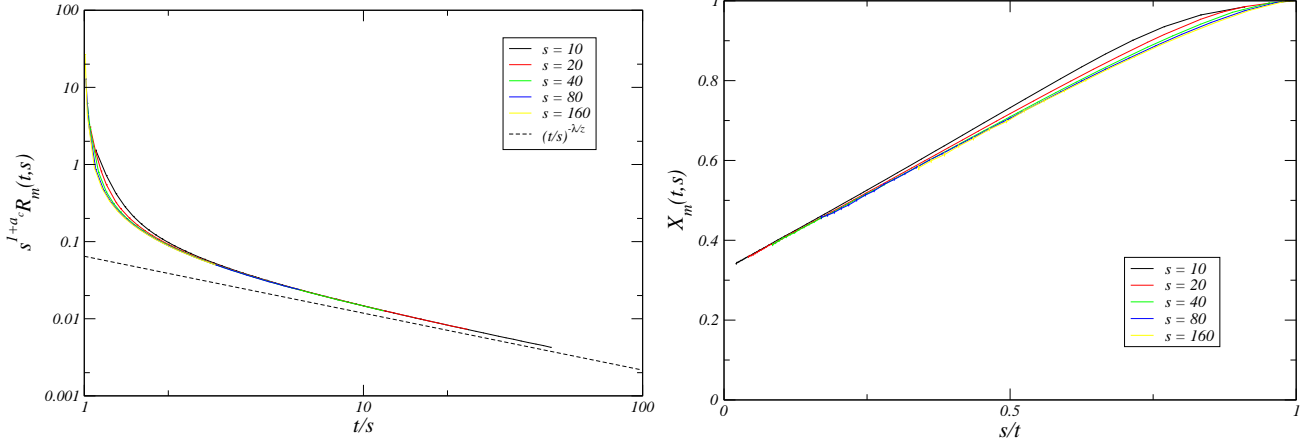


Figure 37 : On the left, scaling function $s^{1+a_c} R(t, s)$ of the linear response function of the two-dimensional Ising model quenched at its critical temperature versus t/s . The data have been averaged over 1.382.017 independent histories. On the right, FDR $X(t, s)$ versus s/t (unpublished).

We have introduced an algorithm allowing for a reduction of the statistical noise of the linear response [104]. Consider a spin model with a Markovian dynamics:

$$\wp(\sigma, t+1) = \sum_{\sigma'} \wp(\sigma', t) W(\sigma \rightarrow \sigma').$$

A magnetic field is coupled to the system by modifying the transition rates W . The response function of the spin σ_i to the introduction of a magnetic field at the site j can be written as

$$\begin{aligned} R_{ij}(t, s) &= \frac{\partial \langle \sigma_i(t) \rangle}{\partial h_j(s)} \\ &= \frac{\partial}{\partial h_j(s)} \left[\sum_{\{\sigma, \sigma'\}} \sigma_i \wp(\sigma, t | \sigma', s+1) \wp(\sigma', s+1) \right] \\ &= \sum_{\{\sigma, \sigma'\}} \sigma_i \wp(\sigma, t | \sigma', s+1) \frac{\partial}{\partial h_j} \wp(\sigma', s+1) \\ &= \sum_{\{\sigma, \sigma', \sigma''\}} \sigma_i \wp(\sigma, t | \sigma', s+1) \frac{\partial}{\partial h_j} W(\sigma'' \rightarrow \sigma') \wp(\sigma'', s) \\ &= \sum_{\{\sigma, \sigma', \sigma''\}} \sigma_i \frac{\partial \ln W}{\partial h_j}(\sigma'' \rightarrow \sigma') \wp(\sigma, t | \sigma', s+1) W(\sigma'' \rightarrow \sigma') \wp(\sigma'', s). \end{aligned}$$

For the Ising-Glauber model, the response reads

$$R_{i,j}(t, s) = \beta \langle \sigma_i(t) [\sigma_j(s+1) - \sigma_j^W(s)] \rangle, \quad (80)$$

where $\sigma_j^W = \tanh(\sum_{k \neq j} J_{jk} \sigma_k)$ is the equilibrium value of σ_j in the Weiss field of its neighbours. The computation of the linear response is reduced to that of a correlation function. Furthermore, there is no need to apply a magnetic field. For this reason, this algorithm was called *no-field* algorithm. Various versions were proposed [427, 326]. From the response, the FDR can be estimated as

$$X(t, s) = \frac{k_B T R(t, s)}{\partial_s C(t, s)} = \frac{\sum_i \langle \sigma_i(t) [\sigma_i(s+1) - \sigma_i^W(s)] \rangle}{\sum_i \langle \sigma_i(t) [\sigma_i(s+1) - \sigma_i(s)] \rangle} \quad (81)$$

An example for the two-dimensional Ising model is presented in figure 37. Using the no-field algorithm, the FDR of the two-dimensional Ising model was estimated to be $X_\infty \simeq 0.328(1)$ [105].

The question of the interpretation of X_∞ as an effective inverse temperature attracted a lot of attention. An important requirement is that the FDR takes the same value for all observables. Many articles pointed out the fact that this is not the case for an aging ferromagnet. RG calculations for the ϕ^4 model give different series expansions for the FDR of magnetisation and energy when $d < 4$ [89]. While $X_\infty \simeq 0.33$, for both magnetisation and energy in the two-dimensional Ising model, the FDR of energy in the Ising-Glauber is $X_E = 0$ (while $X_M = 1/2$) [357]. In the spherical model, the FDR is the same for various local observables (spin, energy, etc.), but not for global magnetisation and global energy in dimensions $d < 4$ [25]. In conclusion, the FDR does not provide a measure of an effective temperature of a ferromagnetic during a quench.

1.3.1.5. Local Scale Invariance

The recent Local Scale Invariance theory provided exact expressions for the response and autocorrelation functions during a quench. It is based on the study of the representations of a Lie group of transformations leaving the Langevin equation invariant [240].

Consider first the simpler case of the diffusion equation $\partial_t \phi = D \Delta \phi$, which is equivalent to a Schrödinger equation with a complex mass $m = i/2D$. The latter is invariant under the transformations of the Galilean group. The quantum wavefunction is however a non-projective representation of this group since it acquires a phase during a Galilean boost. The infinitesimal generators of the group are

$$\begin{cases} X_n = -t^{n+1} \partial_t - \frac{n+1}{2} t^n r \partial_r - \frac{n(n+1)}{4} \mathcal{M} t^{n-1} r^2 - \frac{x}{2} (n+1) t^n, \\ Y_m = -t^{m+1/2} \partial_r - \left(m + \frac{1}{2}\right) \mathcal{M} t^{m-1/2} r, \\ M_n = \mathcal{M} t^n, \end{cases}$$

where $n \in \{-1; 0; 1\}$ and $m \in \{-1; 1/2\}$, and x is the scaling dimension of the quantum field ϕ . X_{-1} is the generator of time translations, X_0 of dilatations, X_1 of conformal special transformations, Y_{-1} of space translations, $Y_{1/2}$ of Galilean boosts and M_0 of the phase change of ϕ . These local transformations generalise the global transformation

$(\vec{r}, t) \rightarrow (\vec{r}/b, t/b^z)$ ensuring the invariance of the growth law (65). The factor $1/2$ appearing in the expression of X_0 is directly related to the dynamical exponent $z = 2$ of diffusion. These generators satisfy the Lie algebra:

$$\begin{cases} [X_n, X_m] = (n - m)X_{n+m}, \\ [X_n, Y_p] = \left(\frac{n}{2} - p\right)Y_{n+p}, \\ [Y_p, Y_q] = (p - q)M_{p+q}, \\ [X_n, M_m] = [Y_n, M_m] = -mM_{n+m}. \end{cases}$$

The idea behind Local Scale Invariance is to consider the representation of a sub-algebra corresponding to the transformations that are supposed to leave invariant the aging dynamics. In particular, the invariance under time translation is broken by the initial conditions. The generator X_{-1} should therefore be excluded. The exact expression of the response function $R(t, s)$ was obtained by imposing its invariance under dilatation and special transformations, i.e. $X_0 R = X_1 R = 0$, [241, 236]

$$R(t, s) = r_0(t - s)^{-1-a} \left(\frac{t}{s}\right)^{1+a-\lambda/z}. \quad (82)$$

This prediction was widely debated in the literature and compared with numerical results, mostly for two and three-dimensional Ising models [239, 330, 422, 327]. Small deviations were usually observed, especially at T_c where thermal fluctuations play an important role. The theory is indeed based on infinitesimal generators X_n , Y_n and M_n corresponding to transformations that leave the noiseless Langevin equation invariant. However, it can be shown that the noise term of the Martin-Siggia-Rose action does not contribute to the response to any order in perturbation. Nevertheless, the limitation to a dynamical exponent $z = 2$ restricts the application of (82) to zero temperature. The infinitesimal generators X_n were later extended to dynamical exponents $z \neq 2$ and a new expression of the response function was obtained [237]:

$$R(t, s) = s^{-1-a} \left(\frac{t}{s}\right)^{1+a'-\lambda/z} \left(\frac{t-s}{s}\right)^{-1-a'}. \quad (83)$$

involving now a new parameter $a' \neq a$. A good agreement with numerical data was reported in the case of the two-dimensional Ising model, even though the presence of small deviations was claimed to prove that (83) was not exact [127]. We will discuss this prediction of the response in the context of the Potts model with an irreversible dynamics.

1.3.2. Out-of-equilibrium dynamics of the Potts model

In this section, we present our results concerning the out-of-equilibrium dynamics of a one-dimensional Ising-like model and of two-dimensional models with the same symmetry as the Potts model.

1.3.2.1. Aging in one-dimensional spin models

In a celebrated paper, Glauber introduced a Markovian dynamics for the Ising model and calculated exactly the one-point and two-point functions in the one-dimensional case [199]. We briefly summarise here these results. Consider a chain of N spins σ_i . The probability to observe a given spin configuration $\sigma = \{\sigma_i\}_i$ at time t evolves according to the master equation

$$\partial_t \wp(\sigma, t) = \sum_{\sigma'} [\wp(\sigma', t)W(\sigma' \rightarrow \sigma) - \wp(\sigma, t)W(\sigma \rightarrow \sigma'),] \quad (84)$$

where $W(\sigma' \rightarrow \sigma)$ is the rate of a transition $\sigma' \rightarrow \sigma$. Glauber assumed that these transition rates are limited to spin flips $\sigma_i \rightarrow -\sigma_i$:

$$W(\sigma \rightarrow \sigma') = \frac{1}{N} \sum_i \omega(\sigma_i) \left[\prod_{j \neq i} \delta_{\sigma_j, \sigma'_j} \right].$$

The most general transition rates depending only on the states of the two neighbouring spins σ_{i-1} and σ_{i+1} and preserving the global symmetry $\sigma_i \rightarrow -\sigma_i$ for all i , is

$$\omega(\sigma_i) = \frac{\alpha}{2} \left[1 - \frac{\gamma}{2} \sigma_i (\sigma_{i-1} + \sigma_{i+1}) + \delta \sigma_{i-1} \sigma_{i+1} \right]. \quad (85)$$

The parameter α can be absorbed into a renormalisation of the time t . Glauber then imposed the constraint that the stationary distribution $\wp_{\text{st.}}(\sigma)$ be the Boltzmann weight for the Ising Hamiltonian. A solution can easily be found if the detailed balance condition holds, i.e. if the expression within the brackets in (84) vanishes. The parameters of the transition rates are then related to the exchange coupling $K = \beta J$ by

$$\gamma = (1 + \delta) \tanh K. \quad (86)$$

Glauber restricted himself to the case $\delta = 0$. He showed that a closed set of linear evolution equations are obtained for the magnetisation, the equal-time correlation functions and the autocorrelation functions. It is instructive to consider the average magnetisation with homogeneous initial conditions. In this case, the decay is $m(t) = e^{-(1-\gamma)t}$, i.e. exponential for $\gamma \neq 1$. At the point $\gamma = 1$, corresponding to a temperature $T = 0$, the relaxation time diverges, as expected since the equilibrium Ising model is critical. The dynamics of the domains walls was observed to be equivalent to a model of particles diffusing and annihilating by pair, i.e. $A + A \rightarrow \emptyset$ in the standard notations [45¹, 45², 15, 153]. The average distance between particles, i.e. the average domain size in the spin language, grows as

$$L(t) = \frac{2\sqrt{\pi}}{1 - m_0^2} t^{1/2}$$

i.e. as expected (65) for an aging ferromagnet. Let us mention finally that some new correlations were calculated exactly: the probability to have n consecutive domain walls [424] or the probability that an interval contains an even number of particles [353] using the method of intervals [87]. We will apply the same techniques to the KDH model.

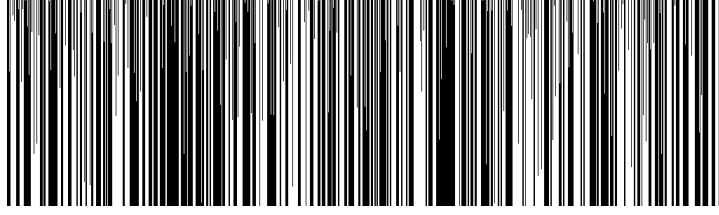


Figure 38 : Typical history of the KDH model near the point $\gamma = 2$ and $\delta = 1$. The vertical direction corresponds to the time direction. The spin configuration of the chain at time $t = 0$ is represented on the upper line.

The full transition rates (85) were considered again by Kimball [301] and Decker and Haake [145]. They showed that a closed set of two evolution equations is obtained for the global magnetisation and a tri-spin product $Q = \sum_i \sigma_{i-1} \sigma_i \sigma_{i+1}$ in the special case $\gamma = 2\delta$, not considered by Glauber. Note that on this line in the $\gamma - \delta$ plane, detailed balance is not satisfied except at the point $\gamma = 2$ and $\delta = 1$, corresponding to zero temperature according to (86). Interestingly, the slowest relaxation time of global magnetisation or tri-spin correlation diverges at this point. The study of its behaviour in the vicinity of $\gamma = 2$ shows that the dynamical exponent is $z = 4$, i.e. very different from the Ising-Glauber value $z = 2$. To understand this difference, it is useful to introduce the following factorisation of the transition rates (85) [407, 128]:

$$\omega(\sigma_i) = \frac{\alpha}{2} \left[1 - \frac{\gamma}{2(1+\delta)} \sigma_i (\sigma_{i-1} + \sigma_{i+1}) \right] \left[1 + \delta \sigma_{i-1} \sigma_{i+1} \right].$$

By absorbing the last term into an effective parameter $\alpha_{\text{eff.}} = \alpha \left[1 + \delta \sigma_{i-1} \sigma_{i+1} \right]$, the usual Glauber transition rates are recovered but with a characteristic time $1/\alpha_{\text{eff.}}$ of the spin flip $\sigma_i \rightarrow -\sigma_i$ that now depends on the relative state of the two neighbours. The dynamics is said to be facilitated. At zero temperature, the transition is allowed only if the two neighbours are in the same state. An example of typical history is presented on figure 38. In contradistinction to the Ising-Glauber model, there exists a macroscopically large number $((1 + \sqrt{5})/2)^L$ of steady states with an arbitrary number of domain walls. The system is not critical, simply frozen in one of the many absorbing states. The divergence of the relaxation time is due to the fact that it is not possible to tunnel from one steady state to the other at zero temperature. Global autocorrelation and response functions were calculated analytically [173]. Both decay exponentially and not algebraically.

Like the Ising-Glauber model, the dynamics of the domain walls in the KDH model consists in pair-annihilation and diffusion. However, in contradistinction to the Ising model for which the domain walls can always hop from one site to the other, diffusion is not allowed anymore in the KDH model at zero temperature. As a consequence, domain walls behave as a gas of immobile particles that can only annihilate with their neighbours. To be more quantitative, define the kink variable

$$\eta_i = \frac{1 - \sigma_i \sigma_{i+1}}{2} \in \{0; 1\}.$$

In the case $\gamma = 2\delta = 2$, the transition rates associated to single-spin flips can be rewritten in terms of kinks as

$$\omega_i(\sigma_i) = \frac{\alpha}{2} (1 - \sigma_i \sigma_{i-1}) (1 - \sigma_i \sigma_{i+1}) = 2\alpha \eta_{i-1} \eta_i.$$

In the following, the parameter α will be absorbed into a redefinition of time. The transition rates vanish unless two kinks occupy the sites i and $i - 1$. Only in this case, the spin-flip $\sigma_i \rightarrow -\sigma_i$ can happen. In terms of kinks, the transition corresponds to

$$\eta_{i-1} \longrightarrow 1 - \eta_{i-1}, \quad \eta_i \longrightarrow 1 - \eta_i$$

i.e. to the annihilation of the two kinks. We showed that for some observables having a simple expression in terms of kinks, a closed set of linear evolution equations can be obtained. This is in particular the case of the probability of occurrence of a string of n consecutive kinks ^[119]:

$$C_n(t) = \langle \eta_1(t) \eta_2(t) \dots \eta_n(t) \rangle.$$

When the initial conditions are homogeneous, the evolution equation reads

$$\frac{d}{dt} C_n(t) = -4C_{n+1}(t) - 2(n-1)C_n(t).$$

We solved this equation by standard techniques: the last term is eliminated by the transformation $C_n(t) = u_n(t) e^{-2(n-1)t}$. A time renormalisation $s = \frac{e^{-2t}-1}{2}$ leaves

$$\frac{d}{ds} u_n(s) = 4u_{n+1}(s),$$

which is solved by means of a generating function. The solution is finally

$$C_n(t) = \sum_{m=0}^{\infty} \frac{2^m}{m!} C_{m+n}(0) (e^{-2t} - 1)^m e^{-2(n-1)t}. \quad (87)$$

The probabilities decay exponentially to zero, apart from the density of kinks $C_1(t)$ which goes to a constant at infinite time t . The average distance between kinks, i.e. the domain size, is asymptotically finite, in contradistinction to the Ising-Glauber model. The calculation was generalised to the case of inhomogeneous initial conditions that allowed us to consider in particular the probability in presence of a boundary. Results similar to (87) were obtained on the Bethe lattice. In the spirit of the empty-interval method, we then considered the correlation between two strings of respectively n and m kinks separated by a hole of k sites (see figure 39):

$$\begin{aligned} C_{n,m}^k(t) &= 2^k \left[\frac{(e^{-2t} - 1)^{k+1}}{(k+1)!} + \frac{(e^{-2t} - 1)^k}{k!} \right] \\ &\times \sum_{p=0}^{+\infty} \frac{2^p u_{n+m+p+k}(0)}{p!} (e^{-2t} - 1)^p e^{-2(n+m-2)t} \\ &+ \sum_{l=1}^k \sum_{\substack{a=n, \\ b=m}}^{+\infty} \left[\sum_{i=0}^{k-l} \frac{u_{a+i, b+k-l-i}^l(0)}{i! (k-l-i)!} \right] \frac{(e^{-2t} - 1)^{k-l+a+b-n-m}}{(a-m)! (b-m)!} e^{-2(n+m-2)t}. \end{aligned}$$

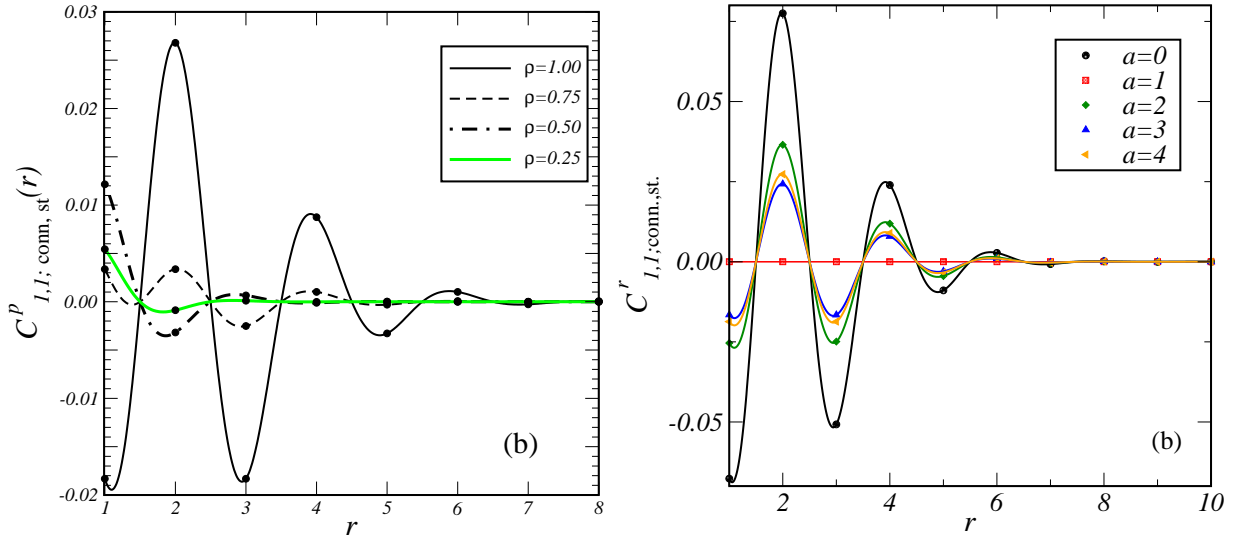


Figure 39 : On the left, density-density connected correlation in the steady state versus the distance r . The different curves correspond to different values of the initial concentration ρ of uncorrelated kinks. On the right, the density-density connected correlation in the steady state is plotted for different distances a between a boundary and the first site in the case $\rho = 1$.

We then extended the problem to the case of two species A and B of immobile particles that can annihilate through the reaction $A + B \rightarrow \emptyset$. The densities of A and B particles are obtained in the same way as the density of kinks presented above:

$$A_n(t) = \frac{1}{2} \left[A_n(0) - B_n(0) + \sum_{m=0}^{\infty} \frac{2^m}{m!} (A_{n+m}(0) + B_{n+m}(0)) (e^{-t} - 1)^m \right] e^{-(n-1)t},$$

$$B_n(t) = \frac{1}{2} \left[B_n(0) - A_n(0) + \sum_{m=0}^{\infty} \frac{2^m}{m!} (A_{n+m}(0) + B_{n+m}(0)) (e^{-t} - 1)^m \right] e^{-(n-1)t}.$$

Finally, we showed that a closed set of evolution equations can be obtained and solved for the correlation of two blocks, of respectively n and m particles, separated by k sites, only if all even sites are occupied by a A particle and odd ones by a B particle (or the opposite).

1.3.2.2. Aging in two-dimensional models in the Potts universality class

We tested the universality of the autocorrelation exponent λ_c and of the asymptotic FDR X_∞ measured during a quench at the critical temperature. To that purpose, we studied by means of Monte Carlo simulations the two-dimensional Potts models with $q = 2, 3$ and 4 states on different lattices. In a second step, numerical estimates of λ_c/z_c and X_∞ for several models in different universality classes were compared [105].

1.3.2.2.1. Lattice-independence of λ_c and X_∞

We considered the Potts model whose Hamiltonian is

$$-\beta H = J \sum_{(i,j)} \delta_{\sigma_i, \sigma_j} - \sum_i h_i \delta_{\sigma_i, 0},$$

where the magnetic field is introduced only to define a response function

$$R_{ij}(t, s) = \frac{\delta \langle \delta \sigma_i(t), 0 \rangle}{\delta h_j(s)}.$$

The system was evolved using the Glauber dynamics and the response was measured with the *no-field* algorithm (80). Three different lattices were considered: square, triangular and honeycomb. In the last two cases, we used the exact critical temperatures obtained from the star-triangle transformation [297]. The autocorrelation exponent was extracted from the decay of the spin-spin autocorrelation functions (77). The response turned out to give less accurate estimates. The FDR is estimated numerically using (81). As can be seen on Tables 6 and 7, the three lattices give estimates of both λ_c/z_c and X_∞ in good agreement. The deviations are systematically smaller than the error bars.

Models	Square	Triang.	Honeyc.
Ising	0.738(21)	0.739(22)	0.731(17)
3-state Potts	0.844(18)	0.845(20)	0.844(16)
4-state Potts	0.99(12)	0.99(17)	0.97(8)

Tableau 6 : Autocorrelation exponents λ_c/z_c of the q -state Potts models with $q = 2, 3$ and 4 on the square, triangular and honeycomb lattices.

Theses values are in good agreement with those found in the literature for a square lattice and based on the Short-Time Dynamics technique. The autocorrelation exponents presented below were recalculated from the initial-slip exponent θ using (73). In the case of the Ising model, our estimates of the autocorrelation exponent is compatible with the values $\lambda_c/z_c \simeq 0.731(3)$ [209], and 0.732 [396] using the dynamical exponent $z_c \simeq 2.1667(5)$ [394]. Our values of the FDR are more accurate than previous estimates [357, 435]. In the case of the three-state Potts model, our autocorrelation exponents are compatible with 0.828(2) [441]. In the case of the four-state Potts model, our values agrees with the estimate 0.919 assuming $z_c = 2.294$ [27], and with 0.917(11) assuming $z_c = 2.296(5)$ [28].

Models	Square	Triang.	Honeyc.
Ising	0.328(1)	0.323(1)	0.328(1)
3-state Potts	0.406(1)	0.402(3)	0.404(1)
4-state Potts	0.459(8) [†]	0.460(4) [†]	0.467(21) [†]

Tableau 7 : Asymptotic FDR X_∞ of the q -state Potts models with $q = 2, 3$ and 4 on the square, triangular and honeycomb lattices. The symbol [†] indicates possible corrections to scaling.

1.3.2.2.2. Models in different universality classes

To test the universal character of both λ_z/z_c and X_∞ , we compared the three-state Potts model to the Ashkin-Teller model at the point of its critical line with the same ν exponent, and the four-state Potts model to the Baxter-Wu and Debierre-Turban models.

The symmetric Ashkin-Teller model corresponds to two Ising models coupled at each site by their energy densities. The Hamiltonian is ^[30]

$$-\beta H = \sum_{(i,j)} [J\sigma_i\sigma_j + J'\tau_i\tau_j + K\sigma_i\sigma_j\tau_i\tau_j],$$

where σ_i and τ_i are Ising spins. This model was shown to provide a good description of the order-disorder phase transition of submonolayers of Selenium adsorbed on Nickel (100) surfaces ^[34]. Obviously, the line $K = 0$ corresponds to two uncoupled Ising models while for $J = J' = K$, the Ashkin-Teller model is equivalent to the four-state Potts model. A four-state spin η_i can indeed be constructed from the Ising spins σ_i and τ_i as

$$\eta_i = \frac{1}{2}(\sigma_i + 1) + (\tau_i + 1).$$

One can then check that when $J = J' = K$, the energy per pair of sites (i, j) is $3J$ if $\sigma_i = \sigma_j$ and $\tau_i = \tau_j$ and $-J$ otherwise. The latter can therefore be rewritten as $4\delta_{\eta_i, \eta_j} - 1$. On a square lattice, the phase diagram of the Ashkin-Teller model displays several critical lines. In the $J - K$ plane, a self-dual line

$$e^{-2K} = \sinh 2J = \sinh 2J', \quad \frac{\ln 3}{4} < K < +\infty,$$

joins the Ising ($J_c = \frac{1}{2} \ln(1 + \sqrt{2})$) and four-state Potts ($J_c = \frac{1}{4} \ln 3$) critical points ^[178]. The critical exponents vary continuously along this line:

$$\nu = \frac{2-y}{3-2y}, \quad \beta_\sigma = \frac{2-y}{24-16y}, \quad \beta_{\sigma\tau} = \frac{1}{12-8y},$$

where the parameter $y \in [0; 4/3]$ is defined by ⁽⁸⁾

$$\cos \frac{\pi y}{2} = \frac{1}{2} [e^{4K} - 1] \Leftrightarrow K = \frac{1}{4} \ln \left[1 + 2 \cos \frac{\pi y}{2} \right].$$

Note that the ratio $\beta_\sigma/\nu = 1/8$ is constant along the critical line. After the four-state Potts critical point $y = 0$, the critical line splits into two branches ^[496, 292] believed to belong to the Ising model universality class. Between these two branches, the two Ising models forming the Ashkin-Teller model are paramagnetic but they are strongly correlated, i.e. their product $\sigma_i\tau_i$ is in a ferromagnetic state. Like the Potts model, the Ashkin-Teller model can be mapped onto a six-vertex model and then onto a Solid-On-Solid model. The critical exponents were determined exactly using the correspondence with the Coulomb gas ^[290, 389, 433]. In the following, we will be interested in the point $y = 3/4$ of the critical line. The thermal exponent ν is the same as for the three-state

⁽⁸⁾ Again, this parameter is not the den Nijs parameter defined in equation (8), nor (31).

Potts model ($\nu = 5/6$)⁽⁹⁾. However, magnetic scaling dimensions are different ($\frac{\beta_\sigma}{\nu} = \frac{1}{8}$ and $\frac{\beta_{\sigma\tau}}{\nu} = \frac{1}{5}$ while $\frac{\beta}{\nu} = \frac{2}{15}$ for the three-state Potts model).

The Baxter-Wu model corresponds to Ising spins on a triangular lattice interacting by triplet inside each plaquette [48, 49, 44]

$$-\beta\Delta H = J \sum_{(i,j,k)\in\Delta} \sigma_i\sigma_j\sigma_k.$$

The partition function was calculated exactly using Bethe ansatz. The system is critical at the coupling $J_c = \frac{1}{2} \ln(1 + \sqrt{2})$ as the Ising model. The similitude does not go further since the Baxter-Wu model belongs to the four-state Potts model universality class [212]. The ground-state is indeed four-fold degenerated: the energy is minimised by the spin configurations $+++$, $+-$, $-+-$ and $- - +$ on the plaquette. Amplitude ratios were also shown to be numerically compatible for the two models [55, 447]. However, logarithmic corrections affect the critical behaviour of the four-state Potts model but not the one of the Baxter-Wu model [387, 99].

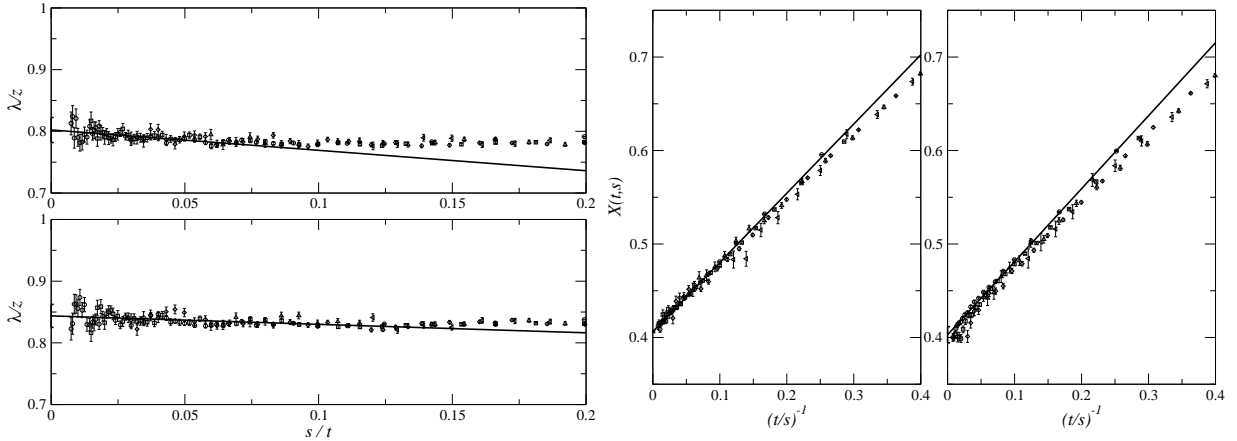


Figure 40 : On the left, effective exponent λ_c/z_c extracted from the decay of the spin-spin autocorrelation functions $C(t, s)$ versus the smallest time t used in the interpolation. The two graphs correspond to the three-state Potts model (top) and the Ashkin-Teller model at the point with the same exponent ν (bottom). On the right, asymptotic FDR for the same models. The different symbols correspond to different waiting times s .

The multispin Ising model introduced by Debierre and Turban is defined on the square lattice by the Hamiltonian [144]

$$-\beta H = \sum_{x,y} [J_1\sigma_{x,y}\sigma_{x+1,y} + J_2\sigma_{x,y}\sigma_{x,y+1}\cdots\sigma_{x,y+m}],$$

where x and y are the lattice coordinates. Spins interact by pairs in the horizontal direction whereas m spins are coupled in the vertical one. Remarkably, the self-dual line is independent of the parameter m and is therefore identical to the Ising

⁽⁹⁾ In reference 105, the two models were incorrectly claimed to be in the same universality class. Only thermal exponents are identical.

one, i.e. $\sinh 2J_1 \sinh 2J_2 = 1$. The critical exponents estimated by transfer matrix diagonalisation [144] and Monte Carlo simulations [68] are compatible with those of the four-state Potts model. As in the case of the Baxter-Wu model, the ground-state is four-fold degenerated with spin configurations homogeneous in the horizontal direction but with alternating pattern $+++$, $+-$, $-+-$ and $---$ in the vertical one. The observation that the two models have equivalent quantum Hamiltonians in the extreme anisotropic limit confirmed that the multispin Ising model belongs to the four-state Potts universality class [257]. The surface exponents were also shown to be the same provided logarithmic corrections are taken into account [258]. For $m = 4$, the transition was conjectured to be of first-order. This was confirmed by Monte Carlo simulations [103].

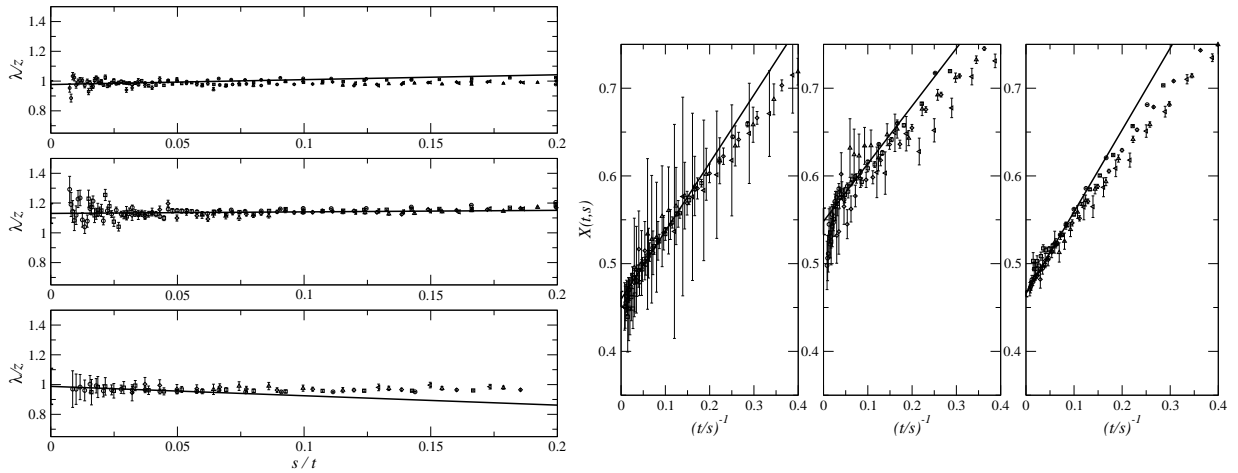


Figure 41 : On the left, effective exponents λ_c/z_c extracted from the decay of the spin-spin autocorrelation functions $C(t, s)$ versus the smallest time t used in the interpolation. The three graphs correspond to the four-state Potts model (top), the Baxter-Wu model (middle) and the Debierre-Turban model (bottom). On the right, asymptotic FDR for the same models. The different symbols correspond to different waiting times s .

For these five models, we computed the spin-spin autocorrelation and response functions and extracted the autocorrelation exponent λ_c/z_c and the asymptotic FDR X_∞ . The numerical data are presented on figures 40 and 41 and the final estimates are summarised in Table 8. For the Ashkin-Teller model at the point with the same thermal exponent as the three-state Potts model, the autocorrelation exponent is compatible with the value 0.798 that can be interpolated from Short-Time Dynamics data [323]. For the Baxter-Wu model, our value is compatible with the previous estimate 1.058(4) [27]. A discrepancy is however observed for the Debierre-Turban model: 0.902(10) [448] and 0.920(10) [28].

The autocorrelation exponent λ_c/z_c of the three-state Potts model and of the Ashkin-Teller model are slightly outside of the error bars, which is not really a surprise since only their thermal exponents are the same. However, the FDR of these two models are in very good agreement which is much more surprising. For the two models belonging to the four-state Potts model universality class, the situation is more complex. The results for the Debierre-Turban model are compatible with those of the four-state Potts model but this not the case for the Baxter-Wu model. The autocorrelation exponent is

compatible within error bars with the estimate of the four-state Potts model. However, since the latter is very noisy, it makes certainly more sense to compare with the Debierre-Turban model, assuming that it gives a better estimate for the four-state Potts model universality class. The autocorrelation exponents of the Baxter-Wu and Debierre-Turban are not compatible. The FDR follows the same trend: the estimates for the four-state Potts and Debierre-Turban models are compatible but not for the Baxter-Wu model. This singular behaviour of the Baxter-Wu model is probably related to the fact that, in contradistinction to the two other models, its critical behaviour is not affected by logarithmic corrections. Such corrections are perhaps also present in the dynamical behaviour of the Potts and Debierre-Turban models. The quality of our data is not sufficient to take into account such corrections. This point is still unsolved.

Models	λ_c/z_c	X_∞
Potts $q = 3$	0.844(18)	0.406(1)
Ashkin-Teller	0.802(20)	0.403(8)
Potts $q = 4$	0.99(12)	0.459(8)
Baxter-Wu	1.13(6)	0.548(15)
Debierre-Turban	0.977(25)	0.466(3)

Tableau 8 : Autocorrelation exponents λ_c/z_c , and asymptotic FDR X_∞ for several models related to the Potts model with three or four states.

1.3.2.3. Potts models with an irreversible dynamics

So far, we have considered only dynamics satisfying the detailed balance condition. The rate of a transition, say $\sigma(t_1) \rightarrow \sigma(t_2)$, was constrained to satisfy

$$\frac{W(\sigma(t_1) \rightarrow \sigma(t_2))}{W(\sigma(t_2) \rightarrow \sigma(t_1))} = \frac{\wp_{st.}(\sigma(t_2))}{\wp_{st.}(\sigma(t_1))},$$

where $\wp_{st.}$ denotes the stationary distribution. Assuming that the latter is the Boltzmann distribution $\wp_{st.} = \frac{1}{Z} e^{-\beta H}$, an Hamiltonian can always be reconstructed from the transition rates. In the case of the discrete-time dynamics governed by the master equation

$$\wp(\sigma, t+1) = \sum_{\sigma'} [\wp(\sigma', t)W(\sigma' \rightarrow \sigma) - \wp(\sigma, t)W(\sigma \rightarrow \sigma')],$$

the probability of an history $\sigma(t_1) \rightarrow \sigma(t_2) \rightarrow \sigma(t_3) \rightarrow \dots \rightarrow \sigma(t_n)$ in the steady state is

$$\wp_{st.}(\sigma(t_1)) W(\sigma(t_1) \rightarrow \sigma(t_2)) W(\sigma(t_2) \rightarrow \sigma(t_3)) \dots W(\sigma(t_{n-1}) \rightarrow \sigma(t_n)).$$

When the detailed balance condition holds, this probability is easily shown to be equal to

$$\wp_{st.}(\sigma(t_n)) W(\sigma(t_n) \rightarrow \sigma(t_{n-1})) W(\sigma(t_{n-2}) \rightarrow \sigma(t_{n-3})) \dots W(\sigma(t_2) \rightarrow \sigma(t_1)),$$

i.e. the probability of the time-reversed history. The dynamics is said to be reversible. However, the detailed balance is not a necessary condition and we are free to consider a dynamics for which it is not satisfied. Such a violation occurs in particular when there exists an absorbing state, i.e. a spin configuration σ^A from which the system cannot escape. This means that the transition rates $W(\sigma^A \rightarrow \sigma)$ vanish for all σ while there exists at least one spin configuration σ for which $W(\sigma \rightarrow \sigma^A) > 0$. The stationary distribution $\wp_{\text{st.}}$ of an irreversible dynamics is usually difficult to compute since the full stationarity condition

$$\partial_t \wp_{\text{st.}}(\sigma) = \sum_{\sigma'} [\wp_{\text{st.}}(\sigma', t) W(\sigma' \rightarrow \sigma) - \wp_{\text{st.}}(\sigma, t) W(\sigma \rightarrow \sigma')] = 0$$

has to be solved. In general, it is not possible to find an Hamiltonian H such that $\wp_{\text{st.}} = \frac{1}{Z} e^{-\beta H}$.

1.3.2.3.1. The Ising model with an irreversible dynamics

In the case of the one-dimensional Ising model, the more general transition rates (85) were introduced by Glauber. As already discussed, detailed balance is satisfied only when the relation (86) between the two parameters γ and δ holds. The two-dimensional case allows for a wider variety of models. Consider a square lattice. The transition rate $\omega(\sigma_0)$, i.e. the probability that the spin σ_0 undergoes a spin-flip, should involve a linear term in σ_0 in order for one of the two states $\sigma_0 = \pm 1$ to be favoured according to the state of the neighbours. The more general transition rate is therefore ^[214]

$$\omega(\sigma_0) = \frac{1}{2} [1 - \sigma_0 f(\sigma_1, \sigma_2, \sigma_3, \sigma_4)],$$

where $\sigma_1, \sigma_2, \sigma_3, \sigma_4$ are the four neighbours of σ_0 on the square lattice. The assumption of up/down symmetry, i.e. of invariance under the reversal of all spins, imposes that the transition rates be a product of an even number of spins. The function f should therefore be an odd function. Finally, the four neighbours are assumed to be equivalent and to contribute in the same way to the transition rates. Therefore, the function f can only depend on $\sum_{i=1}^4 \sigma_i$ and its powers. The more general form of the transition rates is finally

$$\omega(\sigma_0) = \frac{1}{2} \left[1 - \sigma_0 (\gamma + \delta \sigma_1 \sigma_2 \sigma_3 \sigma_4) (\sigma_1 + \sigma_2 + \sigma_3 + \sigma_4) \right]. \quad (88)$$

Since $f(0) = 0$, the transition rates can be equivalently parametrised by the value of the function f when $\sum_{i=1}^4 \sigma_i = 2$ and 4 , i.e. by $f(2) = 2(\gamma - \delta) = x$ and $f(4) = 4(\gamma + \delta) = y$. It follows that this model can be interpreted as a two-dimensional Ising-Glauber model

$$\omega(\sigma_0) = \frac{1}{2} \left[1 - \sigma_0 \tanh \left(\frac{\sum_{i=1}^4 \sigma_i}{k_B T (|\Delta E|)} \right) \right]$$

with a temperature $k_B T(2) = 2 / \text{atanh } x$ and $k_B T(4) = 4 / \text{atanh } y$ depending on the absolute value of the energy variation ΔE caused by the spin-flip. Such a result can be obtained by coupling an Ising model to two reservoirs at different temperatures ^[196, 351]. During each time step, only one of the two reservoirs is coupled to the system and a spin is flipped according to Glauber's transition rates. If the choice of the reservoir is

made randomly, an average transition rate can be defined and it can be shown that it takes the form (88).

As discussed by de Oliveira *et al.* [142], the detailed balance is satisfied only if $y = 2x/(1 + x^2)$. In the steady state, a critical line in the $x - y$ plane separates a ferromagnetic phase from a paramagnetic one at small x and y . Several already-known models appear as special cases of this more general one. The Ising-Glauber model is recovered when the two temperatures $T(2)$ and $T(4)$ are equal, i.e. when $\frac{1}{4} \operatorname{atanh} x = \frac{1}{2} \operatorname{atanh} y$. The intersection with the critical line corresponds to the Onsager critical point $k_B T_c = 2/\ln(1 + \sqrt{2})$. On the line $x = y$, the transition rates (88) become

$$\omega(\sigma_0) = \frac{1}{2} \left[1 - \gamma \sigma_0 S \left(\sum_{i=1}^4 \sigma_i \right) \right],$$

where $S(x) = x/|x|$ if $x \neq 0$ and $S(0) = 0$. This model is known as majority vote model [140]. Imagine that the spins represent individuals that have to vote yes (+1) or no (-1) on a given issue. The transition rates imply that each of them take his decision by adopting the majority vote of his neighbours. In the steady state, Monte Carlo simulations showed that the model belongs to the Ising universality class [140].

When $\delta = 0$, the transition rates (88) become those of the so-called linear Ising-Glauber model [437, 141]

$$\omega(\sigma_0) = \frac{1}{2} \left[1 - \frac{\gamma}{4} \sigma_0 (\sigma_1 + \sigma_2 + \sigma_3 + \sigma_4) \right], \quad (\gamma < 1).$$

The latter may be obtained by replacing the function $\tanh(x)$ present in the usual Glauber transition rates by its first-order Taylor expansion x . At the point $\gamma = 1$, the linear Ising-Glauber model is equivalent to the Voter model: at each time step, a spin chooses randomly one of its neighbours and adopts the same state. Because of the linearity of the transition rates, closed set of linear evolution equations can be written and solved for magnetisation, correlations and autocorrelations in any dimension d [141]. The system is critical at $\gamma = 1$ with correlations decaying algebraically as $r^{-(d-2+\eta)}$ with $\eta = 1$ for $d = 1$ but $\eta = 0$ for $d \geq d_c = 2$. The dimension $d = 2$ is therefore the upper-critical dimension of the system. Magnetisation displays a jump, which means that $\beta = 0$ while the susceptibility diverges as $(1 - \gamma)^{-1}$. At the upper-critical dimension $d_c = 2$, this algebraic behaviour is modified by a multiplicative logarithmic correction.

The aging properties of the general model (88) were studied along its critical line. At the critical point of the majority vote model, the initial-slip exponent was estimated to be $\theta \simeq 0.191(2)$, which means according to (73), that the autocorrelation exponent is $\lambda_c/z_c \simeq 0.731(4)$, in agreement with the two-dimensional Ising-Glauber model [364, 467]. This result strengthens the belief that both the static and dynamical critical behaviours are the same as the Ising-Glauber model at all points of the critical line, except at the Voter point. Indeed, the critical domain coarsening at the Voter point is very different from the usual behaviour discussed in this chapter. The asymptotic density of domain walls behaves as $1/|\ln(1 - \gamma)|$ when $d = 2$ but remains finite for $d > 2$ [141]. The ferromagnetic state is therefore never reached above the upper-critical dimension [52]. Besides the fact that the growth is much slower at $d_c = 2$, $L(t) \sim \ln t$, the curvature does not seem to play any role in the dynamics of domain walls [156]. This was interpreted as a complete vanishing of the surface tension. The dynamics is

governed only by noise fluctuations at the interface. The persistence displays an usual behaviour $P(t) \sim e^{-A(\ln t)^2}$ at the upper-critical dimension [247]. The dynamical and autocorrelation exponents are known to be equal to $z_c = 2$ and $\lambda_c = d$ [52]. At the upper-critical dimension $d_c = 2$, logarithmic corrections affect the algebraic decay of both autocorrelation and response functions. The asymptotic FDR was shown to take the same value $X_\infty = 1/2$ as the one-dimensional Ising-Glauber model [435, 226].

1.3.2.3.2. The Potts model with an irreversible dynamics

In a way similar to the Ising case discussed above, we have constructed the most general transition rates for three-state Potts spins on a square lattice [121]. The transition rates $W(\sigma \rightarrow \sigma')$ are assumed to depend only on the final state σ' and on the states of the four neighbours. For three-state Potts spins, the number of transition rates to specify is therefore $3^5 = 243$. Using the \mathbb{Z}_3 symmetry to permute the three states and the equivalence between the four neighbours, this number is lowered to twelve. These independent transition rates are presented in Table 9. The number of independent parameters can still be reduced by assuming, for instance, that the final states $\sigma' = 2$ and 3 should be equiprobable if the four neighbours are in the state $\sigma_i = 1$. Finally, only five independent parameters, denoted p_1 to p_5 , remain. Note that in the four-dimensional hypervolume defined by $p_1 = 1$, the three ferromagnetic states are absorbing states.

	1	2	3
1 1 1 1	p_1	$(1 - p_1)/2$	$(1 - p_1)/2$
1 1 1 2	p_2	p_5	$1 - p_2 - p_5$
1 1 2 2	$p_3/2$	$p_3/2$	$1 - p_3$
1 1 2 3	p_4	$(1 - p_4)/2$	$(1 - p_4)/2$

Tableau 9 : Inequivalent transition rates $W(\sigma \rightarrow \sigma')$. The final state σ' is given on the first line while the first column corresponds to the state of the four neighbours.

Despite the apparent complexity inherent to the large number of parameters, the situation is similar to the Ising case discussed above. Similar models are encountered in some regions of the five-dimensional phase diagram. The three-state Potts model with a Glauber dynamics is recovered on the line where the five parameters are

$$p_1 = \frac{r^4}{2 + r^4}, \quad p_2 = \frac{r^3}{1 + r + r^3}, \quad p_5 = \frac{r}{1 + r + r^3},$$

$$p_3 = \frac{2r^2}{1 + 2r^2}, \quad p_4 = \frac{r}{2 + r},$$

where r is related to the exchange coupling K by $r = e^K$. The location of the critical point separating ferromagnetic and paramagnetic phases is known exactly on this line : $K_c = \ln(1 + \sqrt{q})$. On the line, parametrised by p ,

$$p_1 = p_2 = p_3 = p_4 = p, \quad p_5 = (1 - p)/2,$$

the final state σ' is the same as the majority of the neighbours with probability p and random otherwise. This model is a generalisation of the majority vote model. Monte Carlo simulations showed that it belongs to the three-state Potts model universality class [81, 82, 466, 468]. The critical point was determined numerically.

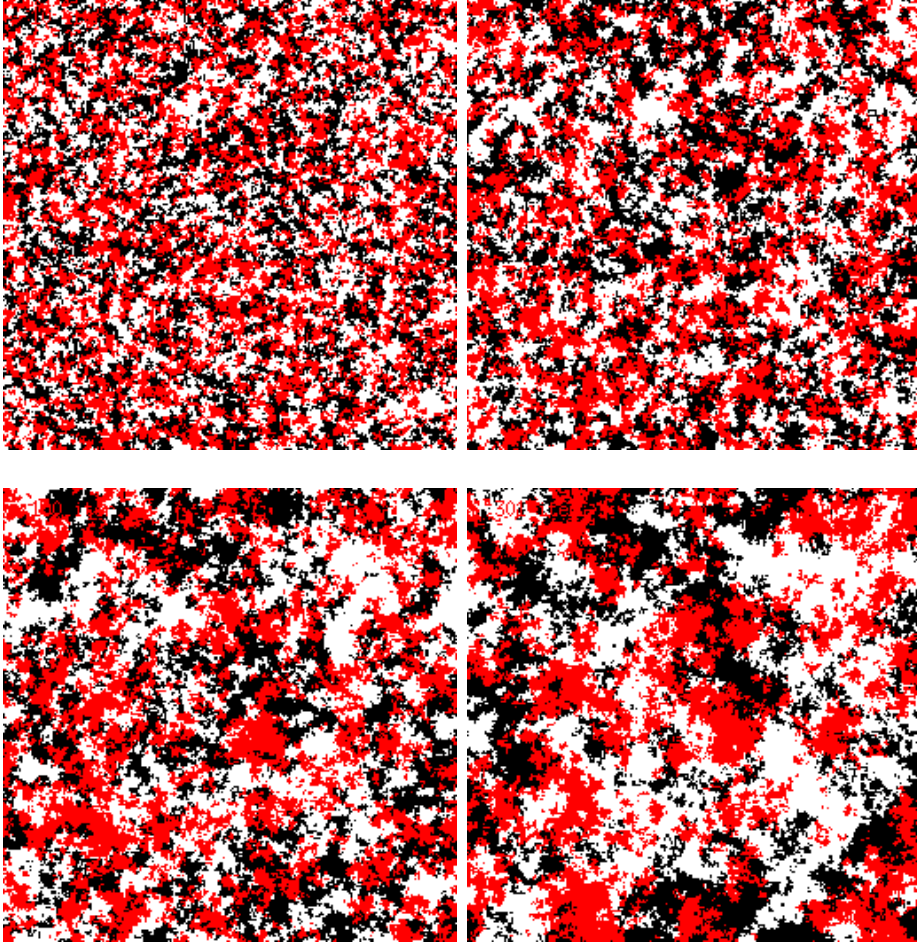


Figure 42 : Spin configurations of the three-state Voter model during a quench. The different snapshots correspond to times $t = 10, 30, 100,$ and 300 (from left to right and top to bottom).

Finally, on the line parametrised by γ

$$p_1 = \frac{1}{3}(1 + 2\gamma), \quad p_2 = \frac{1}{3}\left(1 + \frac{5}{4}\gamma\right), \quad p_5 = \frac{1}{3}\left(1 - \frac{1}{4}\gamma\right),$$

$$p_3 = \frac{1}{3}(2 + \gamma), \quad p_4 = \frac{1}{3}\left(1 + \frac{1}{2}\gamma\right),$$

the model is equivalent to the linear three-state Potts-Glauber model

$$\omega(\sigma_0) = \frac{1 - \gamma}{q} + \frac{\gamma}{4}(\delta_{\sigma_0, \sigma_1} + \delta_{\sigma_0, \sigma_2} + \delta_{\sigma_0, \sigma_3} + \delta_{\sigma_0, \sigma_4})$$

that is obtained by replacing the $\tanh(x)$ function of the Glauber transition rates by its first-order Taylor expansion around $x = 0$. The static critical properties in the

steady state, as well as the dynamical critical behaviour, of this model were calculated exactly [227]. The universal quantities were shown to be independent of the number of states q . Consequently, the conclusions drawn in the Ising case can be extended to the linear three-state Potts model. In particular, the critical point is located at $\gamma = 1$ and the upper-critical dimension is $d_c = 2$. The correlation length diverges as $(1 - \gamma)^{-1/2}$, i.e. $\nu = 1/2$. The critical behaviour $(1 - \gamma)^{-1}$ of the magnetic susceptibility is affected by logarithmic corrections at $d = 2$. Autocorrelation and response function decay algebraically with an autocorrelation exponent $\lambda_c/z_c = d/2$, again with logarithmic corrections in the case $d = 2$. Finally, the asymptotic FDR takes the value $X_\infty = 1/2$. Note that the critical point is the natural generalisation of the Voter model to q states. Comparison of these predictions with Monte Carlo simulations will be presented in the following.

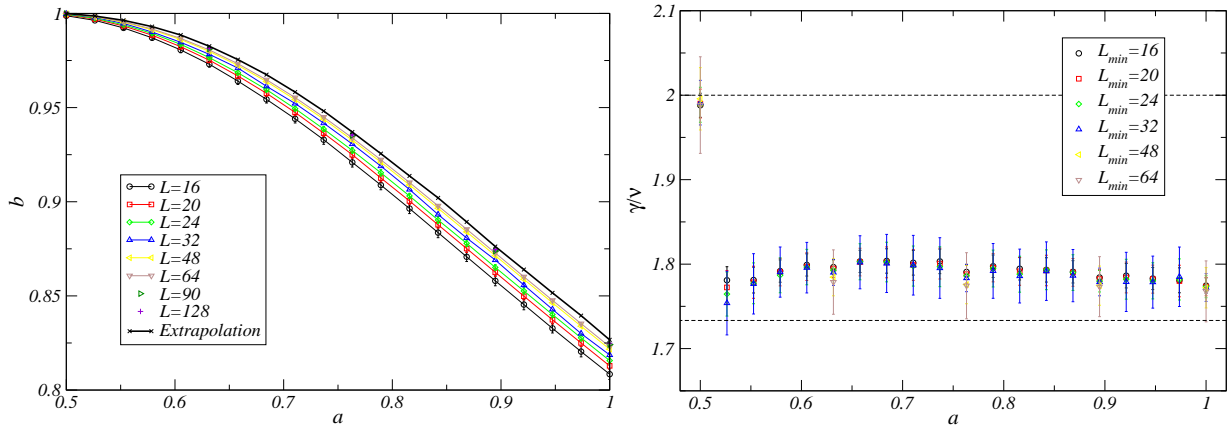


Figure 43 : On the left, critical line in the $a - b$ plane, as obtained from the maximum of the magnetic susceptibility. The different curves correspond to lattice sizes from $L = 16$ to $L = 128$. An extrapolation was then performed. On the right, effective critical exponent γ/ν along the critical line. The dashed line corresponds to the exact values for the three-state Potts model ($\gamma/\nu \simeq 1.733$), and the Voter model ($\gamma/\nu = 2$).

We restricted ourselves to a two-dimensional section

$$p_1 = p_3 = b, \quad p_4 = a, \quad p_2 = b \left(1 + \frac{a-b}{2} \right), \quad p_5 = \frac{b}{2}(1-a) + \frac{1}{2}(1-b)^2.$$

parametrised by a and b of the full five-dimensional phase diagram. The Voter model is expected to be at the point $a = 1/2$ and $b = 1$. The line $b = 1$ corresponds to the absorbing phase. We have performed large-scale Monte Carlo simulations in the steady state. Because the dynamics is local, the autocorrelation time is very large (up to $\tau \simeq 7231$ while $\tau \simeq 25$ with the Swendsen-Wang algorithm). The location of the critical line was determined as the maximum of the magnetic susceptibility and the crossing points of the Binder cumulant. The latter provided an estimate less affected by Finite-Size corrections but nevertheless, a better accuracy was obtained with the former. The critical line is presented on figure 43. We have estimated the critical exponent γ/ν by Finite-Size Scaling. As seen on figure 43, the Voter point $a = 1/2$ displays a behaviour very different from all other points on the critical line. The susceptibility was then studied as a function of b when approaching the Voter point. Evidences of

logarithmic corrections were given. Finally, the exponent ν was estimated from the Finite-Size Scaling of the correlation length. The scaling functions of the correlation length and the Binder cumulant were shown to be universal along the critical line, except for $a = 1/2$.

We then studied the aging proprieties of this model on the critical line. The spin-spin autocorrelation functions $C(t, s)$ were shown to decay algebraically with an autocorrelation exponent estimated to be $\lambda/z \simeq 0.806(5)$, $0.817(4)$, $0.820(4)$ and $0.818(3)$ for $a = 0.63158$, 0.76316 , 0.89474 , and 1 , respectively. These values are close, even though incompatible, to the numerical estimates $0.828(2)$ [44¹] and $0.844(19)$ [105] for the three-state Potts model. The Local Scale Invariance prediction (83) of the response function was shown to provide a better fit of the numerical data than the scaling hypothesis (79) (figure 44). The asymptotic FDR X_∞ is close to the value $X_\infty \simeq 0.406$ of the three-state Potts model [105]. The Voter point was studied separately. As predicted, the autocorrelation functions were shown to display logarithmic corrections and our numerical estimate of the FDR X_∞ was compatible with $1/2$.

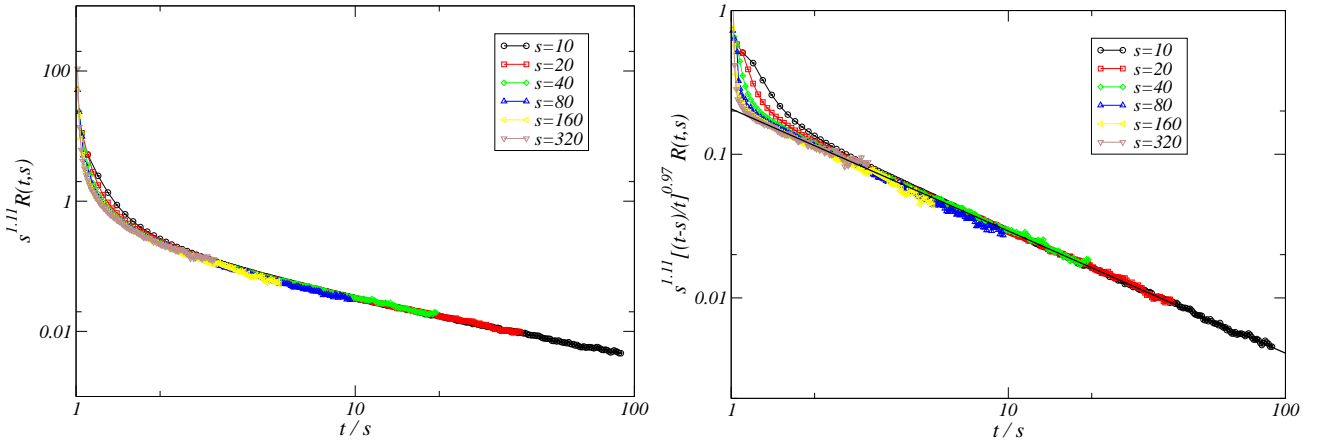


Figure 44 : On the left, scaling function $s^{1+a_c} R(t, s)$ of the response function versus t/s . On the right, scaling function $s^{1+a_c} [(t-s)/t]^{1+a'} R(t, s)$ predicted by Local Scale Invariance at the critical point $a = 1$. The bold line is the expected algebraic decay $(t/s)^{-\lambda/z}$ with $\lambda/z = 0.844$.

1.3.3. Aging in fully-frustrated models

In this section, the aging properties of the fully-frustrated Ising (FFIM) and XY (FFXY) models are discussed. Despite the presence of magnetic frustration, i.e. the impossibility for the system to satisfy simultaneously all bonds, these models display a behaviour during a quench which is similar to that of random ferromagnets.

1.3.3.1. Fully-Frustrated Ising Model

By Fully-Frustrated, it is meant that for each plaquette of the lattice, an odd number of bonds are anti-ferromagnetic while all others are ferromagnetic. As a consequence, one bond is necessarily unsatisfied in the ground state. For a single plaquette, the latter may be constructed in the following way: first choose the sign of one of the spins and then walk around the plaquette, assigning to each newly encountered spin the state imposed by the bond that was followed when leaving the previous spin.

When the initial spin is reached again, the sign has been changed as many times as anti-ferromagnetic couplings were followed around the plaquette. If this number is odd, the final state is opposite to the initial spin. Consequently, one bond cannot be satisfied.

The paradigmatic example of such a FFIM is the anti-ferromagnetic Ising model (AFIM) on a triangular lattice. Because of frustration, no long-range order can develop in the system at finite temperature [246]. The entropy per site was shown to be $s \simeq 0.3383k_B$ at zero temperature, meaning that the number of ground states grows exponentially with the number of sites [219, 220]. The system is critical at zero temperature. An exact calculation of spin-spin correlation functions on a given sublattice indeed showed an algebraic decay at zero temperature with a critical exponent $\eta = 1/2$ [456]. A mapping of the AFIM onto a Solid-On-Solid model was later discovered. As a preliminary, note that each bond of a triangular lattice is shared by two triangular plaquettes so the removal of a bond leads to the union of these two plaquettes into a diamond. Since in the ground states exactly one bond is unsatisfied in each plaquette, the graph of satisfied bonds associated to any spin configuration at zero temperature corresponds to a particular covering of the lattice with diamonds. Seen in three-dimensions, the latter looks like a random surface in the cubic lattice. Another way to construct a mapping of the AFIM onto a Solid-On-Solid model is to sweep each plaquette clockwise if the triangle points upwards and anti-clockwise otherwise. A height difference +1 is affected to satisfied bonds and -2 to unsatisfied ones. The phase transition of the AFIM corresponds to the roughening transition of this Solid-On-Solid model. From this mapping, it was concluded that the specific heat should diverge with an exponent $\alpha = 1/2$ [66, 392]. The mapping onto the Solid-On-Solid model was later confirmed by Monte Carlo simulations [503]. Coarse-grained spin variables were shown to behave as expected for a Gaussian model. At finite temperature, ferromagnetic plaquettes of the triangular lattice are equivalent to vortices of charges ± 6 in the Solid-On-Solid model. These charges were shown to interact via a logarithmic potential, i.e. a two-dimensional Coulomb interaction. This establishes a connection with a Coulomb gas (§ 1.2.1.2). Monte Carlo simulations gave evidences of such a logarithmic interaction between defects [376, 503]. Interestingly, Monte Carlo simulations and transfer matrix calculations provided evidences of a Berezinskii-Kosterlitz-Thouless transition, driven by the magnetic field and not the temperature [71]. The critical phase extends up to $H \simeq 0.27(1)$ [70].

A fully-frustrated Ising model can also be constructed on a square lattice [479]. The Hamiltonian is chosen as

$$-\beta H = J \sum_{x,y} [\sigma_{x,y} \sigma_{x+1,y} + (-1)^{f(x,y)} \sigma_{x,y} \sigma_{x,y+1}],$$

where x and y are the lattice coordinates. The function $f(x,y) \in \mathbb{N}$ is chosen in such a way that each square plaquette contains an odd number of anti-ferromagnetic couplings, i.e. such that the circulation $\sum_{(x,y) \in \square} f(x,y)$ be an odd integer. The cases considered in the literature are $f(x,y) = x + y$ (Zig-Zag configuration), and $f(x,y) = x$ (Piled-up Domino configuration). The Mattis transform $\sigma_{x,y} \rightarrow (-1)^{1+(y \bmod 3)} \sigma_{x,y}$ is equivalent to the exchange of the Zig-Zag and Piled-up Domino coupling configurations [355]. Thanks to the translation invariance of the Piled-up Domino configuration in the y direction, a transfer matrix can be constructed. Exact results were obtained: long-range order was excluded at finite temperature and the entropy per site was shown to be

finite, $s \simeq 0.2406$, at zero temperature [20]. The spin-spin correlation functions decay algebraically with an exponent η that was shown to take the same value $1/2$ as the AFIM, first using a mapping of the ground states of the FFIM onto a special point of the Baxter F model [184] and later using the equivalence of the transfer matrix with a quantum spin chain [411]. Note finally that a Fully-Frustrated three-state Potts model was studied numerically [187, 188, 186]. While the Zig-Zag configuration gives similar results for both Ising and Potts models, the transition of the three-state Potts model with a Pile-Up Domino configuration occurs at finite temperature and displays a reentrant behaviour.

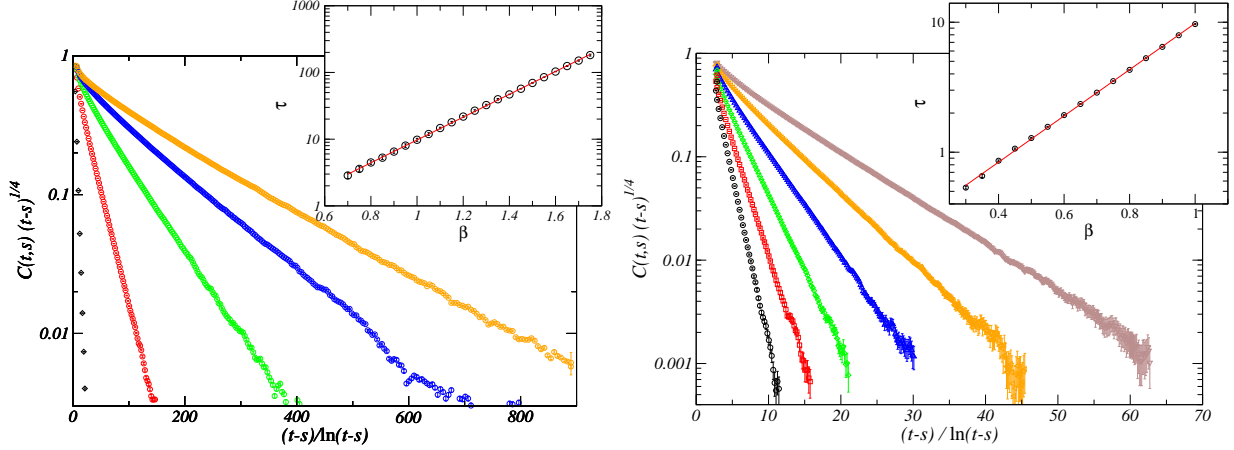


Figure 45 : Scaling function $C(t,s)(t-s)^{\eta z}$ of the equilibrium spin-spin autocorrelation function versus $(t-s)/\ln(t-s)$ for the AFIM (left) and the FFIM (right). The different curves correspond to different temperatures. In the inset, the relaxation time, extracted from a power law interpolation, is plotted versus $\beta = 1/k_B T$. The red line are the interpolations $\tau = \tau_0 e^{3.92(2)\beta}$ (AFIM) and $\tau = \tau_0 e^{4.097(26)\beta}$ (FFIM).

At finite temperature, the system is in the paramagnetic phase and therefore relaxation functions are expected to decay exponentially. However, it was claimed that, below the temperature at which the Fortuin-Kasteleyn clusters percolate in the pure Ising model, the exponential decay of the relaxation functions is replaced by a stretched exponential (63), like in spin-glasses [181, 189]. Monte Carlo estimates of the exponent β of the stretched-exponential law display a strong dependence on temperature. We argued recently that the relaxation is not stretched-exponential but exponential with logarithmic corrections due to the presence free topological defects in the paramagnetic phase [483]. Consider the one-time correlation function $C(\vec{r}, t, |T - T_c|)$. Under a rescaling of lengths by a factor b , we inferred the following behaviour:

$$C(\vec{r}, t, |T - T_c|) = b^{2x_\sigma} C(\vec{r}/b, t/b^z, |T - T_c| b^{1/\nu}).$$

The choice $b = t^{1/z}$ leads in the two-dimensional case to

$$C(\vec{r}, t, |T - T_c|) = t^{-\eta/z} \mathcal{C}(\vec{r}/t^{1/z}, |T - T_c| t^{1/\nu z}).$$

According to (61), the quantity $\tau \sim |T - T_c|^{-\nu z}$ is the relaxation time. In the paramagnetic phase, the correlation functions are expected to decay exponentially as

(62). Since \mathcal{C} depends on t/τ , the usual behaviour $C(t) \sim e^{-t/\tau}/t^{\eta/z}$ is recovered. We made two modifications to apply this scaling behaviour to the FFIM. Since the correlation length is known to diverge as $e^{2\beta}$ as the temperature is decreased, the relaxation time is assumed to behave as

$$\tau \sim \xi^z \sim e^{2\beta z}, \quad (89)$$

where $\beta = 1/k_B T$. Second, we used the modified growth law (66) to take into account the existence of unbounded topological defects in the paramagnetic phase. The correlation function is therefore expected to decay as

$$C(t) \sim \frac{e^{-t/\tau \ln t}}{t^{\eta/z}}. \quad (90)$$

We computed the equilibrium spin-spin autocorrelation function $C(t, s)$ at different temperatures in the paramagnetic phase of both the AFIM and the FFIM. We interpolated the data with a stretched exponential (63), an exponential decay and an exponential with logarithmic corrections (90). These three *ansätze* fit reasonably well the data. From the interpolation, we extracted the relaxation time τ and compared its temperature dependence with (89). For both the AFIM and the FFIM, the relaxation function (90) gives by far a much better compatibility (see figure 45).

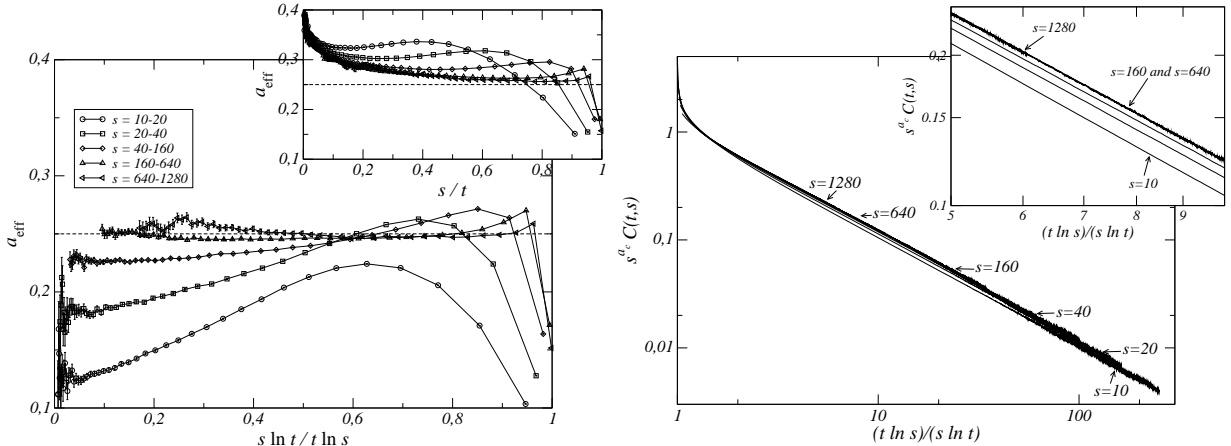


Figure 46 : On the left, effective exponent a_c of the FFIM versus the scaling variable $s \ln t / t \ln s$. The different curves correspond to the different pairs of waiting times s used in the estimation of a_c . In the inset, the same quantity is considered when no logarithmic correction is taken into account. On the right, scaling function $s^{a_c} C(t, s)$ versus the scaling variable $s \ln t / t \ln s$. The different curves correspond to the different waiting times s . Note the collapse of the data for the largest waiting times.

We have also studied the aging of the FFIM during a quench at zero temperature [484]. As a preliminary, we estimated the dynamical exponent z_c by a power-law interpolation of the autocorrelation function $C(t, s) \sim (t - s)^{-\eta/z}$ at equilibrium. Note that we do not have to worry about logarithmic corrections because in the critical phase, vortices are bounded by pair and do not affect the dynamics. Our estimate $z_c = 2.004(9)$ is compatible with the expected value $z_c = 2$ and in disagreement with

the recent claim of a sub-diffusive growth with $z \simeq 2.33$ in the AFIM [298, 299]. The system is then initially prepared in the paramagnetic phase and quenched at $T = 0$. Using the growth law (66) involving logarithmic corrections due to topological defects, spin-spin autocorrelation functions are assumed to scale as

$$C(t, s) \underset{t/s, t-s \gg 1}{\sim} s^{-a_c} \mathcal{F}_C \left(\frac{t \ln s}{s \ln t} \right).$$

We first extracted the exponent a_c by combining data at different times (t_1, s_1) and (t_2, s_2) such that

$$\frac{t_1 \ln s_1}{s_1 \ln t_1} = \frac{t_2 \ln s_2}{s_2 \ln t_2}.$$

An effective exponent a_{eff} can then be computed as

$$a_{\text{eff}} = - \frac{\ln C(t_2, s_2) - \ln C(t_1, s_1)}{\ln s_2 - \ln s_1}.$$

As seen on figure 46, the expected value $a_c = \eta/z_c = 1/4$ is recovered at large waiting times s . If logarithmic corrections are not taken into account, no stable exponent is obtained. Similarly, a collapse of the scaling function $s^{a_c} C(t, s)$ is observed at large waiting times s only with the scaling variable $t \ln s / s \ln t$ and not with t/s . Finally, we extracted the autocorrelation exponent from the decay of $C(t, s)$ with $t/\ln t$. We obtained the value $\lambda_c/z_c \simeq 1.02(2)$ when taking into account logarithmic corrections, in contradistinction to the estimate $\lambda_c/z_c \simeq 0.86$ obtained without logarithmic corrections [298, 299]. The presence of logarithmic corrections was later confirmed in the case of the AFIM [295] and was shown to hold in all the field-induced Berezinskii-Kosterlitz-Thouless critical phase.

1.3.3.2. Fully-Frustrated XY Model

A Fully-Frustrated version of the XY model can be constructed via the Hamiltonian

$$-\beta H = J \sum_{(i,j)} \cos(\theta_i - \theta_j - A_{ij}).$$

This model is relevant for the description of arrays of Josephson junctions in a transverse magnetic field, θ_i being the phase of the superconducting wavefunction and $A_{ij} = \frac{2e}{\hbar c} \int_i^j \vec{A} \cdot d\vec{\ell}$ the circulation along a path joining the sites i and j of the vector potential \vec{A} associated to the applied magnetic field [461]. In the FFXY, the energy of a bond (i, j) is minimal when $\theta_i - \theta_j - A_{ij}$ is a multiple of 2π . However, it is not always possible to find an angle configuration for which this condition is fulfilled at every bond of the lattice. Indeed, the circulation of $\theta_i - \theta_j$ around a closed path is trivially equal to $\sum_{(i,j) \in \text{Loop}} (\theta_i - \theta_j) = 0$. Consequently, the system is not frustrated only if the circulation of A_{ij} along all loops of the lattice is a multiple of 2π . For a Fully-Frustrated system, this condition is expected to be maximally violated around each plaquette of the lattice. On a square lattice, this will be the case with the choice $A_{ij} = \pi/4$. For Josephson-junctions arrays, such a frustration is obtained when the magnetic flux through each plaquette is equal to half a quantum.

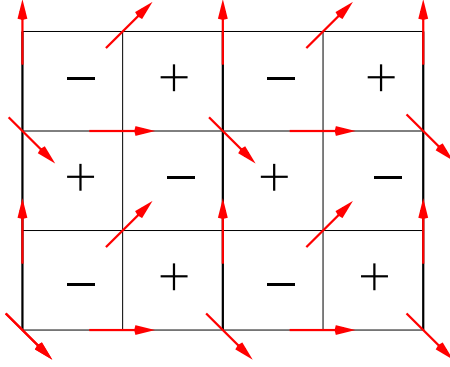


Figure 47 : Example of a spin configuration $\vec{\sigma}_i = (\cos \theta_i \quad \sin \theta_i)$ of the FFXY model on the square lattice at zero temperature. In the plaquettes where the spins turns clockwise (resp. anti-clockwise), chirality is chosen -1 (resp. $+1$).

Another possible definition of a FFXY model on the square lattice may be obtained with the bond configurations discussed above in the case of the FFIM [479]:

$$-\beta H = J \sum_{x,y} [\cos(\theta_{x+1,y} - \theta_{x,y}) + (-1)^{f(x,y)} \cos(\theta_{x,y+1} - \theta_{x,y})],$$

where $f(x,y)$ is defined in such a way that each plaquette of the lattice contains an odd number of anti-ferromagnetic bonds. The ground-state is constructed in the following way: the orientation of a first spin is chosen randomly. This spin belongs to four plaquettes of the square lattice. One of them is swept clockwise or anti-clockwise, starting from the initial spin. Each new spin encountered during the sweeping is given the angle of the previous one plus $\pi/4$ if the bond is ferromagnetic or $3\pi/4$ if it is anti-ferromagnetic. Now, four spins have been defined. Each of them can be used to sweep a new plaquette of the lattice. However, the orientation of the sweeping is now imposed by the spins already defined. An example of spin configuration at zero temperature is shown on figure 47. It can be noticed that the orientation of the plaquettes alternates on the lattice. The chirality of a plaquette is defined as [480]

$$\chi = \text{Sign} \left[\sum_{(i,j) \in \square} (-1)^{f_{ij}} \sin(\theta_i - \theta_j) \right],$$

where i and j denote nearest-neighbouring sites on the edges of a given plaquette. By construction, chirality takes the value -1 (resp. $+1$) if the plaquette was swept clockwise (anti-clockwise) during the construction of the ground-state. As seen on the figure, chiralities are ordered anti-ferromagnetically. The degeneracy of the ground-state is infinite but does not increase with the lattice site, in contradistinction to the FFIM for example. The ground-state is indeed completely defined once the orientation of an initial spin and the chirality of a plaquette are given. This choice breaks the invariance of the Hamiltonian under the global rotation of all spins and the reversal of all chiralities, i.e. under the transformations of the symmetry group $U(1) \otimes \mathbb{Z}_2$. The spontaneous breaking of the \mathbb{Z}_2 symmetry should be followed by a phase transition, possibly in the Ising model universality class. At high-temperature, the anti-ferromagnetic order of chiralities is expected to be destroyed by thermal fluctuations. The order parameter of

the transition is the staggered chirality. The spontaneous breaking of the global $U(1)$ symmetry is accompanied by the proliferation of Goldstone modes, i.e. spin waves in this case, that destroy the order of the ground state at any finite temperature. The system can nevertheless give rise to a Berezinskii-Kosterlitz-Thouless phase transition (BKT) due to the binding of topological defects at low-temperature. This transition is signaled by a jump of the helicity modulus, or spin stiffness, Υ . The question regarding the coincidence of the two phase transitions was widely debated in the literature.

Like in the XY model, the topological charge of the vortices are constrained to be integer. The presence of frustration in the FFXY leads to additional half-integer charges and the walls between domains of different anti-ferromagnetic chirality orderings induce other topological defects of charges $1/4$ [223]. Such a picture is provided by a mapping of the FFXY onto a Coulomb gas on the dual lattice. Topological defects are associated to magnetic charges and frustration manifests itself as a background medium with a charge $f = \frac{1}{2\pi} \sum_{(i,j) \in \square} A_{ij} = \frac{1}{2}$. The Coulomb gas Hamiltonian (6) is therefore

$$H = \frac{g}{2} \sum_{i,j \neq i} \left(m_i + \frac{1}{2} \right) G(\vec{r}_i - \vec{r}_j) \left(m_j + \frac{1}{2} \right)$$

and the ground state corresponds to a chessboard lattice of alternating charges $+1/2$ and $-1/2$. In this framework, each corner of the walls between domains of different chiralities appears to be associated to a charge $\pm 1/4$. Because it consists in two corners, a kink carries a charge $\pm 1/2$. As the \mathbb{Z}_2 transition temperature is approached, the free energy of the domain walls vanishes and these corners become more and more probable. Their fractional charge destabilises the binding of $U(1)$ integer charges by screening individual charges. Consequently, the BKT transition cannot occur above the \mathbb{Z}_2 transition. The same mechanism was discussed in the case of the anti-ferromagnetic XY model on a triangular lattice [304, 305]. The half-integer charges, corresponding to kinks and anti-kinks, also interact logarithmically and so, in principle, they can form bound pairs of opposite signs. Their unbinding leads to a Berezinskii-Kosterlitz-Thouless transition but it was later shown that the associated BKT temperature is lower than the vortex BKT transition and is therefore not realised in the FFXY [303]. Different conclusions were drawn from a mapping of the FFXY onto two coupled XY models that leads by Renormalisation-Group argument to a coupled Ising-XY model [500, 205, 206].

In earlier Monte Carlo simulations, a single phase transition was observed with a specific heat diverging logarithmically, as in the Ising model [460, 373, 60, 477]. Measurements of a central charge larger than $c = 3/2$ [464] ($c = 1/2$ for the Ising transition and $c = 1$ for the BKT transition) and Monte Carlo simulations [207, 316, 426] contradicted this picture of two uncoupled transitions at the same temperature. More recent Monte Carlo simulations proved the existence of two separated transitions, the BKT transition occurring at a slightly lower temperature than the second-order one [317]. This result is compatible with the scenario of vortex screening by fractional charges presented above. Furthermore, it was argued that the free kinks induce a loss of phase coherence between domains of different chirality orderings. Therefore, the long-range interaction between vortices can only develop when the domain walls have vanished or said differently, the BKT transition can only take place at a lower temperature than the \mathbb{Z}_2 transition [303]. This mechanism was confirmed by Monte Carlo simulations [400]. Finally, the critical behaviour at the second-order phase transition was shown to be in

the universality class of the Ising model [398, 399, 230, 375, 231]. Short-Time Dynamics simulations are compatible with these results [341, 342, 343, 340].

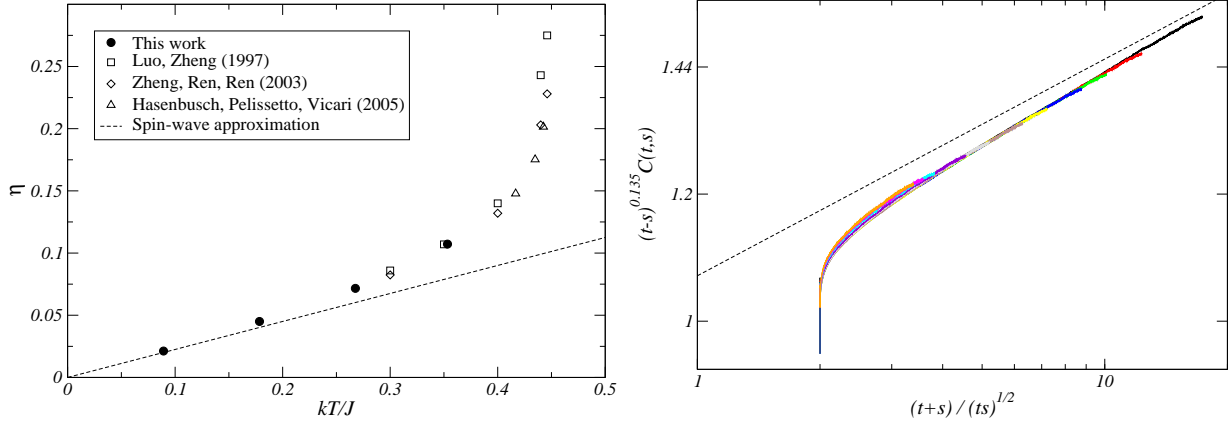


Figure 48 : On the left, critical exponent η extracted from the decay of spin-spin autocorrelation functions in the low temperature phase compared to previous estimates found in the literature and to the prediction of the spin-wave approximation (dashed line). On the right, scaling function $(t-s)^{\eta/2}C(t,s)$ versus $(t+s)/\sqrt{ts}$ at the Berezinskii-Kosterlitz-Thouless temperature.

We studied the aging properties of the FFXY by means of Monte Carlo simulations [482]. We first considered a quench in the low-temperature phase, i.e. at a temperature $T < T_{\text{BKT}}$. The system is initially prepared in the ground state using the algorithm presented at the beginning of this section. We made the assumption that chiralities are frozen so that spin-waves are the only possible excitations of the system. From the mapping of the FFXY onto two coupled XY models, the system is expected to behave as a XY model with an effective exchange coupling $J/\sqrt{2}$ [500]. In the spin-wave approximation, the two-time spin-spin autocorrelation functions of the XY model were predicted to behave as [431]

$$C(t,s) \sim (t-s)^{-\eta/z} \left(\frac{t+s}{\sqrt{ts}} \right)^{\eta/z},$$

where η is the static exponent at the temperature of the quench and the dynamical exponent is equal to $z = 2$. This behaviour is well reproduced by Monte Carlo simulations [63, 5]. We assumed that this behaviour holds for the FFXY too. We first analysed the spin-spin autocorrelation functions along the curves defined by

$$\frac{t+s}{\sqrt{ts}} = \text{Cst.}$$

From the remaining algebraic decay $(t-s)^{-\eta/z}$ of the autocorrelation, we extracted the exponent η/z . As can be seen on figure 48, our estimates are in good agreement with results from different techniques: Short-Time Dynamics [343], Monte Carlo simulations at equilibrium [230, 375] and relaxation of one-time functions [510]. At low temperature, the linear dependence of η with the temperature ($\eta = \sqrt{2} \frac{k_B T}{2\pi J}$) in the spin-wave approximation is reproduced. Note that these results imply that $z = 2$ throughout

the low-temperature critical phase, in contradistinction with strongly temperature-dependent dynamical exponents previously reported [318, 287]. We then tried to extract a second estimate of η from the decay of $(t-s)^{\eta/2}C(t,s)$ with $(t+s)\sqrt{ts}$. The results are compatible at small times t but systematic deviations are observed for large t . A good collapse of the scaling function $(t-s)^{\eta/2}C(t,s)$ versus $(t+s)/\sqrt{ts}$ is nevertheless observed (figure 48). We then studied the behaviour of the response function. In the spin-wave approximation, one expects

$$R(t,s) \sim (t-s)^{-1-\eta/z} \left(\frac{t+s}{\sqrt{ts}} \right)^{\eta/z}.$$

When combining this expression with the behaviour of autocorrelation functions, the FDR can be shown to display a divergence at time $t/s = 2 + \sqrt{5}$:

$$X(t,s) = \frac{k_B T R(t,s)}{\partial_s C(t,s)} \sim \frac{s(t+s)}{t^2 - 4ts - s^2}.$$

This behaviour was observed in the XY model [5]. In the case of the FFX, we showed that the location of the divergence increases with the time s and tends to the expected value $t/s = 2 + \sqrt{5}$.

We then considered the case of a quench at the Berezinskii-Kosterlitz-Thouless temperature when the system is initially prepared at infinite temperature. Since vortices are free in the high-temperature phase, we expect the domain walls to be slowed down. Using the modified growth law (66), the scaling behaviour (77) of autocorrelation functions becomes

$$C(t,s) \sim (t-s)^{-\eta/2} f \left(\frac{\xi(t)}{\xi(s)} \right) \sim (t-s)^{-\eta/2} \mathcal{F}_C \left(\frac{t \ln s}{s \ln t} \right).$$

In the aging regime, the scaling function $\mathcal{F}_C(x)$ is expected to decay as $x^{-\phi}$ with $\phi = \lambda/z - \eta/2$. Our numerical data are in good agreement with such a behaviour. We estimated the autocorrelation exponent to be $\lambda/z \simeq 0.84$, i.e. slightly above the value 0.808(3) obtained by Short-Time Dynamics [340]. Both values are incompatible with the estimates for the XY model: $\lambda/z \simeq 0.625$ [340], 0.738(4) [510], and 0.738(5) [319]. This discrepancy indicates a contribution of the chirality degrees of freedom to this exponent. Similarly, the FDR was estimated to $X_\infty \simeq 0.385(15)$ while we obtained $X_\infty \simeq 0.215(15)$ for the XY model (see figure 49).

Finally, we considered the aging properties of the chirality degrees of freedom. The system is prepared at infinite temperature and then quenched at the \mathbb{Z}_2 critical temperature. Surprisingly, our results are incompatible with those of the Ising model. From the algebraic decay of the chirality-chirality autocorrelation functions $\langle \chi(t)\chi(s) \rangle$, the autocorrelation exponent was estimated to be $\lambda/z = 0.98(5)$, far from the value $\lambda/z \simeq 0.738$ for the Ising model. The FDR $X_\infty = 0.405(5)$ is also incompatible ($X_\infty \simeq 0.328$ for the Ising model). The inclusion of logarithmic corrections influences only very weakly these values, even though a better collapse of $X(t,s)$ is obtained (see figure 49). This discrepancy is still unexplained. We note that, at equilibrium, the critical behaviour of the Ising model is recovered only after a long regime where $\nu \simeq 0.8$ [375]. We note also that we obtained similar values of the FDR for both angle and chirality degrees of freedom. The uncoupling of the two probably occurs at much larger times.

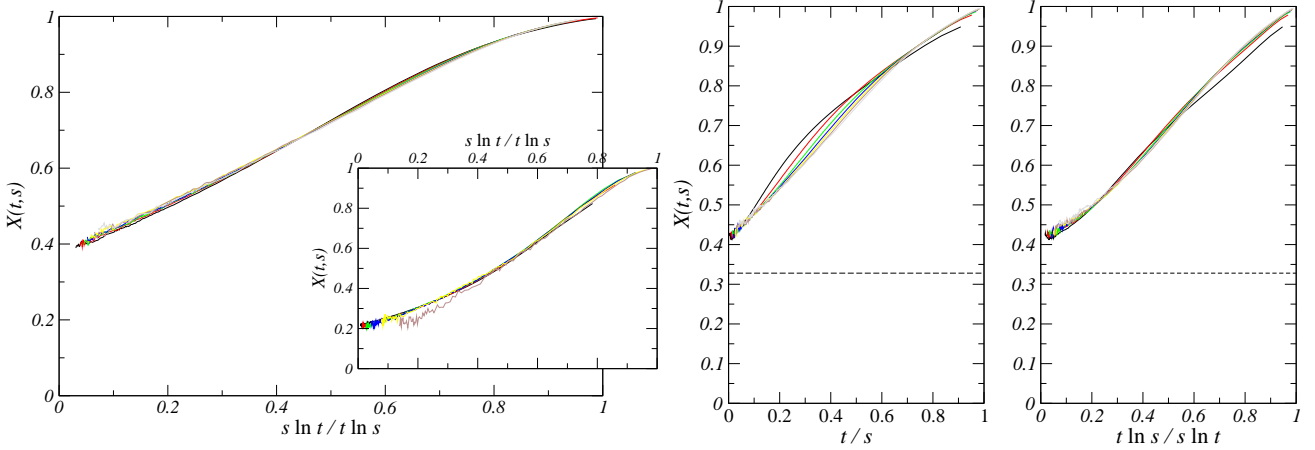


Figure 49 : On the left, fluctuation-dissipation ratio (FDR) $X(t, s)$ of angles during a quench at the Berezinskii-Kosterlitz-Thouless temperature. In the inset, the FDR of the XY model is presented for comparison. The different curves correspond to different waiting times s . On the right, FDR of chiralities during a quench at the critical temperature versus s/t and $s \ln t/t \ln s$.

1.3.4. Jarzynski relation

While equilibrium statistical physics is firmly established since the pioneering works of Boltzmann and Gibbs more than one century ago, general results are still relatively sparse for out-of-equilibrium processes. An important breakthrough was accomplished two decades ago with the discovery of the so-called fluctuation theorems. The Jarzynski relation, to be discussed in this chapter, was recognised as a special case of them.

The second principle of classical thermodynamics introduces a distinction between reversible and irreversible processes. In the former case, the variation of entropy of the system is directly proportionnal to the heat exchanged with the environment and the total entropy is a conserved quantity. In the irreversible case, a production of entropy accompanies the time evolution and provokes an increase of the total entropy. Remarkably, equilibrium statistical mechanics was constructed around another entropy, the statistical or Shannon entropy, which was defined without any relation to the thermodynamical entropy of the second principle. As shown by Boltzmann H theorem, a second principle is recovered for the statistical entropy if the dynamics is not governed by the usual Newtonian equations of motion, which are reversible, but by an effective stochastic dynamics, accounting for the interaction with the many degrees of freedom of the environment. The irreversible nature of the dynamics of a gas of particles is caused by their undeterministic behaviour during a collision.

Statistical entropy is also intimately related to fluctuations. While he was working on the thermodynamics of electromagnetic radiation, Einstein introduced a particularly fruitful derivation of the equilibrium fluctation-dissipation relation between specific heat and energy fluctuations [264]. Combining a second-order Talyor expansion of entropy with the Boltzmann postulate of statistical physics, he wrote the probability distribution of the energy fluctuations as a Gaussian law

$$\wp(E) \sim e^{-S(E)/k_B} \simeq e^{-(E-\langle E \rangle)^2/2k_B T^2 C},$$

whose variance involves the specific heat. In the same spirit, Onsager wrote the probability distribution of a set of observables $\vec{X} = \{X_\alpha\}_\alpha$ with vanishing equilibrium average $\langle X_\alpha \rangle$, as

$$\wp(X_1, X_2, \dots) \sim e^{-S(X_1, X_2, \dots)/k_B} \simeq e^{-\frac{1}{2} \sum_{\alpha, \beta} S_{\alpha\beta} X_\alpha X_\beta},$$

where $S_{\alpha\beta} = \frac{\partial^2 S}{\partial X_\alpha \partial X_\beta}$. With the further assumptions of an exponential relaxation of $\langle X_\alpha(t) \rangle$ and of microscopic reversibility

$$\wp(\vec{X}', t; \vec{X}, 0) = \wp_R(\vec{X}, 0; \vec{X}', t),$$

where \wp_R is the probability distribution when the flow of time is reversed, he derived the celebrated reciprocal relations valid for reversible fluctuations close to equilibrium [401, 402, 102].

A theory of irreversible processes was later derived by Onsager and Machlup [404, 405]. They assumed that the kinetic equations of the observables X_α take the form of (coupled) Langevin equations $\dot{X} + \frac{1}{\tau} X - \eta = 0$ where the random force $\eta(t)$ describes in an effective manner the thermal noise. Since each sequence of random forces $\eta(t)$ leads in a deterministic way to a different history $X(t)$, the probability distribution of $X(t)$ is in the case of a single observable

$$\wp[X(t)] \sim e^{-\frac{1}{2\sigma^2} \int \eta^2 dt} \sim e^{-\frac{1}{2\sigma^2} \int [\dot{X} + \gamma X]^2 dt}.$$

The ‘‘classical’’ path obeys a least-dissipation principle. Far-from-equilibrium, the Onsager-Machlup theory breaks down for complex systems because it is based on linearised kinetic equations. Before introducing recent developments beyond the Onsager-Machlup theory, it is instructive to first consider the simple example of a particule in a potential $V(x)$ and submitted to a time-dependent force $f(t)$. The Newtonian kinetic equation reads

$$m\ddot{x} = -\frac{\partial V}{\partial x_l} + f(t) - m\gamma\dot{x} + \eta(t).$$

Assuming as before that the random force is distributed according to a Gaussian law, the probability distribution of an history $x(t)$, with $t \in [0; t_f]$, is

$$\wp[x(t)] \sim e^{-\frac{1}{2\sigma^2} \int \eta^2 dt} = e^{-\frac{1}{2\sigma^2} \int [m\ddot{x} + \frac{\partial V}{\partial x_l} - f(t) + m\gamma\dot{x}]^2 dt},$$

where $\sigma^2 = 2m\gamma k_B T$ according to the fluctuation-dissipation theorem. The probability $\wp_R[\bar{x}(t)]$ of the time-reversed history $\bar{x}(t) = x(t_f - t)$ is easily obtained by the transformation $\dot{x} \rightarrow -\dot{x}$. The ratio of these two probabilities is [386]

$$\frac{\wp[x(t)]}{\wp_R[\bar{x}(t)]} \sim e^{-\frac{1}{k_B T} \int [m\ddot{x} + \frac{\partial V}{\partial x_l} - f(t)] \dot{x} dt} = e^{-\left(\left[\frac{1}{2}mv^2\right] - W\right)/k_B T} = e^{-Q/k_B T}$$

according to the first principle of thermodynamics. This relation is a special case of a fluctuation theorem. Since the heat Q exchanged with the environment is odd under time-reversal, it is usually written as $\wp(Q)/\wp(-Q) = e^{-Q/k_B T}$. This relation is easily generalised to a Markovian process. When detailed balance holds, the quotient of the

probability of an history (X_1, X_2, \dots, X_N) by the probability of its image under time-reversal is

$$\frac{\wp(X_1, X_2, \dots, X_N)}{\wp(X_N, \dots, X_2, X_1)} = \frac{\wp(X_1)W(X_1 \rightarrow X_2) \dots W(X_{N-1} \rightarrow X_N)}{\wp(X_N)W(X_N \rightarrow X_{N-1}) \dots W(X_2 \rightarrow X_1)} = \frac{\wp(X_1)}{\wp(X_N)} e^{-\Delta E/k_B T} \quad (91)$$

If no work is extracted from the system, the energy variation is $\Delta E = Q$ according to the first principle. If detailed balance does not hold, one may assume that the heat exchange with the environment is defined as $Q = \prod_i W(X_i \rightarrow X_{i+1})/W(X_{i+1} \rightarrow X_i)$. The notion of statistical entropy is generalised by defining $S(X) = -k_B \ln \wp(X)$ so that $S = \langle S(X) \rangle$ [44²]. The ratio (91) leads to the fluctuation theorem [45⁰]

$$\frac{\wp(X_1, X_2, \dots, X_N)}{\wp(X_N, \dots, X_2, X_1)} = e^{-\Delta S/k_B - Q/k_B T} = e^{-\Delta S_{\text{tot.}}/k_B},$$

where $\Delta S_{\text{tot.}}$ is the entropy variation of the universe. Finally, this relation can be recast as

$$1 = \sum_X \wp(X_1, X_2, \dots, X_N) = \sum_X e^{-\Delta S_{\text{tot.}}/k_B} \wp(X_N, \dots, X_2, X_1) = \langle e^{-\Delta S_{\text{tot.}}/k_B} \rangle, \quad (92)$$

known as integrated fluctuation theorem. Remarkably, it follows from Jensen's inequality that $\langle \Delta S_{\text{tot.}} \rangle \geq 0$. Therefore, the second principle of thermodynamics does not apply to each history individually but only to the average.

The previous relations can be applied to a system mechanically coupled to the environment and therefore producing a work W . This coupling is introduced as a perturbation of the Hamiltonian: $H(X) = H_0(X) + \lambda(t)\phi(X)$. If detailed balance holds, transition rates are modified in consequence:

$$\frac{W_i(X_i \rightarrow X_{i+1})}{W_i(X_{i+1} \rightarrow X_i)} = -\beta [E_0(X_{i+1}) - E_0(X_i) + \lambda(t_i)[\phi(X_{i+1}) - \phi(X_i)]] .$$

The quotient of the probability of an history (X_1, X_2, \dots, X_N) by the probability of its image under time-reversal becomes

$$\frac{\wp(X_1, X_2, \dots, X_N)}{\wp(X_N, \dots, X_2, X_1)} = \frac{\wp(X_1)}{\wp(X_N)} e^{-[\Delta E_0 + \sum_i \lambda(t_i)[\phi(X_{i+1}) - \phi(X_i)]]/k_B T}. \quad (93)$$

The last term is the total thermodynamical work W extracted from the system while ΔE_0 is the heat exchanged with the environment. Let us restrict now the discussion to an initial state X_1 at equilibrium, i.e.

$$\wp(X_1) = \frac{e^{-\beta E_0(X_1)}}{\mathcal{Z}} = e^{\beta[F_1 - E_0(X_1)]}.$$

Since detailed balance holds, the final state $\wp(X_N)$ is distributed according to the Boltzmann distribution too. Therefore, the ratio (93) can be recast as a fluctuation theorem [13¹]

$$\frac{\wp(X_1, X_2, \dots, X_N)}{\wp(X_N, \dots, X_2, X_1)} = e^{\beta(\Delta F - W)}.$$

In a way similar to (92), the Jarzynski relation is finally obtained [285, 284]

$$\langle e^{-\beta W} \rangle = e^{-\beta \Delta F}. \quad (94)$$

This result received beautiful experimental confirmations, using a single molecule of RNA submitted to a mechanical stretch [325] or a forced oscillator [167]. For a cyclic transformation, one obtains ⁽¹⁰⁾

$$\langle e^{-\beta W} \rangle = 1.$$

Applying Jensen's inequality to this relation, one recovers Thomson's formulation of the second principle: no work can be extracted from a cyclic transformation at equilibrium. If the work is distributed according to a Gaussian law, i.e.

$$\wp(W) = \frac{1}{\sqrt{2\pi\sigma^2}} e^{-\frac{(W-\langle W \rangle)^2}{2\sigma^2}}$$

then the Jarzynski relation implies

$$\int_{\mathbb{R}} e^{-\beta(W-\langle W \rangle)} \wp(W) dW = e^{\frac{\beta^2 \sigma^2}{2}} = e^{-\beta \Delta F}$$

and therefore the irreversible heat lost during the process is proportional to the fluctuations of the work:

$$\langle Q \rangle - T \Delta S = \Delta F - \langle W \rangle = -\frac{\sigma^2}{2k_B T}. \quad (95)$$

The Jarzynski relation has attracted a lot of attention. It offers the possibility to compute numerically a free energy difference. Therefore, it is widely used in computational chemistry and biophysics. The application of (94) has to be carefully performed. If the perturbation is too strong and therefore the work extracted too large, the average is dominated by rare events that are very difficult to sample numerically.

We studied the distribution of the work $\wp(W)$ when a magnetic field is coupled to a two-dimensional Ising model [120]. Using Monte Carlo simulations, the system is initially prepared at equilibrium and the magnetic field is increased linearly. The work is measured as $W = -\Delta h \sum_i M_i$ where M_i is the total magnetisation at the i -th iteration. In the paramagnetic phase, the work distribution $\wp(W)$ is very close to a Gaussian law. We therefore checked the relation (95) by calculating ΔF from the Jarzynski relation and from the second moment σ^2 of the distribution $\wp(W)$. As expected, a very good agreement is obtained for small fields and low ramps, which are the closest to a reversible transformation. For strongly irreversible transformations, the rare events of the distribution $\wp(W)$ are too badly sampled and the Jarzynski relation becomes biased. In the stable regime, we used the estimate of ΔF provided by the Jarzynski relation to evaluate the correlation length. The system was considered as a set of N uncorrelated Ising magnetic moments. The similarity of our work distributions

⁽¹⁰⁾ This equation was often confused with Bochkov and Kuzovlev relation [72, 73]. The latter differs from the Jarzynski relation by the fact that it involves the mechanical work and not the thermodynamical one.

with those obtained with a single spin supports that idea [350]. The equilibrium free energy differences should therefore be

$$\Delta F = F(h) - F(0) = -Nk_B T \ln \cosh \frac{mh}{k_B T}.$$

We then introduced a phenomenological Langevin equation

$$\frac{\partial M}{\partial t} = -\frac{M(t) - M_{\text{eq.}}(h)}{\tau},$$

where the equilibrium magnetisation is $M_{\text{eq.}}(h) = -\frac{\partial F}{\partial h}$. It can be solved exactly and gives a prediction for the average work $\langle W(t) \rangle$. The numerical data are well reproduced by this simple model. In the ferromagnetic phase, the work distribution displays two peaks corresponding to the two different ferromagnetic states. We checked again the Gaussian approximation (95). We observed that the peak corresponding to a magnetisation initially parallel to the magnetic field is almost immobile while the other one moves very fast as the magnetisation tends to reverse itself. Dissipation is mainly due to these configurations with a magnetisation anti-parallel to the magnetic field. Finally, we considered the Ising model at the critical point. Two peaks are again observed but they are not Gaussian. We used the estimates of ΔF provided by the Jarzynski relation to extract the δ critical exponent as $F_{\text{sing}}(h) \sim h^{1+1/\delta}$. We note finally that the same study has been later conducted to test the Crooks relation [254].

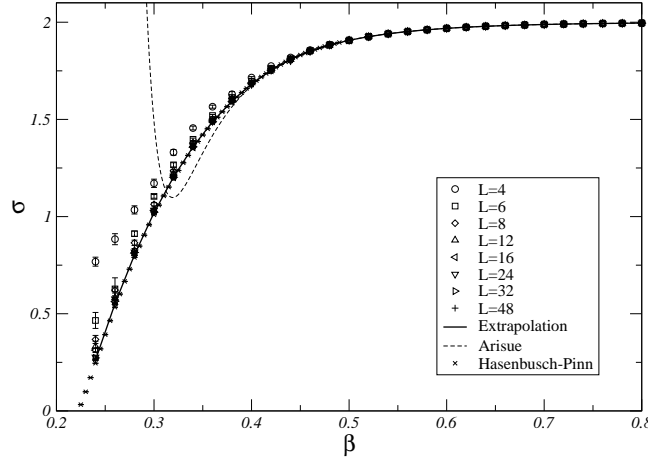


Figure 50 : Order-order surface tension of the three-dimensional Ising model versus temperature. Our data are compared to high-temperature series expansions (Arisue) and Monte Carlo simulations (Hasenbusch-Pinn).

In a second work, we used a Jarzynski relation extended to a protocol involving a time-dependent temperature instead of a magnetic field [106]. Equation (93) is easily adapted to

$$\frac{\wp(X_1, X_2, \dots, X_N)}{\wp(X_N, \dots, X_2, X_1)} = \frac{\wp(X_1)}{\wp(X_N)} e^{-\sum_i \beta(t_i)[E(X_{i+1}) - E(X_i)]}.$$

Using again an equilibrium initial state, we obtained the relation

$$\langle e^{-\int E(t)\dot{\beta}dt} \rangle = e^{-\Delta(\beta F)}. \quad (96)$$

Crooks had already mentioned the possibility to obtain such a relation ^[130]. Equation (96) was later rederived in the case of a deterministic dynamics with a Nosé-Hover thermostat ^[486]. Equation (96) provides a new way to evaluate free energies numerically. It extends the so-called thermodynamical perturbation or the Bennet method ^[53] and fits into the general category of annealed importance sampling ^[388].

We applied equation (96) to measure numerically the surface tension of the three-dimensional Ising model. First, a system with anti-periodic boundary conditions is initially prepared at zero temperature. Because of the boundaries, an interface separates the two different ferromagnetic phases. At sufficiently low temperature, fluctuations can be neglected and the free energy is easily evaluated. The temperature is then increased and the “entropic work” $\int E(t)\beta dt$ is recorded. Because of the large autocorrelation time of the interface, even with the Swendsen-Wang algorithm ^[459], we used an appropriate cluster algorithm introduced by Hasenbusch and Meyer ^[228]. The protocol is repeated 1000 times. To estimate the free energy of the interface, one has to remove from ΔF the contribution of the ferromagnetic phases. The latter is obtained by applying the same procedure to a system with periodic boundary conditions and therefore without interface. On figure 50, our estimates of the order-order surface tension are compared to high-temperature series expansion and Monte Carlo simulations ^[232]. The same technique has been later applied to the two-dimensional Ising model ^[255].

1.3.5. Conclusions

In this second chapter, we considered the dynamics of homogeneous lattice spin models initially prepared in their high-temperature phase and then quenched below or at their critical temperature. The more complex case of spin glasses is out of our scope. In ferromagnets, the existence of a divergent relaxation time is explained by the local growth of domains in competition to impose the global order of the system. While reversible thermal fluctuations occur inside the domains, the growth and coalescence of domain walls are irreversible processes. The Fluctuation-Dissipation Theorem (FDT) is therefore violated. The scaling theory of two-time functions is motivated by the assumption of a single characteristic length growing algebraically with time. Two new universal quantities emerged: the autocorrelation exponent λ associated to the algebraic decay of two-time functions and the asymptotic value of the Fluctuation-Dissipation Ratio (FDR) measuring the degree of violation of the FDT.

We studied several models in this framework. We first discussed the one-dimensional KDH model at zero temperature. Exploiting the equivalence with a gas of immobile particles undergoing pair annihilation, we calculated exactly the time-dependence of some correlation functions. In contradistinction to the Ising-Glauber model, only exponential decays were observed. When prepared out-of-equilibrium, the system does not age but only falls in one of the many ground states of the model. We note that if particle diffusion is allowed, the Ising-Glauber model is recovered. This shows that diffusion of defects is an essential ingredient to observe aging.

We then focused our attention to two-dimensional systems, studied by means of Monte Carlo simulations. We introduced the first estimator of linear response. No magnetic field needs to be applied and the FDR is directly accessible without assuming a dependence on autocorrelations, i.e. $X = X(C)$. In the case of the q -state Potts model with $q = 2, 3$ and 4 , we checked that the autocorrelation exponent and the FDR do not depend on the lattice, as expected for universal quantities. We then compared

several models. In particular, we compared the Baxter-Wu and Debierre-Turban models, both in the same universality class as the four-state Potts model. Our estimates of the autocorrelation exponents show a different behaviour of the Baxter-Wu model, as already observed in Short-Time Dynamics simulations. The FDR displays the same trend. This unexpected result is probably related to the fact that the equilibrium critical behaviour of both four-state Potts and Debierre-Turban models is affected by logarithmic corrections but not that of the Baxter-Wu model. Unfortunately, how logarithmic corrections of the static critical behaviour are translated in the case of aging and even whether they appear at all is still an open question. We note that, surprisingly, no logarithmic correction was found in the aging behaviour of the spherical model at its upper critical dimension ^[174] while such corrections were encountered in the $O(n)$ model ^[125]. We then considered a generalised three-state Potts model with an irreversible dynamics, i.e. without detailed balance. A universal behaviour was observed, independently of whether detailed balance holds or not. Only at the point where the critical line meets the absorbent phase, the model undergoes a different type of coarsening corresponding to the Voter model.

We finally turned our attention to homogeneously frustrated models. Like the anti-ferromagnetic Ising model on a triangular lattice, the Fully-Frustrated Ising model is critical at zero temperature. Despite the existence of a macroscopically large number of ground states, the aging of this model is similar to that of ferromagnetic systems. However, because of the local dynamics, excited ferromagnetic plaquettes can only be annihilated by pair. They behave as topological defects, interacting via a Coulomb potential, as vortices in the XY model. We therefore assumed that these defects pin the domain walls and slow down the dynamics. As a consequence, logarithmic corrections appear in the scaling behaviour of two-time functions. We showed that these corrections explain the slow dynamics reported in the literature and that no stretched exponential law is needed to reproduce relaxation functions. We also considered the Fully-Frustrated XY model which has the particularity to undergo two very close transitions, a Berezinskii-Kosterlitz-Thouless transition followed by a second-order phase transition in the Ising model universality class. We indeed observed the same aging behaviour as the XY model at the first transition. However, we failed to recover that of the Ising model at the second one. Cross-over effects due to the vicinity of the BKT transition is invoked to explain this result. Larger-scale Monte Carlo simulations are needed to resolve this issue.

Finally, we applied the Jarzynski relation to the study of the work distribution in a two-dimensional Ising model under a linearly-increasing magnetic field and to estimate the order-order surface tension of the three-dimensional Ising model. The algorithm introduced in the second case extends thermodynamical perturbation and Bennet method.

1.4. Simulations of experimental systems

Being part of a laboratory mostly composed of experimentalists, I had many opportunities to listen to seminars on experimental topics. Some discussions with colleagues evolved into collaborations. I discuss in this small chapter two applications of numerical techniques to the simulation of real experimental systems.

1.4.1. Magnetic systems

The powerful numerical techniques employed in the simulations of the random Potts model, that were discussed in the first chapter, can, of course, be used to study more realistic magnetic systems.

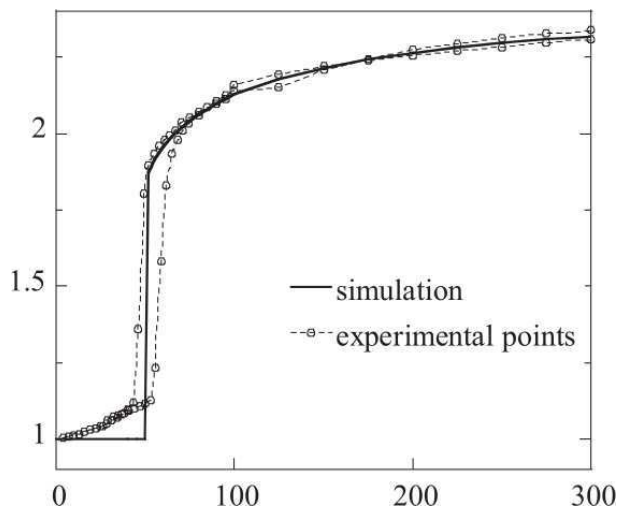


Figure 51 : Total magnetisation versus the applied magnetic field. The jump occurs at non-zero field.

Multilayer magnetic systems deposited by evaporation is one of the speciality of our laboratory. The so-called exchange bias effect attracted the attention of my colleagues. Consider a two-layer system where the upper layer is ferromagnetic while the other is anti-ferromagnetic. As the interface is approached, the ferromagnetic order of the upper layer is progressively destroyed. Because of the coupling with the anti-ferromagnet, magnetisation vanishes at the interface. Under a strong magnetic field, the ferromagnetic order is enhanced in the vicinity of the interface. A small magnetic field is not sufficient to reverse magnetisation. As a consequence, the hysteresis cycle appears to be horizontally shifted. My colleagues studied in particular the system $\text{Fe}_{60}\text{Gd}_{40}/\text{Fe}_{55}\text{Sn}_{45}$ ^[176]. To reproduce the exchange bias, we first assumed the system homogeneous in the planes perpendicular to the magnetic field. The parallel direction is discretised as a chain of N sites. The total energy is chosen as

$$E = \sum_{i=1}^N \left[-J_i \cos(\theta_i - \theta_{i+1}) + D_i \sin^2 \theta_i - \mu_i H \cos \theta_i \right],$$

where θ_i is the angle made by the magnetic moment with the field, J_i is the exchange coupling, D_i the uniaxial anisotropy parameter and μ_i the magnetic moment. These

parameters were adjusted with the experimental data. A low temperature, the equilibrium state is given by the minimum energy. Numerically, we discretised the angles θ_i and constructed a transfer matrix to compute magnetisation profiles. On figure 51, the displacement of the magnetisation jump under a magnetic field is clearly observed.

In a second collaboration, we used Monte Carlo simulations to estimate the magnetic susceptibility of thin magnetic films with an incomplete covering of the last atomic layer [19]. It was usually assumed that the transition temperature was smoothly varying when the thickness of the films was increased by depositing more and more atoms at the surface. We showed that a very different scenario takes place: when a new atomic layer is started, a new susceptibility peak appears roughly at the location of the maximum for an infinite system with the same thickness. As more atoms are deposited, the first peak decreases while the second increases. As shown on figure 52, one peak replaces the other.

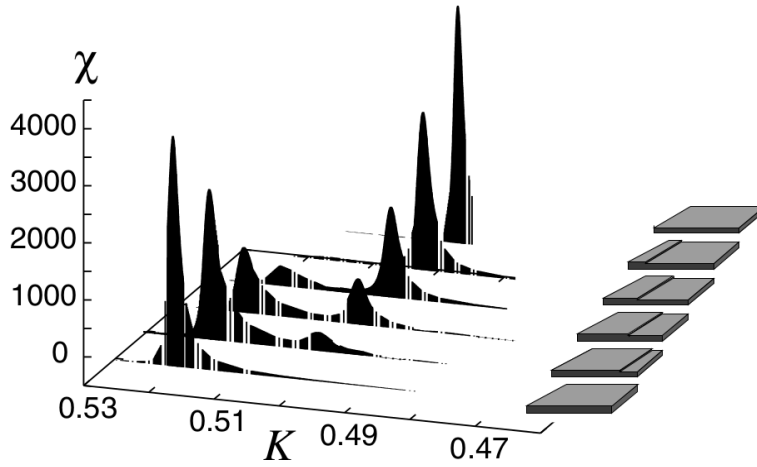


Figure 52 : Evolution of the magnetic susceptibility versus the exchange coupling K when the covering of the top layer is increased.

1.4.2. Electronic systems

We developed a numerical code to estimate the first eigenstates of a single electron in a two-dimensional periodic potential $V(\vec{r})$, i.e.

$$V(\vec{r} + \vec{R}) = V(\vec{r})$$

for any $\vec{R} = n\vec{a} + m\vec{b}$, where n and m are integers. According to Bloch theorem, the eigenvectors of Schrödinger equation are of the form

$$\psi_{\vec{k}}(\vec{r}) = u_{\vec{k}}(\vec{r})e^{i\vec{k}\cdot\vec{r}},$$

where $u_{\vec{k}}(\vec{r})$ are periodic functions on the first Brillouin zone and satisfy the Bloch-Schrödinger equation

$$-\frac{\hbar^2}{2m}(\nabla + i\vec{k})^2 u_{\vec{k}} + V u_{\vec{k}} = E_{\vec{k}} u_{\vec{k}}.$$

To work in non-rectangular cells, we found more convenient to use the tensor formalism:

$$-\frac{\hbar^2}{2m}(\partial_\mu + ik_\mu)(\partial^\mu + ik^\mu)u_{\vec{k}}(\vec{r}) + V(\vec{r})u_{\vec{k}}(\vec{r}) = E_{\vec{k}}u_{\vec{k}}(\vec{r}), \quad (97)$$

where k_μ are the components of the dual vector \vec{k} in the dual basis (\vec{a}^*, \vec{b}^*) while $k^\mu = g^{\mu\nu}k_\nu$. The metric tensor $g_{\mu\nu}$ is defined as the dot product of basis vectors, for example $g_{12} = \vec{a} \cdot \vec{b}$. Note that the unit vectors \vec{a} and \vec{b} are constant so the tensor metric is uniform and the Laplacian $\Delta = \frac{1}{\sqrt{g}}\partial_\mu(g^{\mu\nu}\sqrt{g}\partial_\nu \cdot)$ is reduced to $\partial_\mu\partial^\mu$.

The unit cell is discretised by introducing a rectangular mesh. Functions on the unit cell, as $u_{\vec{k}}(\vec{r})$ and $V(\vec{r})$, are replaced by vectors. The Bloch-Schrödinger equation is reduced to a linear relation $H|u\rangle = E|u\rangle$. To find the first eigenvectors, we used a projective method. Let $|\phi_i\rangle$ the eigenvectors of H for the eigenvalues ε_i . Then, for most of the trial vectors $|u_0\rangle$,

$$H^N|u_0\rangle = \sum_i \varepsilon_i^N |\phi_i\rangle \langle \phi_i | u_0 \rangle \xrightarrow{N \rightarrow +\infty} \varepsilon_{\max}^N |\phi_{\max}\rangle \langle \phi_{\max} | u_0 \rangle,$$

where ε_{\max} is the largest eigenvalue of H . The eigenvector $|\phi_{\max}\rangle$ is obtained after normalisation of $H^N|u_0\rangle$. The eigenvalue is computed by applying once more H . The second largest eigenvalue can be estimated by considering a second trial vector $|u_1\rangle$. Applying N times the operator H and using the Gramm-Schmidt orthogonalisation procedure at each application, $H^N|u_1\rangle$ tends to the second eigenvector. In quantum mechanics, we are actually not interested in the largest eigenvalues but in the lowest. In principle, the latter can be obtained by applying the above procedure to the operator $\Lambda - H$, where Λ has to be chosen larger than ε_{\max} in order to avoid an oscillatory behaviour. Numerically, Λ cannot be too large compared to the smallest eigenvalue, otherwise truncation errors would accumulate at each application of $\Lambda - H$. We found easier to use the following algorithm to estimate the n eigenvectors corresponding to the smallest eigenvalues:

1. Choose randomly n trial vectors $|u_1\rangle, \dots, |u_n\rangle$,
2. Construct n new vectors $|v_i\rangle = H|u_i\rangle$,
3. Apply the Gramm-Schmidt orthogonalisation procedure to the $2n$ vectors $|u_1\rangle, \dots, |u_n\rangle, |v_1\rangle, \dots, |v_n\rangle$. A basis $|e_1\rangle, \dots, |e_{2n}\rangle$ of a subspace of the Hilbert vector space is obtained.
4. Construct the $2n \times 2n$ Hamiltonian matrix whose elements are $H_{ij} = \langle e_i | H | e_j \rangle$.
5. Diagonalise this matrix. Sort the eigenvalues. Select the n eigenvectors associated to the n smallest eigenvalues

$$|\phi_i\rangle = \sum_{j=1}^{2n} \phi_{ij} |e_j\rangle$$

and reconstruct their components in the full Hilbert space using the known components of $|e_i\rangle$.

6. Go to step 1 using $|\phi_i\rangle$ as new trial vectors.

A criterion has to be introduced to stop the iteration when a sufficient convergence has been achieved. During step 3, we computed the component of $H|u_i\rangle$ orthogonal to $|u_i\rangle$. The trial vector $|u_i\rangle$ was considered sufficiently close to the exact eigenvector when this component was smaller than a pre-defined parameter ϵ , i.e. when

$$||u_i\rangle - |H|u_i\rangle|| < \epsilon.$$

The algorithm is stopped when all eigenvectors have converged.

The operator H of the above algorithm has to be replaced by the Bloch-Schrödinger Hamiltonian (97). The fastest implementation of the derivatives consists in replacing them by finite differences on the lattice:

$$\partial_\mu u(\vec{r}) \simeq \frac{u(n+1, m) - u(n, m)}{a}.$$

However, the spectral approach provides a more stable implementation. A Discrete-Fourier Transform of $u(\vec{r})$ is first calculated. The derivative $\partial_\mu u(\vec{r})$ is then estimated by taking the inverse Discrete-Fourier Transform of $ik_\mu u(\vec{k})$. The computational cost of these two steps is of order $\mathcal{O}(N \ln N)$ when Fast-Fourier Transforms are employed. The application of the potential $V(\vec{r})$ on the wavefunctions is more suitably performed in real space and not in Fourier space. The algorithm requires therefore to go back and forth between real and Fourier spaces.

The convergence can be significantly improved by first starting with a small lattice. We chose initial lattices allowing for an exact diagonalisation. The number of lattice points is then slightly increased. The wavefunctions on the new lattice are extrapolated from the previous one. The best results were obtained using the following algorithm:

1. Perform a Discrete-Fourier Transform of the wavefunction u on the $N \times N$ lattice.
2. To extrapolate to a $N' \times N'$ lattice, extend the $N \times N$ Fourier spectrum of u to a $N' \times N'$ one by filling the new high frequencies with zeroes.
3. Perform an inverse Discrete-Fourier Transform.

A plane-wave shape is preserved by this extrapolation. Moreover, high-frequencies have high kinetic energies so they do not contribute much to the lowest states. This explains why the method works well with free electrons confined in a potential.

This technique has been used to compare theoretical predictions with images obtained by Scanning Tunnelling Microscope (STM) ^[155]. The system under consideration was a surface reconstruction Au(23 23 21) of gold. Different steps between hcp and fcc phases are self-organised on the surface and form a regular lattice. They act as a potential barrier for conduction electrons. Schockley states, i.e. electronic states corresponding to evanescent wavefunctions and therefore localised at the surface, are trapped between these steps. Using STM images of the surface reconstruction, we made numerical calculations for different potential shapes and compared to STM images of the electronic density inside the wells (see figure 53).

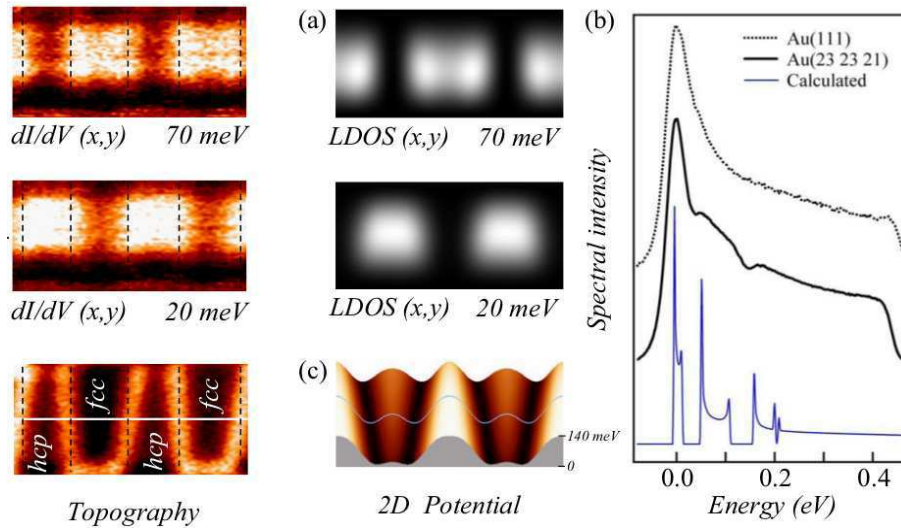


Figure 53 : On the left, electronic density measured by STM inside the wells formed by the surface reconstruction. On the centre, the numerically calculated densities. On the right, comparison between the computed density of states and the photo-emission spectrum. Below (c), the reconstructed potential used in the numerical calculations.

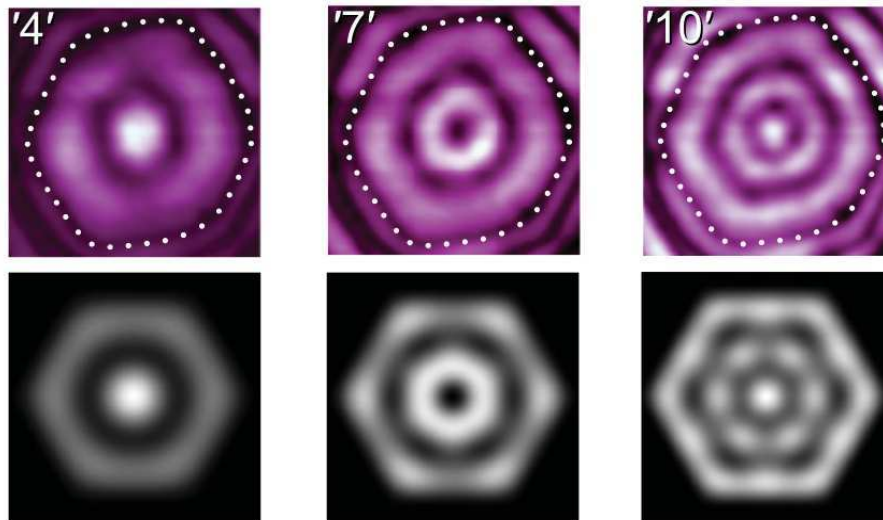


Figure 54 : Electronic density of Schockley states trapped in truncated hexagonal Ag pyramids obtained by STM (above) compared to numerical calculations (below).

The numerical method was then employed to reproduce the electronic density of Schockley states trapped in isolated truncated hexagonal Ag pyramids, grown by epitaxy on Cu(111) (figure 54) [469]. The pyramids are four to six atomic layers high.

BIBLIOGRAPHY

- [1] A.J.Bray, A.J. Briant, and D.K. Jervis (2000), *Phys. Rev. Lett.* **84**, 1503.
- [2] F.D.A. Aarão Reis, S.L.A. de Queiroz, and R.R. dos Santos (1996), *Phys. Rev. B* **54**, R9616.
- [3] F.D.A. Aarão Reis, S.L.A. de Queiroz, and R.R. dos Santos (1997), *Phys. Rev. B* **56**, 6013.
- [4] M. Abramowitz, and I.A. Stegun (1970) In *Handbook of Mathematical Functions*, (Dover, New-York).
- [5] S. Abriet, and D. Karevski (2004), *Eur. Phys. J. B* **37**, 47.
- [6] D.A. Adams, L.M. Sander, and R.M. Ziff (2010), *J. Stat. Mech.* , P03004.
- [7] A. Aharony, and J. Asikainen (2002) *cond-mat/0206367*.
- [8] A. Aharony and A.B. Harris (1996), *Phys. Rev. Lett.* **77**, 3700.
- [9] A. Aharony, A.B. Harris, and S. Wiseman (1998), *Phys. Rev. Lett.* **81**, 252.
- [10] M. Aizenman, B. Duplantier, and A. Aharony (1999), *Phys. Rev. Lett.* **83**, 1359.
- [11] M. Aizenman, and J. Wehr (1989), *Phys. Rev. Lett.* **62**, 2503.
- [12] M. Aizenman, and J. Wehr (1990), *Comm. Math. Phys.* **130**, 489.
- [13] E.V. Albano, M.A. Bab, G. Baglietto, R.A. Borzi, T.S. Grigera, E.S. Loscar, D.E. Rodriguez, M.L Rubio Puzzo, and G.P. Saracco (2011), *Rep. Prog. Phys.* **74**, 026501.
- [14] S.M. Allen, and J.W. Cahn (1979), *Acta Metall.* **27**, 1085.
- [15] J.G. Amar, and F. Family (1990), *Phys. Rev. A* **41**, 3258.
- [16] C. Amoruso, A.K. Hartmann, M.B. Hastings, and M.A. Moore (2006), *Phys. Rev. Lett.* **97**, 267202.
- [17] D. Andelman, and A.N. Berker (1984), *Phys. Rev. B* **29**, 2630.
- [18] P.W. Anderson (1958), *Phys. Rev.* **109**, 1492.
- [19] S. Andrieu, C. Chatelain, M. Lemine, B. Berche, and Ph. Bauer (2001), *Phys. Rev. Lett.* **86**, 3883.
- [20] G. André, R. Bidaux, J.-P. Carton, R. Conte, and L. de Seze (1979), *J. Phys. France* **40**, 479.
- [21] C.A. Angell (1995), *Science* **267**, 1924.
- [22] J-Ch. Anglès d'Auriac, and F. Iglói (2003), *Phys. Rev. Lett.* **90**, 2003.
- [23] J-Ch. Anglès d'Auriac, F. Iglói, M. Preissmann, and A. Sebö (2002), *J. Phys. A* **35**, 6973.
- [24] A. Annibale and P. Sollich (2006), *J. Phys. A* **39**, 1.

- [25] A. Annibale and P. Sollich (2006), *J. Phys. A* **39**, 2853.
- [26] A. Annibale and P. Sollich (2008), *J. Phys. A* **41**, 135001.
- [27] E. Arashiro, and J.R. Drugowich de Felício (2003), *Phys. Rev. E* **67**, 046123.
- [28] E. Arashiro, H.A. Fernandes, and J.R. Drugowich de Felício (2009), *Physica A* **388**, 4379.
- [29] J.J. Arenzon, A.J. Bray, L.F. Cugliandolo, and A. Sicilia (2007), *Phys. Rev. Lett.* **98**, 145701.
- [30] J. Ashkin and E. Teller (1943), *Phys. Rev.* **64**, 178.
- [31] J. Asikainen, A. Aharony, B.B. Mandelbrot, E. Rausch, and J.-P. Hovi (2003), *Eur. Phys. J. B* **34**, 479.
- [32] R. B. Potts (1952), *Math. Proc. Camb. Phil. Soc.* **48**, 106.
- [33] C.F. Baillie, W. Janke, and D.A. Johnston (1996), *Phys. Lett. B* **388**, 14.
- [34] Per Bak, P. Kleban, W. N. Unertl, J. Ochab, G. Akinici, N. C. Bartelt, and T. L. Einstein (1985), *Phys. Rev. Lett.* **54**, 1539.
- [35] H.G. Ballesteros, L.A. Fernández, V. Martín-Mayor, A. Muñoz Sudupe, G. Parisi, and J.J. Ruiz-Lorenzo (1998), *Phys. Rev. B* **58**, 2740.
- [36] H.G. Ballesteros, L.A. Fernández, V. Martín-Mayor, A. Muñoz Sudupe, G. Parisi, and J.J. Ruiz-Lorenzo (2000), *Phys. Rev. B* **61**, 3215.
- [37] A. Barrat (1998), *Phys. Rev. E* **57**, 3629.
- [38] M. Bauer, and D. Bernard (2002), *Phys. Lett. B* **543**, 135.
- [39] M. Bauer, and D. Bernard (2003), *Comm. Math. Phys.* **239**, 493.
- [40] M. Bauer, and D. Bernard (2006), *Phys. Rep.* **432**, 115.
- [41] R. Bausch, V. Dohm, H.K. Janssen and R.K.P. Zia (1981), *Phys. Rev. Lett.* **47**, 1837.
- [42] R. Bausch, H.K. Janssen, and H. Wagner (1976), *Z. Phys. B* **24**, 113.
- [43] R.J. Baxter (1973), *J. Phys. C* **6**, L445.
- [44] R.J. Baxter (1974), *Aust. J. Phys.* **27**, 369.
- [45] R.J. Baxter (1982), *J. Phys. A* **15**, 3329.
- [46] R.J. Baxter (1982) In *Exactly solved models of statistical mechanics*, (Academic Press, London).
- [47] R.J. Baxter, S.B. Kelland, and F.Y. Wu (1976), *J. Phys. A* **9**, 397.
- [48] R.J. Baxter, and F.Y. Wu (1973), *Phys. Rev. Lett.* **31**, 1294.
- [49] R.J. Baxter, and F.Y. Wu (1974), *Aust. J. Phys.* **27**, 357.
- [50] V. Beffara (2004), *Ann. Prob.* **32**, 2606.
- [51] V. Beffara and H. Duminil-Copin (2010) *arxiv/1006.5073*.
- [52] E. Ben-Naim, L. Frachebourg, and P.L. Krapivsky (1996), *Phys. Rev. E* **53**, 3078.
- [53] C.H. Bennett (1976), *J. Comput. Phys.* **22**, 245.
- [54] B. Berche, P.-E. Berche, C. Chatelain, and W. Janke (2005), *Cond. Matt. Phys.* **8**, 47.
- [55] B. Berche, P. Butera, W. Janke, and L. Shchur (2009), *Comp. Phys. Comm.* **180**, 493.

- [56] B. Berche, and C. Chatelain (1999), *Comp. Phys. Comm.* **121-122**, 191.
- [57] P.-E. Berche, C. Chatelain, and B. Berche (1998), *Phys. Rev. Lett.* **80**, 297.
- [58] P.-E. Berche, C. Chatelain, B. Berche and W. Janke (2002), *Comp. Phys. Comm.* **147**, 427.
- [59] P.-E. Berche, C. Chatelain, B. Berche and W. Janke (2004), *Eur. Phys. J. B* **38**, 463.
- [60] B. Berge, H.T. Diep, A. Ghazali, and P. Lallemand (1986), *Phys. Rev. B* **34**, 3177.
- [61] D. Bernard, P. Le Doussal, and A.A. Middleton (2007), *Phys. Rev. B* **76**, R020403.
- [62] L. Berthier, J.L. Barrat, and J. Kurchan (1999), *Eur. Phys. J. B* **11**, 635.
- [63] L. Berthier, P.C.W. Holdsworth, and M. Sellitto (2001), *J. Phys. A* **34**, 1805.
- [64] J.L. Black, and V.J. Emery (1981), *Phys. Rev. B* **23**, 429.
- [65] R. Blumenhagen, and E. Plauschinn (2009) In *Introduction to Conformal Field Theory: With Applications to String Theory*, Springer-Verlag.
- [66] H.W.J Blöte and H.J. Hilborst (1982), *J. Phys. A* **15**, L631.
- [67] H.W.J. Blöte, J.L. Cardy, and M.P. Nightingale (1986), *Phys. Rev. Lett.* **56**, 742.
- [68] H.W.J. Blöte, A. Compagner, P.A.M. Cornelissen, A. Hoogland, F. Mallezie, C. Vanderzande (1986), *Physica A* **139**, 395.
- [69] H.W.J. Blöte, and M.P. Nightingale (1982), *Physica A* **112**, 405.
- [70] H.W.J. Blöte and M.P. Nightingale (1993), *Phys. Rev. B* **47**, 15046.
- [71] H.W.J. Blöte, M.P. Nightingale, X.N. Wu, and A. Hoogland (1991), *Phys. Rev. B* **43**, 8751.
- [72] G.N. Bochkov, and Y.U. Kuzovlev (1981), *Physica A* **106**, 443.
- [73] G.N. Bochkov, and Y.U. Kuzovlev (1981), *Physica A* **106**, 480.
- [74] C. Borgs, and J.T. Chayes (1996), *J. Stat. Phys.* **82**, 1235.
- [75] P. Braun, and M. Fähnle (1988), *J. Stat. Phys.* **52**, 775.
- [76] A.J. Bray (1990), *Phys. Rev. B* **41**, 6724.
- [77] A.J. Bray (1994), *Adv. Phys.* **43**, 357.
- [78] A.J. Bray, B. Derrida and C. Godrèche (1994), *Europhys. Lett.* **27**, 175.
- [79] A.J. Bray, K. Humayun, and T.J. Newman (1991), *Phys. Rev. B* **43**, 3699.
- [80] A.J. Bray and M.A. Moore (1985), *J. Phys. C* **18**, L927.
- [81] A. Brunstein, and T. Tomé (1998), *Physica A* **257**, 334.
- [82] A. Brunstein, T. Tomé (1999), *Phys. Rev. E* **60**, 3666.
- [83] E. Buffenoir, and S. Wallon (1993), *J. Phys. A* **26**, 3045.
- [84] T.W. Burkhardt, and B. Derrida (1985), *Phys. Rev. B* **32**, 7273.
- [85] T.W. Burkhardt, and E. Eisenriegler (1985), *J. Phys. A* **18**, L83.
- [86] T.W. Burkhardt, and T. Xue (1991), *Phys. Rev. Lett* **66**, 895.
- [87] M.A. Burschka, C.R. Doering, D. ben-Avraham (1989), *Phys. Rev. Lett.* **63**, 700.

- [88] P. Calabrese and A. Gambassi (2002), *Phys. Rev. E* **65**, 066120.
- [89] P. Calabrese and A. Gambassi (2004), *J. Stat. Mech.* , P07013.
- [90] P. Calabrese and A. Gambassi (2005), *J. Phys. A* **38**, R133.
- [91] P. Calabrese, V. Martín-Mayor, A. Pelissetto, and E. Vicari (2003), *Phys. Rev. E* **68**, 036136.
- [92] J. Cardy (2008) In *Conformal Field Theory and Statistical Mechanics in Exact Methods in Low-dimensional Statistical Physics and Quantum Computing*, Oxford University Press.
- [93] J.L. Cardy (1984), *J. Phys. A* **17**, L385.
- [94] J.L. Cardy (1984), *Nucl. Phys. B* **240**, 514.
- [95] J.L. Cardy (1999), *J. Phys. A* **32**, L177.
- [96] J.L. Cardy (1999), *Physica A* **263**, 215.
- [97] J.L. Cardy (2005), *Ann. Phys.* **318**, 81.
- [98] J.L. Cardy, and J.L. Jacobsen (1997), *Phys. Rev. Lett.* **79**, 4063.
- [99] J.L. Cardy, M. Nauenberg and D.J. Scalapino (1980), *Phys. Rev. B* **22**, 2560.
- [100] E. Carlon, C. Chatelain and B. Berche (1999), *Phys. Rev. B* **60**, 12974.
- [101] M. Caselle, S. Lottini and M.A. Rajabpour (2011), *J. Stat. Mech.* , P02039.
- [102] H.B.G. Casimir (1945), *Rev. Mod. Phys.* **17**, 343.
- [103] N. Caticha, J. Chahine, and J.R. Drugowich de Felício (1991), *Phys. Rev. B* **43**, 1173.
- [104] C. Chatelain (2003), *J. Phys. A.* **36**, 10739.
- [105] C. Chatelain (2004), *J. Stat. Mech.* , P06006.
- [106] C. Chatelain (2007), *J. Stat. Mech.* , P04011.
- [107] C. Chatelain (2010), *J. Stat. Mech.* , P08004.
- [108] C. Chatelain (2012), *Springer Lecture Notes Physics* **853**, 113.
- [109] C. Chatelain, and B. Berche (1998), *Phys. Rev. E* **58**, R6899.
- [110] C. Chatelain, and B. Berche (1998), *Phys. Rev. Lett.* **80**, 1670.
- [111] C. Chatelain, and B. Berche (1999), *Phys. Rev. E* **60**, 3853.
- [112] C. Chatelain, and B. Berche (2000), *Nucl. Phys. B* **572**, 626.
- [113] C. Chatelain, B. Berche, W. Janke, and P.-E. Berche (2001), *Phys. Rev. E* **64**, 036120.
- [114] C. Chatelain, B. Berche, W. Janke, and P.-E. Berche (2005), *Nucl. Phys. B* **719**, 275.
- [115] C. Chatelain, B. Berche, and L.N. Shchur (2001), *J. Phys. A* **34**, 9593.
- [116] C. Chatelain, P.-E. Berche, and B. Berche (1999), *Eur. Phys. J. B* **7**, 439.
- [117] C. Chatelain, P.-E. Berche, and B. Berche (1999), *Comp. Phys. Comm.* **122**, 197.
- [118] C. Chatelain, P.-E. Berche, B. Berche, and W. Janke (2002), *Comp. Phys. Comm.* **147**, 431.
- [119] C. Chatelain, M. Henkel, M. de Oliveira, and T. Tomé (2012), *J. Stat. Mech.* , P11006.

- [120] C. Chatelain, and D. Karevski (2006), *J. Stat. Mech.* , P06005.
- [121] C. Chatelain, T. Tomé, M.J. de Oliveira (2011), *J. Stat. Mech.* , P02018.
- [122] J.T. Chayes, L. Chayes, D.S. Fisher, and T. Spencer (1986), *Phys. Rev. Lett.* **57**, 2999.
- [123] S. Chen, A.M. Ferrenberg, and D. P. Landau (1992), *Phys. Rev. Lett.* **69**, 1213.
- [124] S. Chen, A.M. Ferrenberg, and D. P. Landau (1995), *Phys. Rev. E* **52**, 1377.
- [125] Y. Chen, S.H. Guo, and Z.B. Li (2001), *Phys. Status Solidi B* **223**, 599.
- [126] A. Coniglio (1989), *Phys. Rev. Lett.* **62**, 3054.
- [127] F. Corberi, A. Gambassi, E. Lippiello and M. Zannetti (2008), *J. Stat. Mech.* , P02013.
- [128] R. Cordery, S. Sarker, and J. Tobochnik (1981), *Phys. Rev. B* **24**, 5402.
- [129] A. Crisanti, and F. Ritort (2003), *J. Phys. A* **36**, R181.
- [130] G.E. Crooks (1999) In *Excursions in statistical dynamics*, Dissertation, University of California at Berkeley.
- [131] G.E. Crooks (1999), *Phys. Rev. E* **60**, 2721.
- [132] L.F. Cugliandolo (2011), *J. Phys. A* **44**, 483001.
- [133] L.F. Cugliandolo, and D.S. Dean (1995), *J. Phys. A* **28**, 4213.
- [134] L.F. Cugliandolo, and J. Kurchan (1993), *Phys. Rev. Lett.* **71**, 173.
- [135] L.F. Cugliandolo, and J. Kurchan (1994), *J. Phys. A* **27**, 5749.
- [136] L.F. Cugliandolo, and J. Kurchan (2008), *J. Phys. A* **41**, 324018.
- [137] C. Dasgupta, and S.K. Ma (1980), *Phys. Rev. B* **22**, 1305.
- [138] L. de Arcangelis, S. Redner, and A. Coniglio (1985), *Phys. Rev. B* **31**, 4725.
- [139] C. De Dominicis, E. Brézin, and J. Zinn-Justin (1975), *Phys. Rev. B* **12**, 4945.
- [140] M.J. de Oliveira (1992), *J. Stat. Phys.* **66**, 273.
- [141] M.J. de Oliveira (2003), *Phys. Rev. E* **67**, 066101.
- [142] M.J. de Oliveira, J.F.F Mendes and M.A. Santos (1993), *J. Phys. A* **26**, 2317.
- [143] S.L.A. de Queiroz, and R.B. Stinchcombe (1996), *Phys. Rev. E* **54**, 190.
- [144] J.-M. Debierre and L. Turban (1983), *J. Phys. A* **16**, 3571.
- [145] U. Decker and F. Haake (1979), *Z. Phys. B* **35**, 281.
- [146] M.P.M. den Nijs (1979), *J. Phys. A* **12**, 1857.
- [147] M.P.M. den Nijs (1983), *Phys. Rev. B* **27**, 1674.
- [148] Y. Deng, H.W.J. Blöte, and B. Nienhuis (2004), *Phys. Rev. E* **69**, 026123.
- [149] B. Derrida, A.J. Bray and C. Godrèche (1994), *J. Phys. A* **27**, L357.
- [150] B. Derrida, and E. Gardner (1984), *J. Phys. A* **17**, 3223.
- [151] B. Derrida, V. Hakim, and V. Pasquier (1995), *Phys. Rev. Lett.* **75**, 751.
- [152] B. Derrida and H. Hilhorst (1981), *J. Phys. C* **14**, L539.
- [153] B. Derrida, and R. Zeitak (1996), *Phys. Rev. E* **54**, 2513.

- [154] P. di Francesco, P. Mathieu, and D. Sénéchal (1997) In *Conformal Field Theory*, Springer-Verlag.
- [155] C. Didiot, Y. Fagot-Revurat, S. Pons, B. Kierren, C. Chatelain, D. Malterre (2006), *Phys. Rev. B* **74**, 081404.
- [156] I. Dornic, H. Chaté, J. Chave, and H. Hinrichsen (2001), *Phys. Rev. Lett.* **87**, 045701.
- [157] V. Dotsenko, A.B. Harris, D. Sherrington, and R.B. Stinchcombe (1995), *J. Phys. A* **28**, 3093.
- [158] V.S. Dotsenko (1985), *J. Phys. A* **18**, L241.
- [159] V.S. Dotsenko, and Vl.S. Dotsenko (1983), *Adv. Phys.* **32**, 129.
- [160] V.S. Dotsenko, and Vl.S. Dotsenko (1984), *J. Phys. A* **17**, L301.
- [161] V.S. Dotsenko, Vl.S. Dotsenko, and M. Picco (1998), *Nucl. Phys. B* **520**, 633.
- [162] V.S. Dotsenko, Vl.S. Dotsenko, M. Picco, and P. Pujol (1995), *Eur. Phys. Lett.* **32**, 425.
- [163] Vl.S. Dotsenko, and V.A. Fateev (1984), *Nucl. Phys. B* **240**, 312.
- [164] Vl.S. Dotsenko, M. Picco, and P. Pujol (1995), *Proceedings of the Trieste Conference on Recent Developments in Statistical Mechanics and Quantum Field Theory* , April 1995.
- [165] Vl.S. Dotsenko, M. Picco, and P. Pujol (1995), *Phys. Lett. B* **347**, 113.
- [166] Vl.S. Dotsenko, M. Picco, and P. Pujol (1995), *Nucl. Phys. B* **455**, 701.
- [167] F. Douarche, C. Ciliberto, and A. Petrosyan (2005), *J. Stat. Mech.* , P09011.
- [168] J. Dubail, J.L. Jacobsen, and H. Saleur (2010), *J. Stat. Mech.* , P12026.
- [169] J. Dubail, J.L. Jacobsen, and H. Saleur (2010), *J. Phys. A* **43**, 482002.
- [170] H. Duminil-Copin, and S. Smirnov (2011) *arxiv/1109.1549*.
- [171] B. Duplantier (1998), *Phys. Rev. Lett.* **81**, 5489.
- [172] B. Duplantier (2003), *J. Stat. Phys.* **110**, 691.
- [173] S.B. Dutta, M. Henkel, and H. Park (2009), *J. Stat. Mech.* , P03023.
- [174] M. Ebbinghaus, H. Grandclaude, and M. Henkel (2008), *Eur. Phys. J. B* **63**, 85.
- [175] V.J. Emery (1975), *Phys. Rev. B* **11**, 239.
- [176] F. Canet, C. Bellouard, S. Mangin, C. Chatelain, C. Senet, R. Siebrecht, V. Leiner, and M. Piccuch (2003), *Eur. Phys. J. B* **34**, 381.
- [177] A. Falicov and A.N. Berker (1996), *Phys. Rev. Lett.* **76**, 4380.
- [178] C. Fan (1972), *Phys. Rev. B* **6**, 902.
- [179] S. Fan, and F. Zhong (2009), *Phys. Rev. E* **79**, 011122.
- [180] A.M. Ferrenberg, and R.H. Swendsen (1988), *Phys. Rev. Lett.* **61**, 2635.
- [181] A. Fierro, G. Franzese, A. de Candia, and A. Coniglio (1999), *Phys. Rev. E* **59**, 60.
- [182] D. Fisher, and D. Huse (1988), *Phys. Rev. B* **38**, 373.
- [183] H.C. Fogedby (2007) *arxiv/0706.1177*.
- [184] G. Forgacs (1980), *Phys. Rev. B* **22**, 4473.

- [185] C.M. Fortuin, and P.W. Kasteleyn (1972), *Physica* **57**, 536.
- [186] D.P. Foster and C. Gérard (2004), *Phys. Rev. B* **70**, 014411.
- [187] D.P. Foster, C. Gérard and I. Puha (2001), *J. Phys. A* **34**, 5183.
- [188] D.P. Foster, C. Gérard and I. Puha (2002), *J. Phys. A* **35**, L75.
- [189] G. Franzese, and A. Coniglio (1999), *Phys. Rev. E* **59**, 6409.
- [190] D. Friedan, Z. Qiu and S. Shenker (1984), *Phys. Rev. Lett.* **52**, 1575.
- [191] H. Furukawa (1989), *Phys. Rev. B* **40**, 2341.
- [192] H. Furukawa (1989), *J. Phys. Soc. Jpn.* **58**, 216.
- [193] N.G. Fytas, and P.E. Theodorakis (2010), *Phys. Rev. E* **82**, 062101.
- [194] A. Gambassi (2006), *J. Phys. Conf. Ser.* **40**, 13.
- [195] A. Gamsa, and J. Cardy (2007), *J. Stat. Mech.* , P08020.
- [196] P.L. Garrido, A. Labarta and J. Marro (1987), *J. Stat. Phys.* **49**, 551.
- [197] A. Garriga, P. Sollich, I. Pagonabarraga, and F. Ritort (2005), *Phys. Rev. E* **72**, 056114.
- [198] D. Girardi, and N.S. Branco (2011), *Phys. Rev. E* **83**, 061127.
- [199] R. Glauber (1963), *J. Math. Phys. (N. Y.)* **4**, 294.
- [200] F. Gliozzi, and M.A. Rajabpour (2010), *J. Stat. Mech.* , L05004.
- [201] C. Godrèche and J.M. Luck (2000), *J. Phys. A* **33**, 1151.
- [202] C. Godrèche, and J.M. Luck (2000), *J. Phys. A* **33**, 9141.
- [203] C. Godrèche, and J.M. Luck (2002), *J. Phys. C* **14**, 1589.
- [204] S. Gong, F. Zhong, X. Huang, and S. Fan (2010), *New J. Phys.* **12**, 043036.
- [205] E. Granato and J.M. Kosterlitz (1986), *J. Phys. C* **19**, L59.
- [206] E. Granato and J.M. Kosterlitz (1986), *Phys. Rev. B* **33**, 4767.
- [207] E. Granato, J.M. Kosterlitz, J. Lee, and M.P. Nightingale (1991), *Phys. Rev. Lett.* **66**, 1090.
- [208] Y. Grandati (1992), *Ann. de Physique* **17**, 159.
- [209] P. Grassberger (1995), *Physica A* **214**, 547.
- [210] M.B. Green, J.H. Schwartz, and E. Witten (1987) In *Superstring theory: Introduction*, Cambridge University Press.
- [211] R.L. Greenblatt, M. Aizenman, and J.L. Lebowitz (2009), *Phys. Rev. Lett.* **103**, 197201.
- [212] H.P. Griffiths and D.W. Wood (1973), *J. Phys. C* **6**, 2533.
- [213] G. Grimmett (2006) In *The Random Cluster Model*, Springer-Verlag.
- [214] G. Grinstein, C. Jayaparakash and Y. He (1985), *Phys. Rev. Lett.* **55**, 2527.
- [215] G. Grinstein, and A. Luther (1976), *Phys. Rev. B* **13**, 1329.
- [216] T Grossman, and A. Aharony (1987), *J. Phys. A* **20**, L1193.
- [217] T. Grossman, and A. Aharony (1986), *J. Phys. A* **19**, L745.
- [218] I.A. Gruzberg (2006), *J. Phys. A* **39**, 12601.
- [219] G. H. Wannier (1950), *Phys. Rev.* **79**, 357.
- [220] G. H. Wannier (1973), *Phys. Rev. B* **7**, 5017.

- [221] B.I. Halperin, P.C. Hohenberg, and S.-K. Ma (1972), *Phys. Rev. Lett.* **29**, 1548.
- [222] B.I. Halperin, P.C. Hohenberg, and S.-K. Ma (1974), *Phys. Rev. B* **10**, 139.
- [223] T.C. Halsey (1985), *J. Phys. C* **18**, 2437.
- [224] T.C. Halsey, P. Meakin, and I. Procaccia (1986), *Phys. Rev. Lett.* **56**, 854.
- [225] A.B. Harris, and T.C. Lubensky (1974), *Phys. Rev. Lett.* **33**, 1540.
- [226] M.O. Hase, S.R. Salinas, T. Tomé, and M.J. de Oliveira (2006), *Phys. Rev. E* **73**, 056117.
- [227] M.O. Hase, T. Tomé, and M.J. de Oliveira (2010), *Phys. Rev. E* **82**, 011133.
- [228] M. Hasenbusch, and S. Meyer (1991), *Phys. Rev. Lett.* **66**, 530.
- [229] M. Hasenbusch, F. Parisen Toldin, A. Pelissetto, and E. Vicari (2007), *J. Stat. Mech.* , P02016.
- [230] M. Hasenbusch, A. Pelissetto, and E. Vicari (2005), *Phys. Rev. B* **72**, 184502.
- [231] M. Hasenbusch, A. Pelissetto, and E. Vicari (2006), *J. Phys.: Conf. Ser.* **42**, 124.
- [232] M. Hasenbusch, and K. Pinn (1994), *Physica A* **203**, 189.
- [233] M. Hellmund, and W. Janke (2002), *Nucl. Phys. B - Proc. Suppl* **106**, 923.
- [234] M. Hellmund, and W. Janke (2003), *Phys. Rev. E* **67**, 026118.
- [235] M. Henkel (1999) In *Conformal invariance and critical phenomena*, Springer-Verlag.
- [236] M. Henkel, and F. Baumann (2007), *J. Stat. Mech.* , P07015.
- [237] M. Henkel, T. Enss and M. Pleimling (2006), *J. Phys. A* **39**, L589.
- [238] M. Henkel, M. Paessens, and M. Pleimling (2003), *Europhys. Lett.* **62**, 664.
- [239] M. Henkel, and M. Pleimling (2003), *Phys. Rev. E* **68**, 065101(R).
- [240] M. Henkel, and M. Pleimling (2010) In *Non-Equilibrium Phase Transitions, Volume 2: Ageing and Dynamical Scaling Far from Equilibrium*, Springer-Verlag.
- [241] M. Henkel, M. Pleimling, C. Godrèche, and J.-M. Luck (2001), *Phys. Rev. Lett.* **87**, 265701.
- [242] M. Henkel and G.M. Schütz (2004), *J. Phys. A* **37**, 591.
- [243] H.J. Herrmann (1990), *Physica A* **168**, 516.
- [244] H.O. Heuer (1993), *J. Phys. A* **26**, L333.
- [245] P.C. Hohenberg, and B.I. Halperin (1977), *Rev. Mod. Phys.* **49**, 435.
- [246] R.M.F. Houtappel (1950), *Physica* **16**, 425.
- [247] M. Howard and C. Godrèche (1998), *J. Phys. A* **31**, L209.
- [248] K. Hui, and A.N. Berker (1989), *Phys. Rev. Lett.* **62**, 2507.
- [249] K. Hui, and A.N. Berker (1989), *Phys. Rev. Lett.* **63**, 2433.
- [250] K. Humayun and A.J. Bray (1991), *J. Phys. A* **24**, 1915.
- [251] D.L. Hunter, L. de Arcangelis, R. Matz, P.H. Poole, and N. Jan (1993), *Physica A* **196**, 188.
- [252] D. Huse (1989), *Phys. Rev. B* **40**, 304.

- [253] D.A. Huse and C.L. Henley (1985), *Phys. Rev. Lett.* **54**, 2708.
- [254] H. Híjar, J. Quintana-H, and G. Sutmann (2007), *J. Stat. Mech.* , P04010.
- [255] H. Híjar, and G. Sutmann (2008), *J. Stat. Mech.* , P07012.
- [256] D. Hérisson and M. Ocio (2002), *Phys. Rev. Lett.* **88**, 257202.
- [257] F. Iglói (1987), *J. Phys. A* **20**, 2651.
- [258] F. Iglói (1987), *J. Phys. A* **20**, 5319.
- [259] F. Iglói (1993), *J. Phys. A* **26**, L703.
- [260] F. Iglói, and H. Rieger (1998), *Phys. Rev. B* **57**, 11404.
- [261] Y. Ikhlef, and M.A. Rajabpour (2012), *J. Stat. Mech.* , P01012.
- [262] Y. Imry and S.K. Ma (1975), *Phys. Rev. Lett.* **35**, 1399.
- [263] Y. Imry, and M. Wortis (1979), *Phys. Rev. B* **19**, 3581.
- [264] F.E. Irons (2004), *Am. J. Phys.* **72**, 1059.
- [265] E. Ising (1925), *Z. Phys.* **31**, 253.
- [266] N. Ito (1993), *Physica A* **192**, 604.
- [267] N. Ito (1993), *Physica A* **196**, 591.
- [268] J.L. Jacobsen, and J.L. Cardy (1998), *Nucl. Phys. B* **515**, 701.
- [269] J.L. Jacobsen, P. Le Doussal, M. Picco, R. Santachiara, and K.J. Wiese (2009), *Phys. Rev. Lett.* **102**, 070601.
- [270] J.L. Jacobsen, and M. Picco (2000), *Phys. Rev. E* **61**, R13.
- [271] W. Janke, and D.A. Johnston (2000), *Nucl. Phys. B* **578**, 681.
- [272] W. Janke, D.A. Johnston, and R. Villanova (2001), *Physica A* **281**, 207.
- [273] W. Janke, and S. Kappler (1995), *Phys. Rev. Lett.* **74**, 212.
- [274] W. Janke, and A.M.J. Schakel (2004), *Nucl. Phys. B* **700**, 385.
- [275] W. Janke, and A.M.J. Schakel (2005), *Phys. Rev. E* **71**, 036703.
- [276] W. Janke, and R. Villanova (1995), *Phys. Lett. A* **209**, 179.
- [277] W. Janke, and R. Villanova (1996), *Nucl. Phys. B* **47**, 641.
- [278] W. Janke and R. Villanova (1997), *Nucl. Phys. B* **489**, 679.
- [279] W. Janke and R. Villanova (2000), *Nucl. Phys. B - Proc. Suppl.* **83**, 697.
- [280] W. Janke and R. Villanova (2002), *Phys. Rev. B* **66**, 134208.
- [281] W. Janke, and M. Weigel (2004), *Phys. Rev. B* **69**, 144208.
- [282] H.K. Janssen, B. Schaub, and B. Schmittmann (1989), *Z. Phys. B* **73**, 539.
- [283] M. Janssen (1998), *Phys. Rep.* **295**, 1.
- [284] C. Jarzynski (1997), *Phys. Rev. E* **56**, 5018.
- [285] C. Jarzynski (1997), *Phys. Rev. Lett.* **78**, 2690.
- [286] H.R. Jauslin, and R.H. Swendsen (1981), *Phys. Rev. B* **24**, 313.
- [287] G.S. Jeon, S.J. Lee, and M.Y. Choi (2003), *Phys. Rev. B* **67**, 014501.
- [288] G. Jug, and B.N. Shalaev (1996), *Phys. Rev. B* **54**, 3442.
- [289] R. Juhász, H. Rieger, and F. Iglói (2001), *Phys. Rev. E* **64**, 056122.
- [290] L.P. Kadanoff, and A.C. Brown (1979), *Ann. Phys.* **121**, 318.
- [291] W. Kager and B. Nienhuis (2004), *J. Stat. Phys* **115**, 1149.

- [292] G. Kamieniarz, P. Kozłowski, and R. Dekeyser (1997), *Phys. Rev. E* **55**, 3724.
- [293] D. Karevski, G. Palágyi, and L. Turban (1995), *J. Phys. A* **28**, 45.
- [294] M. Karsai, J.-Ch. Anglès d'Auriac, and F. Iglói (2010), *J. Stat. Mech.* , P08027.
- [295] M. Karsai, J.-Ch. Anglès d'Auriac, and F. Iglói (2009), *J. Stat. Mech.* , P07044.
- [296] K.K. Kaski and J. Nieminen, and J.D. Gunton (1985), *Phys. Rev. B* **31**, 2998.
- [297] D. Kim, and R.I. Joseph (1974), *J. Phys. C* **7**, L167.
- [298] E. Kim, B. Kim and S.J. Lee (2003), *Phys. Rev. E* **68**, 066127.
- [299] E. Kim, S.J. Lee, and B. Kim (2007), *Phys. Rev. E* **75**, 021106.
- [300] J.K. Kim (1996), *Phys. Rev. B* **53**, 3388.
- [301] J.C. Kimball (1979), *J. Stat. Phys.* **21**, 289.
- [302] W. Kinzel, and E. Domany (1981), *Phys. Rev. B* **23**, 3421.
- [303] S.E. Korshunov (2002), *Phys. Rev. Lett.* **88**, 167007.
- [304] S.E. Korshunov, and G.V. Uimin (1986), *J. Stat. Phys.* **43**, 1.
- [305] S.E. Korshunov, and G.V. Uimin (1986), *J. Stat. Phys.* **43**, 17.
- [306] H.A. Kramers, and G.H. Wannier (1941), *Phys. Rev.* **60**, 252.
- [307] S. Kumar, J.D. Gunton, and K.K. Kaski (1987), *Phys. Rev. B* **35**, 8517.
- [308] D.P. Landau (1980), *Phys. Rev. B* **22**, 2450.
- [309] P. Langevin (1908)), *C.R. Acad. Sci. (Paris)* **146**, 530.
- [310] M. Lau, C. Dasgupta, and O.T. Valls (1988), *Phys. Rev. B* **38**, 9024.
- [311] G.F. Lawler, O. Schramm, and W. Werner (2004), *Ann. Prob.* **32**, 939.
- [312] D. Ledue, and D.P. Landau (2001), *Phys. Rev. B* **63**, 054425.
- [313] D. Ledue, D.P. Landau, and J. Teillet (1995), *Phys. Rev. B* **51**, 12523.
- [314] D. Ledue, D.P. Landau, and J. Teillet (1998), *J. Appl. Phys.* **83**, 6305.
- [315] J. Lee and J.M. Kosterlitz (1990), *Phys. Rev. Lett.* **65**, 137.
- [316] J. Lee, J.M. Kosterlitz, and E. Granato (1991), *Phys. Rev. B* **43**, 11531.
- [317] S. Lee and K.-C. Lee (1994), *Phys. Rev. B* **49**, 15184.
- [318] S.J. Lee, J.R. Lee, and B. Kim (1995), *Phys. Rev. E* **51**, R4.
- [319] X.W. Lei, and B. Zheng (2007), *Phys. Rev. E* **75**, 040104(R).
- [320] J.C. Lessa and S.L.A. de Queiroz (2006), *Phys. Rev. E* **74**, 021114.
- [321] M.A. Lewis (1998), *Eur. Phys. Lett.* **43**, 189.
- [322] M.A. Lewis (1999), *Eur. Phys. Lett.* **47**, 129.
- [323] Z.B. Li, X.W. Liu, L. Schülke, and B. Zheng (1997), *Physica A* **245**, 485.
- [324] F.W.S. Lima (2012), *Physica A* **389**, 3039.
- [325] J. Liphardt, S. Dumont, S.B. Smith, I. Tinoco, and C. Bustamante (2002), *Science* **296**, 1832.
- [326] E. Lippiello, F. Corberi, and M. Zannetti (2005), *Phys. Rev. E* **71**, 036104.

- [327] E. Lippiello, F. Corberi, and M. Zannetti (2006), *Phys. Rev. E* **74**, 041113.
- [328] E. Lippiello and M. Zannetti (2000), *Phys. Rev. E* **661**, 3369.
- [329] F. Liu, and G.F. Mazenko (1991), *Phys. Rev. B* **44**, 9185.
- [330] E. Lorenz, and W. Janke (2007), *Europhys. Lett.* **77**, 10003.
- [331] M.P.O Loureiro, J.J. Arenzon, L.F. Cugliandolo and A. Sicilia (2010), *J. Phys. Conf. Ser.* **246**, 012022.
- [332] M.P.O. Loureiro, J.J. Arenzon, L.F. Cugliandolo, A. Sicilia (2010), *Phys. Rev. E* **81**, 021129.
- [333] T.C. Lubensky (1975), *Phys. Rev. B* **11**, 3573.
- [334] J.M. Luck (1993), *Eur. Phys. Lett.* **5**, 359.
- [335] J.M. Luck (1993), *J. Stat. Phys.* **72**, 417.
- [336] A.W.W. Ludwig (1987), *Nucl. Phys. B* **285**, 97.
- [337] A.W.W. Ludwig (1988), *Phys. Rev. Lett.* **61**, 2388.
- [338] A.W.W. Ludwig (1990), *Nucl. Phys. B* **330**, 639.
- [339] A.W.W. Ludwig, and J.L. Cardy (1987), *Nucl. Phys. B* **285**, 687.
- [340] H.J. Luo, M. Schulz, L. Schülke, S. Trimper, and B. Zheng (1998), *Phys. Lett. A* **250**, 383.
- [341] H.J. Luo, L. Schülke, and B. Zheng (1998), *Phys. Rev. E* **57**, 1327.
- [342] H.J. Luo, L. Schülke, and B. Zheng (1998), *Phys. Rev. Lett.* **81**, 180.
- [343] H.J. Luo and B. Zheng (1997), *Mod. Phys. Lett. B* **11**, 615.
- [344] K. Löwner (1923), *Math. Annal.* **89**, 103.
- [345] K. MacIsaac and N. Jan (1992), *J. Phys. A* **25**, 2139.
- [346] S.N. Majumdar (1992), *Phys. Rev. Lett.* **68**, 2329.
- [347] S.N. Majumdar, A.J. Bray, S.J. Cornell, and C. Sire (1996), *Phys. Rev. Lett.* **77**, 3704.
- [348] S.N. Majumdar, A.M. Sengupta (1996), *Phys. Rev. Lett.* **76**, 2394.
- [349] B.B. Mandelbrot (1982) In *The Fractal Geometry of Nature*, Freeman (San Francisco).
- [350] R. Marathe and A. Dhar (2005), *Phys. Rev. E* **72**, 066112.
- [351] M.C. Marques (1989), *J. Phys. A* **22**, 4493.
- [352] P.C. Martin, E. Siggia, and H.A. Rose (1973), *Phys. Rev. A* **8**, 423.
- [353] T. Masser, and D. ben-Avraham (2000), *Phys. Lett. A* **275**, 382.
- [354] D. Matthews-Morgan, and D.P. Landau (1984), *Phys. Rev. Lett.* **53**, 679.
- [355] D.C. Mattis (1976), *Phys. Lett. A* **56**, 421.
- [356] R. Matz, D.L. Hunter and N. Jan (1994), *J. Stat. Phys.* **74**, 903.
- [357] P. Mayer, L. Berthier, J.P. Garrahan, and P. Sollich (2003), *Phys. Rev. E* **68**, 016116.
- [358] G. Mazzeo, and R. Kühn (1999), *Phys. Rev. E* **60**, 3823.
- [359] B.M. McCoy (1969), *Phys. Rev.* **188**, 1014.
- [360] B.M. McCoy (1970), *Phys. Rev. B* **2**, 2795.
- [361] B.M. McCoy, and T.T. Wu (1968), *Phys. Rev.* **176**, 631.

- [362] B.M. McCoy, and T.T. Wu (1969), *Phys. Rev.* **188**, 982.
- [363] D. McMahon (2009) In *String theory demystified*, McGraw Hill.
- [364] J.F.F. Mendes and M.A. Santos (1998), *Phys. Rev. E* **57**, 108.
- [365] M.T. Mercaldo, J.-Ch. Anglès d'Auriac, and F. Iglói (2004), *Phys. Rev. E* **69**, 056112.
- [366] M.T. Mercaldo, J.-Ch. Anglès d'Auriac, and F. Iglói (2005), *Europhys. Lett.* **70**, 733.
- [367] M.T. Mercaldo, J.-Ch. Anglès d'Auriac, and F. Iglói (2006), *Phys. Rev. E* **73**, 026126.
- [368] N. Metropolis A.W. Rosenbluth, M.N. Rosenbluth, A.H. Teller, E. Teller (1953), *J. Chem. Phys.* **21**, 1087.
- [369] M. Mezard, G. Parisi, and M.A. Virasoro (1987) In *Spin glass theory and beyond*, World Scientific.
- [370] A.A. Middleton, and D.S. Fisher (2002), *Phys. Rev. B* **65**, 134411.
- [371] J.D. Miller, and K. De'Bell (1993), *J. Phys. I* **3**, 1717.
- [372] A.D. Mirlin, Y.V. Fyodorov, A. Mildenberger, and F. Evers (2006), *Phys. Rev. Lett.* **97**, 046803.
- [373] S. Miyashita and H. Shiba1 (1984), *J. Phys. Soc. Jpn.* **53**, 1145.
- [374] F. Montani, E.V. Albano (1995), *Phys. Lett. A* **202**, 253.
- [375] C. Monthus, B. Berche, and C. Chatelain (2009), *J. Stat. Mech.* , P12002.
- [376] C. Moore, M.G. Nordahl, N. Minar, and C.R. Shalizi (1999), *Phys. Rev. E* **60**, 5344.
- [377] A.K. Murtazaev, and A.B. Babaev (2009), *J. Mag. Mag. Mat.* **321**, 2630.
- [378] A.K. Murtazaev, and A.B. Babaev (2012), *J. Mag. Mag. Mat.* **324**, 3870.
- [379] A.K. Murtazaev, A.B. Babaev, and G.Ya. Aznaurova (2007), *Bull. Russ. Acad. Sci. Phys.* **71**, 707.
- [380] A.K. Murtazaev, A.B. Babaev, and G.Ya. Aznaurova (2008), *Physics of the Solid State* **50**, 733.
- [381] A.K. Murtazaev, A.B. Babaev, and G.Ya. Aznaurova (2009), *Journal of Experimental and Theoretical Physics* **109**, 442.
- [382] A.K. Murtazaev, A.B. Babaev, and G.Ya. Aznaurova (2010), *Bull. Russ. Acad. Sci. Phys.* **74**, 686.
- [383] A.K. Murtazaev, A.B. Babaev, and G.Ya. Aznaurova (2011), *Low Temp. Phys.* **37**, 134.
- [384] A.K. Murtazaev, I.K. Kamilov, and A. B. Babaev (2004), *Journal of Experimental and Theoretical Physics* **99**, 1201.
- [385] A.K. Murtazaev, I.K. Kamilov, and A.B. Babaev (2007), *Bull. Russ. Acad. Sci. Phys.* **71**, 1586.
- [386] O. Narayan, and A. Dhar (2004), *J. Phys. A* **37**, 63.
- [387] M. Nauenberg and D.J. Scalapino (1980), *Phys. Rev. Lett.* **44**, 837.
- [388] R.M. Neal (2001), *Stat. Comput.* **11**, 125.
- [389] B. Nienhuis (1984), *J. Stat. Phys.* **34**, 731.

- [390] B. Nienhuis (1987) In *Phase Transitions and Critical Phenomena*, volume 11, Academic Press, Eds C. Domb and J.L. Lebowitz.
- [391] B. Nienhuis, A.N. Berker, E.K. Riedel, and M. Schick (1979), *Phys. Rev. Lett.* **43**, 737.
- [392] B. Nienhuis, H.J. Hilhorst and H.W.J. Blöte (1984), *J. Phys. A* **17**, 3559.
- [393] B. Nienhuis, E.K. Riedel and M. Schick (1980), *J. Phys. A* **13**, L189.
- [394] M.P. Nightingale, and H.W.J. Blöte (2000), *Phys. Rev. B* **62**, 1089.
- [395] M.A. Novotny, and D.P. Landau (1981), *Phys. Rev. B* **24**, 1468.
- [396] K. Okano, L. Schülke, and B. Zheng (1997), *Nucl. Phys. B* **485**, 727.
- [397] T. Olson, and A.P. Young (1999), *Phys. Rev. B* **60**, 3428.
- [398] P. Olsson (1995), *Phys. Rev. Lett.* **75**, 2758.
- [399] P. Olsson (1997), *Phys. Rev. B* **55**, 3585.
- [400] P. Olsson and S. Teitel (2005), *Phys. Rev. B* **71**, 104423.
- [401] L. Onsager (1931), *Phys. Rev.* **37**, 405.
- [402] L. Onsager (1931), *Phys. Rev.* **38**, 2265.
- [403] L. Onsager (1944), *Phys. Rev.* **65**, 117.
- [404] L. Onsager, and S. Machlup (1953), *Phys. Rev.* **91**, 1505.
- [405] L. Onsager, and S. Machlup (1953), *Phys. Rev.* **91**, 1512.
- [406] G. Palagyi, C. Chatelain, B. Berche, and F. Iglói (2000), *Eur. Phys. J. B* **13**, 357.
- [407] R. Pandit, G. Forgacs, and P. Rujan (1981), *Phys. Rev. B* **24**, 1576.
- [408] R. Paredes, and J. Valbuena (1998), *Phys. Rev. E* **59**, 6275.
- [409] R.B. Pearson (1980), *Phys. Rev. B* **22**, 2579.
- [410] A. Pelissetto, and E. Vicari (2000), *Phys. Rev. B* **62**, 6393.
- [411] I. Peschel (1982), *Z. Phys. B* **45**, 339.
- [412] J.C Phillips (1996), *Rep. Prog. Phys.* **59**, 1133.
- [413] M. Picco (1996), *Phys. Rev. B* **54**, 14930.
- [414] M. Picco (1997), *Phys. Rev. Lett.* **79**, 2998.
- [415] M. Picco (1998) *cond-mat/9802092*.
- [416] M. Picco, and R. Santachiara (2008), *Phys. Rev. Lett.* **100**, 015704.
- [417] M. Picco, and R. Santachiara (2010), *J. Stat. Mech.* , P07027.
- [418] M. Picco, and R. Santachiara (2011), *Phys. Rev. E* **83**, 061124.
- [419] M. Picco, R. Santachiara, and A. Sicilia (2009), *J. Stat. Mech.* , P04013.
- [420] A. Picone, and M. Henkel (2002), *J. Phys. A* **35**, 5575.
- [421] A. Picone, M. Henkel, and J. Richert (2003), *J. Phys. A* **36**, 1249.
- [422] M. Pleimling and A. Gambassi (2005), *Phys. Rev. B* **71**, 180401(R).
- [423] R.B. Potts (1952), *Proc. Camb. Phil. Soc* **48**, 106.
- [424] A. Prados and J.J. Brey (2001), *J. Phys. A* **34**, L453.
- [425] V.V. Prudnikov, P.V. Prudnikov, A.S. Krinitsyn, A.N. Vakilov, E.A. Pospelov, and M.V. Rychkov (2010), *Phys. Rev. E* **81**, 011130.

- [426] G. Ramirez-Santiago, and Jorge V. José (1994), *Phys. Rev. B* **49**, 9567.
- [427] F. Ricci-Tersinghi (2003), *Phys. Rev. E* **68**, 065104.
- [428] S. Risau-Gusman, and F. Romá (2008), *Phys. Rev. B* **77**, 134435.
- [429] A. Roder, J. Adler, and W. Janke (1998), *Phys. Rev. Lett.* **80**, 4697.
- [430] C. Roland and M. Grant (1990), *Phys. Rev. B* **41**, 4663.
- [431] A.D. Rutenberg and A.J. Bray (1995), *Phys. Rev. E* **51**, R1641.
- [432] P.S. Sahni, G.S. Grest, M.P. Anderson, and D.J. Srolovitz (1983), *Phys. Rev. Lett.* **50**, 263.
- [433] H. Saleur (1987), *J. Phys. A* **20**, L1127.
- [434] H. Saleur, and B. Duplantier (1987), *Phys. Rev. Lett.* **58**, 2325.
- [435] F. Sastre, I. Dornic, and H. Chaté (2003), *Phys. Rev. Lett.* **91**, 267205.
- [436] D. Schechtman, I. Blech, D. Gratias, and J.W. Cahn (1984), *Phys. Rev. Lett.* **53**, 1951.
- [437] M. Scheucher and H. Spohn (1988), *J. Stat. Phys.* **53**, 279.
- [438] O. Schramm (2000), *Isr. J. Math.* **118**, 221.
- [439] O. Schramm (2001), *Electron. Comm. Probab.* **6**, 115.
- [440] K. Schwarz, A. Karrenbauer, G. Schehr, and H. Rieger (2009), *J. Stat. Mech.*, P08022.
- [441] L. Schülke, and B. Zheng (1995), *Phys. Lett. A* **204**, 295.
- [442] U. Seifert (2005), *Phys. Rev. Lett.* **95**, 040602.
- [443] T. Senthil, and S.N. Majumdar (1996), *Phys. Rev. Lett.* **76**, 3001.
- [444] B.N. Shalaev (1984), *Sov. Phys. Solid State* **26**, 1811.
- [445] B.N. Shalaev (1994), *Phys. Rep.* **237**, 129.
- [446] R. Shankar (1988), *Phys. Rev. Lett.* **61**, 2390.
- [447] L. Shchur and W. Janke (2010), *Nucl. Phys. B* **840**, 491.
- [448] C.S. Simões, and J.R. Drugowich de Felício (2001), *Mod. Phys. Lett. B* **15**, 487.
- [449] S. Smirnov (2001), *C.R. Acad. Sci. Paris Sér. I Math.* **333**, 239.
- [450] R.E. Spinney, and I.J. Ford (2012) In *Nonequilibrium Statistical Physics of Small Systems: Fluctuation Relations and Beyond*, R. Klages, W. Just, C. Jarzynski (Eds.), Wiley-VCH, Weinheim.
- [451] J.L. Spouge (1988), *Phys. Rev. Lett.* **60**, 871.
- [452] J.L. Spouge (1988), *Phys. Rev. Lett.* **60**, 1885.
- [453] H.E. Stanley (1977), *J. Phys. A* **10**, L211.
- [454] H.E. Stanley, D. Stauffer, J. Kertész, and H.J. Herrmann (1987), *Phys. Rev. Lett.* **59**, 2326.
- [455] A.L. Stella, and C. Vanderzande (1989), *Phys. Rev. Lett.* **62**, 1067.
- [456] J. Stephenson (1964), *J. Math. Phys.* **5**, 1009.
- [457] J.D. Stevenson, and M. Weigel (2011), *Eur. Phys. Lett.* **95**, 40001.
- [458] J.D. Stevenson, and M. Weigel (2011), *Comp. Phys. Comm.* **182**, 1879.
- [459] R.H. Swendsen, and J.S. Wang (1987), *Phys. Rev. Lett.* **58**, 86.

- [460] S. Teitel and C. Jayaprakash (1983), *Phys. Rev. B* **27**, 598.
- [461] S. Teitel and C. Jayaprakash (1983), *Phys. Rev. Lett.* **51**, 1999.
- [462] H.N.V. Temperley, and E.H. Lieb (1971), *Proc. R. Soc. London Ser. A* **322**, 251.
- [463] P.E. Theodorakis and N.G. Fytas (2011), *Eur. Phys. J. B* **81**, 245.
- [464] J.M. Thijssen and H.J.F. Knops (1990), *Phys. Rev. B* **42**, 2438.
- [465] Y. Tomita, and Y. Okabe (2001), *Phys. Rev. E* **64**, 036114.
- [466] T. Tomé, A. Brunstein, and M.J. de Oliveira (2000), *Physica A* **283**, 107.
- [467] T. Tomé, and M.J. de Oliveira (1998), *Phys. Rev. E* **58**, 4242.
- [468] T. Tomé, and A. Petri (2002), *J. Phys. A* **35**, 5379.
- [469] C. Tournier-Colletta, B. Kierren, Y. Fagot-Revurat, C. Chatelain, D. Malterre (2011), *Phys. Rev. B* **84**, 165420.
- [470] J. Trenkler, H. Abe1, P. Wochner, D. Haeffner, J. Bai, H.D. Carstanjen, and S.C. Moss (2000), *Modelling Simul. Mater. Sci. Eng.* **8**, 269.
- [471] L. Turban (1980), *J. Phys. C* **13**, L13.
- [472] L. Turban (1980), *Phys. Lett. A* **75**, 307.
- [473] L. Turban, and F. Igóí (1994), *Eur. Phys. Lett.* **27**, 91.
- [474] L. Turban, F. Igóí, and B. Berche (1994), *Phys. Rev. B* **49**, 12695.
- [475] K. Uzelac, A. Hasmy, and R. Jullien (1995), *Phys. Rev. Lett* **74**, 422.
- [476] K. Uzelac, A. Hasmy, and R. Jullien (1995), *J. Non-Cryst. Solids* **186**, 365.
- [477] J.E. Van Himbergen (1986), *Phys. Rev. B* **33**, 7857.
- [478] C. Vanderzande (1992), *J. Phys. A* **25**, L75.
- [479] J. Villain (1977), *J. Phys. C* **10**, 1717.
- [480] J. Villain (1977), *J. Phys. C* **10**, 4793.
- [481] R.F. Voss (1984), *J. Phys. A* **17**, L373.
- [482] J.-C. Walter and C. Chatelain (2009), *J. Stat. Mech.* , P10017.
- [483] J.-C. Walter and C. Chatelain (2012), *J. Stat. Mech.* , P02010.
- [484] J.C. Walter, and C. Chatelain (2008), *J. Stat. Mech.* , P07005.
- [485] S. Wansleben and D.P. Landau (1991), *Phys. Rev. B* **43**, 6006.
- [486] S.R. Williams, D.J. Searles, and D.J. Evans (2008), *Phys. Rev. Lett.* **100**, 250601.
- [487] W.G. Wilson, and C.A. Vause (1988), *Phys. Lett. A* **126**, 471.
- [488] W.G. Wilson, and C.A. Vause (1989), *Phys. Rev. B* **39**, 689.
- [489] W.G. Wilson, and C.A. Vause (1989), *Phys. Rev. B* **39**, 4651.
- [490] S. Wiseman, and E. Domany (1995), *Phys. Rev. E* **51**, 3074.
- [491] S. Wiseman and E. Domany (1995), *Phys. Rev. E* **52**, 3469.
- [492] S. Wiseman and E. Domany (1998), *Phys. Rev. E* **58**, 2938.
- [493] S. Wiseman and E. Domany (1998), *Phys. Rev. Lett.* **81**, 22.
- [494] F.Y. Wu (1982), *Rev. Mod. Phys.* **54**, 235.
- [495] F.Y. Wu (1982), *Rev. Mod. Phys.* **55**, 315.

- [496] F.Y. Wu and K.Y. Lin (1974), *J. Phys. C* **7**, L181.
- [497] X. Wu, W.I. Goldberg, M.X. Liu, and J.Z. Xue (1992), *Phys. Rev. Lett.* **69**, 470.
- [498] W. Xiong, F. Zhong, and S. Fan (2012), *Comp. Phys. Comm.* **183**, 1162.
- [499] W. Xiong, F. Zhong, W. Yuan, and S. Fan (2010), *Phys. Rev. E* **81**, 051132.
- [500] M. Y. Choi and S. Doniach (1985), *Phys. Rev. B* **31**, 4516.
- [501] F. Yaşar, Y. Gündüç, and T. Çelik (1998), *Phys. Rev. E* **58**, 4210.
- [502] C. Yeung, M. Rao, and R.C. Desai (1996), *Phys. Rev. E* **53**, 3073.
- [503] H. Yin, B. Chakraborty, and N. Gross (2000), *Phys. Rev. E* **61**, 6426.
- [504] J.Q. Yin, B. Zheng, V.V. Prudnikov, and S. Trimper (2006), *Eur. Phys. J. B* **49**, 195.
- [505] J.Q. Yin, B. Zheng, and S. Trimper (2004), *Phys. Rev. E* **70**, 056134.
- [506] J.Q. Yin, B. Zheng, and S. Trimper (2005), *Phys. Rev. E* **72**, 036122.
- [507] H.P. Ying, and K. Harada (2000), *Phys. Rev. E* **62**, 174.
- [508] A.P. Young (1998) In *Spin Glasses and Random Fields*, World Scientific.
- [509] A. Zatelepin, and L. Shchur (2010) *arxiv/1008.3573*.
- [510] B. Zheng, F. Ren, and H. Ren (2003), *Phys. Rev. E* **68**, 046120.
- [511] R.M. Ziff, P.T. Cummings, and G. Stell (1984), *J. Phys. A* **17**, 3009.
- [512] B. Zwiebach (2004) In *A first course in string theory*, Cambridge University Press.